NEW APPROACHES IN AVOIDING GAS HYDRATE PROBLEMS IN OFFSHORE AND DEEPWATER OPERATION

The Thesis by

Zahidah Md Zain

Submitted for the Degree of

Doctor of Philosophy in Petroleum Engineering

Institute of Petroleum Engineering
Heriot-Watt University
Edinburgh, Scotland, UK

June 2013

ABSTRACT

Oil industry is facing with challenging gas hydrates and flow assurance issues in deepwater developments. The situation is not any better for Brown fields as a result of increasing water cut. The other factor which is playing an increasing role is product quality and environmental concerns, demanding reduction in chemical usage. The current industry practice for hydrate prevention is injecting hydrate inhibitors at the upstream end of pipelines based on the calculated or measured hydrate phase boundary, water cut, worst pressure and temperature conditions, and the amount of inhibitor lost to non-aqueous phases. In general, systematic ways of controlling and monitoring along the pipeline and/or downstream to examine the degree of inhibition are very limited.

Monitoring changes in the pipeline pressure drop is inadequate to provide reliable indicator for hydrate formation and deposition. Therefore, early hydrate warning and online hydrate monitoring techniques are demanded to optimise inhibitor dosage, reduce the risk of gas hydrate formation/deposition and the cost of mitigating the blockage in subsea pipelines.

The primary part of this thesis is to develop a new approach for early warning system and monitoring against initial hydrate formation. It is known that the formation of hydrates changes the water structure, which is claimed to remain in the aqueous phase for a period of time even after the dissociation of gas hydrates. This change of water structure is hypothesized to be in the form of water memory. Therefore, two hydrate early warning techniques are investigated based on the presence of water memory resulted from hydrate formation. The techniques investigated in this thesis are dielectric properties and onset of ice formation.

In this thesis, the new approach demonstrate that dielectric properties at microwave frequencies has the potential to be used as a downstream and online analysis for detecting the initial hydrate formation and/or presence of hydrate particles and/or changes in water structure due to hydrate formation. Characteristic of onset of ice formation by freezing

method for water samples with and without hydrate water memory shows that samples with water memory nucleate faster than that without water memory. It is concluded that the new approach described above have potential to be developed for early warning and online hydrate monitoring. The results are very encouraging and could potentially change the industrial approach to gas hydrate control strategy.

Low Dosage Hydrate Inhibitors (LDHIs) have been applied in the field to prevent gas hydrate problems by delaying gas hydrate nucleation and/or growth and to prevent agglomeration of hydrates from growing larger enough to plug the flowline. However, the mechanism of hydrate formation and inhibition is still not well understood. It is believed micro-scale investigation could provide vital clues.

The second aim of this thesis is to investigate the inhibition mechanism of Low Dosage Hydrate Inhibitors (LDHIs) by visual observation of gas hydrate formation, growth, and morphology by means of high-pressure glass micromodels, multichanel flow conduits, and glass capillary tubes. Extensive novel data and knowledge was generated from these techniques. The finding of this study shows that various hydrate morphologies formed in the presence of different KHIs for Natural Gas Hydrate and Methane Hydrate.

It was concluded that these techniques provides a new data to supplement the lacking of knowledge on the kinetics of gas hydrate inhibition and morphologies.

Dedicated to:

my parents, **Md Zain** and **Halimah**,

for their prayers and sacrifice,

my husband, **Zairul Bakry**,

for his patience and encouragement,

my beloved son, **Fadhlul Wafi**,

the rainbow and the strength of my life

ACKNOWLEDGEMENTS

I would like to take this opportunity to express my gratitude and appreciation to all people – my supervisors, officemates, colleagues, family and friends – whose encouragement have served as a constant inspiration throughout the course of my study. This thesis is dedicated to them.

I am very fortunate to have the opportunity to be a member of Centre for Gas Hydrate Research of Heriot-Watt University, the highly recognised centre for gas hydrate research in the world. My sincere appreciation and gratitude to Professor Bahman Tohidi for his excellent supervision, guidance and continues support throughout my study. I am also deeply grateful to Professor Adrian C. Todd for his illuminating discussions and invaluable suggestions on the thesis. A special appreciation to Professor Ken Sorbie and the late Professor Ali Danesh for providing my linkage to this Institute to pursue my degree at Heriot-Watt University.

Special gratitude to Dr. Jinhai Yang for his invaluable supervision on the experimental techniques and his kind hearted. I owe appreciation to other colleague particularly Mr. Rod Burgess, Mr. Ross Anderson, Dr. Antonin Chapoy, Mr. Jahan Arjmandi, Mr. Jim Pantling and Mr. Colin Flockhart for helping me in the laboratory and on specific discussions. Everlasting friendship from Dr. Saeid Mazloum, Dr. Roghie Azarinezhad and Dr. Manoocher Salehabadi will be remembered forever.

The financial support from PETRONAS, National Oil Company of Malaysia, through their full scholarship to pursue my degree is greatly acknowledged. Special appreciation to PETRONAS management and colleagues within the company who provided continuous encouragement and support for me during this study.

This work was part of two Joint Industrial projects funded by BASF, British Petroleum Plc., Clariant Oil Services, Gaz de France, OMV Aktiengesellschaft, TOTAL, the UK Department of Trade and Industry, PETRONAS, National Iranian Gas Company, Norsk Hydro, Chevron and Statoil whose supports are gratefully acknowledged.

Finally, I will always remember the sacrifice, love, patience and encouragement from all my family members, without which it will be impossible for me to complete this degree.

TABLE OF CONTENTS

LIST OF TABLES

TABLES

LIST OF FIGURES

FIGURES

NOMANCLATURE

NOMANCLATURE

AAs	Anti-Agglomerates
AFP	Anti freeze Protein
Ar	Argon
C_1	Methane
C_2	Ethane
C_3	Propane
CfAFP	choristoneura fumiferama anti freeze protein
CO_2	Carbon Dioxide
DW	Deionised water
HDW	Hydrate deionised water
HDWV	Vacuumed hydrate deionised water
HWHYD	The Heriot-Watt HYDrate model
i-C_4	iso-butane
K	degree Kelvin
KHIs	Kinetic Hydrate Inhibitors
Kr	Krypton
LDHIs	Low Dosage Hydrate Inhibitors
MPa	Mega pascal
N_2	Nitrogen
n-C_4	normal butane
nm	nanometer
O_2	Oxygen
Psia	pound per square inch absolute
SDW	Saturated deionised water
SDWV	Vacuumed saturated deionised water
SEM	Scanning Electron Microscope
THF	Tetrahydrofuran
THI's	threshold hydrate inhibitors
wfAFP	winter flounder anti freeze protein

LIST OF PUBLICATIONS AND REPORTS BY CANDIDATE

B. Tohidi, A. Chapoy, F. Ahmadloo, I. Valko, **Z. Zain**, " Developing Hydrate Monitoring and Early Warning Systems", *OTC 19247, presented at Offshore Technology Conference*, Houston, Texas, U.S.A., 5 – 8 May (2008)

Z.M. Zain, J. Yang, B. Tohidi, "Hydrate Monitoring and Warning System for Reducing Gas Hydrate Risk", *paper no. CE057, presented at 21st Symposium of Malaysian Chemical Engineers*, University Putra Malaysia, Malaysia, 11 – 14 December (2007)

Chapoy, A., Yang, J., **Zain, Z.** and Tohidi, B., "Hydrate Monitoring and Early Warning System", *presented at Deepwater Drilling and Field Production Asia*, Kuala Lumpur, Malaysia, 5-6 December (2006).

Tohidi, Bahman., **Zain, Zahidah, Md.,** Yang, Jinhai, Burgass, Rod., "Methods for Monitoring Hydrate Inhibition, and Early Warning System for Hydrate Formation", World Intellectual Property Organization, International Publication date 26 May 2006, International Publication Number WO 2006/054076 A1.

Zain, M.Z., Yang, J. and Tohidi, B., "New Approaches in Gas Hydrate Flow Assurance Control**",** *poster presented at SPE Forum*, Portugal, 23-28 November (2005).

Zain, M.Z., Yang, J., Tohidi, B., Cripps A., and Hunt A., "Hydrate Monitoring and Warning System for Reducing Gas Hydrate Risks"**,** *presented at PRSS Technology Forum***,** Kuala Lumpur Malaysia, 24-26 July (2005).

Zain, M.Z., Yang, J., Tohidi, B., Cripps A., and Hunt A., "Hydrate Monitoring and Warning System: A New Approach for Reducing Gas Hydrate Risks**",** SPE 94340**,** *presented at EAGE/SPE International Conference and Exhibition*, Madrid, Spain, 13-16 June (2005).

Zain, M.Z., Yang, J. and Tohidi, B., "Developing Early Warning System for Reducing Gas Hydrate Risks", *poster presentation at Devex 2005 Conference***,** Aberdeen, UK, 18 – 19 May (2005).

Research Report, Flow Assurance: Hydrate Monitoring and Warning System, Institute of Petroleum Engineering, Heriot-Watt University, Edinburgh, 2005-2006.

Research Report, Flow Assurance: Micro and Macro-Scale Evaluation of Low Dosage Hydrate Inhibitors, Institute of Petroleum Engineering, Heriot-Watt University, Edinburgh, 2002-2005.

Tohidi, B., Danesh, A., Todd, A.C., Anderson, R., Burgass, R., Arjmandi, M., Masoudi, R., Ji, H., Mohammadi, A., Yang, J., Ren, S., **Zain, M.Z**., Mali, G., and Jadhawar, P., "Gas Hydrate and Flow Assurance Studies", *presented at the DTI IOR Research Dissemination Seminar*, Aberdeen, UK, 24 June (2004).

Tohidi, B., Danesh, A., Todd, A.C., Anderson, R., Burgass, R., Arjmandi, M., Masoudi, R., Ji, H., Mohammadi, A., Yang, J., Ren, S., **Zain, M.Z.**, Mali, G., and Jadhawar, P., "Gas Hydrates: Friend or Foe?**"**, *presented at the DTI IOR Research Dissemination Seminar*, Aberdeen, UK, 24 June (2004).

Tohidi, B., Danesh, A., Todd, A.C., Yang, J., Ren, S.R., Arjmandi, M., Burgass, R.W., Carnegie, E., Anderson, R., Biderkab, A.-B., and **Zain, M.Z**., **"**Flow assurance: micro- and macro-scale evaluation of low dosage hydrate inhibitors"**,** *presented at UK DTI IOR Seminar*, Aberdeen, Scotland, UK, 24 June (2003).

CHAPTER 1

INTRODUCTION

The past decade has witnessed dramatic changes in the oil and gas industry with the advent of deepwater exploration and production. A major challenge in deep water and offshore field development is to ensure unimpeded flow of hydrocarbons to the host platform or processing facilities. Managing solids such as hydrates, waxes, asphaltene and scale is key to the viability of developing a deepwater prospect.

This thesis is concerned with the challenging gas hydrates and flow assurance issues particularly in deepwater developments. The situation is not any better for Brown fields as a result of increasing water cut. The other factor which is playing an increasing role is product quality and environmental concerns, demanding reduction in chemical usage.

The current industry practice for hydrate prevention is injecting hydrate inhibitors at the upstream end of pipelines based on the calculated/measured hydrate phase boundary, water cut, worst pressure and temperature conditions, and the amount of inhibitor lost to non-aqueous phases. In general, systematic ways of controlling and monitoring along the pipeline and/or downstream to examine the degree of inhibition are very limited.

Early hydrate warning and online hydrate monitoring techniques are needed to optimise inhibitor dosage, reduce the risk of gas hydrate formation/deposition and the cost of mitigating the blockage in subsea pipelines. In general monitoring changes in the pipeline pressure drop is inadequate to provide reliable indicator for hydrate formation and deposition. Therefore new techniques are necessary.

In the recent years, a family of Low Dosage Hydrate Inhibitors (LDHIs) known as kinetic hydrate inhibitors (KHIs) have been applied in the field to prevent gas hydrate problems by delaying gas hydrate nucleation and/or growth. However, the mechanism of hydrate formation and inhibition is still not well understood. It is believed micro-scale investigation could provide vital clues.

The scope of this thesis is illustrated in Figure 1.1. The primary part of this thesis is to develop a new approach for early warning system and monitoring against initial hydrate formation. It is known that the formation of hydrates changes the water structure, which is claimed to remain in the aqueous phase even after the dissociation of gas hydrates. Therefore, it should be possible to detect initial hydrate formation by detecting these changes. The techniques investigated for this thesis include the use of dielectric constant and onset of ice formation. The purpose is to provide the operator adequate time to initiate remedial steps prior to massive hydrate formation/build up which could result in pipeline blockage.

The second aim of this thesis is to investigate the inhibition mechanism of Low Dosage Hydrate Inhibitors (LDHIs) by visual observation of gas hydrate formation, growth, and morphology. These techniques are based on visual observation in high pressure glass micromodel and glass capillary tubes.

1.1. GAS HYDRATES

Gas hydrates or clathrate hydrates are the second commonly found water crystal, after ice, which formed when small (<0.9 nm) nonpolar molecules contact water at ambient temperatures (typically <300 K) and moderate pressure (typically > 0.6 MPa). A large fraction of the earth's natural gas is stored in the form of clathrate hydrates. Much of the natural gas-containing hydrates are in the deep bottom and while production of gas from such deep-lying hydrates is too expensive now, it could be in the future as a source of energy supplies (Sloan, 2000).

On a molecular scale, single small guest molecules are encaged by hydrogen-bonded water cavities. Guest repulsions prop open different sizes of water cages, which combine to form three well-defined unit crystals structure which are structure-I (sI), structure-II (sII) and structure-H (sH). Figure 1.2 presents the shape of different gas hydrate cavities in the three structures. Not all cavities structure needs to be occupied by a guest molecule in order for the structure to be stable, hence gas hydrates are nonstoichiometric. Some properties of the three hydrate crystals structures are given in Table 1.1.

Table 1.1. Hydrate unit cell characteristics of structure-I, II, and H (Sloan, 2000; Tohidi, 1995)

Structure	I		II		H		
	small	large	small	large	small	medium	large
Crystal system	Cubic		Cubic		Hexagonal		
Lattice parameter/ Å	12		17.3		a = 12.26, c = 10.17		
H_2O/unit cell	46		136		34		
Total no. of cavities/ unit cell	8		24		6		
Cavity type	5^{12}	$5^{12}6^2$	5^{12}	$5^{12}6^4$	5^{12}	$4^35^66^3$	$5^{12}6^8$
Radius of cavity/Å	3.95	4.3	3.91	4.73	3.91	4.06	5.71
Cavities /unit cell	2	6	16	8	3	2	1
Coordination no.	20	24	20	28	20	20	36

Hydrate sI consists of 46 water molecules with a 12 Å body centred cubic unit cell of small and large cavities. The small cavities are dodecahedrons, i.e. polyhedra with 12 pentagonal faces (5^{12}). The large cavities have 12 pentagonal faces and 2 hexagonal faces ($5^{12}6^2$). Combination of two 5^{12} and six $5^{12}6^2$ form hydrate sI which can accommodate guests with diameters up to 6 Å in size.

Hydrate sII also consists of two different polyhedral cavities with 136 water molecules. The small cavities, similar to sI, which is dodecahedrons (5^{12}) whereas the large cavities have 12 pentagonal faces and four hexagonal faces ($5^{12}6^4$). Combination of sixteen 5^{12} and eight $5^{12}6^4$ cavities form a diamond cubic lattice with a cell parameter of 17.3 Å. Hydrate sII accommodates molecules up to approximately 7 Å in diameter. The information on properties of hydrate sI and sII was detailed by Jeffrey (Jeffrey, 1984).

Hydrate sH forms a hexagonal crystal lattice with the lattice parameters, a = 12.26 Å and c = 10.17 Å consists of 34 water molecules. It was discovered recently and reported by Ripmeester et al. (Ripmeester et al., 1987). It has three different types of cavities, the dodecahedron (5^{12}) which is common to hydrate sI and SII, a medium sized cavity with 3 square faces, 6 pentagonal faces and 3 hexagonal faces ($4^35^66^3$), and a large cavity with 12 pentagonal faces and 8 hexagonal faces ($5^{12}6^8$). Combination of three 5^{12}, two $4^35^66^3$ and one $5^{12}6^8$ cavities form a hydrate sH crystal lattice. The large

$5^{12}6^8$ cavity can accommodate molecules as large as almost 10 Å in diameter (Sloan, 1998).

The 5^{12} cavity can accommodate guests such as methane and hydrogen sulphide and the $5^{12}6^2$ cavity which can fit slightly larger guests such as ethane and carbon dioxide. The $5^{12}6^4$ cavity can fit guests such as propane and n-butane. sI hydrates are typically found in situ in deep oceans with biogenic gases such as methane and hydrogen sulphide. sII hydrates are found predominantly in natural gas pipelines due to the presence of molecules such as propane and butane.

1.2. GAS HYDRATE CONTROL AND PREVENTION

The conventional ways to prevent and reduce hydrate risks in transfer line and process facilities is to remove one of the elements favouring hydrate formation (Fu et al., 2001). For example, thermal insulation and external heating (Urdahl et al., 2004) techniques are used to remove the low temperature element. Water can be removed by dehydration of the natural gas using glycol system and lowering the operating pressure can reduce the tendency for hydrates to form in the production system. However, these conventional techniques may not be feasible for some fields especially in offshore and deepwater environment due to space limitation and high insulation or heating cost. The deepwater insulation costs are reported typically US$1 million per kilometre of flowline (Sloan, 2005).

Another option is to use the “Thermodynamic Inhibitors”. Thermodynamic inhibitors such as methanol and ethylene glycol, or salts are injected to compete for water molecules with the hydrate structure. These are water soluble chemicals that reduce the water activity, hence shifting the hydrate phase boundary to higher pressure and/or lower temperature conditions.

The current methods of determining the dosage required include determining the hydrate phase boundary for the fluid under consideration, experimentally and/or through modelling. The amount of thermodynamic inhibitor required to keep the fluid outside the hydrate stability zone, even when under the worst operating conditions, is then calculated and/or experimentally determined. Generally the worst conditions are those of the highest pressure and lowest temperature. Finally, an estimated amount of

inhibitor is added, including an allowance for what is lost from the aqueous phase to the vapour and liquid hydrocarbon phases, whilst also taking into account a safety margin. However, due to high dosage requirement, it can result in significant increase in capital and operational expenditure, in particular at high water cut conditions, as well as logistical and environmental problems.

In the last 10 years, the industry has focused on the application of a new family of inhibitors which are applied at low concentrations and prevent gas hydrate problems. These inhibitors are classified as Low Dosage Hydrate Inhibitors (LDHIs). The LDHIs is classified into the Kinetic Hydrate Inhibitors (KHIs) and Anti-Agglomerants (AAs) (Frostman et al., 2001; Oskarsson et al., 2005). The KHIs work by delaying nucleation and/or growth of crystals. However, they generally fail to inhibit the agglomeration of crystals once nucleation/growth occurs. AAs allow gas hydrates to form but prevent the agglomeration of hydrate crystals and thus minimize the risk of pipeline plugging.

The procedure for applying KHIs is somehow different from that of THIs. It is based on the hydrate stability zone calculation (i.e. the conditions in which hydrate formation is thermodynamically favoured for a given fluid composition) and the worst operating conditions expected. A degree of subcooling, defined as the hydrate dissociation temperature minus the lowest expected operating temperature at the system pressure ($T_{Equilibrium}$-$T_{Operating}$), is considered. Then, fluid residence time in the pipeline is estimated. Following this, the inhibitor is experimentally tested at the same (or a slightly greater) degree of subcooling. The requirement of the inhibitor is that it prevents hydrate formation under these conditions for a period longer than the estimated fluid residence time in the system. Generally 0.5 – 2 mass % may be sufficient for delaying the onset of hydrate formation (Tohidi et al., 2003). While KHIs have limitation on the amount of subcooling they can sustain, AAs are generally less dependent on the subcooling. However, AAs do have a fundamental limitation in that they require a liquid hydrocarbon phase to be present in order to transport hydrates that may form.

In the past, kinetic hydrate inhibitors (KHIs) and anti-agglomerants (AAs) were complementary in the pipeline flow assurance toolbox for hydrate prevention while thermodynamic inhibitors were extensively used (Sloan, 2000). However, the thermodynamic inhibitors are replaced by kinetic hydrate inhibitors for several field

applications in the recent years after many proven field trials. There are on going research and development to improve the existing formulations and/or develop new formulations. Zeng et al (Zeng et al, 2005) suggested refinement of LDHIs classification. This refinement was to classify LDHIs into three groups according to their inhibition mechanism namely, nucleation inhibitors (delay hydrate nucleation), crystal growth inhibitors (inhibit hydrate crystal growth) and memory effect inhibitors (alter or eliminate the memory effect). In this classification, the memory effect inhibitors was suggested based on the finding that Anti freeze Protein (AFP) of winter flounder (wfAFP) and budworm insect, choristoneura fumiferama (CfAFP) were effective at suppressing the memory effect in the reformation of Tetrahydrofuran (THF) hydrates. Although it was not clearly mentioned by Zeng et al the usage of the memory effect inhibitors, it is assumed that it would be suitable to avoid hydrate reformation from water with hydrate memory.

Practically, in most cases too much inhibitor is used. Excessive use of an inhibitor has environmental and economical consequences. However from an industrial standpoint this is viewed as acceptable, as the problems caused by the formation of hydrates have much greater economical consequences.

However, despite all these measures, hydrates do still form and cause serious operational and safety concerns. Their formation often takes place due to problems with injection pumps, a sudden increase in the water cut (water content of the fluid in the system), reducing the concentration of inhibitor, a change in fluid flow rate, emergency shut-downs, problems associated with start-ups, lack of reservoir fluid samples, lack of information on the composition of produced water, changes in the system temperature and pressure, uncertainty concerning the performance of the utilised inhibitor(s), and deleterious synergy between various inhibitors.

It is also acknowledged that the elucidation of a mechanism for hydrate inhibition is still very much in its infancy and that novel approaches will be required to give additional insights (Zeng et al, 2005; Frostman et al, 2001). Therefore, a part of this thesis provides some additional insight into the mechanism of LDHIs inhibition and its effect on morphology using visualization techniques.

The first step prior to hydrate control and prevention is to have an early warning and monitoring system in place which is briefly described next.

1.3. EARLY WARNING AND MONITORING SYSTEM

Early warning sign of hydrate formation in the pipeline and also in onshore processes and platforms is very important to ensure appropriate measure is taken to prevent the blockage and rupture of pipeline and vessels. Sloan (Sloan, 2000) pointed out that not a single indicator gives the best warning of hydrate formation. In general, there are several methods for warning of hydrate formation which are applied and considered for testing. These are pigging return, changes in fluid rates and compositions at the separator, pressure drop increases, acoustic detection, thermocamera, gamma ray densitometer, pressure pulse technology and fibre optic technique. However, each of this method has its own limitation and it is described in Chapter 2.

In this thesis a novel approach proposed for early warning to avoid unplanned hydrate formation is related the phenomenon known as “hydrate water memory”. In a system that has previously contained hydrates or in which the nucleation of hydrates has already occurred, the degree or amount of subcooling (at a given pressure), which is required to induce hydrate formation, can be substantially reduced. This can lead to hydrate formation occurring unexpectedly when a system is within a range of temperature and pressure conditions where hydrate formation would not normally be expected on the basis of the composition of the mixture present. This reduction in the amount of “sub-cooling” required to induce hydrate formation is believed to be attributed to residual structure of the water, or residual hydrate nuclei that can persist for prolonged periods. In this thesis, the techniques used to identify the presence of hydrate water memory as an indicator for early warning system was investigated. Further evidence on the main factor influence the hydrate memory was also reported.

1.4. THESIS OUTLINE

This thesis reports a number of novel findings and techniques as indicated in the thesis abstract, appropriate chapters and summarized in the final chapter. The structure of the thesis is shown in Figure 1.3. There are eight chapters with the introduction in Chapter1. Then the thesis is divided into the development of novel methods for early warning (Chapter 2,3,4) and the prevention by LDHI which focused on understanding

the mechanism of growth and inhibition and novel methods for evaluation of LDHI (Chapter 5,6,7). Finally, Chapter 8 contains conclusions and recommendations.

In Chapter 2, current techniques available for early warning system are reviewed to address its applications and limitations. A literature review on hydrate water memory which is the main focus of phenomena for novel technique for early warning indicator is covered.

In Chapter 3, a new approach for hydrate early warning system using dielectric properties was investigated. Dielectric theory and its application on gas hydrate and oil & gas industry was reviewed. Important factors were investigated such as the effect of water structure, sustainability of water memory, effect of heating, effect of sample preparation path on water memory, effect of sample preparation path on water structure and the effect of impurities.

In Chapter 4, a new approach based on investigating water memory by onset of ice formation by freezing technique under controlled laboratory environment was described. This chapter provides the background theory of ice nucleation and the technique adopted in this study to describe the stochastic nature of ice nucleation, nucleation probability distribution. The experimental measurement and analysis of results are described in this chapter.

In Chapter 5, details a literature review on the mechanism of gas hydrate formation, crystal growth and hydrate crystal morphology, and inhibition by Low Dosage Hydrate Inhibitor (LDHI). Available experimental techniques to study gas hydrate formation and evaluating performance of LDHI was reviewed. A novel visual technique applied for this study was presented.

In Chapter 6, the novel visual observation to understand the mechanism of crystals growth, inhibition, mophology and methods for evaluation of Kinetic Inhibitors (KHIs) by static glass micromodel was demonstrated. The investigation covers natural gas-water and methane-water system with and without various kinetic hydrate inhibitors. Hydrate crystals morphology and the effect of inhibitor on hydrate structure were also investigated.

In Chapter 7, investigating inhibition mechanism of LDHIs by dynamic visual observation using multi-channel flow conduit and capillary glass tube blockage techniques were demonstrated for several cases. These cases covers evaluation of both kinetic hydrate inhibitor for gas system and anti-agglomerant for natural gas condensate system. The effect of selected synergist, carrier fluid and corrosion inhibitor on kinetic hydrate inhibitor for gas-water system were investigated. Evaluation of anti-agglomerant for gas condensate with and without salt was also presented. A brief investigation of hydrate particle size and distribution for natural gas- condensate-water system was reported.

Chapter 8, presents a summary of the main contributions and discussions of this thesis followed by a suggested future work programme.

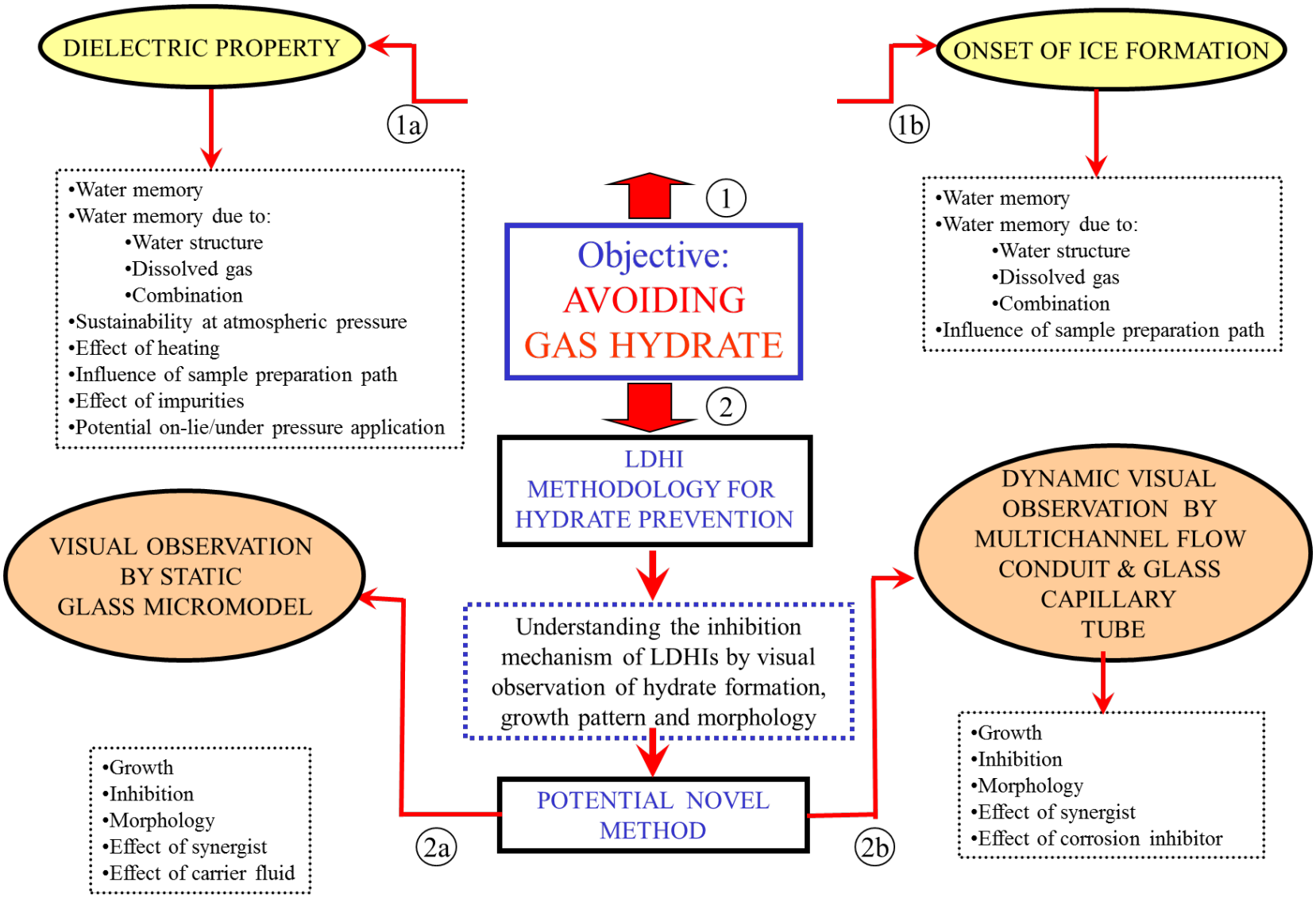

Figure 1.1. Scope of thesis.

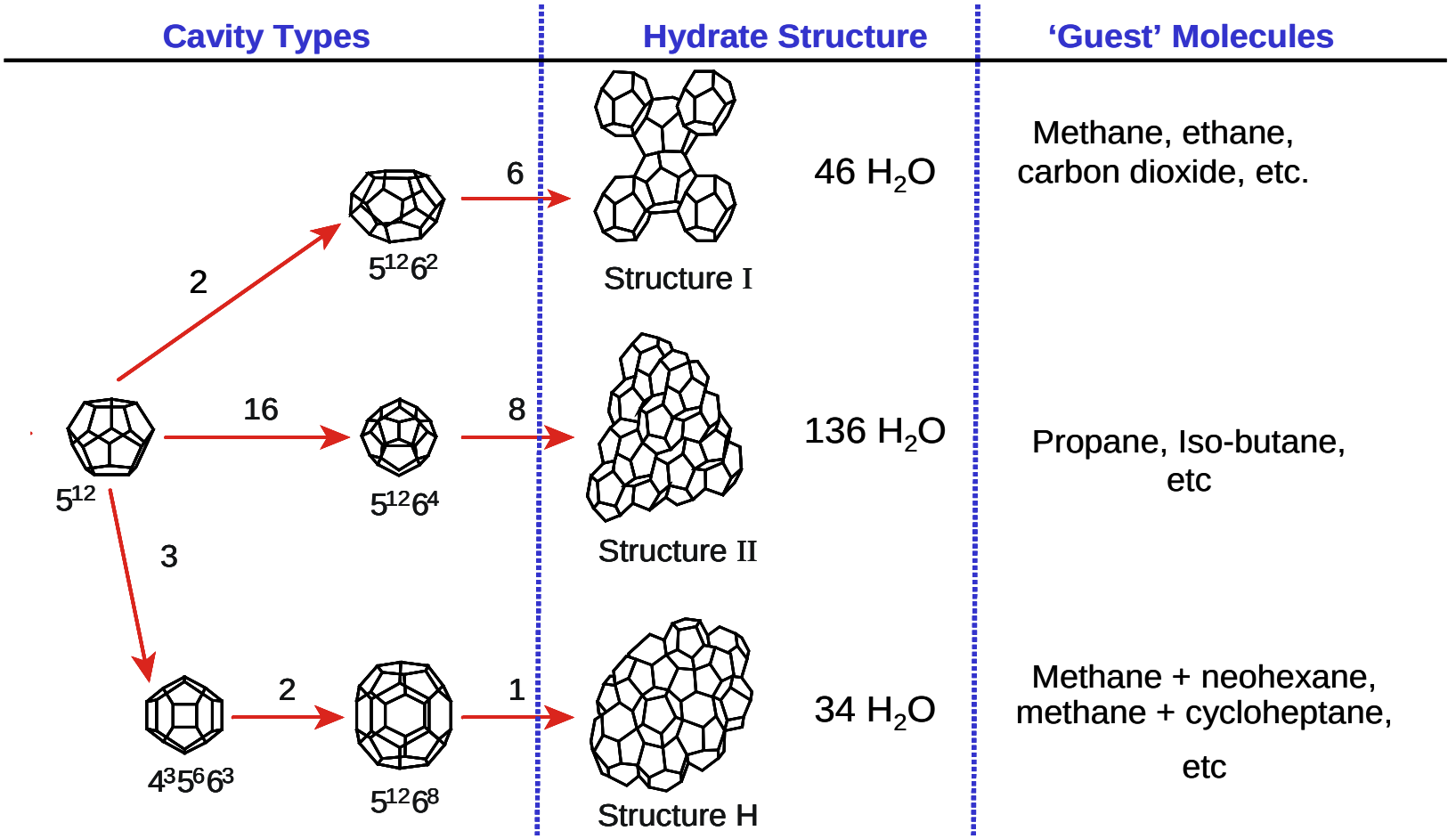

Figure 1.2. Three common hydrate unit crystal structures. Nomenclature: $5^{12}6^4$ indicates a water cage composed of 12 pentagonal and 4 hexagonal faces; along the lines are indicated the numbers of cage types. Example: the structure I unit crystals is composed of 2 5^{12} cages, 6 $5^{12}6^2$ cages, and 46 water molecules (Sloan, 2000).

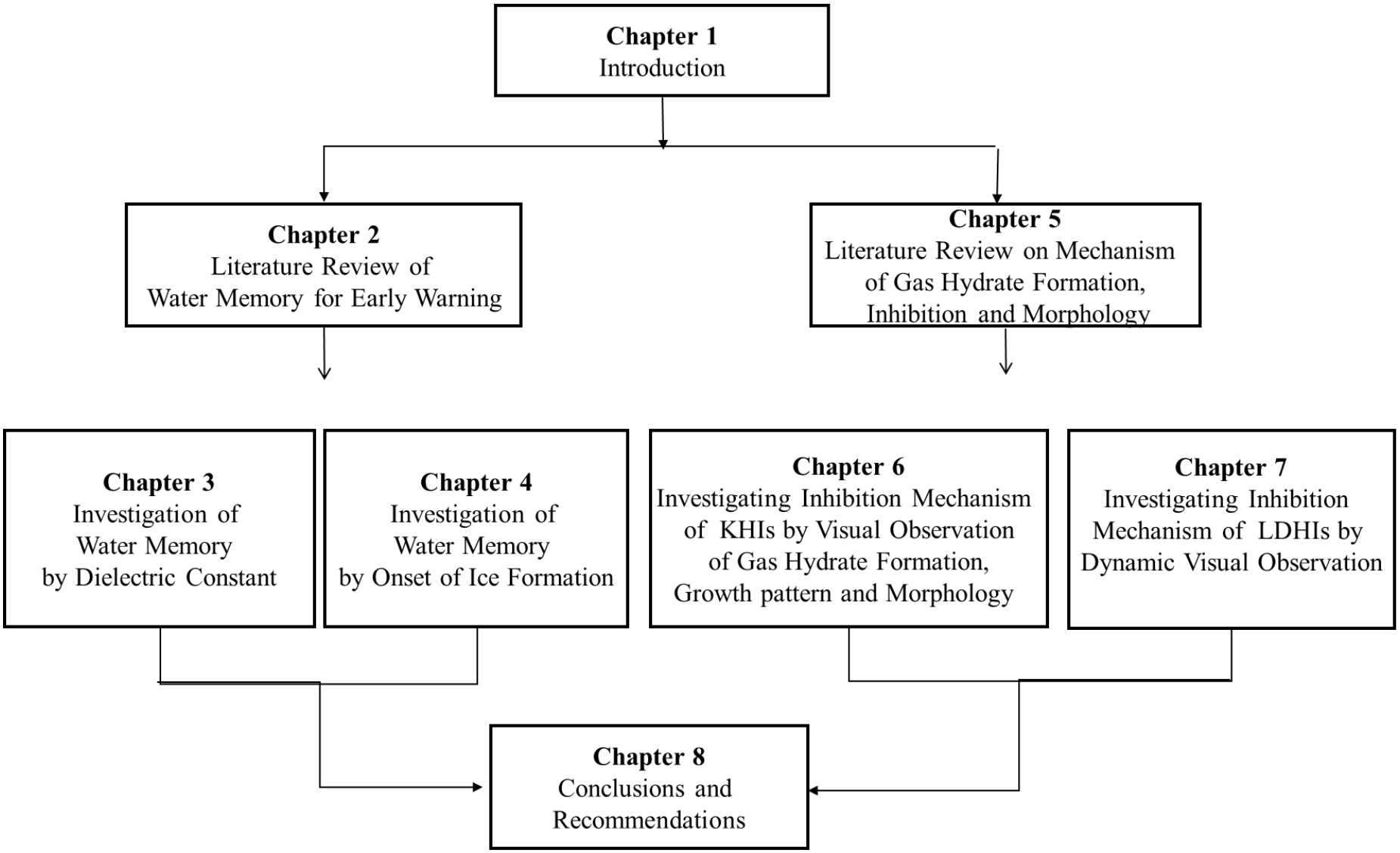

Figure 1.3. Structure of the thesis

CHAPTER 2

LITERATURE REVIEW ON HYRATE WATER MEMORY[1] FOR EARLY WARNING

In this chapter, current techniques available for early warning system are reviewed to address the applications and limitations. Subsequently, a detailed literature review on water memory due to hydrate formation and dissociation and water memory in general are covered.

2.1. REVIEW TECHNIQUES FOR EARLY WARNING SYSTEM.

Several methods for warning of hydrate formation which are applied and considered for testing. These are pigging return, changes in fluid rates at the separator, pressure drop increases, acoustic detection, thermocamera and gamma ray densitometer (Sloan, 2002). Recent development on techniques for monitoring hydrate are pressure pulse technology (Gudmundsson, 2005) and fibre optic (Brower et al., 2005). However, each of this method has its own limitation which it is described next.

Pigging Returns. The flexible plastic balls or cylinders called pigs are launched through the pipeline by pressure driven to sweep debris from the pipeline into a pig trap. The pig trap provides valuable information about solid deposition in the pipeline such as hydrates, wax, scale and sand. In the case of hydrate, frequently hydrate particles are found in pig traps before hydrate blockages occur in the pipelines. Pigging returns is carefully examined for evidence of hydrate particles. Hydrate masses are stable even at atmospheric pressure in a pig receiver discharge. The endothermic process of hydrate dissociation causes released water to form ice, which inhibits rapid dissociation. Although, onshore pigging is commonly done to keep lines clear, it may be very expensive to provide offshore pigging either through a mobile pigging vessel over the well or from the wellhead without round trip pigging capability. Therefore, high costs limit the frequent examination of offshore pigging returns (Sloan, 2000).

[1] Water memory is referred to the memory of hydrate formation in the aqueous phase which is believed to remain even after hydrate dissociation.

Changes in Fluid Rates at Separators. When the water production is small, it may be possible to monitor the rate of water production. If the water arrival decreases significantly at the separator, hydrate may be forming in the line. In this case, separator water rate provides an early indication of hydrate formation in a gas line that has no oil/condensate and little water production. Corrigan et al (Corrigan et. al., 1996) reported the loss of water production from the pipeline as a sensitive indication of hydrate formation which occurred many hours before observing an increase in the differential pressure for BP-operated assets in the North Sea. This was monitored during blank trials for testing KHIs. In this case study, the first indication of hydrate formation was observed 30 hours after ceasing methanol injection. This was based on constant water level in the slug-catcher while the water-outlet in the slug-catcher was closed (meaning that there is no water production to the slug-catcher). It worth mentioning that the gas flow rates during this period remained steady and the pipeline pressure drop did not change. This demonstrates that pressure drop is probably not a good indicator for detecting initial hydrate formation. In fact, the first significant increase in the differential pressure was observed 46 hours after the start of the test followed by large fluctuations in the gas flow and further increase in the differential pressure after 74 hours. However, when water production is substantially higher or intermittent, this technique (i.e., monitoring water production) will not be applicable as an early warning.

Pressure Drop Increases. A line-pressure drop build-up is a less direct flow indicator. Hydrate formation at the wall in the gas pipeline will cause the pressure drop (Δp) increases and the flow rate decrease due to decrease in the pipe diameter. Pressure drop increases are usually more noticeable than flow rate changes. The change in Δp is more sensitive than the change in flow because the Δp in pipes is proportional to the square of turbulent flow rates. However, in the presence of hydrate, a large restriction may be necessary over a long length before a substantial pressure drop occurs as illustrated in Figure 2.1 (a). While a gradual pressure increase in hydrate formation occurs for gas systems, a gradual pressure increase is not typical for a gas/oil/condensate systems. In gas/oil/condensate systems, hydrates usually cause a series of sharp spikes (Figure 2.1 (b)) in pressure as hydrate masses form, slough, agglomerate and break before final blockage without advance warning. In addition, the Δp trace usually contains

substantial noise, making it difficult to observe small changes or trends in Δp as an early warning.

Acoustic Sensing Along Subsea Pipeline. This technique has been widely used for sand monitoring by detecting sand impingement on pipe. Application of acoustic sensor for hydrate particles is limited to onshore pipeline. However, this unit has yet to be field tested in a subsea application (Sloan, 2000).

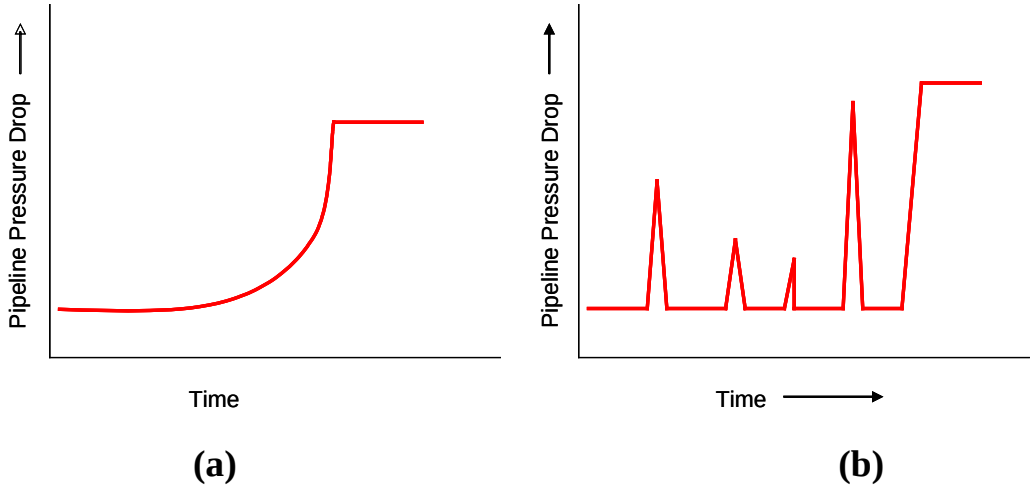

Figure 2.1 Pipeline pressure drops because of hydrates (a) hydrate build-up on walls and (b) hydrate-particles agglomeration (Sloan, 2000).

Thermocamera. It is a hand-held device that measures the infrared spectral transmission as an indicator of system temperature (Sloan, 2000). It is used only onshore or topside offshore with air between the detector and the suspected hydrate plug because water absorbs infrared transmission. This device enables determination of temperature variations in the system, particularly at points where hydrates might form but where a thermocouple is not provided such as downstream of a valve. It was mentioned that this thermocamera is very sensitive to pipe coating, variation in wall thickness and pipe roughness (Sloan 2000).

Gamma Ray Densitometers with Temperature Sensing. A gamma ray densitometer uses an emitter and sensor on opposite external of pipe walls. The transmission of the gamma ray to the sensor is a function of the density of the pipe contents. This technique is based on combined gamma ray densitometry with the temperature downstream of densitometry to indicate changes in conditions that could be hydrate present. This

combination is needed since the gamma ray alone will not be able to discriminate density of water and hydrate. Hydrates are indicated by a low temperature (due to the Joule-Thomson effect) and an increase in density as cited by Sloan (Sloan 2000), whereas the water temperature is similar to that of gas. A high-density, low temperature mass in the pipeline is likely to be hydrates, whereas a high density slug without a temperature drop is probably water. This technique is useful tool for onshore but it could not be applied to sub sea due to limitation on temperature sensing requirement (Sloan, 2000).

Some recent developments on the techniques for monitoring hydrate deposits in the pipeline are reported. Gudmundsson et al (Gudmundsson, 2005) reported techniques developed for monitoring deposits in pipelines using pressure pulse technology. It is based on high speed measurements of pressure transient (i.e. the physics of pressure propagation in fluids, single phase and multiphase) that arise when a valve is activated and closed for a few seconds. It was claimed that this technology is field proven for measuring gas-liquid flow rate in production wells and to locate and quantify deposits in a pipeline between platforms. However, there is no further report on what types of deposits would be applicable using this technology.

Brower et al (Brower et al, 2005) reported the development of non-intrusive fibre-optic sensor for managing flow assurance risks. This sensor can measure temperature, pressure, heat flux, strain and acoustic measurement. The measurement can be used to detect gas hydrate blockage, to estimate paraffin deposition, locate pigs and to detect passage of liquid slugs. Detection of hydrate blockage is via pressure measurement from increasing in pressure drop. Pressure measurement from multiphase pipelines and flowlines are potentially highly transient due to hydrodynamic slugging, terrain slugging and inherent oscillations in other flow regimes even without hydrate formation. It is recognised that, the trend of increasing pressure drop particularly in the early stages of hydrate formation may not be readily identifiable. Brower et al. suggested that other methods to enhance early detection of hydrate can be used in conjunction with fibre optic based pressure measurement. The authors suggest that these methods could be real time online simulations, statistical analysis, pattern recognition techniques and other monitoring techniques.

As described in the abstract and introduction chapter, the primary part of this thesis is to develop a new approach for early warning system and monitoring against initial hydrate formation. The presence of water memory due to hydrate formation and dissociation has been studied as an indicator for early warning and monitoring. The following sections provide some review of literature related to the phenomena on water memory due to hydrate formation and dissociation and also water structure in general.

2.2 REVIEW OF WATER MEMORY

The idea of memory effects in water has been a question of debate for many years. This phenomenon on the water memory has gained researchers' interest and its mechanism has been considered and discussed from various aspects. The concept of memory effect has emerged from empirical observations that the induction time[2], the duration for which a hydrate forming system remain in the metastable hydrate free state, for hydrate nucleation strongly depends on the thermal history of the system (Vysniauskas et al., 1982; Hwang et al., 1990; Parent et al., 1996; Sloan et al., 1998; Ohmura et al. 2003; Lee et al., 2005). A clathrate hydrate forms more easily from water which has been obtained by melting the hydrate compared to water with no previous hydrate memory.

Vysniauskas and Parent (Vysniauskas et al., 1982; Parent et al., 1996) reported the experimental data on induction time for nucleation behaviour of methane gas hydrates. They found that there is significant reduction of induction time as a result of prior hydrate formation in the system and proposed that the residual structure was the cause of reduce induction time. This leads to industry implication that once a hydrate plug has been formed and dissociated, subsequent hydrate formation will occur more readily until the water has been removed from the pipeline.

The sign of residual water structure for hydrate forming system after dissociation was also studied using physical properties measurement such as refractive index, viscosity and interfacial tension (Sloan et al., 1998; Bylov et al., 1997; Kato et al., 1998; Ohmura et al., 2000). However, the studies reveal supporting the hypothesis on residual water (Sloan et al., 1998; Kato et al., 1998) and also demonstrate the negative results (Bylov et al., 1997; Ohmura et al., 2000).

[2] Induction time is defined as the elapsed time from the start of the experiment to the onset of hydrate formation. The experiments are usually conducted at isothermal and/or isobaric conditions to simulate the field operating condition

There are two hypotheses that have been proposed to explain this memory effect. First, which is the most commonly hypothesised, is that the memory effect contributed by the residual structure remains in solution after hydrate dissociation as schematically illustrated in Figure 2.2. The residual structure is hypothesised to consist of remnant water structure or partial hydrate cage-like structures of water molecules surviving after hydrate dissociation. Makagon presented the data to support the concept that on dissociation hydrates do not totally decompose but leave a partial structure which enables hydrates to form more easily with a second decrease in temperature. Then a molecular dynamic studies by Chen confirmed Makagon suggestions that both the pentamer ring and the residual structure are stable up to 315 K (Sloan, 1998).

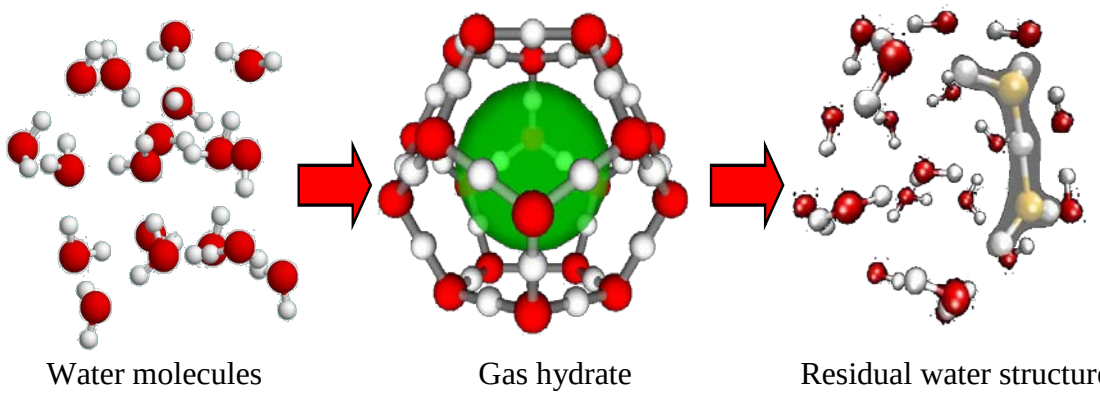

Figure 2.2 Schematic illustration of residual water structure remain after hydrate dissociation

The second hypothesis is that a dissolved gas remains in the solution after hydrate dissociation which causes the water memory. Molecular dynamic simulation studies by Rodger (Rodger, 2000) on melting of methane hydrate provide a clue to the second hypothesis. This study concluded that the memory effect relates more to the persistence of high concentration and retarded diffusion of methane in melt than it does to the persistence of metastable hydrate precursors. However, there is some limited literature published on this hypothesis. The cause of the memory effect has not been clarified yet at a molecular level. The nature and the mechanism of the memory effect in relation to the hydrate nucleation require more investigation. In the recent years some studies were published to investigate further on the nature of memory effect (Takeya et al., 2000; Ohmura et al., 2003; Buchanan et al., 2005).

A study by Takeya et al. (Takeya et al., 2000) was the first that investigated the stochastic nature of hydrate nucleation to characterise the memory effect. Takeya et al. measured the nucleation rate of CO_2 gas hydrates at 4.7 MPa and 275K for different types of water samples. These samples were untreated water, melted ice, degassed ice and degassed melted ice. They found that the nucleation rate is significantly increased when formed from melted ice than from a fresh water sample. However, no memory effect was observed if the melted ice was heated to 298K for 1 hour which is 15K above dissociation temperature of CO_2 gas hydrates.

Following the study by Takeya, Ohmura et al. (Ohmura et al., 2003) investigated the statistical nature of memory effect for Clathrate-Hydrate Nucleation in a hydrochlorofluorocarbon (CH_3CCl_2F)/water system. The primary objective was to investigate how hydrate nucleation in the system depends on its thermal history[3] through which the preceding hydrate dissociation was carried out. The study was performed for 30 to 50 samples with prior hydrate formation and dissociation under atmospheric pressure. The hydrate was formed by cooling the sample to 277.2 K which is 4 K below the hydrate stability temperature. It was then heated to 282 or 283 K (1 or 2 K above the three-phase water/CH_3CCl_2F/hydrate equilibrium temperature) for 40 or 720 minutes to dissociate the hydrate and then reform the hydrate. The finding of this investigation was that the hydrate nucleation in a system with a memory is an intrinsically stochastic event and that the rate of nucleation strongly depends on the thermal history of the system.

Phenomena on the hydrate water memory effect based on water structure were also investigated by Buchanan et al. (Buchanan et al., 2005) for methane – water system. Neutron diffraction with H/D isotope substitution was applied to examine the water structure before hydrate formation and after hydrate decomposition. The neutron diffraction scans were recorded continuously over a period of approximately 8 hours to track the decomposition of the methane hydrate. The result based on neutron-scattering

[3] Thermal history is defined as time evolution of system temperature. It is characterised by the temperature at which the hydrate covering the drops dissociated and also by the length of time for which the samples were held at that temperature before they were cooled again to a prescribed level of induce hydrate nucleation.

curves and the empirical potential structure refinement (EPSR) analysis of data reveals that there is no significant difference in the water structure between these samples.

Experimental work has shown that preheating a sample will remove any hydrate water memory, as discussed by Sloan et al. (Sloan et al., 1998) where they reported macroscopic evidence of residual structures using a sapphire multi-tube apparatus with a steel ball for a methane gas system with deionised water. They reported that the apparent viscosity of the solution returned to baseline after heating to 28 ºC and that residual liquid water was destroyed at this temperature. Makagon (Makagon, 1997) reports that in the heating of water above 30 ºC, the structured state of water almost completely disappears, and that the temperature at which the effect of initial hydrate formation is removed ranges from 30 to 35 ^{o}C. He stated that heating of water above these temperatures does not produce a noticeable difference.

In general, it is cited in publications related to understanding the properties of water that water "memory" has been the most controversial of all claims made for water (Matthews, 2006). The idea that water can retain some kind of imprint of compounds dissolved in it has long been cited as a possible mechanism for homeopathy which claims to treat ailments using solutions of certain compound. However, some homeopathic remedies are so dilute that they no longer contain a single molecule of the original compound which prompted many scientists to dismiss homeopathic effects as imaginary. Roy et al. (Roy et al., 2005) argues that the water has proved itself capable of effect that go beyond simple chemistry, and these may imbue water with a memory. One of the ways this may occur is through an effect known as epitaxy which is using the atomic structure of one compound as a template to induce the same structure in others.

Water is a liquid with extraordinary properties. It has a very high cohesion and an exceptionally strong dielectric cohesion, yet it is a fluid at ambient temperature and pressure. It also has an open structure that is full of voids, especially at low temperatures. Some of these properties are found in other fluids, but the combination of all these anomalies makes liquid water unique among all other fluids (Cabane et al. 2005). The most distinctive feature of bonding in liquid water is not only the well known hydrogen bonds, but the necessary presence of a wide range of van der Waals bonds between and among the various oligomeric (cluster) structure units. It is this range of very weak bonds that could account for the remarkable ease of changing the

structure of water. This could help explain the well-known anomalies in its properties (Roy et el., 2005).

Cabane et al. (Cabane et al., 2005) recently provide a review of the physics of water. In this review it was stated that despite great progress in reproducing the interactions of water molecules, none of the numerical simulations can reproduce simultaneously the three basic features of the liquid, i.e. the liquid gas coexistence curve up to the critical point, the temperature of maximum density and the dielectric constant. It was also recognised that the properties of water is quite a tough problem to describe and to understand. To some extend, the difficulties have their origin in the limitations of experimental techniques.

Based on the above reported literatures related to hydrate water memory, one can say that the presence of hydrate water memory in some cases is depending on the techniques, selection of suitable test condition and types of fluid system. In this thesis, the main aim was to detect the presence of hydrate water memory as an indicator for early warning system. In the next two chapters of this thesis, dielectric constant (Chapter 2) and onset of ice formation (Chapter 3) techniques were proposed as potential novel early warning methods.

CHAPTER 3

INVESTIGATION OF WATER MEMORY BY DIELECTRIC CONSTANT

In this chapter, a new approach for hydrate early warning using dielectric properties is studied. Dielectric theory and its application to gas hydrate and oil & gas industry is reviewed. Detection of water memory at atmospheric pressure by dielectric constant is demonstrated. Important factors are investigated which are the effect of water structure, sustainability of water memory, effect of heating, effect of sample preparation path, compositional changes in liquid phase and effect of impurity (salt). Potential online measurement at low pressure was reported in this chapter. The study covers the detection of initial hydrate formation, sustainability of water memory and the effect of heating.

3.1. INTRODUCTION

A new approach for hydrate early warning and monitoring against initial hydrate formation using dielectric properties is discussed in this chapter. A brief on dielectric theory and the application of dielectric properties are described in Section 3.1.1 and Section 3.1.2 of this Chapter respectively.

The technique is primarily used to detect the present of water memory in the system after hydrate formation and dissociation. It has also been used to provide clues whether water clustering structure or dissolved gas is the dominant factor that influences water memory. The phenomenon of water memory is reviewed in Section 2.2 of this thesis. In this work, the hypothesis of dissolved gas as a main factor influencing the water memory instead of water structure has been investigated. Other important factors have also been investigated such as sustainability for hydrate water memory at various conditions, the effect of impurities, the effect of heating and hydrate memory under pressure.

In this thesis, detection of water memory using a new performance probe is studied and reported based on following key questions:

- Can dielectric constant be used as an indicator for early warning system to detect the presence of hydrate water memory?
- Can hydrate water memory be attributed to changes in water structure or dissolved gas or combination of both?
- How long does the hydrate water memory remain in the system?
- Does heating significantly affect water memory?
- Does samples preparation path influence the water memory?
- Is water memory affected by impurities?
- Can water memory be detected under pressure for potential on-line application using dielectric properties?

The above key questions are studied by designing appropriate experiments to test different procedure of preparing water samples. Water samples with prior hydrate formation and dissociation designated as hydrates deionised water (HDW) was tested to detect the presence of water memory using dielectric constant. This sample was compared with water samples saturated with gas without hydrate formation (SDW). The difference in the measured dielectric constants between SDW and HDW provided the indicator if hydrate memory is detectable by this technique. In this case, the hydrate memory was assumed to be a combination of both water structure and dissolved gas in water.

Further tests were performed to study if the water memory was mainly a function of water structure or dissolved gas. The water sample was prepared using similar procedure as hydrate deionised water but this sample was placed under vacuum for some duration to remove excess soluble gas. This sample was designated as vacuumed hydrate deionised water (HDWV). This sample was compared with vacuumed saturated deionised water (SDWV) and the difference in dielectric properties was measured. For all cases the sustainability of water memory was monitored.

The effect of heating on water memory was studied by heating samples to 35 ^{o}C to confirm the removal of water memory at this temperature. Another key question which was considered was the influence of sample preparation path on water memory. Both water samples prepared inside hydrate phase boundary and outside hydrate phase boundary were compared. The effect of impurities specifically salinity of water was

also studied considering the presence of salt (3 weight % of NaCl) in produced water samples. Finally a test was designed under pressure for two reasons. First, to investigate the potential on-line application and second, to study the sustainability of water memory under pressure. The memory effect was also studied for a water soluble hydrate former, i.e., Tetrahydrofuran (THF). The objective was to investigate if water memory could be detected for these systems using dielectric technique and also to eliminate the effect of dissolved gas on water memory. The detail of sample preparation and procedure are discussed in Section 3.2.3 of this chapter.

3.1.1 Dielectric Theory

The dielectric properties or permittivity is one of the factors that determine how a material interacts with an applied electromagnetic field. A dielectric material must contain localised charge that can be displaced by the application of an electric field and also store part of the applied field. This charge displacement is referred to as polarization. The polarization of a polar molecule is made up of orientation, atomic, electronic and interfacial polarization as illustrated in Figure 3.1. Based on this Figure, a dielectric material has an arrangement of electric charge carriers that can be displaced by an electric field. The charges become polarized to compensate for the electric field such that the positive and negative charges move in opposite directions. At microscopic level, several dielectric mechanisms can contribute to dielectric behaviour. Dipole orientation and ionic interact strongly at microwave frequencies as shown in Figure 3.2. Water molecules are permanent dipoles which rotate to follow an electric field. It exhibits a strong orientation polarization. Atomic and electronic mechanisms are relatively weak and usually constant over microwave region.

The orientation polarization can be determined from complex permittivity or so-called dielectric spectroscopy measurements. The complex permittivity, $\varepsilon^*(\omega)$ is a function of the angular frequency ($\omega = 2\pi f$) and is defined as:

$$\varepsilon^*(\omega) = \varepsilon'(\omega) + i\varepsilon''(\omega) \qquad (3.1)$$

where:

$\varepsilon'(\omega)$ = the real part of the relative permittivity (i.e. dielectric constant) which characterises a material ability to store a charge

$\varepsilon''(\omega)$ = the imaginary part of the relative permittivity which is a measure of the heat related loss in the material.

As the frequency of the applied field is varied from low frequency to high frequency, dielectric storage capacity given by $\varepsilon'(\omega)$ is decreases and energy loss given by $\varepsilon''(\omega)$, increases.

Dielectric constant or relative permittivity is dimensionless number. Relative is used in front of permittivity because the number is reported relative to the dielectric properties of a vacuum. Relative permittivity (ε') is defined as

$$\varepsilon' = C_p / C_v \qquad (3.2)$$

where:

C_p = Capacitance of dielectric between two parallel plates

C_v = Capacitance of the same thickness of air (vacuum) between the same two parallel plate

A more detail description of dielectric properties theory is described in Section A.1 of Appendix A.

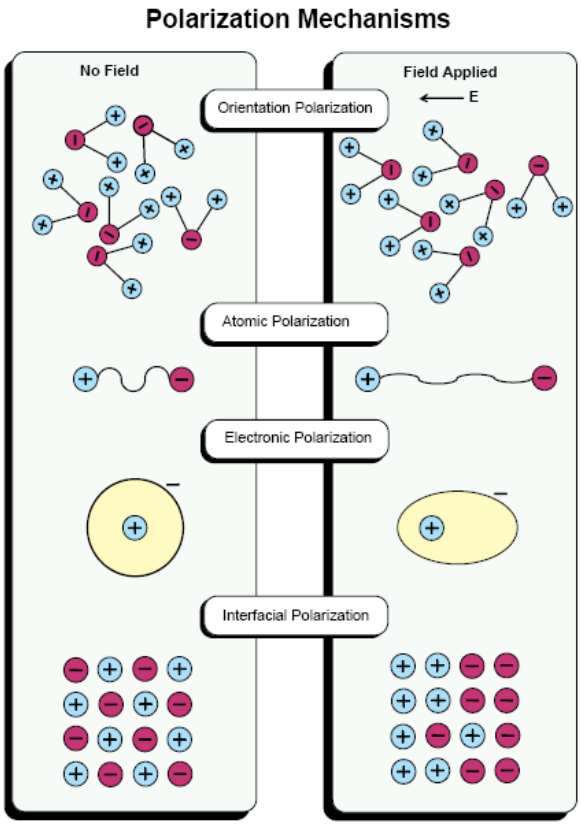

Figure 3.1 Schematic representation of the different polarization mechanism (Hass, 1996)

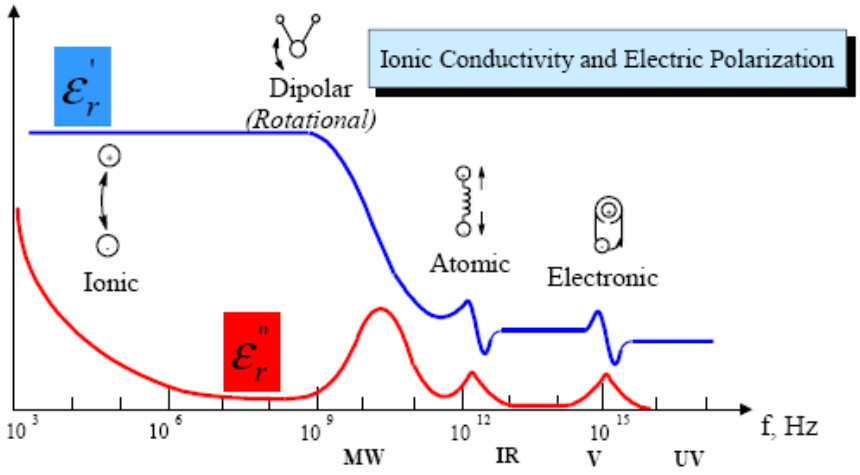

Figure 3.2 Frequency response of dielectric mechanism (Agilent Technologies, 2005)

3.1.2 Application of Dielectric Properties

Based on literature studies, reported application of dielectric properties on gas hydrate formation is very limited. Jakobsen et al. (Jakobsen, et al., 1996) studied the kinetics of trichlorofluoromethane (CCl_3F) hydrate formation in water-in-oil emulsions stabilised by a non-ionic surfactant using dielectric spectroscopy at frequency range of 10 MHz to 1 GHz. They (Jakobsen, et al., 1997) extended the frequency range to 10 GHz for studying gas hydrate formation in water-oil emulsion. During the formation of gas hydrates, decreases in the relaxation time and the static high frequency permittivities were observed. Their study showed that gas hydrate formation in water-oil emulsions can be monitored by permittivity measurements with open-ended probes.

There are several applications of dielectric properties reported in the literature which are not relevant to gas hydrate application. These are the study on different behaviour of crude oil emulsions stability (Fordedal, et al., 1996), simple sensor system for measuring dielectric properties of saline solutions (Hilland, 1997), measurement of dielectric constant for gas condensate (May, et al., 2004), study on rock – water interaction (Knight, et al., 1995), and study on rock wettability (Bona, et al., 2002) and high pressure liquid and gases (Smith, et al., 2002).

In this work, the change in the water memory was detected using dielectric constant/permittivity measurement, which could be used as an indicator for warning system. Part of this work had been reported (Zain et al., 2005). Further development of this technique using a New Performance Probe is described in the following section of this chapter.

3.2. EXPERIMENTAL METHODOLOGY

3.2.1 Experimental facilities

3.2.1.1 Kinetic rigs for sample preparation

Kinetic Rig 3. This rig (Figure 3.3) consists of a 500 ml high-pressure cell (4500 psia/300 bar), a magnetic bar for stirring, coolant jacket and temperature/pressure recording equipment controlled by computer. It has an operating temperature range of – 30 to 75 ^{o}C with temperature being controlled within +/-0.05 ^{o}C. Temperature is measured by a PRT and pressure by a Quartzdyne pressure transducer. The rig was

utilised for studies at atmospheric pressure (Zain et al., 2005) and also measurement at low pressure.

Kinetic Rig 1. The rig (Figure 3.4) consists of a 2400 ml high-pressure vessel up to 6000 psia/400 bar. The cell temperature is controlled by circulating coolant inside a jacket in the cell wall, and measured by a thermocouple. The system has an operating temperature range of –30 to 75 ^{o}C with +/-0.05 ^{o}C accuracy. The cell pressure is monitored by a Quartzdyne pressure transducer (accuracy of 0.007 MPa). A magnetic stirrer with adjustable rotation speed (i.e., rpm) is used to agitate the test fluids. The torque required to drive the stirrer at a constant speed is measured and related to the viscosity of the system. A computer is used to collect data for pressure, temperature and torque. The rig is utilized for experiment at atmospheric pressure using New Performance Probe.

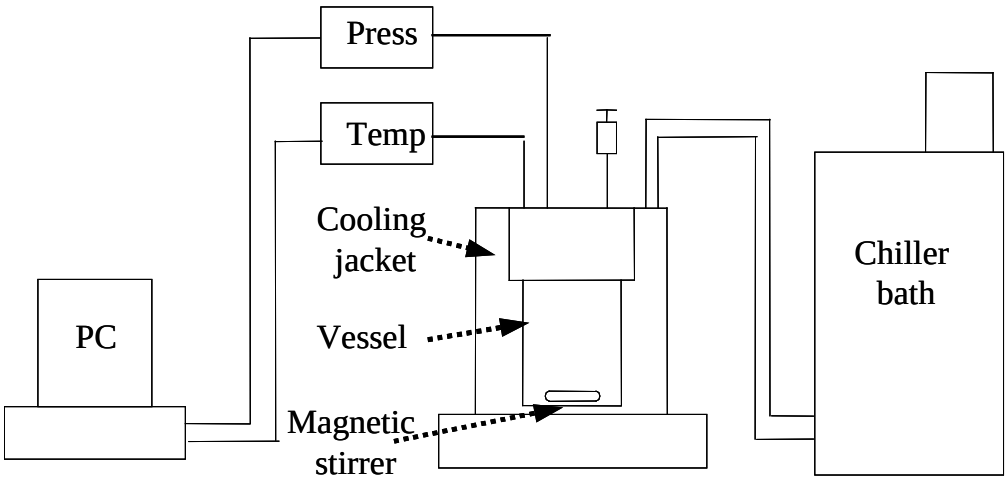

Figure 3.3 Schematic diagram of the High Pressure Kinetics Rig 3

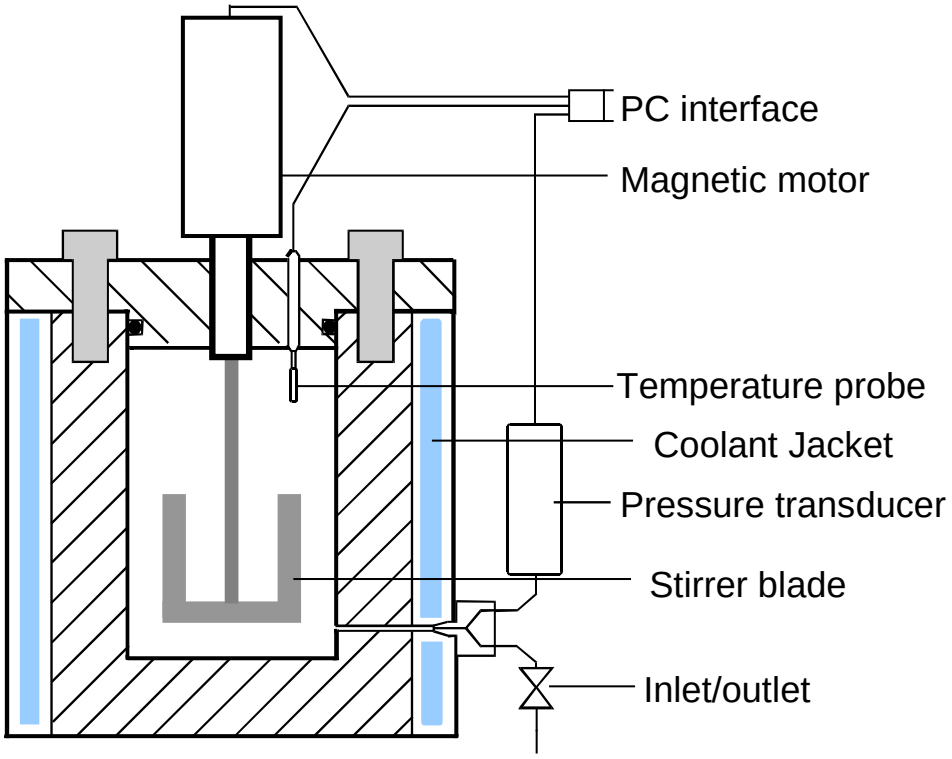

Figure 3.4 Schematic diagram of the High Pressure Kinetics Rig 1

Titanium Equilibrium Cell. Various types of water samples from hydrate formation/dissociation and gas saturation were prepared using a high-pressure titanium equilibrium cell (Figure 3.5). This rig is equipped with high-pressure cell of 300 ml volume, coolant jacket and temperature/pressure recording equipment controlled by computer. It has an operating temperature range of –30 to 75 ^{o}C with +/-0.05 ^{o}C accuracy. Temperature is measured by a PRT and pressure by a pressure transducer. This rig is not equipped with stirrer for mixing. The mixing is achieved by manually turning the vessel upside down.

Titanium Vessel Rig 1. Selected series of experiments were conducted by preparing water samples from hydrate formation/dissociation and gas saturation using a high-pressure Titanium vessel rig (Figure 3.6). This rig, similar design to Kinetic Rig 1, is equipped with a high-pressure cell of 2400 ml volume, coolant jacket and temperature/pressure recording equipment controlled by computer. It has an operating temperature range of -30 to 75 ^{o}C with +/-0.05 ^{o}C accuracy. Temperature is measured by a PRT and pressure by a pressure transducer. The rig is made of Titanium to withstand corrosive material such as salt. Summary of kinetic rigs used for this experiment is tabulated in Table 3.1.

Figure 3.5 Titanium Equilibrium Cell

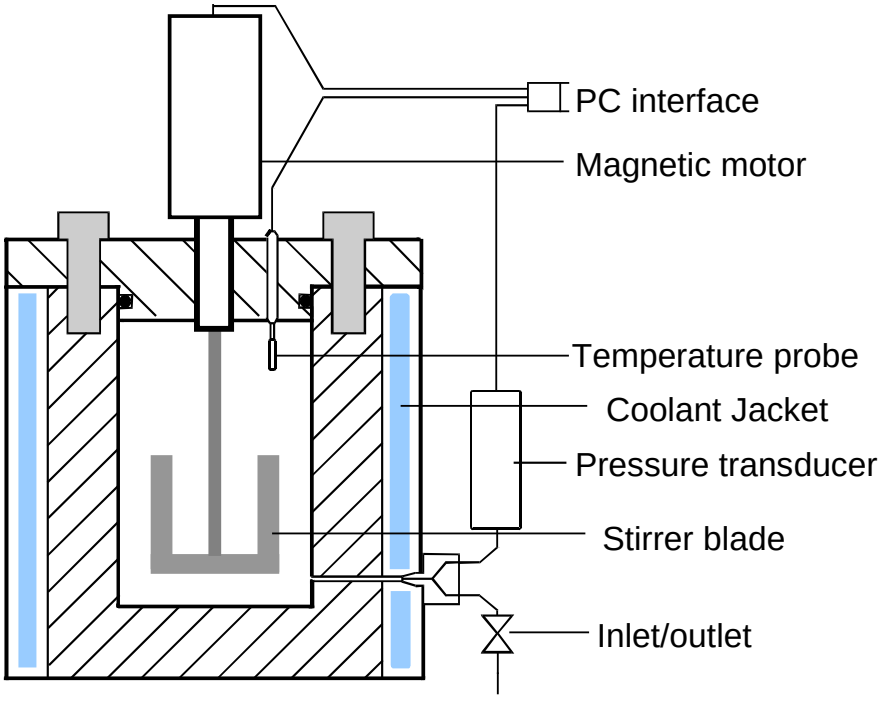

Figure 3.6 Schematic diagram of the Titanium Vessel Rig 1

Table 3.1 Summary of rigs for experiment

Name	Volume (mL)	Remarks
Kinetic rig 3	500	Magnetic bar stirrer
Titanium vessel rig	2400	Magnetic stirrer with adjustable rotation speed
Kinetic rig 1	2400	Magnetic stirrer with adjustable rotation speed
Titanium rig 1	300	Manually stir by turning upside down

3.2.1.2 PNA Network Analyser and dielectric probes for sample measurement

PNA Network Analyser with Slim Probe. The dielectric measurements (Figure 3.7) were performed using a PNA Series Network Analyser (Model no: E8364B) with frequency range of 10 MHz – 50 GHz. The electronic calibration module (Part no: N4691-60001) for 10 MHz – 26.5 GHz attached to the analyser with flexible cable was used to calibrate the system. Measurements were made using a 20 cm slim open-ended coaxial probe. The measurement was made at atmospheric conditions with the probe immersed in the beaker containing sample or at pressure with the probe is placed inside the Kinetic Rig 3. In this thesis, data analysis of experiment at low pressure using this probe is included. Data analysis at atmospheric pressure is detailed in SPE 94340. Extensive data analysis at atmospheric pressure is performed using an improved version of probe called New Performance Probe described next.

PNA-L network analyser with New Performance Probe. A PNA-L network analyser (Model N5230A) with frequency range of 10 MHz – 20 GHz supplied by Agilent was used to measure dielectric properties of the samples as shown in Figure 3.8. The electronic calibration module (Part no: N4691-60005) for 300 KHz – 26.5 GHz attached to the analyser with flexible cable was used to calibrate the system. Measurements were made using a New Performance Probe. The measurements were made at atmospheric conditions (within the scope of this work) with the probe immersed in the beaker containing sample at frequency range of 0.2 GHz – 20 GHz.

Detail configuration of each probes used for this study is given in Appendix A.3.

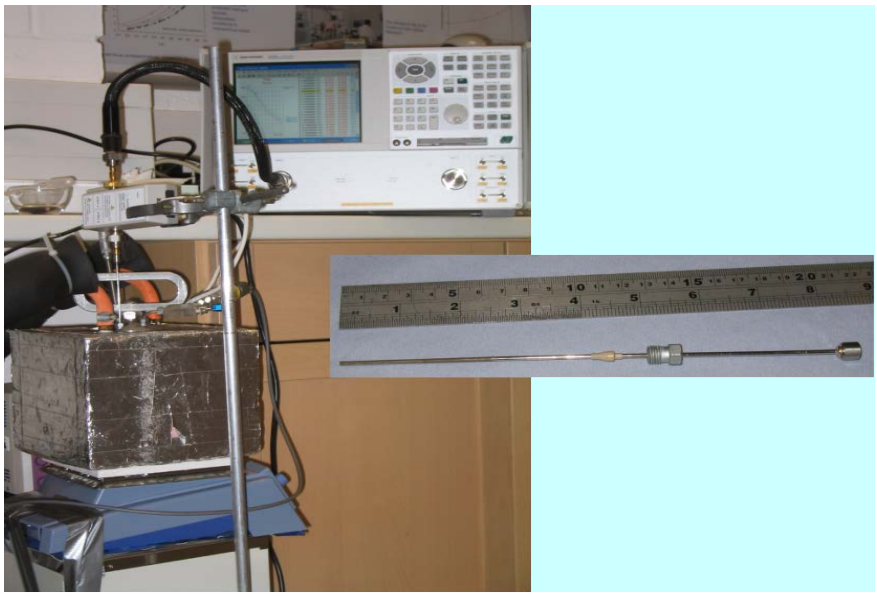

Figure 3.7 Dielectric constant measurement set-up: PNA Network Analyzer with Slim Probe

Figure 3.8 Dielectric constant measurement set-up: PNA-L Network Analyzer with New Performance Probe

3.2.2 Materials

Several different types of water samples were prepared for studying water memory to answer the key questions described in Section 3.1.2. These samples are classified as deionised water (DW), hydrate deionised water (HDW), vacuumed hydrate deionised water (HDWV), saturated deionised water (SDW) and vacuumed saturated deionised water (SDWV). Sample preparation and procedure for different types of water is

described in sample preparation section (Section 3.2.3). Another series of samples was prepared to investigate the effect of impurities (salt) on sustainability of water memory. These samples are classified as deionised water with salt (DWS), hydrates deionised water with salt (HDWS) and saturated deionised water with salt (SDWS). In this study, 3 weight % of Sodium Chloride, 99+% AR grade supplied by Aldrich was used.

Tetrahyrofuran (THF) with chemical formula of C_4H_8O and boiling point of 67 ^oC was supplied by Merck Eurolab. THF forms structure II hydrates with water (THF:17 H_2O). Natural gas supplied by Air Products with the composition listed in Table 3.2 was used in this study.

Table 3.2 Natural Gas Composition

Components	Composition 1 (mole%)	Composition 2 (mole%)
N_2	1.70	2.16
C_1	89.00	89.69
CO_2	1.65	1.69
C_2	5.50	4.62
C_3	1.50	1.26
iC_4	0.16	0.17
nC_4	0.31	0.30
iC_5	0.07	0.06
$nC_5 + C_6$	0.11	0.05
TOTAL	100	100

3.2.3 Sample preparation and procedure

3.2.3.1 Presence of water memory at atmospheric pressure

Hydrate deionised water (HDW) and saturated deionised water (SDW) were prepared to investigate the presence of water memory at atmospheric pressure. The samples were prepared in Titanium Equilibrium Cell with non-continuous and limited mixing. HDW sample was prepared by charging approximately 180 ml of deionised water into the rig at 20 ^oC. The equilibrium cell was pressurised to about 103 bar/1500 psia by injecting

natural gas. The water-natural gas system was directly cooled to 4 ^{o}C (inside the hydrate phase boundary), following path shown schematically in Figure 3.9 to form hydrates. The hydrate formation is detected based on pressure drop and the sudden temperature rise due to the release of latent heat of hydrate formation. After gas hydrates formation the system pressure was reduced to atmospheric pressure to dissociate the hydrates. 60 ml of water sample was transferred into a beaker in a bath where the temperature was kept at 4 ^{o}C in advance. The system was allowed to equilibrate for 30 minutes before measurement.

SDW sample was prepared in the same cell by saturating deionised water with natural gas at about 103 bar/1500 psia and 20 ^{o}C for several hours. The system pressure was reduced to 10.3 bar/150 psia followed by temperature reduction to 4 ^{o}C outside the phase boundary to avoid any hydrate formation as shown schematically in Figure 3.9. The system was allowed to equilibrate for 2 hours before releasing pressure to atmospheric and sampling the water.

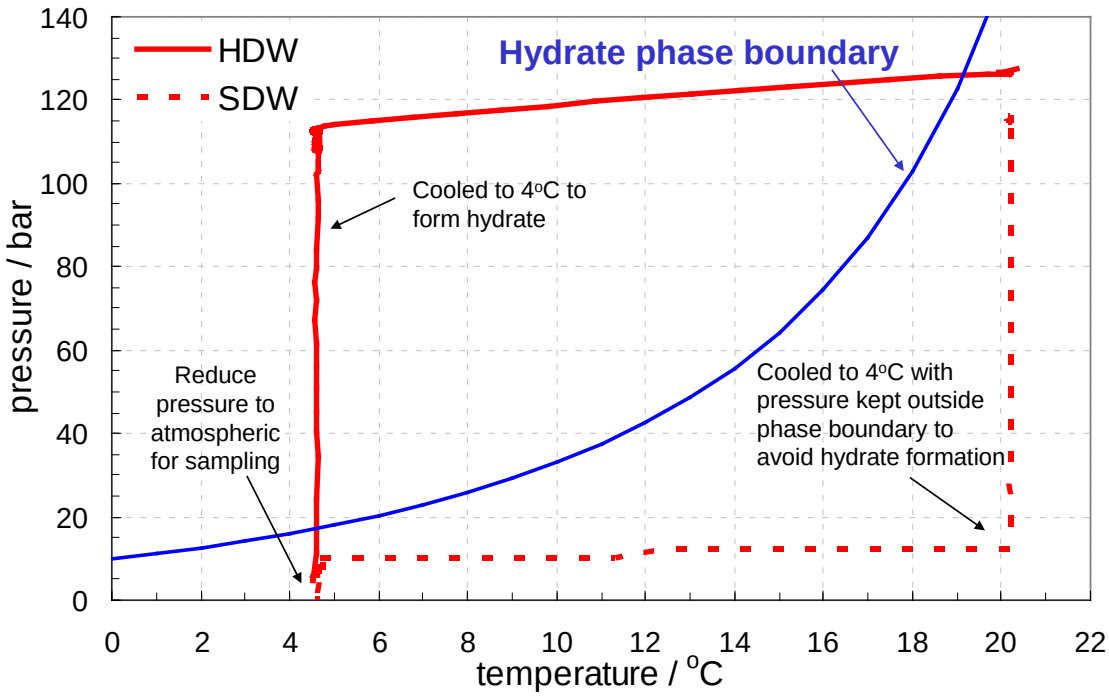

Figure 3.9 Preparation Path of HDW and SDW samples

3.2.3.2 Effect of water structure at atmospheric pressure

HDWV and SDWV samples were prepared using similar procedure described in Section 3.2.3.1 for HDW and SDW samples. The samples were vacuumed for 1 hour to remove excess dissolved gas. This procedure is adopted to clarify if water structure remains as memory without the influence of soluble gas.

3.2.3.3 Effect of heating

The effect of heating to remove water memory was investigated. HDW sample was prepared based on the procedure described in Section 3.2.3.1. Two samples were prepared. The first sample was taken after hydrate dissociation. The second sample, similar to the first sample, was heated to 35 ^{o}C for 20 hours in the beaker. Both samples were cooled down to 4 ^{o}C. The dielectric properties were measured and compared between these samples.

3.2.3.4 Effect of different sample preparation paths

Sample preparation procedure adopted for various studies described in Section 3.2.3.1, 3.2.3.2 and 3.2.3.3 is based directly depressurizing sample to atmospheric pressure at 4 ^{o}C, which obviously different from the situation practically occurring in pipelines. In pipelines, hydrates may be dissociated through gradual change in temperature or pressure. To simulate this process, the hydrate water samples were prepared following different paths, along a depressurisation track inside or just outside the hydrate stability zone. The study was also performed at atmospheric conditions.

The effect of different sample preparation path on water memory was investigated. It is divided into two series of experiments. In the first series, hydrate deionised water (HDW) and saturated deionised water (SDW) were prepared to investigate the presence of water memory. The HDW sample was prepared by charging approximately 1100 ml of deionised water into the Kinetic Rig 1 at 20 ^{o}C. Then the system was placed under vacuum for more than 1 hour to remove any trapped air in the water. The kinetic rig was pressurised to about 103 bar/1500 psia by injecting natural gas. The water-natural gas system was directly cooled to about 4 ^{o}C, inside the hydrate phase boundary, to form hydrates. The hydrate formation is detected based on pressure drop and the sudden temperature rise due to the release of latent heat of hydrate formation.

After gas hydrates formation, the hydrate was dissociated based on two paths. These paths were considered as the worst case scenarios for detection of hydrate water memory. Path 1 designated as Case 1, was the path followed inside hydrate phase boundary as schematically shown in Figure 3.10. Path 2, designated as Case 2, was the path followed outside hydrate phase boundary indicated schematically in Figure 3.11. The system temperature and pressure were reduced step by step along the paths 2 – 3 ^{o}C inside or outside the hydrate phase boundary. The system was released to atmospheric pressure at 4 ^{o}C for sampling. 60 ml of water sample was transferred into a beaker in a bath where the temperature was kept at 4 ^{o}C in advance. The system was allowed to equilibrate for 30 minutes before measurement.

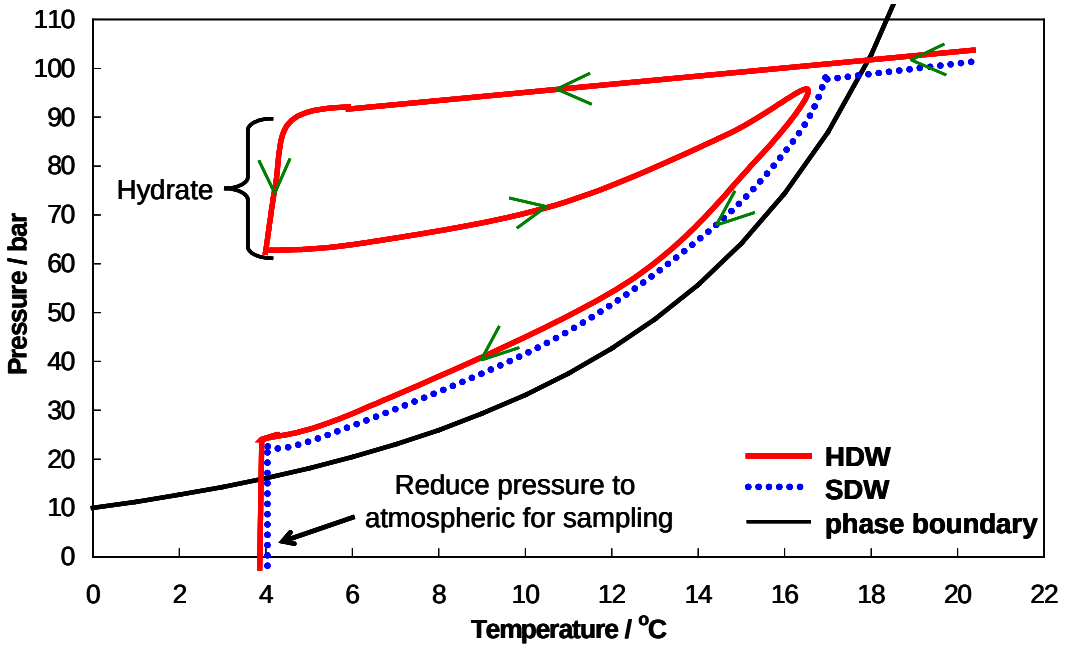

Figure 3.10 Preparation of HDW and SDW samples: Depressurization followed path inside hydrate phase boundary (Case 1)

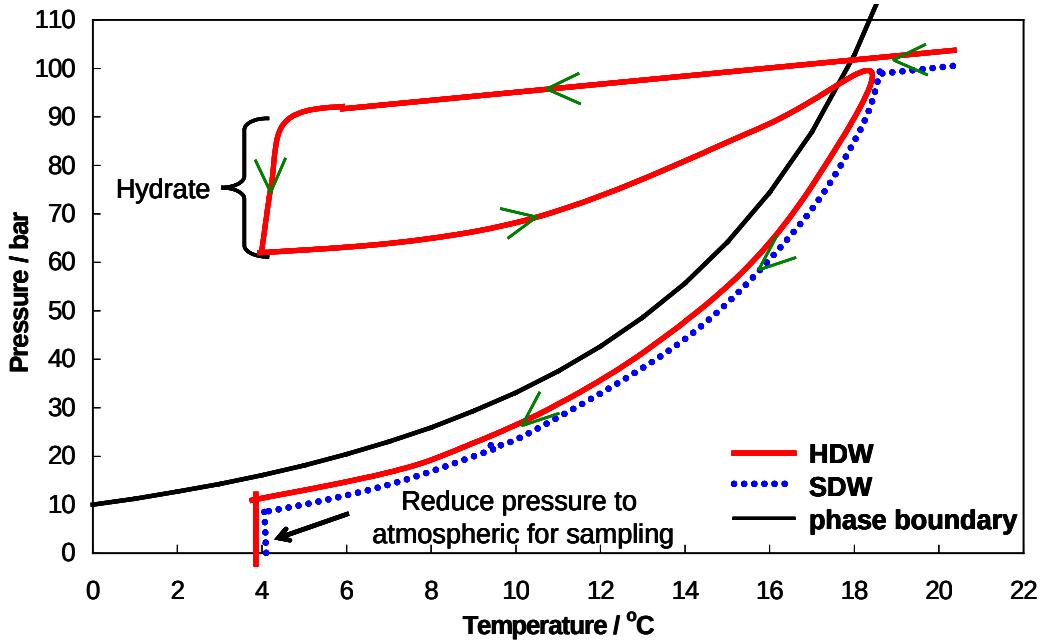

Figure 3.11 Preparation of HDW and SDW samples: Depressurisation followed path outside hydrate phase boundary (Case 2)

SDW sample was used to study the effect of dissolved gas on water memory. It was prepared in the high-pressure Kinetic Rig 1 by saturating deionised water with natural gas at about 103 bar/1500 psia and 20 °C for several hours. The deionised water was placed under vacuum for about 1 hour to remove trapped air. Similarly, the system temperature and pressure were reduced step by step along the paths 2 – 3 °C inside or outside the hydrate phase boundary. The system pressure was reduced to atmospheric at 4 °C for sampling. 60 ml of water sample was transferred into a beaker in a bath where the temperature was kept at 4 °C in advance. The system was allowed to equilibrate for 30 minutes before measurement.

For the second experiment, HDWV and SDWV samples were prepared using similar procedure described above for HDW and SDW samples. The excess dissolved gas was removed from both samples by applying vacuum to the system in two stages. In the first stage, the sample was under vacuum for 30 minutes, and then it was left at atmospheric pressure for 10 minutes. In the second stage, the sample was under vacuum for 10 minutes then left for another 10 minutes. Then the top cap of the Kinetic Rig 1 was opened for water sampling. This procedure is adopted to clarify if water structure remains as memory and is independent of dissolved gas.

Compositional analysis was performed for hydrate deionised water (HDW) and saturated deionised water (SDW) prepared through different paths for studying hydrate water memory using dielectric constant. In addition, analysis was also done for vacuumed hydrate deionised water (HDWV) and vacuumed saturated deionised water (SDWV) for studying the effect of water structure. The objective was to investigate any compositional changes in liquid sample (i.e. water samples) subjected to various treatment described above. This analysis was part of preliminary study to investigate the possibility of monitoring compositional changes of liquid and vapour phases to detect the hydrate formation and memory effect. (Details are described in Appendix C).

3.2.3.5 Effect of impurities

The effect of impurities on hydrate water memory was investigated. These impurities could be salt, kinetic hydrate inhibitor or alcohol. Salt (3 weight % Sodium Chloride) was selected to be investigated in this thesis. This is to mimic the presence of salinity in produced water from reservoir. Similar procedures were followed for sample preparation of hydrate deionised water with salt (HDWS) and saturated deionised water with salt (SDWS) as described for HDW and SDW samples in Section 3.2.3.4. The dissociation/depressurisation process followed a path 2 – 3 ^{o}C inside the hydrate phase boundary.

3.2.3.6 Hydrate water memory under pressure

Potential on-line measurement of dielectric properties for natural gas hydrate was investigated. The path followed for cooling and heating process which divided into 4 steps is illustrated in Figure 3.12. In this experiment, 450 ml of deionised water was pressurised with natural gas at 25 bar/364.7 psia (the working pressure of slim probe) and room temperature in the kinetic rig 3. The slim probe was inserted inside Kinetic Rig 3 to obtain direct measurement of dielectric properties.

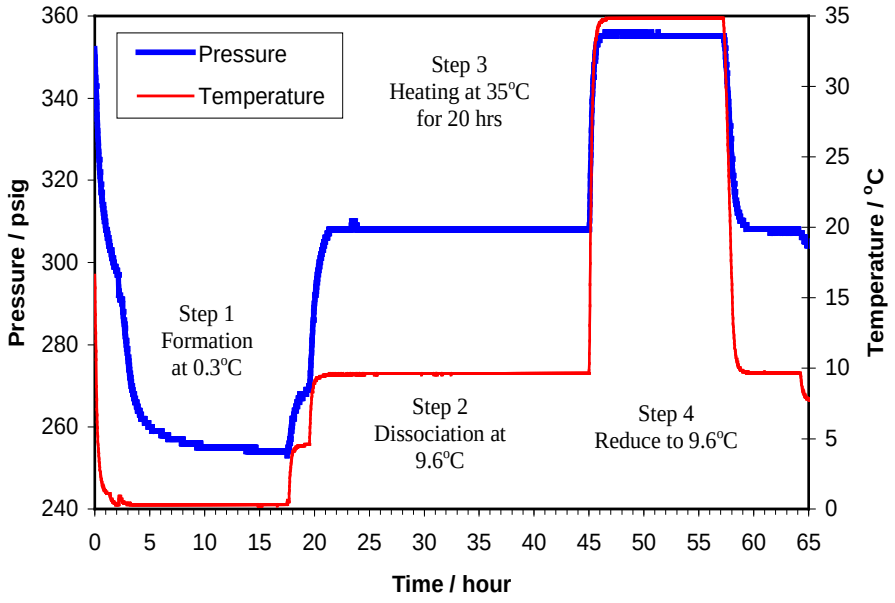

Figure 3.12 Sample preparation paths for under pressure. Natural gas hydrates formation, dissociation and heating.

In the first step, the temperature was reduced to 0.3 ^{o}C inside the phase boundary to form hydrates. Then hydrates were dissociated by increasing the temperature to 9.6 ^{o}C in Step 2. The system was heated to 35 ^{o}C for 20 hours to investigate the effect of time and heating on water memory in Step 3. Finally in Step 4, the system temperature was reduced to 9.6 ^{o}C to measure the changes in the sample's dielectric constant, as a result of heating and gas release.

3.2.3.7 THF-water system

The presence of water memory was investigated for water soluble hydrate former. Water soluble hydrate former was selected for the reason to focus on the influence of water structure as the factor contributing to the presence of the water memory after hydrate dissociation. Among several compounds known as hydrate former, tetrahydrofuran (THF) is a unique in that (a) it is in the state of a liquid under atmospheric pressure, (b) it is unlimitedly soluble in liquid water and (c) it forms a hydrate under atmospheric pressure. Due to unique nature mentioned above, THF has received the attention of hydrate researchers interested in studying the physical properties (Tomoyuki et al., 2001). In contrast to hydrophobic hydrate formers that allow hydrate crystals to form, in general, only at the interfaces where they meet a

liquid-water phase, THF mixed with water into a solution allows hydrate crystals to form and grow anywhere within the confines of the solution.

A 19 mass % tetrahydrofuran (THF) aqueous solution, was used in this study. This is corresponding to the stochiometric composition of THF hydrate (THF-17H_2O) of structure II. Hydrates were formed in the beaker by reducing the system temperature to 1 ^oC at atmospheric pressure and dissociated above the hydrate phase boundary at 6 ^oC. The reported dissociation temperature with 19 mass% is 4.4 ^oC (Pinder et al., 1965, Handa et al., 1984, Hanley et al., 1989, Nagashima et al., 2000, Bollavaram et al., 2000). The aqueous solution was heated to 15 ^oC for 15 hours to study the effect of heating.

3.2.4 Dielectric Constant Measurement and Data Analysis

For all the experiments at atmospheric pressure, the samples were placed in a beaker inside the bath and allowed to equilibrate before measuring dielectric properties using the probe immersed in the sample. In the case of measurement under pressure, the probe was inserted inside the Kinetic Rig 3 where the changes in dielectric properties will be measured as a result of dynamic changes in the pressure and temperature of the system.

The Performance Network Analyzer (PNA) system provides direct reading of dielectric constant or relative permittivity (real part), imaginary part and also loss tangent for the measured samples. For this study dielectric constant measurement was used for data analysis. In some analysis, the dielectric constant measurements were repeated in various intervals for several hours to investigate the change in the water memory as a function of time (and its lifetime) under atmospheric and low pressure. For all analysis, the average data was taken for at least 5 set of data generated from various experiments.

It is important to highlight that the focus of this study is to observe differences or changes in dielectric constant based of various experimental procedure. Therefore, experimental data was analysed based on magnitude of the dielectric constant reading to observe changes. The analysis is performed based on the following categories:

- Difference in dielectric constant with DW (e.g. $\varepsilon'_{DW} - \varepsilon'_{HDW}$)

  - presence of water memory
  - effect of water structure on water memory
  - effect of heating
- Difference in dielectric constant ($\varepsilon'_{SDW} - \varepsilon'_{HDW}$, $\varepsilon'_{SDWV} - \varepsilon'_{HDWV}$ and $\varepsilon'_{SDWS} - \varepsilon'_{HDWS}$)
  - effect of time (sustainability of water memory)
  - effect of water structure on water memory
  - effect of impurity (NaCl)
- Dielectric constant (ε')
  - natural gas hydrate formation under pressure
  - detection of hydrate formation
  - presence of water memory and sustainability with time under pressure
  - effect of temperature
  - THF hydrate formation and dissociation
  - THF-water system
- Difference in dielectric constant under pressure ($\varepsilon'_{\text{before formation}} - \varepsilon'_{\text{after dissociation}}$ and $\varepsilon'_{\text{before formation}} - \varepsilon'_{\text{after heating}}$)

3.3. WATER MEMORY AT ATMOSPHERIC PRESSURE: RESULTS AND DISCUSSIONS

3.3.1 Presence of Water Memory

In this section, it is demonstrated that the dielectric constant measurement has a potential application to detect water memory from hydrate formation and dissociation at atmospheric pressure using a New Performance Probe.

The experiments were designed to test water samples after hydrate formation and dissociation (HDW) that indicated the water memory was a combined effect of changes in water structure and dissolved gas. Water samples saturated with natural gas outside hydrate phase boundary (SDW) was analysed to investigate the effect of dissolved gas. Deionised water was used in all experiment as a reference data for determining changes in dielectric constant with respect to various types of water samples. The measurement was made for DW, HDW and SDW at atmospheric pressure and 4 ^{o}C. It is important to note that these experiments were conducted in Titanium Equilibrium Cell (described in Section 3.2.1.1) with limited mixing based on manually turning the cell up and down

based on sample preparation path shown in Figure 3.9 (HDW prepared inside hydrate phase boundary and SDW prepared outside hydrate phase boundary). The fluid sample was allowed to equilibrate for more than 12 hours before reducing pressure and temperature for each experimental set-up.

The difference in dielectric constant with DW for both HDW and SDW ($\varepsilon'_{DW} - \varepsilon'_{HDW}$ and $\varepsilon'_{DW} - \varepsilon'_{SDW}$) are shown in Figure 3.13. The results indicate that the difference between the HDW and the DW and between the SDW and the DW are similar after 0.5 hour. This similarity might be attributed to the presence of significant gas bubbles in the HDW sample which would affect the measurement. However, the difference is very significant after 1 hour as seen in the Figure 3.13. The difference for HDW is between two to four times of that for SDW. The significant difference observed in HDW is attributed to both dissolved gas effect and changes in water structure/clustering as a result of hydrate formation. In the case of SDW it was primarily due to dissolved gas effect. The result also suggests that water memory in HDW sample remains for a longer time as compared to the SDW sample with soluble gas based on measured difference in dielectric constant.

This result also shows that the new performance probe has higher sensitivity to detect changes for different types of water samples as compared to slim probe[1] (comparison is provided in Section A.4 of Appendix A). The improvement in sensitivity was significant even with the worst case scenario where the sample prepared did not have continuous mixing in the Titanium Equilibrium Cell as compared to the sample prepared with continuous mixing in Kinetic Rig 3 (for the result using slim probe).

[1] The result of analysis using the slim probe was published in paper SPE 94340

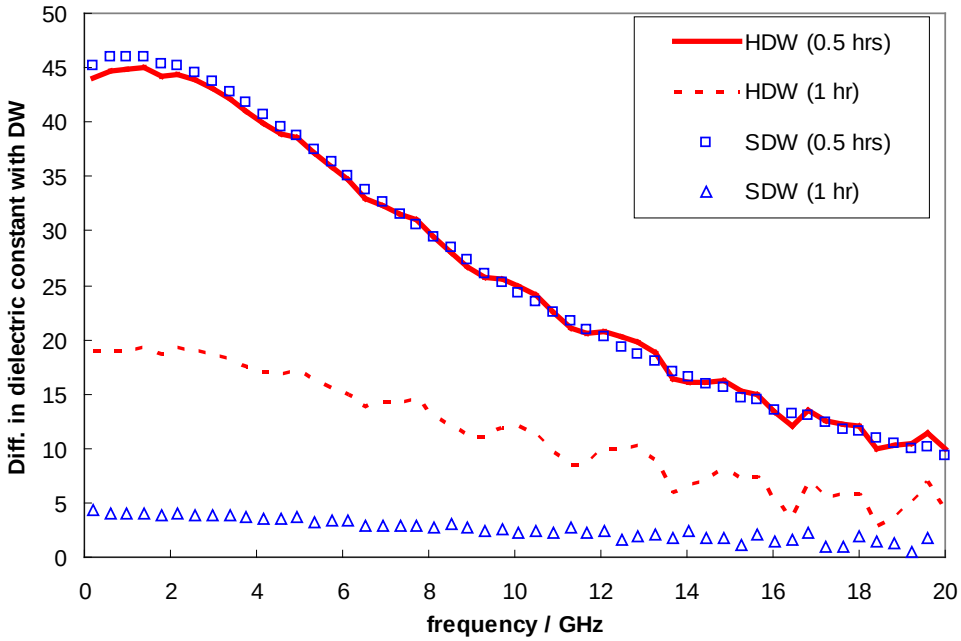

Figure 3.13 Differences in dielectric constant with DW for HDW ($\varepsilon'_{DW} - \varepsilon'_{HDW}$) and SDW ($\varepsilon'_{DW} - \varepsilon'_{SDW}$) at 4 ^{o}C and 1 atm. The presence of water memory is detectable by dielectric properties[2]

3.3.2 Effect of Water Structure on Water Memory

A series of experiments were performed to confirm that water memory is mainly attributed to dissolved gas, which keeps the structure of water until the excess gas is evolved from solution. The experiments were designed similar to preparation of HDW and SDW as described in Section 3.2.3.2. These samples were placed under vacuum for 1 hour to remove excess gas before measuring dielectric constant. The sample designated as HDWV was analysed if changes in water structure remain (i.e., water memory) after applying vacuum to the system with the aim of removing/minimizing the dissolved gas. Similarly, samples designated as SDWV was also analysed to compare with HDWV.

The result of dielectric properties based on differences in dielectric constant with DW for HDWV ($\varepsilon'_{DW} - \varepsilon'_{HDWV}$) and SDWV ($\varepsilon'_{DW} - \varepsilon'_{SDWV}$) at 4 ^{o}C and 1 atm (after leaving the system for about 0.5 hours to stabilise) is plotted in Figure 3.14. The results show

[2] HDW prepared inside hydrate phase boundary and SDW prepared outside hydrate phase boundary as illustrated in Figure 3.9

that the differences with DW are higher for HDWV as compared to SDWV. This difference may suggest the water structure do contribute to the presence of water memory at the test conditions. It shows that removing excess dissolved gas from the samples clearly has effect on the water memory. This is further clarified by comparing differences in dielectric constant with DW for HDW (Figure 3.13) and HDWV (Figure 3.14) after 0.5 hour of stabilisation. The comparison is made at 4 GHz and 8 GHz. It is observed that the difference in dielectric constant with DW for HDW (40 at 4 GHz and 30 at 8 GHz) is in the order of 17 times higher than that for HDWV (2.4 at 4 GHz and 1.8 at 8 GHz). These differences suggest that the contribution of water structure to the presence of water memory was very weak and limited extend. Therefore, the water memory is mainly magnified by the presence of dissolved gas in the water sample to keep the remnant water structure after hydrate dissociation. Once most of the soluble gas evolved from water sample, the water structure will be removed.

It is important to note that the sample preparation path for both HDWV and SDWV for these samples does not follow similar path for depressurising to atmospheric. Therefore the effect of sample preparation path on water structure is investigated and reported in Section 3.3.5.

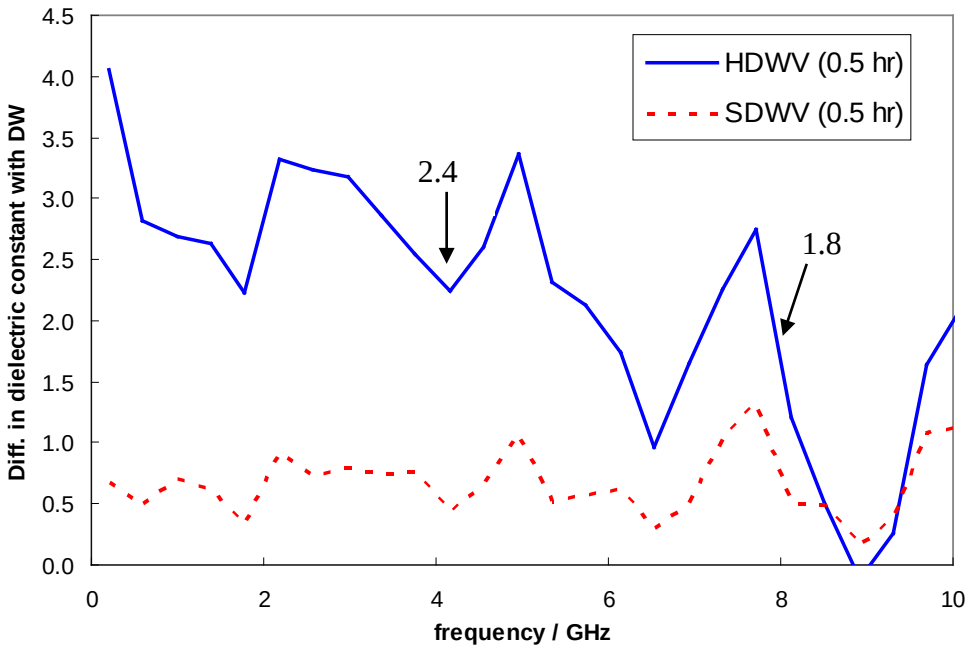

Figure 3.14 Differences in dielectric constant with DW for HDWV ($\varepsilon'_{DW} - \varepsilon'_{HDWV}$) and SDWV ($\varepsilon'_{DW} - \varepsilon'_{SDWV}$) at 4 ^{o}C and 1 atm. Effect of water structure on water memory after 0.5 hour.

3.3.3 Sustainability of Water Memory: Effect of Time

Analysis of time dependence of water memory and its lifetime under atmospheric pressure were investigated. Based on the difference in dielectric constant between SDW and HDW ($\varepsilon'_{SDW} - \varepsilon'_{HDW}$) shown in Figure 3.15, it is clearly observed that at test conditions, the water memory become weaker after 3 hours. Generally, it can be concluded that water memory is time dependent at atmospheric pressure and 4 ^{o}C and its lifetime is about 2 to 3 hours for the systems investigated.

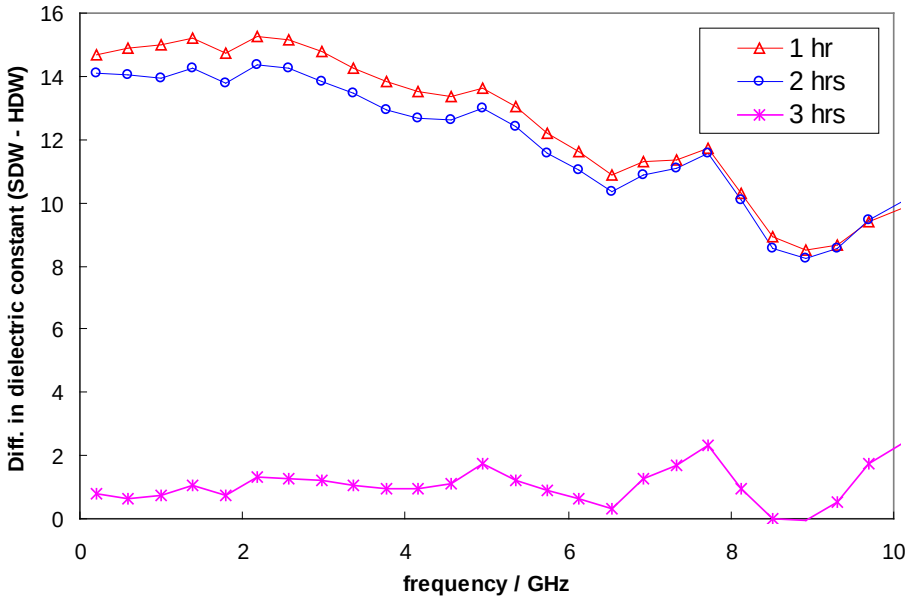

Figure 3.15 Effect of time on differences in dielectric constant between SDW and HDW ($\varepsilon'_{SDW} - \varepsilon'_{HDW}$) at 4 ^{o}C and 1 atm. Water memory remain for 2 to 3 hours

.

3.3.4 Effect of Heating on Water Memory

The effect of heating on the water memory was investigated. It has been reported that water memory is dependent on thermal history (Sloan, 1998; Ohmura, 2003). Water memory will be removed with heating at high temperature. From the dielectric spectrum shown in Figure 3.16, it was observed that there is significant different of the dielectric constant for the sample after hydrate dissociation ($\varepsilon'_{DW} - \varepsilon'_{HDW}$). The difference reduces with increasing frequency. Dielectric constant measurement for the water samples measured after heating shows insignificant difference with DW. The result shows that water memory is totally removed after keeping the sample at 35 ^{o}C for more than 12 hours. It was recognized that 12 hours heating time is too long for

practical purposes. The effect of time required further investigation which could not be covered within the scope of this thesis.

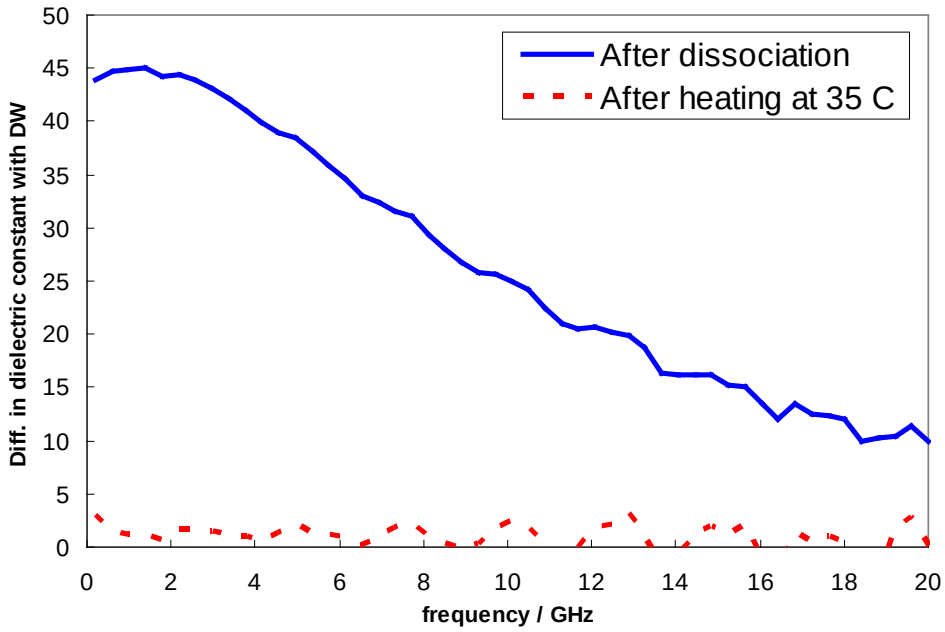

Figure 3.16 Effect of heating on hydrate water memory based on the differences in dielectric constant between DW and HDW ($\varepsilon'_{DW} - \varepsilon'_{HDW}$) at 4 ^{o}C and 1 atm for water sample after hydrate dissociation and after subjected to heating at 35^{o}C. Water memory can be removed subjected to increasing the temperature to 35 ^{o}C.

3.3.5 Effect of Sample Preparation Path on Water Memory

In pipelines, hydrates may be dissociated through gradual change in temperature or pressure. To simulate this process, the hydrate water samples were prepared following different paths, along a depressurisation track inside or just outside the hydrate stability zone.

The dielectric constant measurement for detecting hydrate water memory was conducted at 4 ^{o}C and atmospheric pressure using New Performance Probe based on the different sample preparation paths as described in Section 3.2.3.4. The main objective was to investigate the influence of similar sample path on water memory. Studies described in Section 3.3.1 to 3.3.4 were based on different paths for preparing sample with and without hydrate water memory. In this case, the HDW and SDW were prepared using similar paths by dissociating/reducing pressure steps by steps within 2 -

3 ^{o}C along hydrate phase boundary (both inside and outside the hydrate phase boundary).

Case 1: Sample preparation path inside the hydrate phase boundary.

Both HDW and SDW were prepared based on the actual path shown in Figure 3.17. The sample pressure was released to atmospheric for surface sampling. Figure 3.18 shows the effect of time on hydrate water memory which was presented by the differences between SDW and HDW (ε'_{SDW} - ε'_{HDW}). The dielectric constant measurement shows that the hydrate water memory remains up to 1 hour and it diminishes after 2 hours. The low sustainability of hydrate water memory is believed to be due to the step by steps dissociation to maintain within 2 - 3 ^{o}C inside hydrate phase boundary.

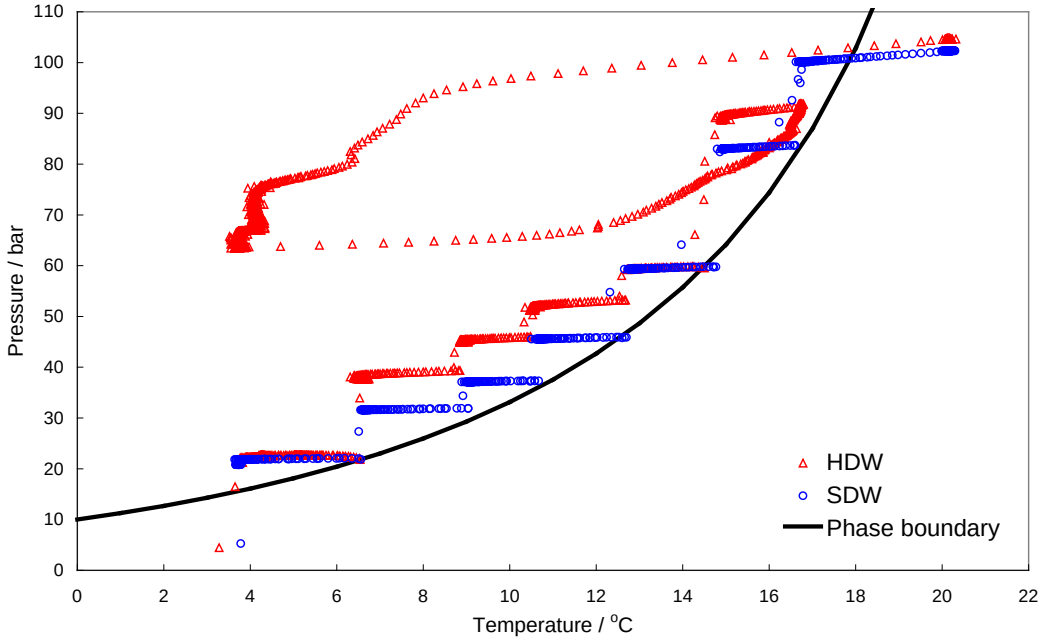

Figure 3.17 Sample preparation paths inside hydrate phase boundary (Case 1).

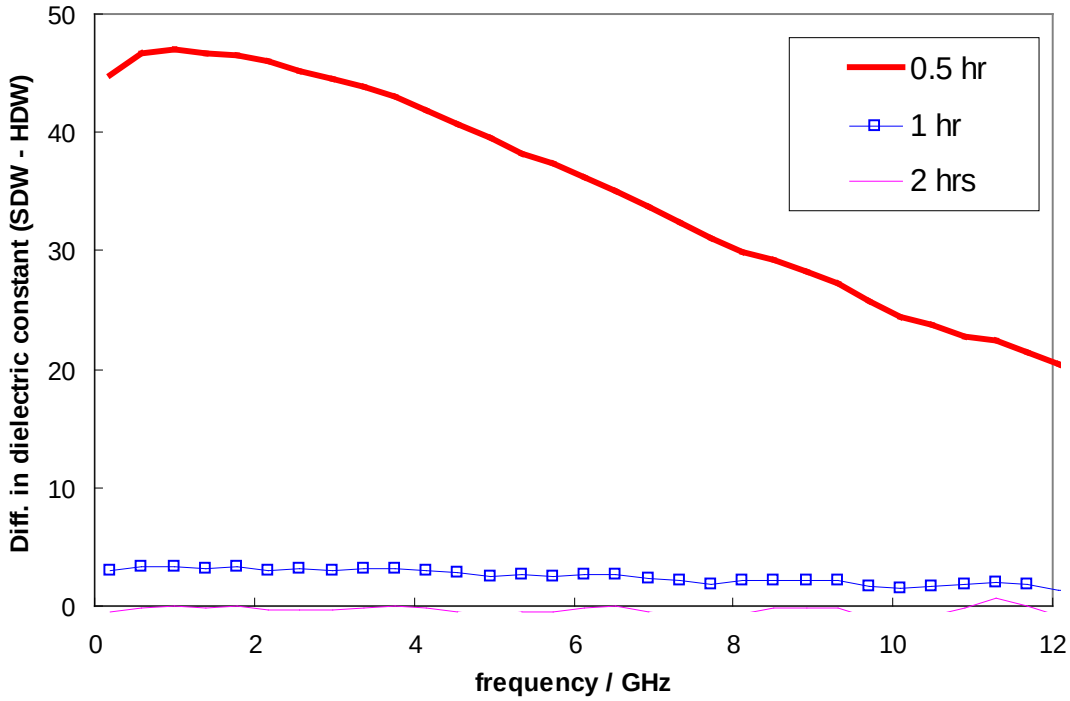

Figure 3.18 Effect of time on the differences in dielectric constant between SDW and HDW ($\varepsilon'_{SDW} - \varepsilon'_{HDW}$) at 4 ^{o}C and 1 atm for case 1. Water memory remains for 1 hour.

Case 2: Sample preparation path outside hydrate phase boundary.

For Case 2, the sample preparation path is shown in Figure 3.19. In this case the hydrate water memory remains approximately around 0.5 hour (Figure 3.20). It was observed that the difference between SDW and HDW ($\varepsilon'_{SDW} - \varepsilon'_{HDW}$) outside phase boundary (Case 2) is significantly lower than that inside phase boundary (Case 1). This is believed to be due to step by step dissociation outside hydrate stability zone which caused significant release of soluble gas compared to the path inside hydrate stability zone), and hence reducing the stability of water memory.

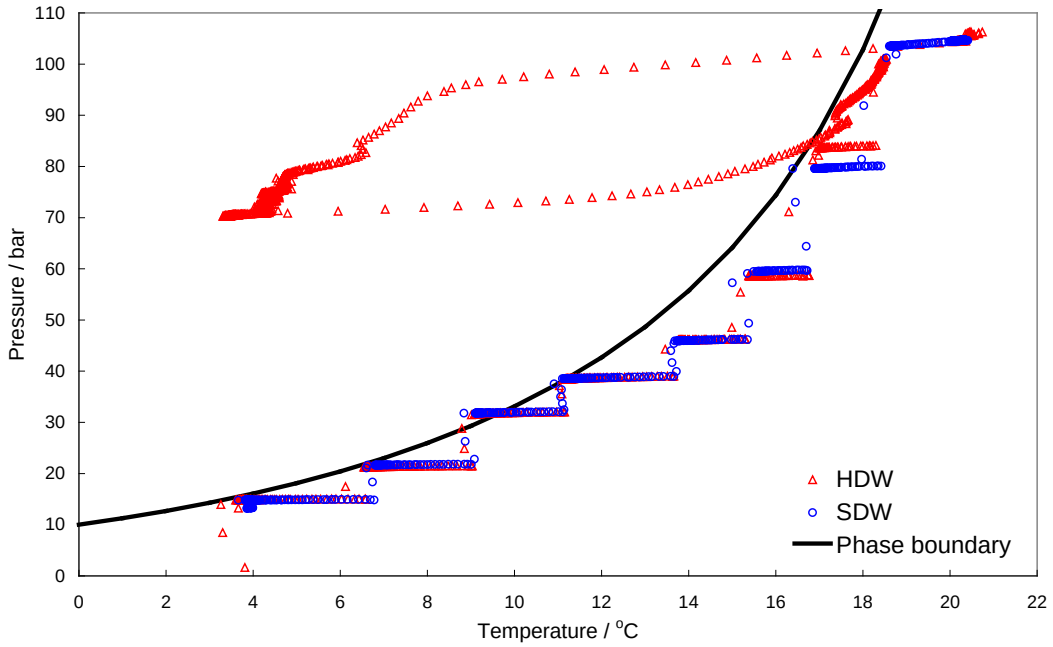

Figure 3.19 Sample preparation paths outside hydrate phase boundary (Case 2).

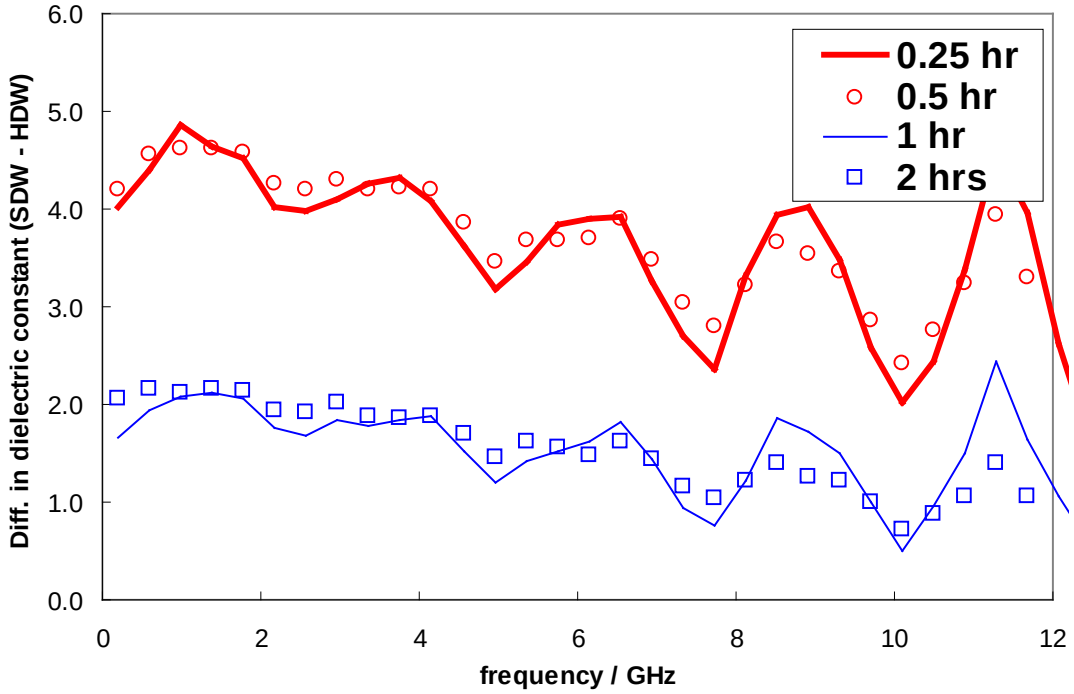

Figure 3.20 Effect of time on the differences in dielectric constant between SDW and HDW ($\varepsilon'_{SDW} - \varepsilon'_{HDW}$) at 4 °C and 1 atm for case 2. Water memory remains for about 0.5 hour.

3.3.6 Effect of water structure on water memory

Another experiment was performed to confirm that water memory is mainly attributed to dissolved gas, which keeps the structure of water until the gas evolved from solution. The samples are designated as HDWV (Hydrate Deionised Water after Vacuum) and SDWV (Saturated Deionised Water after Vacuum). Both samples are prepared by dissociating/depressurising step by step along the path 2 – 3 ^{o}C inside the hydrate phase boundary as shown in Figure 3.21.

Figure 3.22 shows the effect of time on hydrate water memory due to changes in water structure which was presented by the differences in dielectric constant between SDWV and HDWV (ε'_{SDWV} - ε'_{HDWV}). The dielectric constant measurement shows that the water structure remains approximately 0.5 hour and it disappears after around 1 hour at the test conditions.

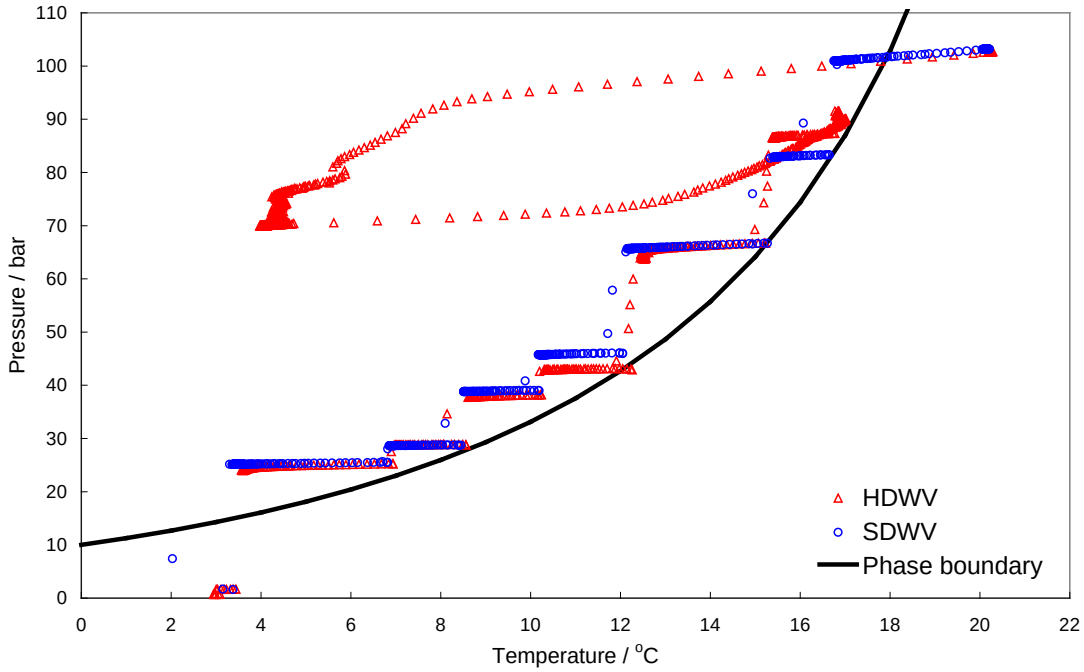

Figure 3.21 Sample preparation paths inside hydrate phase boundary for the effect of water structure on water memory.

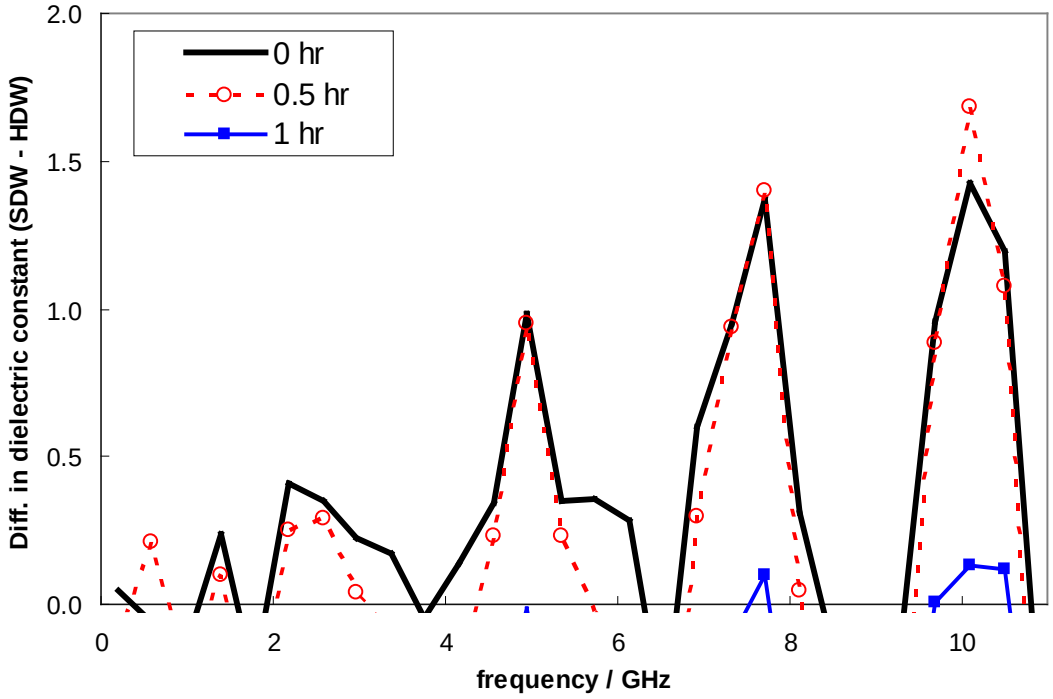

Figure 3.22 Effect of time on the differences in dielectric constant between SDWV and HDWV (ε'_{SDWV} - ε'_{HDWV}) at 4 ^{o}C and 1 atm. Water memory remains for about 0.5 hour.

Influence of water structure on hydrate water memory based on the procedure adopted during this experiment was analysed by comparing the difference in dielectric constant between samples with and without vacuum. The results are shown in Figure 3.23. It is observed that the effect of water structure is very weak after removing most of excess dissolved gas by applying vacuum based on the magnitude of the dielectric constant. For example, at 5 GHz, the difference is increased by 40 in the case of samples without vacuum. Therefore, this result supports the notion that hydrate water memory is influenced significantly by dissolved gas which causes the water memory to remain for some time.

Phenomena on the hydrate water memory effect based on water structure were reported by Buchanan et al. (Buchanan et al., 2005). The result reveals that there is no significant difference between structure of water before hydrate formation and the structure of water after the hydrate decomposition using Neutron diffraction technique. However, based on our study, we had observed the effect of water structure at certain frequency range, but it is obviously very small as compared to the influence of

dissolved gas. This result further confirms that the hydrate water memory is mainly a function of dissolved gas (i.e., extra dissolved gas due to hydrate formation).

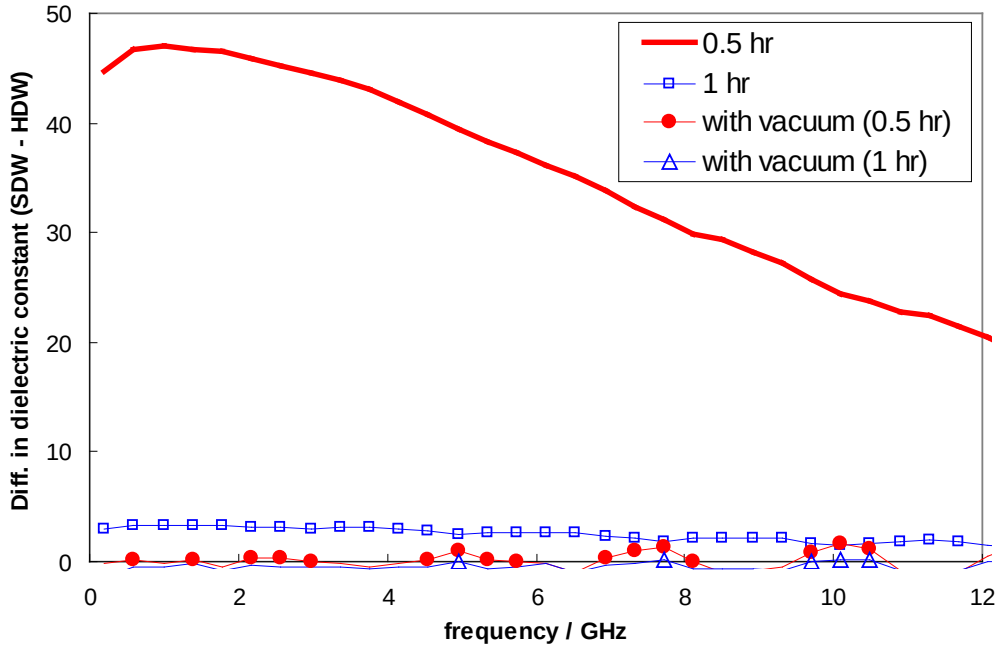

Figure 3.23 Influence of water structure on hydrate water memory. Comparison between sample without vacuum ($\varepsilon'_{SDW} - \varepsilon'_{HDW}$) and with vacuum ($\varepsilon'_{SDWV} - \varepsilon'_{HDWV}$) after 0.5 hour and 1 hour at 4 ^{o}C and 1 atm. Hydrate water memory is influenced significantly by dissolved gas which causes the water memory to remain for some time.

3.3.7 Compositional changes of aqueous phase

The compositional analysis of each aqueous phase was conducted at atmospheric pressure and room temperature after dissociation/depressurisation based on different paths (as discussed in Sections 3.3.5 and 3.3.6 of this chapter). For all samples, concentrations of hydrocarbons which constitute N_2, C_1, CO_2 and C_2 were detected in both HDW and SDW. Example of compositional analysis is shown in Table 3.3.

In another experiment for investigating the potential application of compositional changes of vapour and liquid phases for early warning system (details in Appendix B), it was observed that C_1 concentration remains in the phases, while there were significant changes in C_2 concentration in different samples. Therefore the ratio of C_2 to C_1 concentration was used as a possible indicator for detecting changes in composition due to hydrate formation.

The results of analysis for aqueous samples from HDW (inside hydrate phase boundary), SDW (inside hydrate phase boundary), HDW (outside hydrate phase boundary) and SDW (outside hydrate phase boundary) are shown in Figure 3.24. In the presence of hydrate water memory (for HDW samples) the ratio of C_2 to C_1 concentration is higher than that without water memory (for SDW samples). The ratio is significantly higher in the case of HDW depressurised along the path inside hydrate phase boundary. This is likely due to the longer sustainability of water memory as detected by dielectric constant technique.

Similarly, the aqueous composition was monitored in HDWV and SDWV samples. The result is shown in Figure 3.25. The ratio of C_2 to C_1 concentration was higher in the case of HDWV as compared to SDWV. This indicated that even with the two stages vacuum procedure to remove excess dissolved gas, there was detectable dissolved gas present in the aqueous sample which may contribute to the water memory at the test conditions. The result was also compared with the previous data for HDW and SDW. As expected, the ratio of C_2 to C_1 concentration in HDWV is significantly lower than that of HDW. However, the opposite was observed in the case of SDWV and SDW. In this case, the vacuum process has significantly removed C_1 from the liquid sample while C_2 appeared to be relatively more difficult to be removed and still remain in the liquid sample.

Table 3.3 Compositional analysis of liquid phase for HDW and SDW

Component	Concentration / mole %			
	Inside hydrate phase boundary		Outside hydrate phase boundary	
	HDW	SDW	HDW	SDW
N_2	0.11	2.21	1.71	49.46
C_1	90.45	31.37	22.93	93.19
CO_2	0.14	5.80	37.77	71.83
C_2	40.23	2.36	4.09	9.62
C_2/C_1 (%)	44.48	7.52	17.83	10.32

Note:

*The concentration is based on free water. Detail is in Appendix B.4

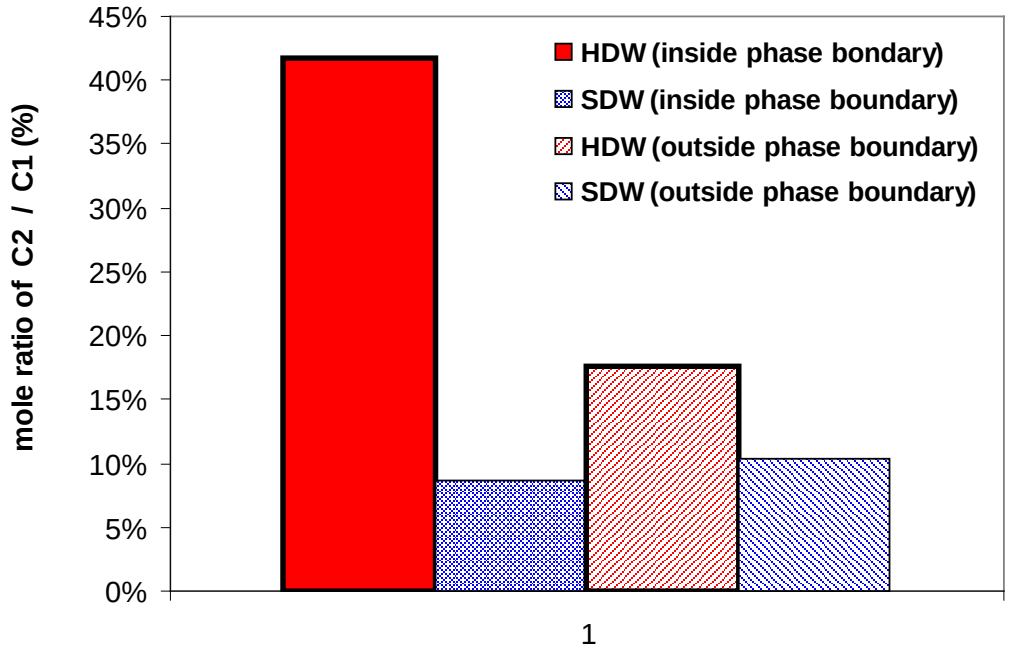

Figure 3.24 Monitoring C_2/C_1 ratios in aqueous phase sample for HDW and SDW based on percent mole ratio of C_2 to C_1.(% = mole C_2/mole C_1 x 100). Comparison between samples prepared inside and outside phase boundary.

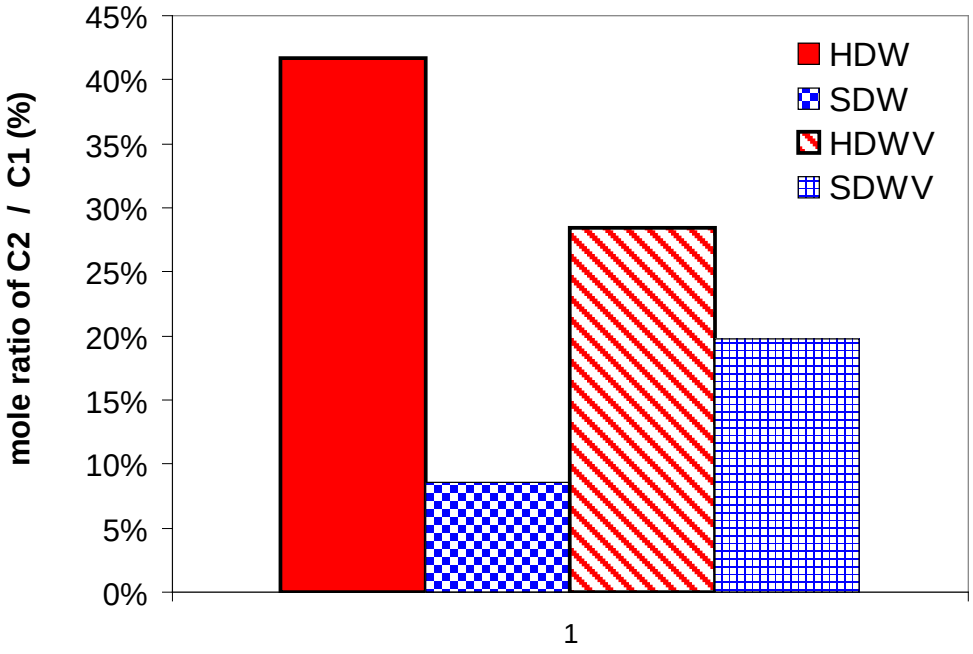

Figure 3.25 Monitoring C_2/C_1 ratios in aqueous phase sample based on percent mole ratio of C_2 to C_1.(% = mole C_2/mole C_1 x 100). Comparison between samples with and without vacuum.

3.3.8 Effect of impurity (salt)

The effect of salt (3 wt% NaCl) on hydrate water memory was investigated. The samples were prepared based on the path shown in Figure 3.26. The results, based on the difference between SDWS and HDWS (ε'_{SDWS} - ε'_{HDWS}), suggest that the water hydrate memory is detectable in the presence of salts as shown in Figure 3.27. Analysis of time dependency of water memory in the presence of salt (presented in Figure 3.27) shows that the water memory becomes weaker after about 1 hour at the test conditions.

Comparing the water memory in the presence and absence of salt shows that the presence of salt has a negative effect on the memory, as can be clearly observed from Figure 3.28. For example, sample measured at 0.5 hour, the magnitude of the difference in dielectric constant for the sample without salt is significantly higher than that of sample with salt. At 2 GHz, the difference for sample without salt is more than four times that of with salt. It is understood that presence of salt in water reduces the activity of water and solubility of natural gas in the water. It is expected that, the amount of gas hydrate form is less for the system with salt as impurity and hence reduce the water memory.

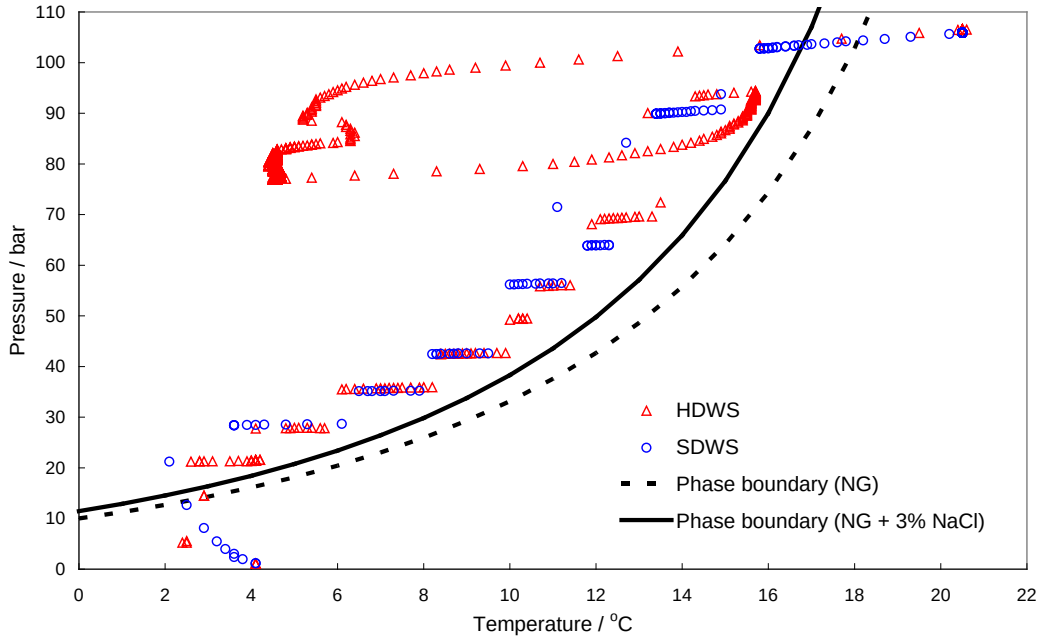

Figure 3.26 Sample preparation paths inside hydrate phase boundary for HDWS and SDWS.

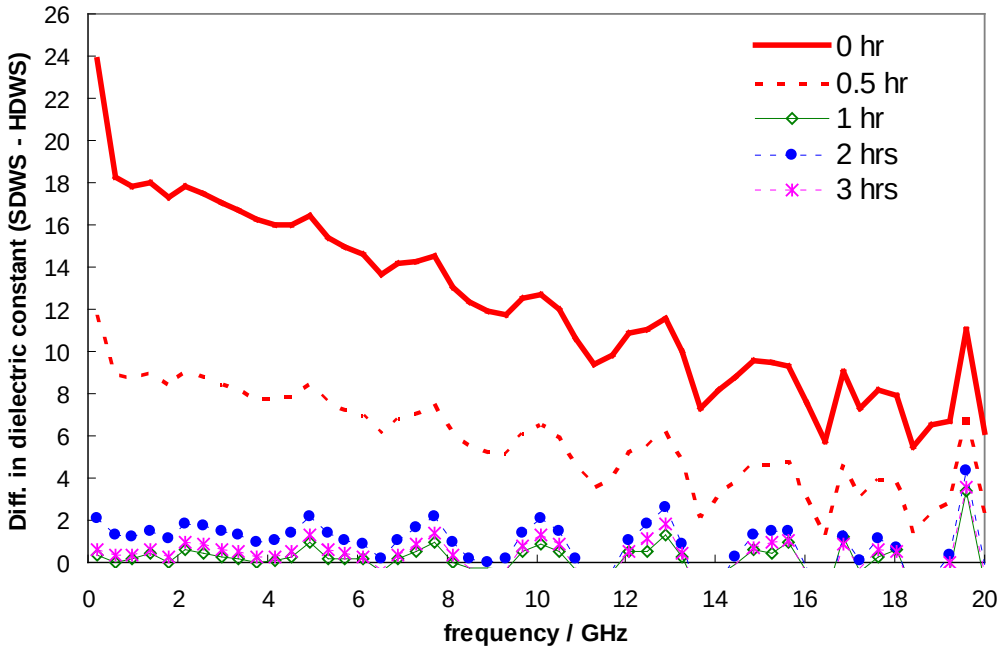

Figure 3.27 Effect of time on differences in dielectric constant between SDWS and HDWS ($\varepsilon'_{SDWS} - \varepsilon'_{HDWS}$) at 4 ^{o}C and 1 atm. Water memory remain for about 1- 2 hour.

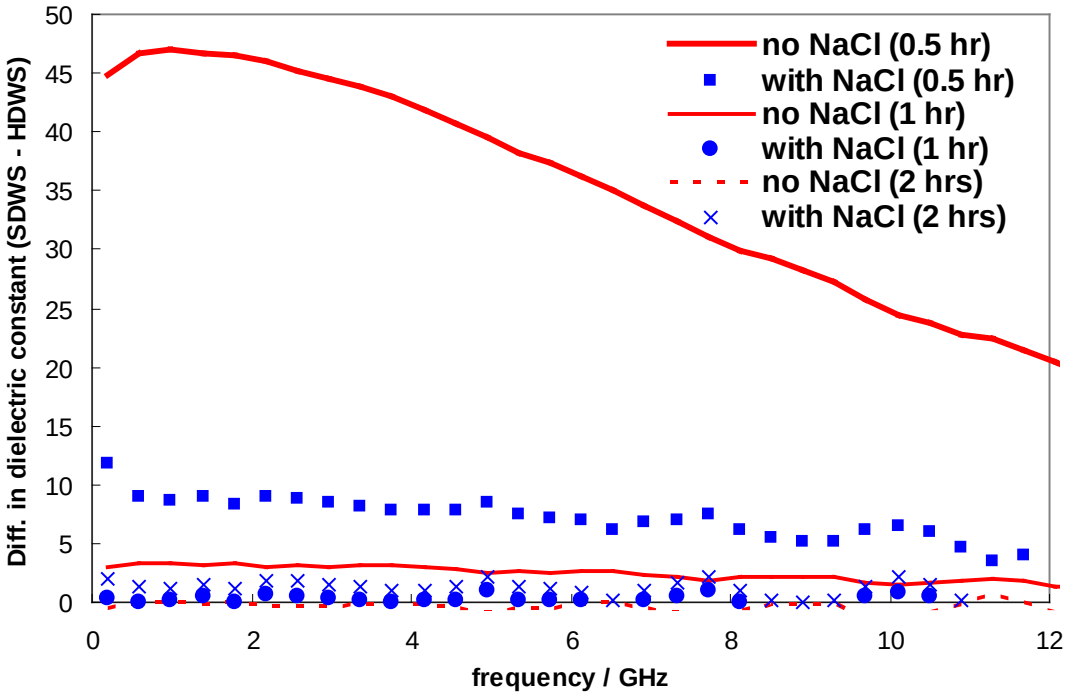

Figure 3.28 Effect of time on differences in dielectric constant for samples without NaCl ($\varepsilon'_{SDW} - \varepsilon'_{HDW}$) and with NaCl ($\varepsilon'_{SDWS} - \varepsilon'_{HDWS}$) at 4 ^{o}C and 1 atm.

3.4. WATER MEMORY UNDER PRESSURE: RESULTS & DISCUSSIONS

3.4.1 Detection of initial hydrate formation

Potential online measurement technique for monitoring and early warning of hydrate formation in the pipeline is of interest to oil companies and field operators. In this thesis, the potential application of dielectric properties measurement at low pressure in the kinetic rig was investigated.

The experiment was carried out in several steps as shown in Figure 3.12 and the path followed within the hydrate phase boundary is shown in Figure 3.29. In Step 1, the dielectric properties were measured at several points during temperature reduction to form hydrate as shown in Figure 3.30. It was observed those dielectric constants are slightly increased below 3 – 4.5 GHz with a decrease in the system temperature. On the contrary the dielectric constant values were significantly reduced with an increase in temperature for frequency above this range inside the hydrate phase boundary.

This trend is related to the data reported by Chaplin, M. (Chaplin, M., 2004) on the effect of increasing temperature or water activity on dielectric constant for water as shown in Figure 3.31. In this reference data, the dielectric constant values are reduced with an increase in the temperature. It converged to the same value at about 5 GHz for temperature ranges from 0 ^{o}C to 20 ^{o}C. Then the values will have the opposite trend with increasing frequency. There was no clear explanation as to why this shifting was observed. As explained by Chaplin it is known that the strength and extent of hydrogen bonding decreases with increasing temperature. This effect lowers dielectric permittivities, lessens the difficulty for dipole movement and allows the water molecule to oscillate at higher frequencies. This behaviour was observed at frequencies lower than 3 GHz as indicated in Figure 3.31.

The comparison between before hydrate formation (at 7 ^{o}C) and in the presence of hydrates (at 0.3 ^{o}C) is shown in Figure 3.32. During the experiments it was observed that as the temperature reached 0.5 ^{o}C, there is significant reduction in the dielectric constant at frequencies above 3 GHz, which could be attributed to the initial hydrate formation (Figure 3.30). As temperature was further reduced to 0.3 ^{o}C, significant growth of hydrates was observed based on sudden increase in the rig temperature due to the release of latent heat of hydrate formation. The value of dielectric constant remains

the same even after leaving the system at 0.3 °C for 14 hours, which is attributed to the presence of solid hydrate crystals.

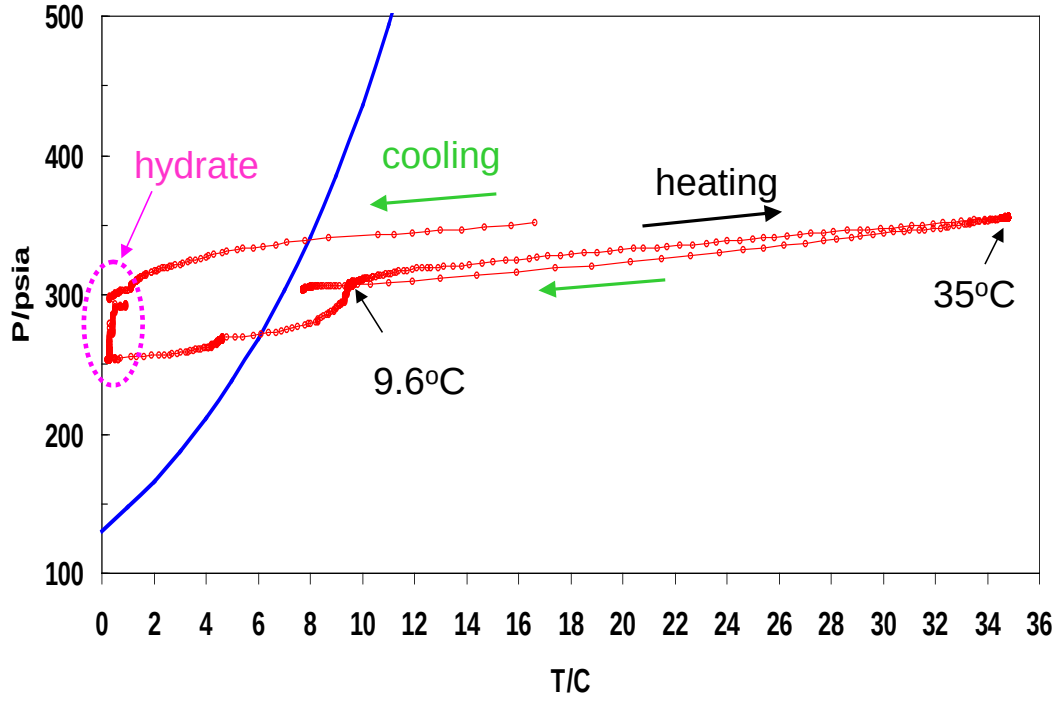

Figure 3.29 Hydrate phase boundary for measurement under pressure

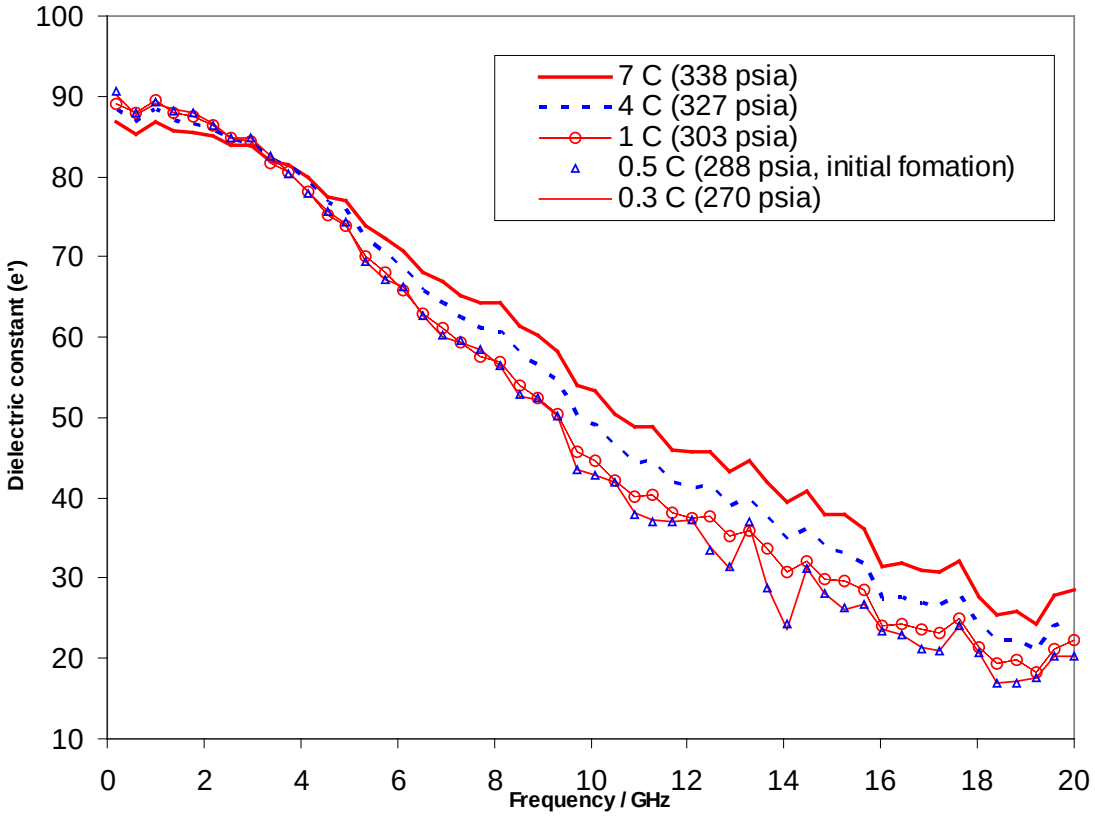

Figure 3.30 Natural gas hydrate formation.

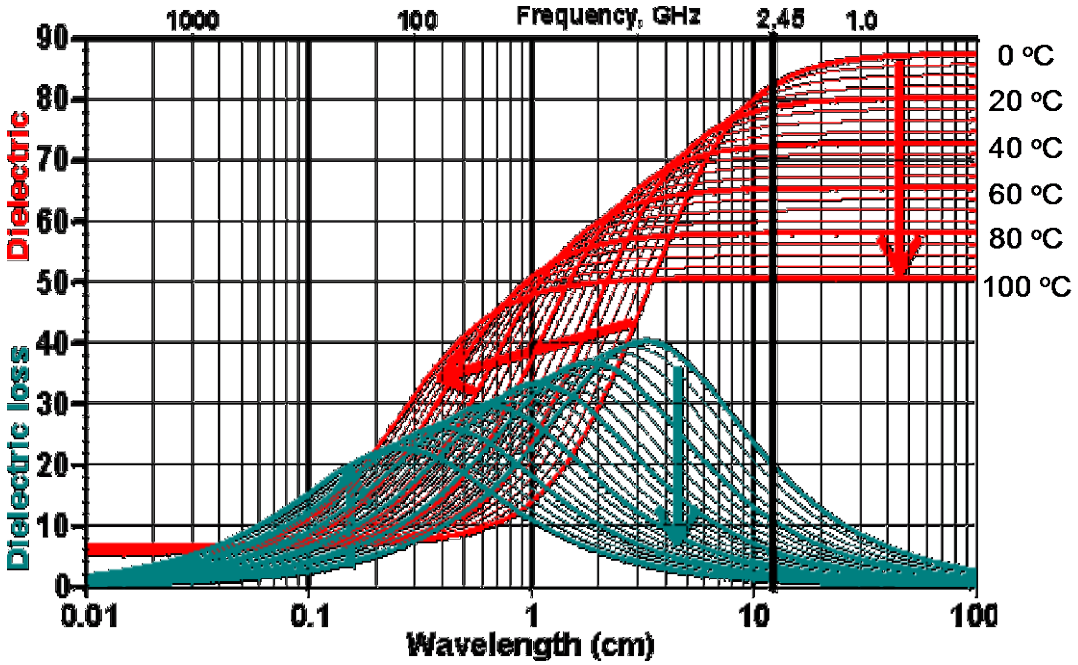

Figure 3.31 Dielectric permittivity and dielectric loss of water between 0 °C and 100 °C (Chaplin, M., 2004).

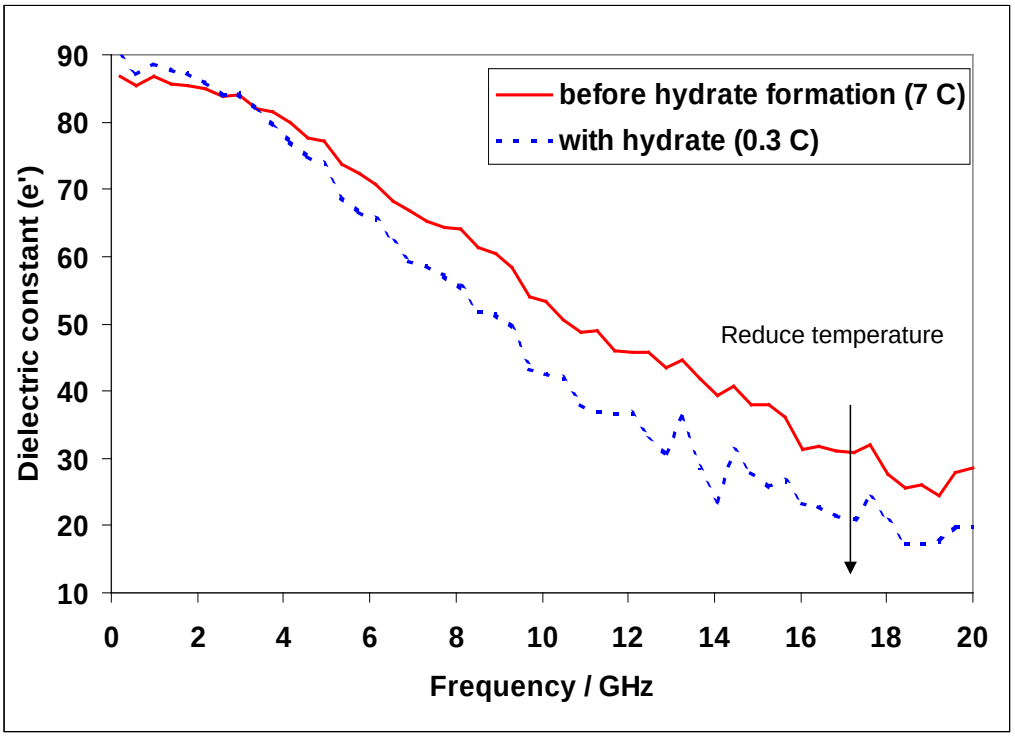

Figure 3.32 Detection of hydrate formation

3.4.2 Sustainability of water memory: Effect of Time

During hydrate dissociation in Step 2, the bath temperature was increased to 9 ^{o}C (i.e., outside the hydrate phase boundary). The system temperature was then stabilised at 9.6 ^{o}C for about 20 hours and several measurements were made at various time intervals. As shown in Figure 3.33, there is a gradual increase in dielectric constant at frequencies below 16 GHz as a function of time. However, at frequencies above 16 GHz, the value remains almost constant. We believe that this observation could be due to changes in the water memory and also slow release of gas from remnant hydrate memory. These have a more pronounced effect on the dielectric measurements at low frequencies. The differences in dielectric constant between before hydrate formation (measured at 7 ^{o}C) and after hydrate dissociation (measured at 9.6 ^{o}C) for 0 to 12 GHz with time (shown in Figure 3.34) clearly demonstrate this effect. As seen for the plot, the difference in dielectric constant is significantly reduced after 12 hours.

This result shows that the effect of hydrate water memory could remain for a much longer time in systems under pressure than that at atmospheric conditions. This could be evidence that the water memory is a strong function of dissolved gas, as the driving force for gas coming out of solution is reduced with an increase in the system pressure. This is also good news with respect to detecting any sign of hydrate formation in the pipeline using monitoring devices that are far away from the point of hydrate formation. The results of this work show that the effect of hydrate formation is still detectable 12 hours after hydrate dissociation in system under moderate pressure (i.e., 350 psia).

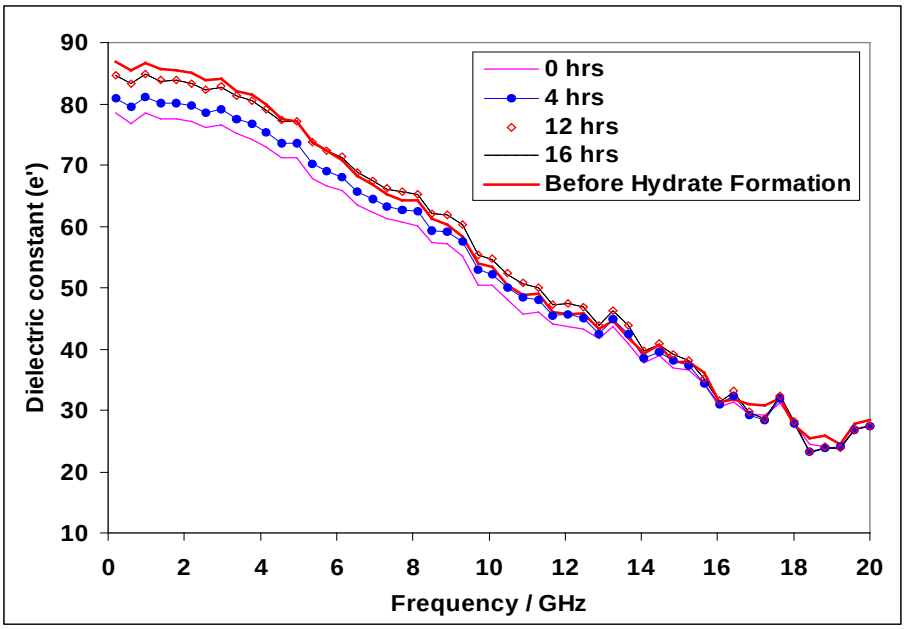

Figure 3.33 Presence of water memory and sustainability with time at 9 ^{o}C.

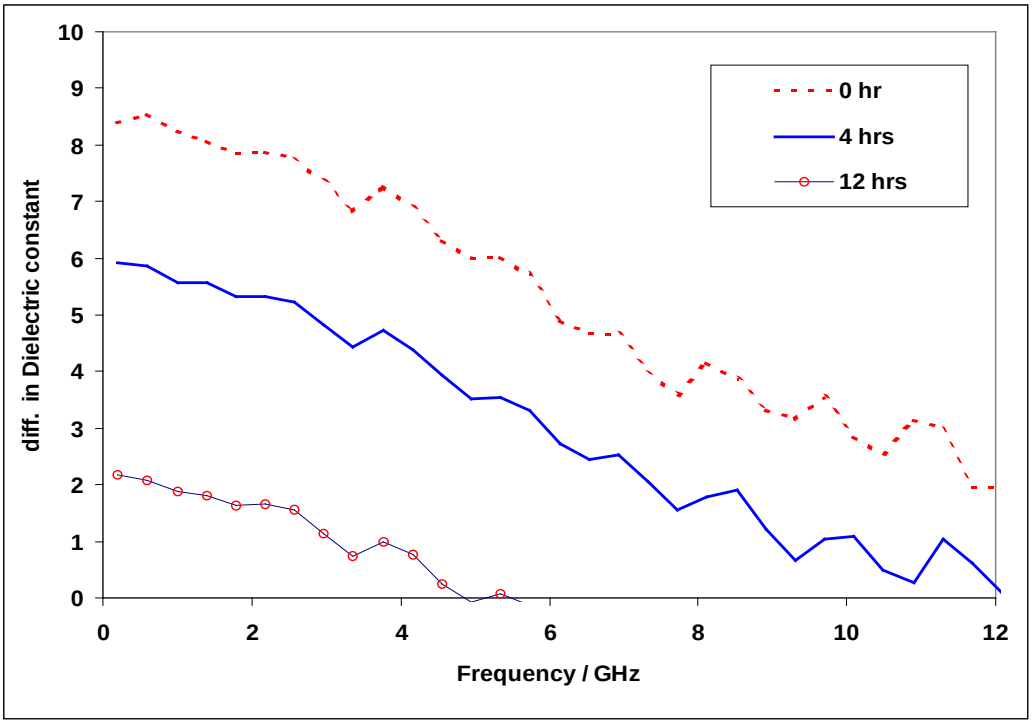

Figure 3.34 Effect of time. Differences in dielectric constant between before hydrate formation (measured at 7 ^{o}C) and after dissociation (measured at 9.6 ^{o}C), $\varepsilon'_{\text{before formation}} - \varepsilon'_{\text{after dissociation}}$);

3.4.3 Effect of heating

In Step 3 of the experiment, the system was further heated to 35 ^{o}C to observe the effect of heating on water memory. Dielectric constant measurements were made during heating process. As shown in Figure 3.35, there is a significant increase in dielectric constant with temperature at frequencies above 6 GHz. Opposite trend was observed at frequencies below 6 GHz. Again this observation is agreeable with that reported by Chaplin, M. (Chaplin, M., 2004) and shown in Figure 3.31. The system was stabilised at 35 ^{o}C for about 10 hours with dielectric constant reading remain unchanged with time.

In the final step of experiment, the system temperature was reduced to 9.6 ^{o}C (i.e., the initial hydrate dissociation temperature). The temperature was stabilised for 5 hours before measuring dielectric properties. Figure 3.36 shows the differences in dielectric constant between before hydrate formation (measured at 7 ^{o}C) and after dissociation & heating (measured at 9.6 ^{o}C). They illustrate the effect of heating on the water memory. It is important to note that comparison was made at different temperatures due to limited

data that could be generated using that set-up. The difference in dielectric constant between DW and HDW ($\varepsilon'_{DW} - \varepsilon'_{HDW}$) is significantly lower after heating as compared to after dissociation. This suggests that most of water memory was removed after heating.

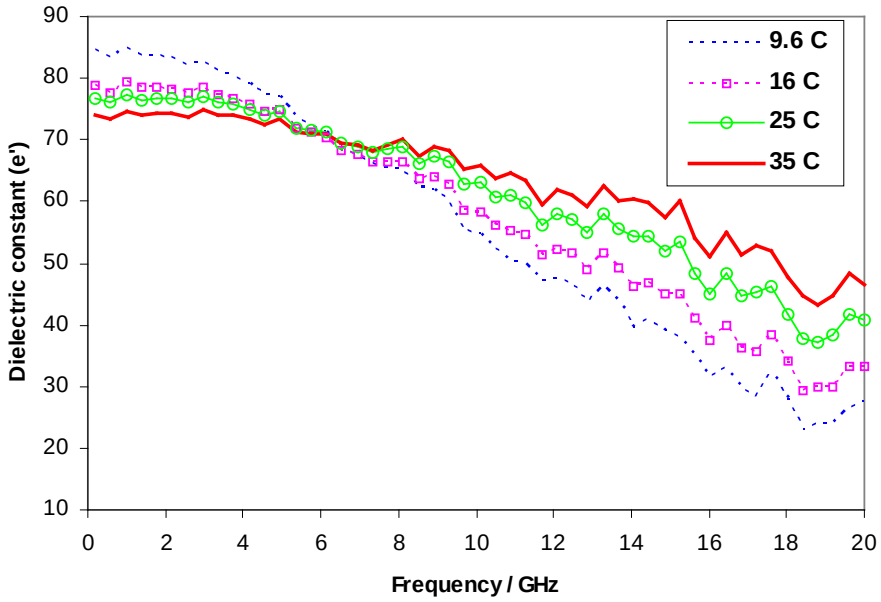

Figure 3.35 Effect of temperature on dielectric constant.

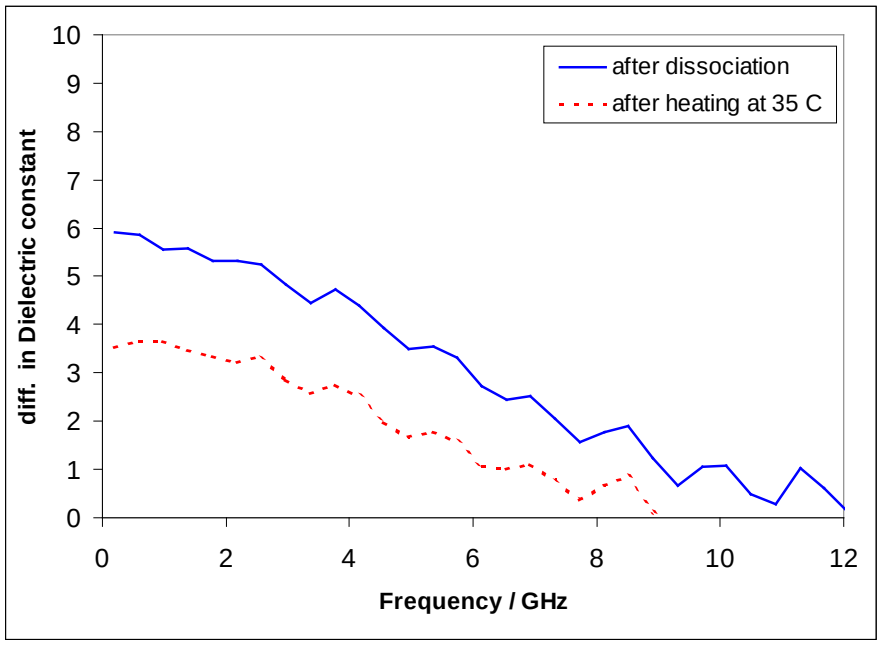

Figure 3.36 Effect of heating. Differences in dielectric constant between before hydrate formation (measured at 7 ^{o}C) and after dissociation & heating (measured at 9.6 ^{o}C), $\varepsilon'_{\text{before formation}} - \varepsilon'_{\text{after dissociation}}$); $\varepsilon'_{\text{before formation}} - \varepsilon'_{\text{after heating at 35 }^{o}\text{C}}$

3.4.4 THF-water system

Tetrahydrofuran **(**THF), as a water-soluble hydrate former, was studied. The objective was to investigate if water memory could be detected for these systems that do not have dissolved gas molecules in the system using dielectric technique. The dielectric constant was measured during THF hydrate formation and dissociation. The presence of water memory was also investigated for this system. The results as shown in Figure 3.37 indicate that dielectric constant is significantly reduced in the presence of solid hydrates (represented by circle). The dielectric constant is also sensitive to the presence of some hydrate particles (represented by triangle) during dissociation. Based on result in Figure 3.38, it was observed that there is no significant difference between dielectric constant after dissociation and after heating. This could be attributed to a very weak water memory presence in water-soluble hydrate former at atmospheric pressure, which is agreeable with the conclusion that dissolved gas plays an important role as a main factor contributed to water memory.

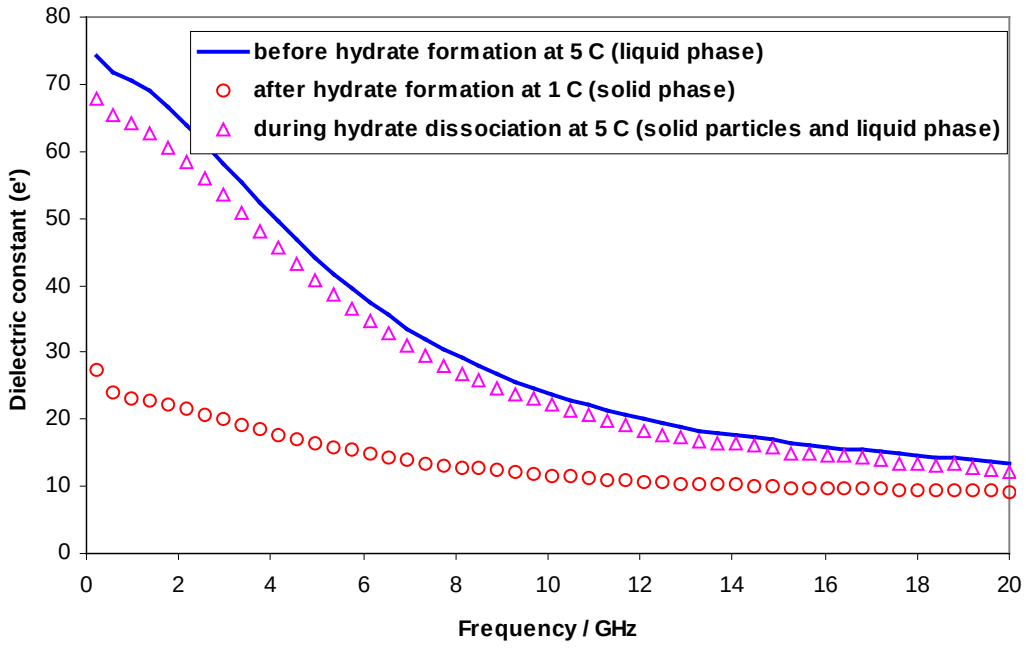

Figure 3.37 THF hydrate formation and dissociation

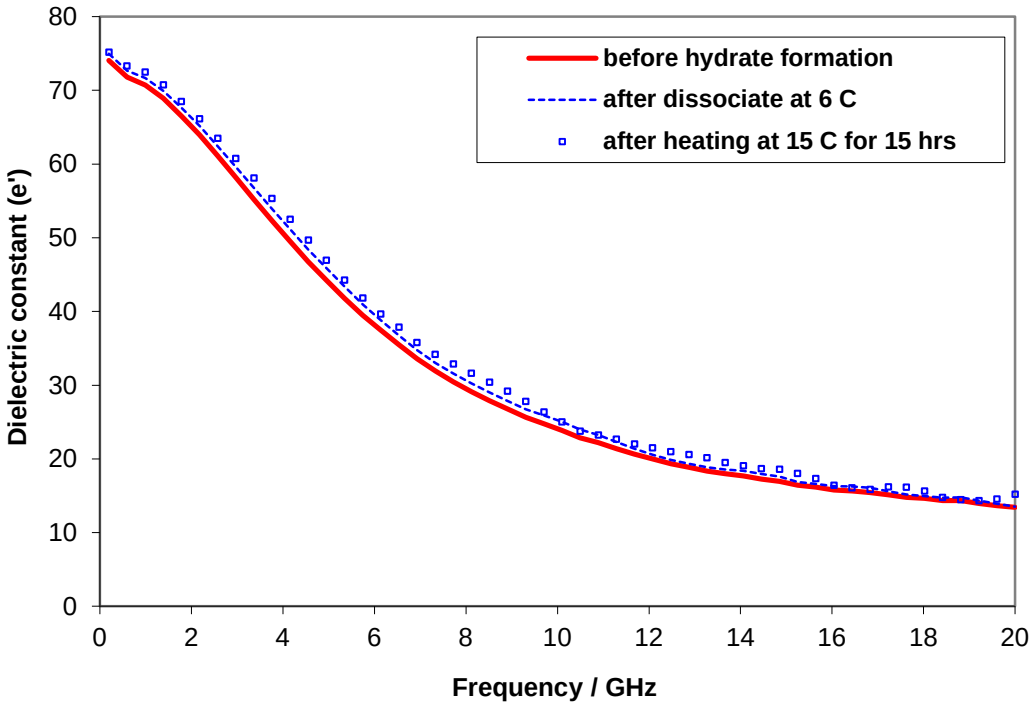

Figure 3.38 THF-Water system at 5 ^{o}C

3.5. SUMMARY AND CONCLUSIONS

In this chapter, a new approach for hydrate early warning system using dielectric properties was studied. The main idea was based on the phenomena of water memory which was extensively reviewed in Chapter 2. The experiments were designed to answer several key questions. These key questions are the potential application of dielectric constant as an indicator to detect the presence of water memory, the main factors contributed to the water memory (changes in water structure or dissolved gas or combination of both), the sustainability of water memory, the effect of heating, the effect of sample preparation path on water memory, the effect of sample preparation path on water structure, the effect of impurities and the water memory under pressure for potential on-line application. In addition, the presence of water memory was investigated for water soluble hydrate former, i.e. Tetrahydrofuran (THF).

The dielectric constant can be applied to detect the presence of water memory in a water sample after hydrate formation and dissociation. This is based on significant different in dielectric constant (measure with DW) between HDW and SDW. The results also suggested the presence of water memory is a combined effect of both dissolved gas and

presence of remnant water structure which remains for a longer time (2 to 3 hours) after hydrate dissociation as compared to the sample with dissolve gas at atmospheric and 4 ^{o}C. In practice, this result implies the produced water must be analysed within 2 to 3 hours after sampling to detect the presence of water memory as hydrate early warning.

The debatable phenomena on the hypothesis of main factors contributing to the presence of water memory were investigated in this thesis. The experiments was designed to confirm that water memory is mainly attributed to dissolved gas, which keeps the structure of water until the excess gas is evolved from solution. Investigation on the presence of water structure suggests that hydrate water memory is influenced significantly by dissolved gas which causes the water memory to remain for some time. The presence of water structure was found to be very weak based on the procedure adopted for this study. This results support the notion that hydrate water memory is mainly a function of dissolved gas.

The effect of heating on the water memory was investigated. The result confirmed that water memory is totally removed after heating at 35 ^{o}C for more than 12 hours. It was recognized that 12 hours heating time is too long for practical purposes. The effect of time required further investigation which could not be covered in this thesis.

In pipelines, hydrates may be dissociated through gradual change in temperature or pressure. To simulate this process, the hydrate water samples were prepared following different paths, along a depressurization track inside or just outside the hydrate stability zone. The effect of different depressurisation path on water memory was investigated. The result shows that the hydrate memory remain up to 1 hour for depressurization path inside hydrate phase boundary and approximately 0.5 hour for that outside hydrate phase boundary. Reduction in temperature and pressure from step by step dissociation cause significant release of soluble gas especially outside hydrate phase boundary and hence reduce the stability of water memory.

The compositional analysis of each aqueous phase was conducted at atmospheric pressure and room temperature after dissociation/depressurisation based on different paths. The results of analysis show that in the presence of hydrate water memory (for HDW samples), the ratio of C_2 to C_1 concentration is higher than that without water memory (for SDW samples). The ratio is significantly higher in the case of HDW

depressurised along the path inside hydrate phase boundary. This is likely due to the longer sustainability of water memory as detected by dielectric constant technique. The ratio of C_2 and C_1 concentration was higher in the case of HDWV as compared to SDWV. This indicated that even with the two stages vacuum procedure to remove excess dissolved gas, there was detectable dissolved gas present in the aqueous sample which may contribute to the water memory at the test conditions. This results support the finding from dielectric constant study that dissolved gas is the main factor contributing to the water memory of hydrates.

Investigation was done on Tetrahydrofuran (THF), a water soluble hydrate former, to further understand the influence of water structure on water memory in the absence of dissolved gas. The result shows that there is no significant difference between dielectric constant after dissociation and after heating. This could be attributed to a very weak water memory presence in water-soluble hydrate former and reduction of water activity at atmospheric pressure, which is agreeable with the conclusion that dissolved gas plays an important role as a main factor contributed to water memory.

The effect of salt (3 wt% NaCl) as impurities on hydrate water memory was investigated. The finding shows that the presence of salt has a negative effect on the memory. It is understood that the presence of salt in water, similar to THF, reduces the activity of water and solubility of natural gas in the water. It is expected that, the amount of gas hydrate form is less for the system with salt as impurity and hence reduces the water memory.

Potential online measurement technique for monitoring and early warning system of hydrate formation in the closed system such as pipeline is of interest to oil companies and filed operators. In this thesis, the potential application of dielectric properties measurement at medium pressure was investigated. The result shows that dielectric properties measurement can be applied to detect the initial hydrate formation and the presence of solid hydrate particles based on reduction of dielectric constant value demonstrated in this study. The water memory remains for a much longer time (12 hours) in the system under pressure than that of atmospheric conditions. This could be evidence that the water memory is a strong function of dissolved gas and remnant of hydrate nuclei which keep the memory for some period of time. The difference in dielectric constant between DW and HDW is significantly lower after heating as

compared to after dissociation. This again suggests that most of water memory was removed after heating.

The results demonstrate that dielectric properties at microwave frequencies has potential to be used as a downstream analysis and/or online system for detecting the initial hydrate formation and/or changes in the water memory due to hydrate formation. This could be used as an indicator for early warning system. The results are very encouraging and could make significant impact on the industrial approach to gas hydrate control strategy.

CHAPTER 4

INVESTIGATION OF WATER MEMORY BY ONSET OF ICE FORMATION

This chapter provides a background theory of ice nucleation and the technique adopted in this study to describe the stochastic nature of ice nucleation, nucleation probability distribution. The experimental measurement and analysis of results are discussed.

4.1. INTRODUCTION

The detection of water memory using onset of ice formation by freezing method was investigated as one of the potential techniques for hydrate monitoring and early warning system.

As discussed in previous chapters, hydrate formation and dissociation is known to change the water structure. It is believed that the resulting change in the water structure could have an impact on the ice formation. Therefore, it should be possible to detect the memory of hydrate formation by measuring the onset of ice formation. In this study, the nucleation probability distribution was employed to describe and analyse the random behaviour of onset of ice formation on selected water samples prepared for detection of water memory by dielectric constant described in Chapter 3 of this thesis.

4.1.1 Ice Nucleation Theory

Ice nucleation is conventionally divided into two categories: homogenous nucleation and heterogeneous nucleation. Homogeneous nucleation which is caused by the water itself, in that water molecules unite into a sufficiently large ice-like aggregate. Heterogeneous nucleation, where the nucleus formation is promoted by foreign substances with the capacity to organise water molecules into an ice-like pattern.

Freezing processes are initiated from a nucleus, which is assumed to organise the water molecules into an ice-like pattern. Pure water freezes at −42°C rather than at its freezing

temperature of 0°C if no crystal nuclei, such as dust particles, are present to form an ice nucleus.

The nucleation rate, I, depends on the average number of critical clusters, n* and the diffusion of molecules to the cluster, β.

$$I = \eta^* \beta \tag{4.1}$$

The average population of critical nuclei is

$$\eta^* = N \exp(-\Delta G^* / k_B T) \tag{4.2}$$

where:

- ΔG^* is critical free energy needed.
- N is the number of potential nucleation sites per unit volume
- k_B is the Boltzmann constant
- T is temperature

4.1.2 Nucleation Probability Distribution

Nucleation is a random phenomenon. The number of nuclei forming in a supersaturated medium within a given time interval is a random quantity. The kinetics theory of nucleation considers the average number of nuclei and relates it to the macroscopic parameters and properties of the system including the time (Toschev et al, 1972).

Takeya et al. (Takeya et al, 2000) investigated the stochastic nature of CO_2 hydrate nucleation to characterise the memory effect. It was reported that the nucleation rates significantly increased when the water had previously frozen as ice and melted (freezing-memory effect), except when the meltwater was heated to 298 K before nucleation. The nucleation rates also increased with O_2-saturated meltwater, but decreased with degassed water.

In this study, the nucleation probability distribution was employed to analyse the random behaviour of onset of ice formation for various types of samples. Based on nucleation theory (Toschev et al, 1972, Ohmura et al, 2000), the nucleation probability distribution P(t) can be expressed by

$$P(t) = 1 - \exp\{-J(t - \tau_o)\} \quad (4.3)$$

Where:

J = nucleation rate in a given volume of liquid

τ_o = the onset time of nucleation (i.e. the shortest induction time for onset of ice formation in this experiment).

The nucleation probability distribution for each water samples was obtained by repeating measurement of induction time under the same experimental conditions. The measurement was conducted using fresh sample each time. This was done for 16 samples based on maximum number of samples analysed within same day. The nucleation probability distribution $P(t)$ for nucleation occurring on or before time t_m (induction time measured for the m^{th} shortest induction time among 16 measurements) is given by $P(t_m) = m/16$. The nucleation probability distribution for various water samples was plotted against time. Figure 4.1 illustrates an example of the sample analysis. The nucleation rates J and the onset time of nucleation τ_o for various types of water samples were determined using best-fit to the experimental data of Equation (4.3).

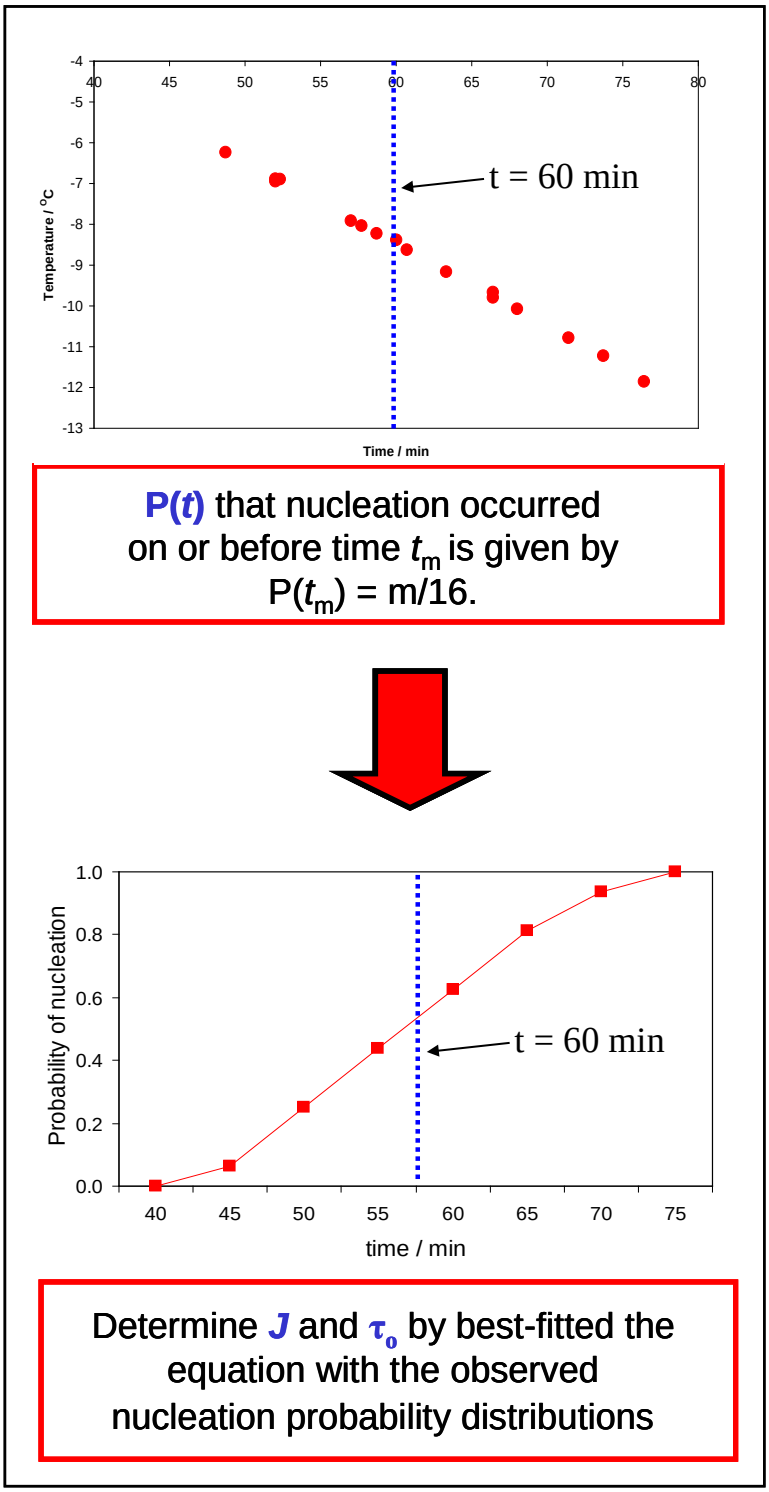

Figure 4.1 Determination of nucleation probability distribution

4.2. EXPERIMENTAL METHODOLOGY

4.2.1 Experimental facilities and material

Water samples prepared for detection of water memory using dielectric constant technique described in Section 3.2.3.4 of Chapter 3 was analysed. These samples are

hydrate deionised water (HDW), saturated deionised water (SDW), vacuumed hydrate deionised water (HDWV) and vacuumed saturated deionised water (SDWV) which was prepared using high pressure kinetic rig 2 described in Chapter 3.

The samples were analysed using freezing point depression apparatus shown in Figure 4.2. The apparatus consists of five platinum resistance temperatures (PRT) probes, four stainless steel tubes, and a controlled-temperature bath. Test samples of 1 ml volume are placed in the stainless steel tubes. These tubes are fitted with PRT probes and all tubes are immersed in the bath. The temperatures of all probes are recorded by feeding the analogue signal into a computer equipped with interface board. Natural gas supplied by Air Products with the composition listed in Table 4.1 was used in this study.

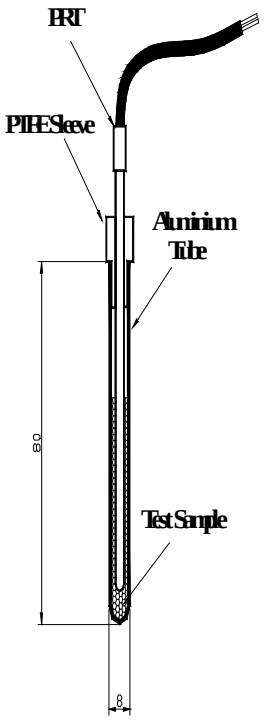

Figure 4.2 Freezing point depression apparatus (sample probe)

Table 4.1: Natural Gas Composition

Component	N_2	C_1	CO_2	C_2	C_3	iC_4	nC_4	iC_5	$nC5+C_6$	Total
Mole (%)	2.16	89.69	1.69	4.62	1.26	0.17	0.30	0.06	0.05	100

4.2.2 Experimental procedure

Water samples prepared by the different paths (inside and outside hydrate phase boundary) described in detail in Section 3.2 of Chapter 3 to study the onset of ice formation by freezing method. Each water samples were kept at constant temperature of 4 ^{o}C in the bath and atmospheric pressure. The onset of ice formation from various types of water samples was determined using the freezing point apparatus developed by HWU. The temperature of the system was reduced from 4 ^{o}C to -15 ^{o}C at a constant rate of 0.2 ^{o}C/min. The onset of ice formation was detected based on the rise of sample temperature as the latent heat of ice formation is released, as shown schematically in Figure 4.3. The onset temperature and corresponding induction time were recorded as the point at which ice crystals started to form. Due to stochastic nature of ice nucleation, several experimental data were generated to investigate the distribution of onset ice formation for these water samples.

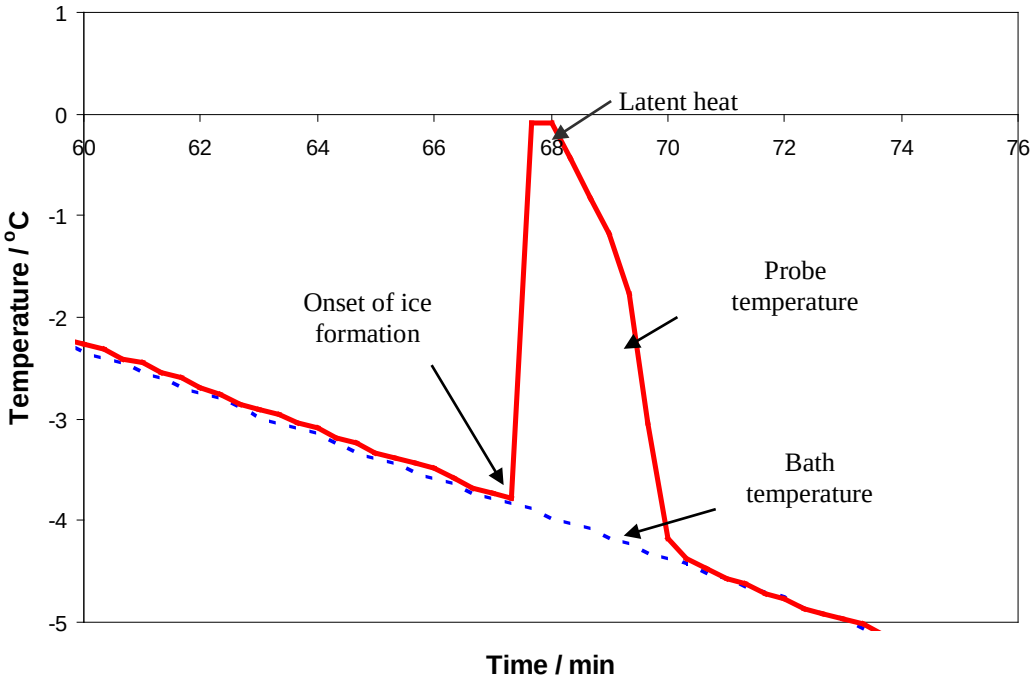

Figure 4.3 Determination of onset of ice formation

4.3. ICE NUCLEATION RATE: RESULTS AND ANALYSIS

4.3.1 Presence of water memory

Case 1: Sample preparation paths inside the hydrate phase boundary

The HDW and SDW samples preparation followed the path shown in Figure 4.4. Onset of ice formation was measured 16 times for each water sample to describe the distribution in terms of ice nucleation. The temperature distribution for onset of ice nucleation is plotted against time for all measured points as shown in Figure 4.5(a). These data are converted to the probability of nucleation for every 5 minutes time range (Figure 4.5(b)). In the last step, the nucleation rate is calculated using nucleation probability distribution described in the previous section by finding the best-fit to the relevant experimental data (Figure 4.6). The ice nucleation rate is used as an indicator for determining the presence of water memory. The ice nucleation rates for all samples measured for this study are tabulated in Table 4.1.

The result for this case shows that the ice nucleation for HDW equally distributed within 50 – 65 minutes (Figure 4.5 (b)). However, the distribution for SDW appeared to be more scattered within 70 - 75 minutes. The ice nucleation rate for HDW is higher than that of SDW (Table 4.1 and Figure 4.6) shows that samples with water memory nucleate faster most likely due to the presence of remnant water structure and dissolved gas from hydrate formation.

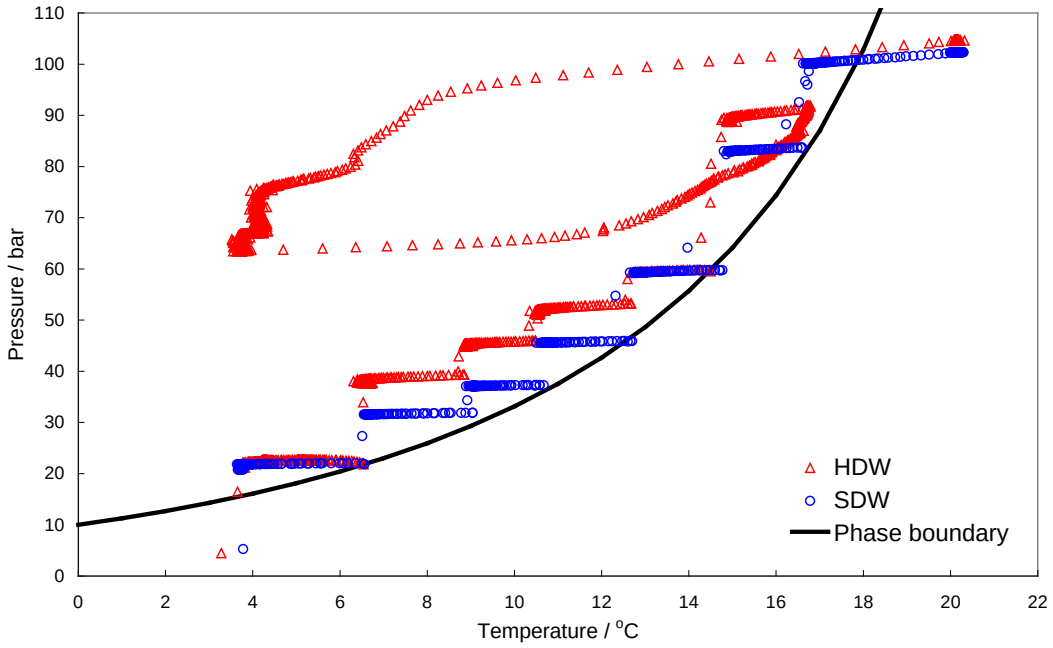

Figure 4.4 Sample preparation paths inside the hydrate phase boundary (Case 1)

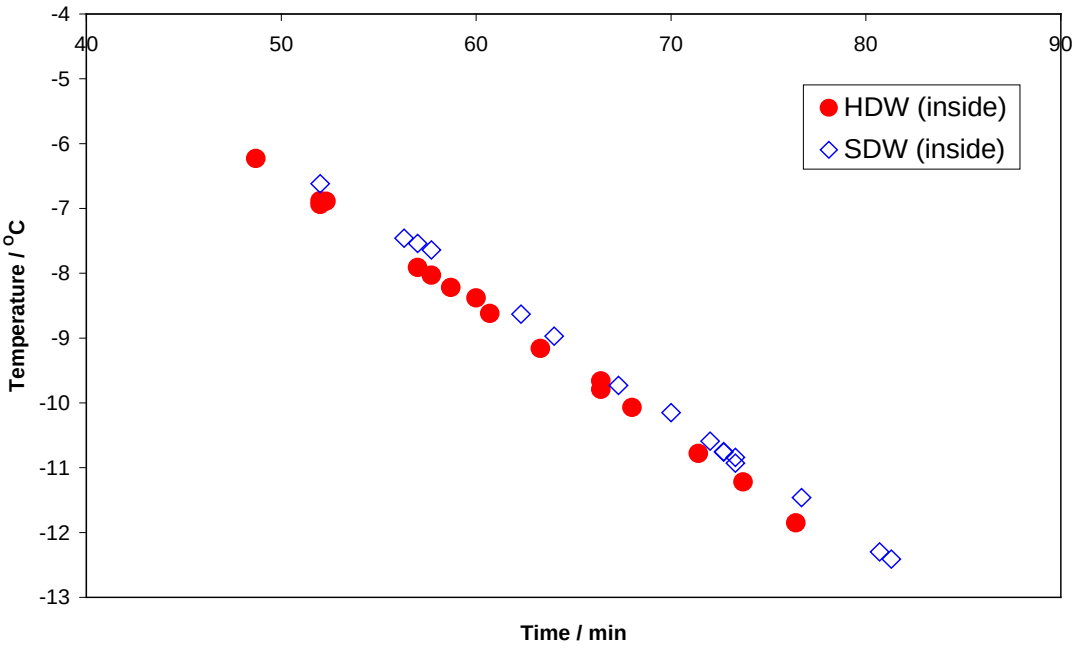

4.5 (a) Distribution of onset ice nucleation

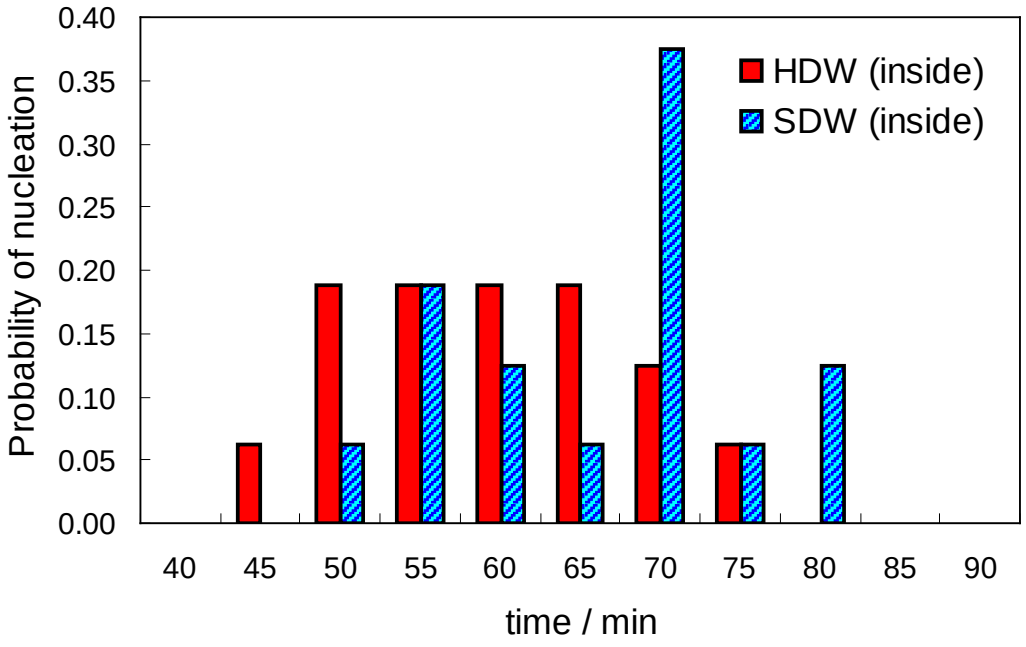

4.5 (b) Probability of ice nucleation

Figure 4.5 Onset ice nucleation for sample preparation paths inside hydrate phase boundary (Case 1).

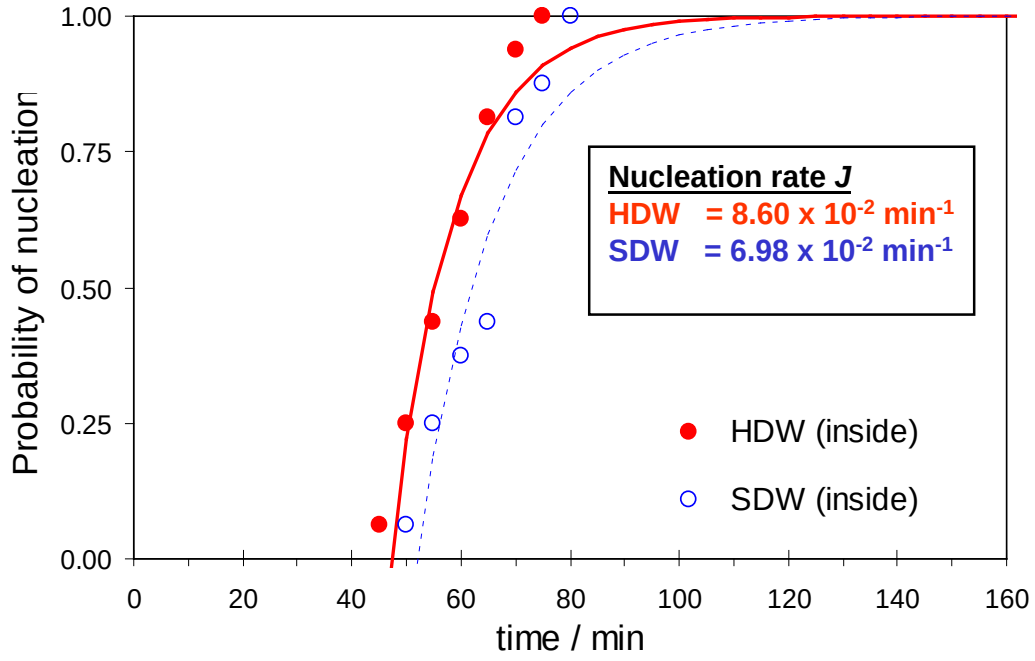

Figure 4.6 Nucleation probability distribution (inside hydrate phase boundary). The circles represent experimental data and the lines represent the best-fit relevant to experimental data.

Table 4.1 Nucleation rates for various waters

Experimental Cases	**Sample name**	***J* (x 10^{-2}) / min^{-1}**	**τ_0 / min**	**Sum Squared Error $\sum (P(t)_{exp.} - P(t)_{pred.})^2$**
Presence of water memory Case 1	HDW (inside)	8.60	47.1	0.013
	SDW (inside)	6.98	52.0	0.055
Presence of water memory Case 2	HDW (outside)	19.48	49.8	0.014
	SDW (outside)	8.75	48.1	0.015
Presence of water memory Case 3	HDW (inside)*	12.40	63.0	0.023
	SDW (outside)#	9.62	49.5	0.008
Presence of water structure	HDWV	10.88	52.5	0.058
	SDWV	9.16	48.2	0.056

Note:

** depressurised to atmospheric pressure to dissociate hydrate at 4 ^oC*

 # depressurised and reduced temperature with limited steps to reach 4 ^oC

Sum Squared Error: $\sum (P(t)_{observed\ value} - P(t)_{fitted\ value})^2$

Case 2: Sample preparation paths outside the hydrate phase boundary

The samples preparation paths outside hydrate phase boundary are shown in Figure 4.7. The distribution of ice nucleation for HDW is clustered within 50 – 65 minutes with the highest at 55 minutes as shown in Figure 4.8. For SDW, it is distributed within 45 – 80 minutes and peak at 60 minutes. The ice nucleation rate based on nucleation probability distribution showed that the rate for HDW is more than twice of SDW (Table 4.1 and Figure 4.9). This demonstrates that hydrate water memory does have significant effect on the ice nucleation. Hydrate water memory promotes higher rate of ice nucleation in comparison with that of dissolved gas. This is consistent with the trend observer in Case 1.

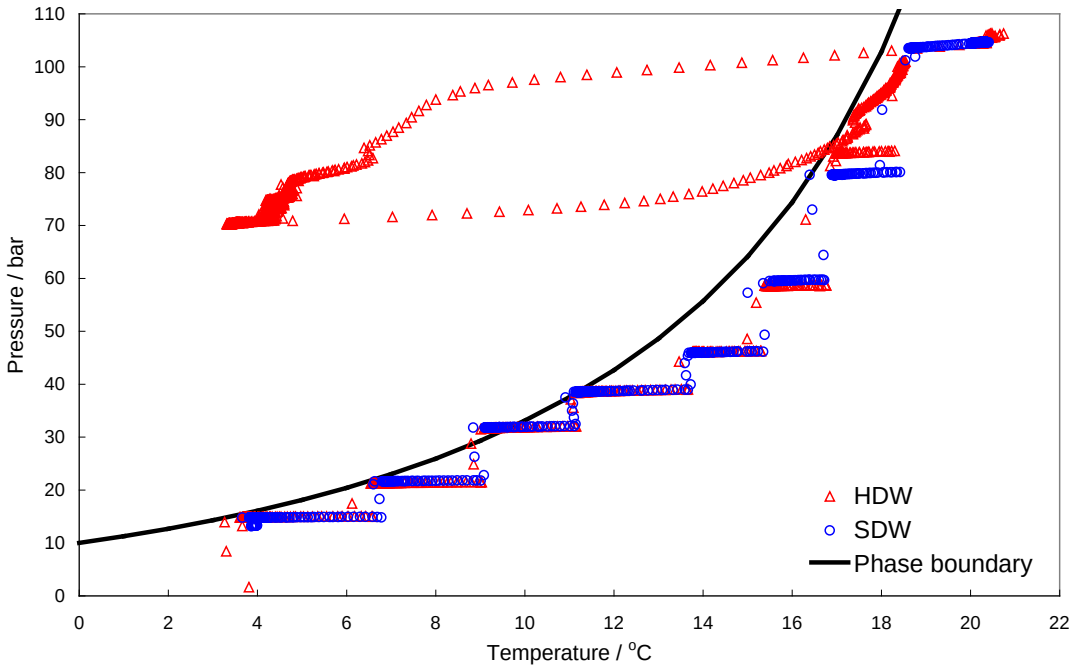

Figure 4.7 Sample preparation paths outside the hydrate phase boundary (Case 2)

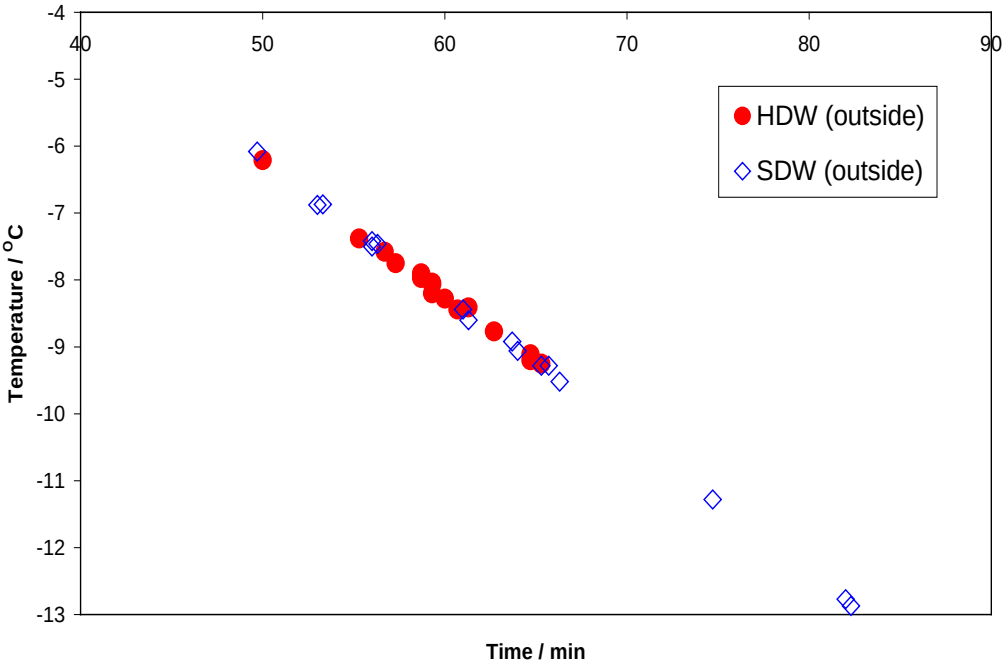

4.8 (a) Distribution of onset ice nucleation

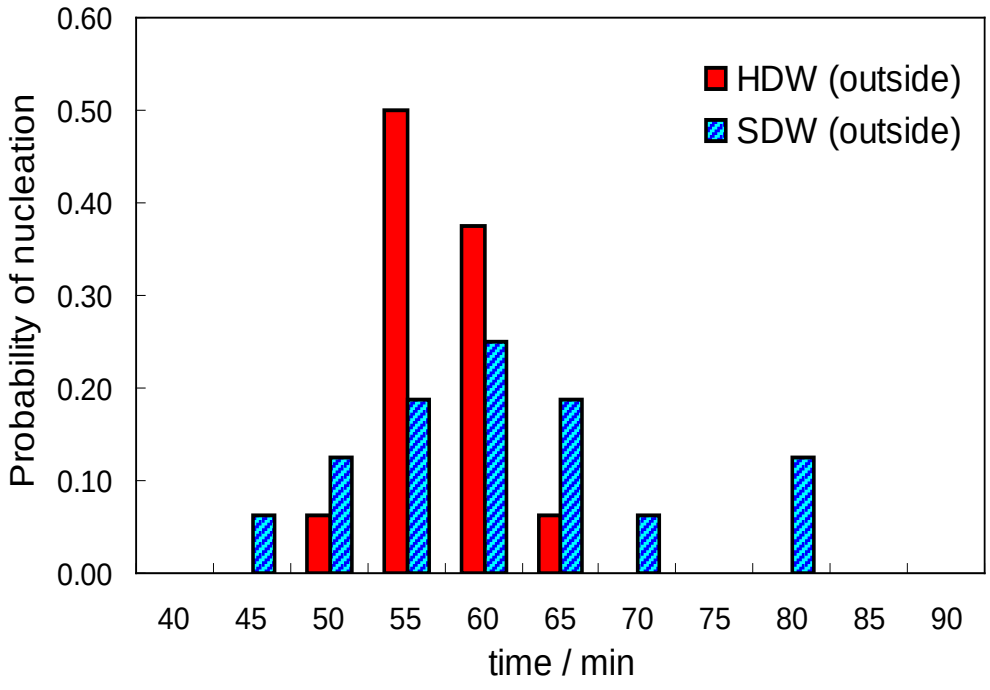

4.8 (b) Probability of ice nucleation

Figure 4.8 Onset ice nucleation for sample preparation paths outside hydrate phase boundary (Case 2).

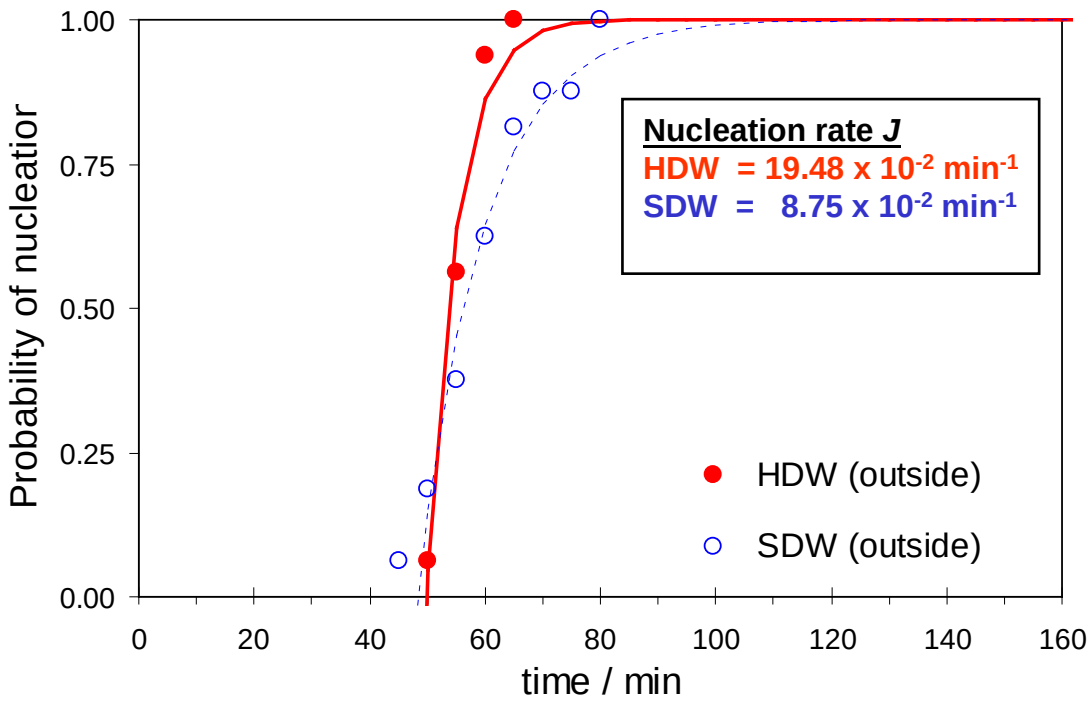

Figure 4.9 Nucleation probability distribution (outside hydrate phase boundary). The circles represent experimental data and the lines represent the best-fit relevant to experimental data.

Case 3: Sample preparation paths inside and outside the hydrate phase boundary

A different path was followed (as shown in Figure 4.10) for sample preparation to investigate the effect of dissolved gas and test procedure (and sample preparation) on the results. Here the SDW was prepared following much lower pressure conditions before measuring the onset of ice formation. The results of the onset of ice formation are presented in Figures 4.11(a) and (b). As shown in the figure the onset points of ice nucleation for the HDW sample appeared latter than that of SDW. The probability of ice nucleation for HDW is equally distributed between 65 – 80 minutes while that of SDW spread within 50 – 75 minutes and peak at 55 minutes. This could be due to higher gas concentration in the HDW than SDW, cancelling the promoting effect of water structure (as a result of hydrate memory) on onset of ice formation. It should be noted that ice structure excludes most hydrocarbon gases; therefore the presence of hydrocarbon gases could delay ice formation. On the other hand, the presence of hydrate structure could promote ice formation. Therefore, there are two competing factors, they are; 1) dissolved gas and 2) remnant hydrate structure. In the former cases, the presence of remnant hydrate structure was the dominating factor in ice formation, probably due to

similar gas concentrations. In the latter case, the high gas concentration in HDW seems to be the dominating factor in delaying onset of ice formation. Although HDW appeared to freeze later than that of SDW, the nucleation rate is higher for HDW as compared to SDW (Table 4.1 and Figure 4.12).

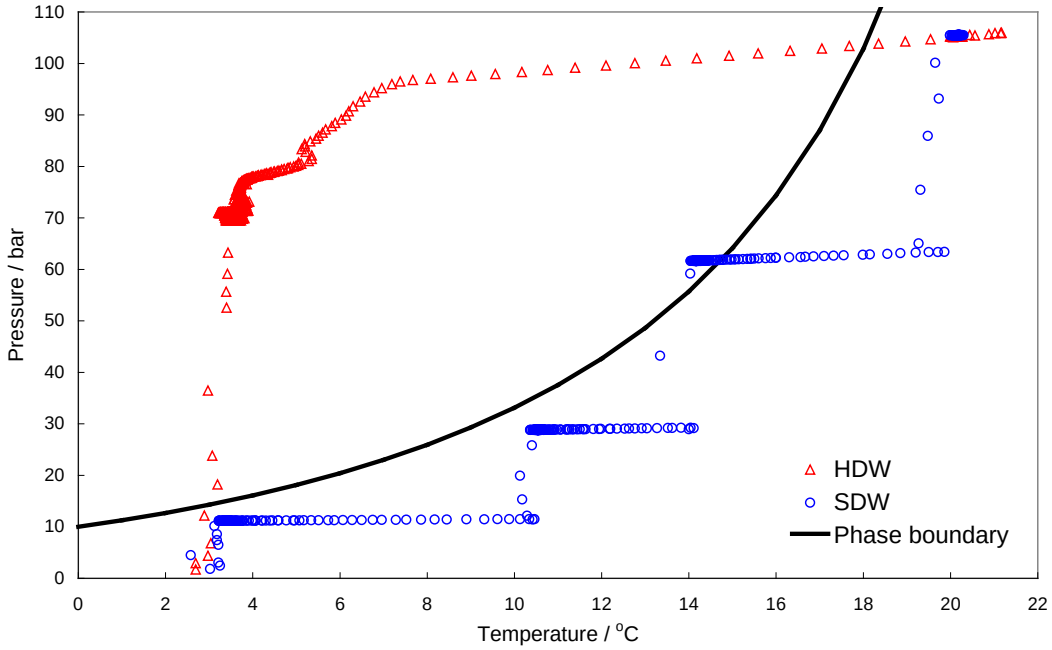

Figure 4.10 Sample preparation paths for HDW (inside the hydrate phase boundary) and SDW (outside the hydrate phase boundary).

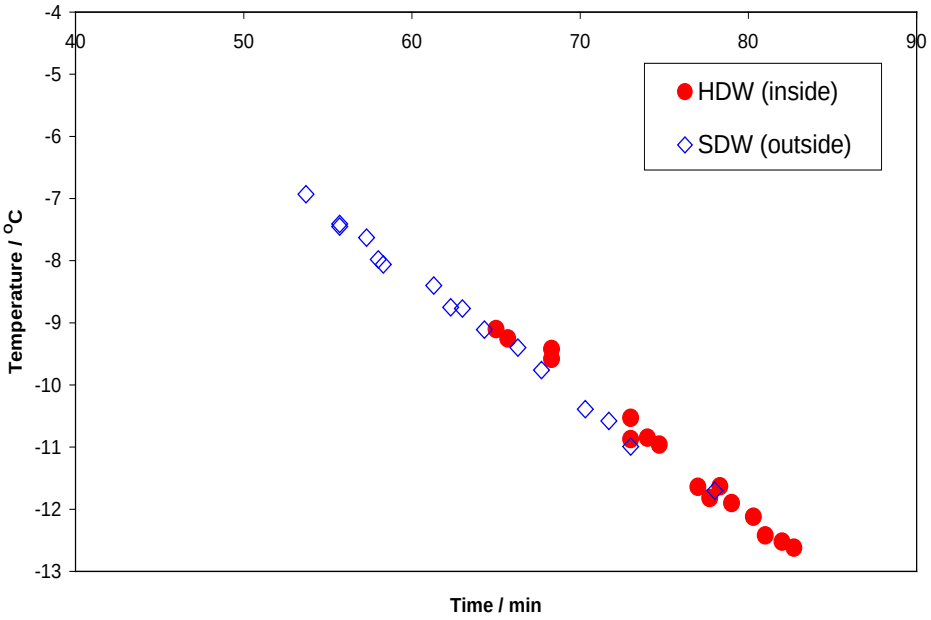

4.11 (a) Distribution of onset ice nucleation

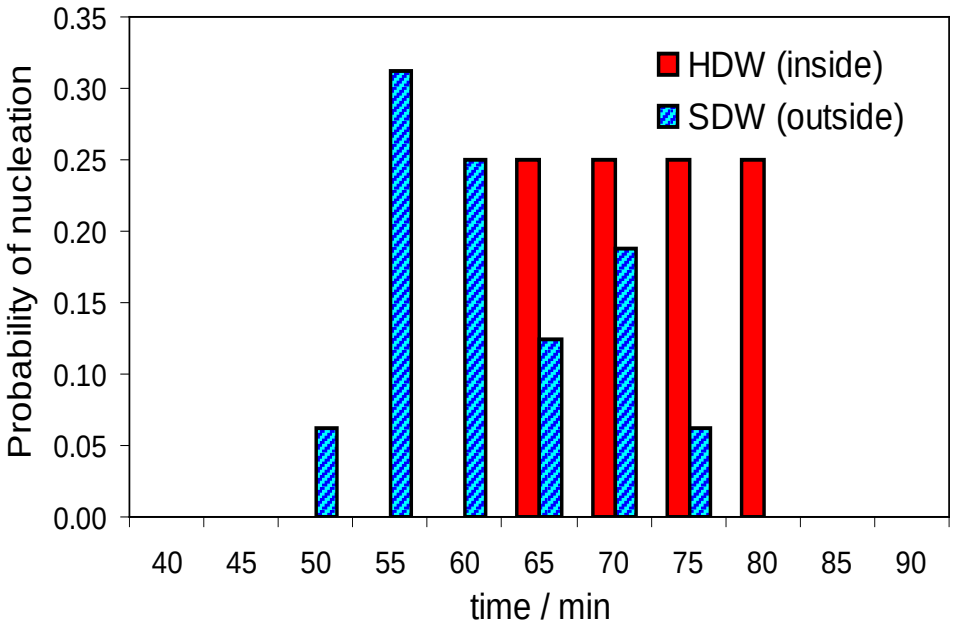

4.11 (b) Probability of ice nucleation

Figure 4.11 Onset ice nucleation for sample preparation paths inside and outside hydrate phase boundary.

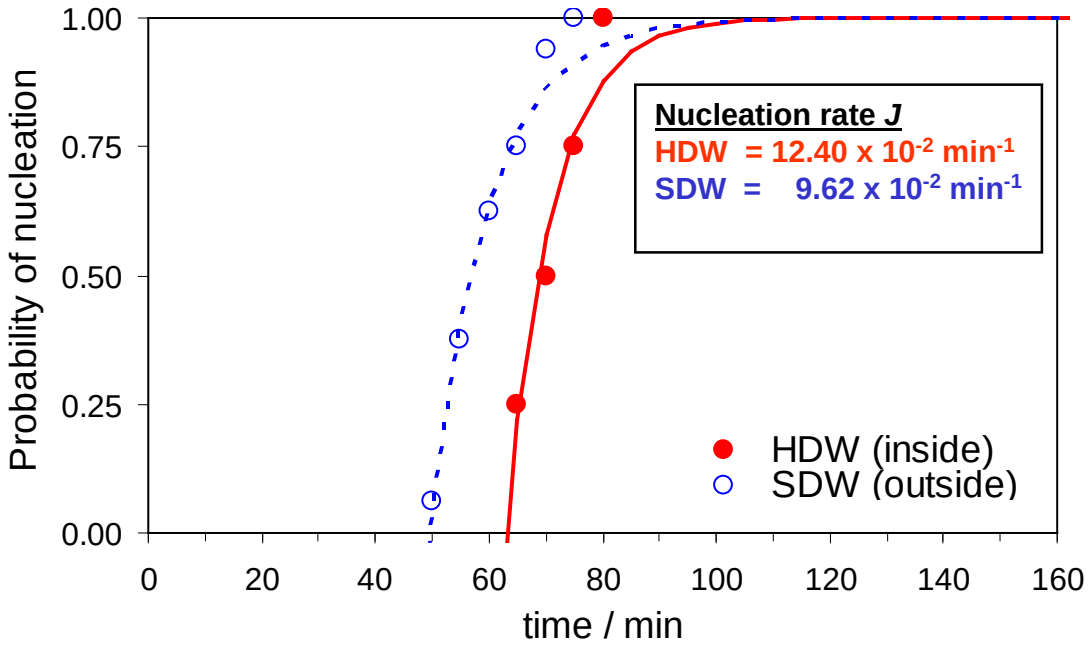

Figure 4.12 Nucleation probability distribution (inside and outside hydrate phase boundary). The circles represent experimental data and the lines represent the best-fit relevant to experimental data.

4.3.2 Presence of water structure

The effect of water structure on the onset ice nucleation was investigated by removing excess dissolved gas. The sample preparation paths are shown in Figure 4.13. The distribution of onset of ice nucleation for both HDWV and SDWV are almost overlapping, as shown in Figure 4.14 (a) and Figure 4.14 (b). Both samples have peaks at 65 minutes. This may indicate that by removing dissolved gas, there is no significant difference in the onset of ice formation. However, the ice nucleation rate for HDWV is slightly higher than that of SDWV (Table 4.1 and Figure 4.15), which may be contributed to the remaining water structure to some extent.

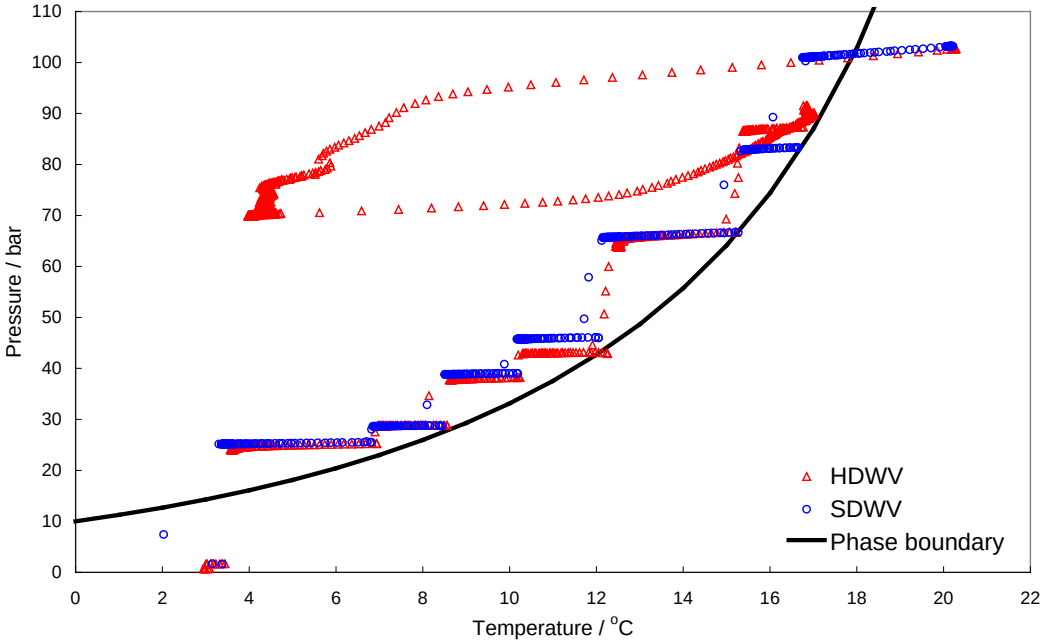

Figure 4.13 Sample preparation paths inside the hydrate phase boundary after removing excess dissolved gas

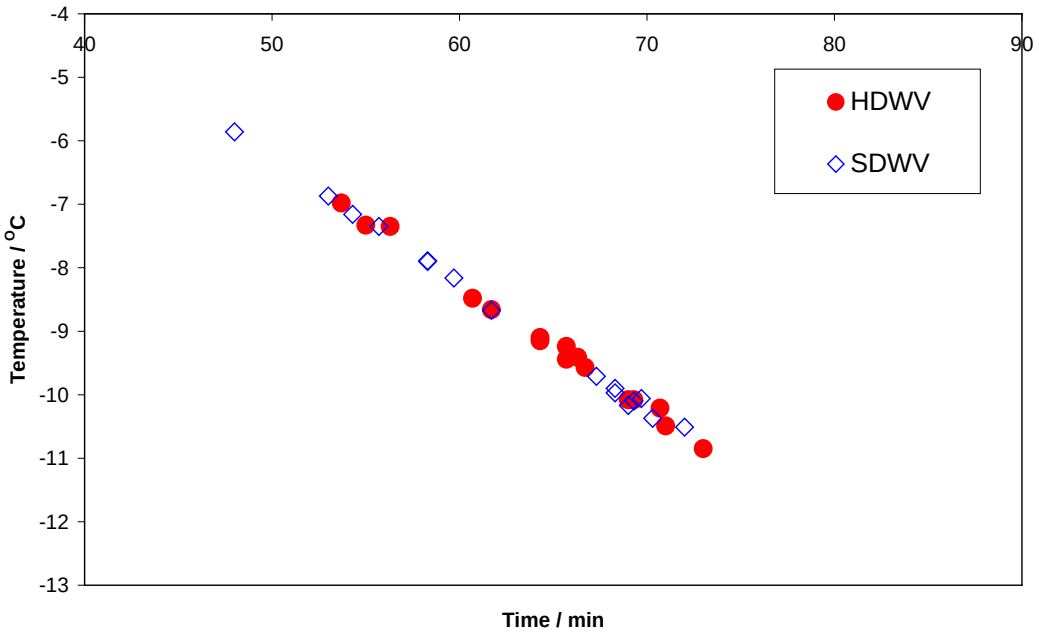

4.14 (a) Distribution of onset ice nucleation

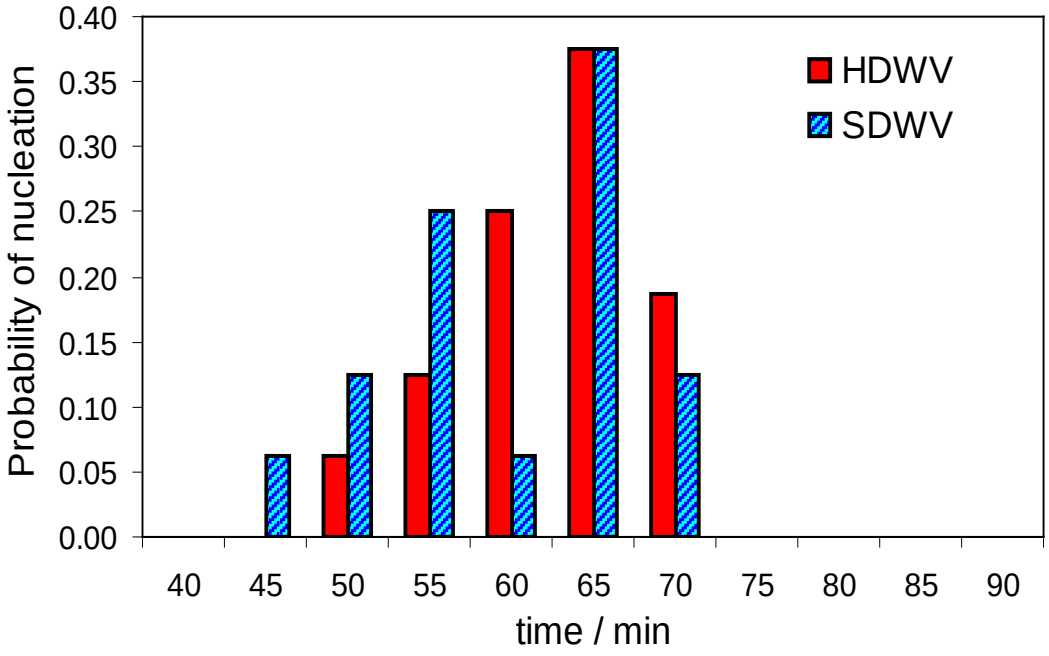

4.14 (b) Probability distribution of ice nucleation

Figure 4.14 The effect of removing excess dissolved gas on onset ice nucleation by depressurizing inside hydrate phase boundary

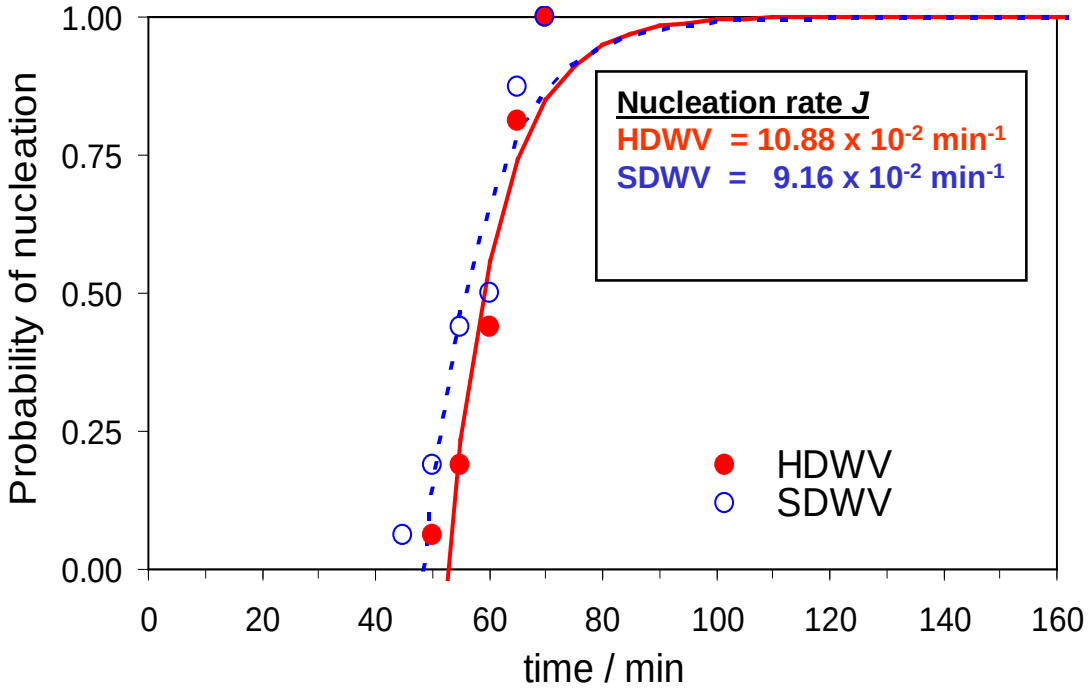

Figure 4.15 Nucleation probability distribution after removing excess dissolved gas (inside hydrate phase boundary). The circles represent experimental data and the lines represent the best-fitted relevant to experimental data.

4.4. SUMMARY AND CONCLUSIONS

Onset of ice formation by freezing method was considered as one of the potential techniques for early warning system. The main idea in this thesis is to generate data to investigate the applicability of onset of ice formation method, which could provide a simple method to detect memory of hydrate formation in produced water from the field.

In this work, two key factors influencing onset of ice formation were investigated. These factors are water memory and water structure due to presence of dissolved gas. The effect of different sample preparation paths on water memory was investigated. The nucleation probability distribution based on classical nucleation theory was applied to describe the stochastic nature of the nucleation data. The results suggest that the samples with water memory tend to freeze earlier and to nucleate faster than those without water memory regardless of the sample preparation paths are inside or outside the hydrate stability zone.

The role of dissolved gas in the sustainability of water structure was studied by removing excess dissolved gas. The results suggest that removing dissolved gas could

significantly eliminate the effect of water structure on ice nucleation, but the presence of water memory is still measurable based on the observed effect on ice nucleation rate.

As a conclusion, the results demonstrate that changes in water memory due to hydrate formation could be detected using freezing method. This could provide a simple method to identify the memory of hydrate formation in produced water, hence an early warning against pipeline blockage.

CHAPTER 5

LITERATURE REVIEW ON MECHANISM OF GAS HYDRATE FORMATION, INHIBITION AND MORPHOLOGY

In this chapter, a review of mechanisms of gas hydrate formation, inhibition and morphology is discussed. Available techniques for studying this aspect of gas hydrate were reviewed. Application of visual techniques in other petroleum related studies were described. The objective of the investigation under the scope of work of this thesis was detailed.

5.1. INTRODUCTION

Hydrate problems become more severe in deepwater developments due to higher pipeline pressures, lower temperature conditions and longer residence times associated with long tiebacks. Greater pressures are required to overcome the hydrostatic head of the fluid column produced at sea level as well as higher frictional pressure drop. Temperature conditions also tend to be below the hydrate formation temperature in most portions of the pipeline system. The potential for the formation of hydrates leading to blockages both during flow and restart of the cooled flow line are significant. Therefore, development of a hydrate prevention strategy is a crucial part of all deepwater projects. Uncertainty in a design resulted from imperfect knowledge of how hydrate behave in the systems leads to over design and increase in both capital and operating expenditure.

The equilibrium thermodynamic and structural properties of gas hydrates have been well established. However, there still remains a need for a fundamental understanding of the kinetic mechanisms of gas hydrate formation, decomposition and inhibition. Hydrate kinetic prediction in oil and gas production systems is a serious challenge for the industry due to limited tools to provide information such as rate of hydrate formation/growth or the morphology of crystals formed, the mechanism of hydrate formation and inhibition, the effects of multiphase flow regimes on the rate of mass

transfer of reactants and the rate of heat dissipation away from growing crystals (Matthews et al., 2002). Understanding these mechanisms will be critical to the development of new and improved technologies for controlling gas hydrate formation in subsea pipelines (Koh et al., 2002).

The focus of this study is to generate novel data on understanding mechanisms of gas hydrate formation and inhibition by Low Dosage Hydrate Inhibitors (LDHIs) for various fluid systems using visual techniques. In particular, understanding kinetic hydrate inhibitor (KHI) failure with the objective of finding clues to explain reason for their failure, hence hydrate formation mechanism.

LDHIs are described in detail in the following subsection (Section 5.1.1) of this chapter. In this work, the effect of various LDHIs on the hydrate inhibition and crystals morphology was studied. The efficiency of inhibitor with synergist and carrier fluid as well as compatibility of Kinetic Hydrate Inhibitors (KHIs) with corrosion inhibitor under dynamic condition was examined.

Several techniques are used to study kinetic of gas hydrate at macroscopic level which may not sufficient to understand and explain the phenomena involved. Hence, the visual technique provides the understanding at mesoscopic level of kinetic hydrate formation. The visual technique will be a new procedure incorporated into laboratory protocol for investigating kinetics of hydrate formation, inhibition and evaluating performance of LDHI under both static and dynamic conditions.

5.1.1 Low Dosage Hydrate Inhibitor (LDHI)

In the recent years, kinetics inhibition of hydrates with/without controlling the growth and agglomeration of gas hydrates has been implemented by the industry as an alternative technology to avoid hydrate in the pipeline, due to various constraints posed by thermodynamic inhibitor. Developing low dosage chemical such as kinetic (Sloan et al., 1995) or anti-agglomerant (Long et al., 1996) inhibitors is an alternative technology to thermodynamic inhibitions.

The idea of low dosage hydrate inhibitors (LDHI's) came from a simple observation that certain fish did not freeze in sub-zero temperature waters (Franks et al., 1987). This is due to the secretion of a protein that bound itself on microscopic ice crystals and prevented their subsequent growth. Evidence of antifreeze proteins lead to the discovery of kinetic hydrate inhibitors (KHI's), sometimes also referred to as threshold hydrate inhibitors (THI's).

LDHIs are divided into two basic categories; Kinetics Hydrate Inhibitors (KHIs) and Anti-Agglomerants (AAs). KHIs delay the nucleation and growth of hydrate crystals for substantial periods of time. It prevents the formation of hydrate crystals by docking on extremely small microscopic crystals and retards their further growth. These polymers are added at a low concentration typically less than 1 weight%. The first generation of KHIs were all water soluble polymers that were either polyvinylpyrolidone (PVP) or polyvinylcaprolactam (PVCap) ring based compounds (Sloan, 1994; Kelland et al., 1995). The basic structure of these polymers is shown in Figure 5.1. In this thesis, most of the KHIs tested are polyvinylcaprolactam based polymer.

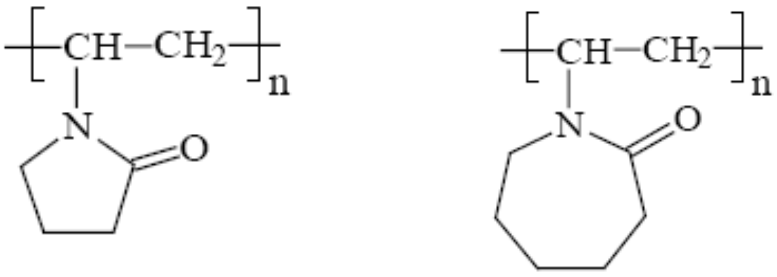

(a) (b)

Figure 5.1. The structure of (a) polyvinylprrolidone and (b) polyvinylcaprolactam (Kelland, 2006)

AAs work to prevent agglomeration of hydrates so that the hydrate crystals do not grow large enough to plug the flowlines, hence hydrates transported as slurry. The action of AAs is based upon having "hydratephilic" head that is incorporated within hydrate crystals and a "hydratephobic" or "oleophilic" tail that disperses the hydrates into liquid

hydrocarbon phase (Mehta et al, 2002). Organic quaternary ammonium and phosphonium salts with one or two long oleophilic tails are the most powerful types of AAs. The basic structure is shown in Figure 5.2. Sloan (Sloan et al, 2008) recently summarised the development of both kinetic inhibitors and anti-agglomerant in chronological order.

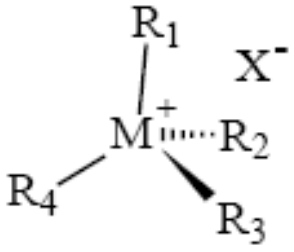

Figure 5.2. The structure of quaternary ammonium or phosphonium hydrate growth inhibitors, where M = N or P and at least 2 of the R groups are n-butyl, n-pentyl or iso-pentyl (Kelland, 2006)

The performance of LDHI's for required inhibition is based on induction time and subcooling. These are usually evaluated using kinetics rigs, autoclaves and/or flow loops. The induction time is defined in practice as the time elapsed until the appearance of a detectable volume of hydrate (Sloan, 2000). Figure 5.3 illustrate typical profile of measuring induction time at isothermal and/or isobaric conditions to simulate the field operating conditions. The subcooling (ΔT_{sub}) is a measure of the driving force for hydrate formation in systems which represent the difference between the hydrate dissociation temperature (T_{eq}) and the operating temperature at a given pressure (T), where $\Delta T_{sub} = T_{eq} - T$.

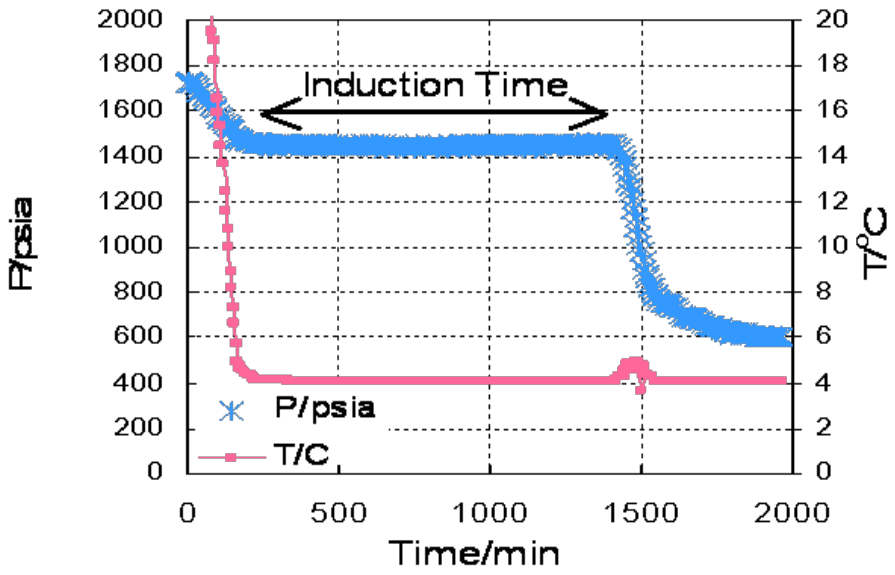

Figure 5.3. Typical plot for induction time determination.

There is a relationship between degree of subcooling and induction time. The higher the degree of subcooling (i.e. driving force for hydrate formation) the lower the induction time. However, AA's is reported to be independent of subcooling and it requires the presence of a liquid hydrocarbon phase to suspend the hydrate crystals. Mehta et al (Mehta et al., 2002) noted that the new KHI's have an upper subcooling limitation of approximately 20 ^{o}F while deepwater developments often have subcooling requirement of 35 – 40 ^{o}F. With this limitation, AAs represents an important hydrate inhibitor particularly in ultra deepwater.

Kelland (Kelland, 2006) extensively reviewed the research and history of the development of LDHIs with emphasis on the chemical structures that have been designed and tested. The mechanism for kinetic hydrate inhibition by water-soluble polymers is still not fully understood although several models have been presented. Despites successful field trials and applications of KHI (Bloys, et al., 1995; Corrigan, et al., 1996; Notz, et al., 1996; Leporcher, et al., 1998; Pakulski, et al. 1998; Argo, et al. 1999; Talley, et al, 1999; Mitchell, et al, 1999; Fu et al., 2001; Lovell, et al., 2002; Boyne et al., 2003; Budd et al., 2004; Glénat, et al., 2004), the mechanism remains unclear and required further understanding.

Research for the development of new experimental techniques for probing and recording microscopic interactions with time is required (Paez et al., 2001). Therefore, this study aims at contributing to the understanding of mechanism of hydrate inhibition using visual techniques.

5.1.2. Kinetic of Gas Hydrate Formation, Inhibition and Morphology

The mechanism of gas hydrate formation and inhibition by KHI had been previously reported by various researchers using several techniques (Koh et al., 2002; Lee et al., 2005, 2006; Ohmura et al., 2003; Taylor et al. 2007). For example, Koh et al. (2002) studied the structural transformation of water around methane during methane hydrate formation using neutron diffraction over temperature range of 4 – 18 ^{o}C and at pressures of 3.4 – 14.5 MPa. The result shows that the hydration sphere around methane in liquid change significantly when methane hydrate is formed, with the water shell in the crystalline hydrate being larger than the shell in liquid. The effect of Poly(N-Vinylpyrrolidone (PVP), VC-713[1] and Quaternary Ammonium Bromide (QAB) on Tetrahydrofuran (THF) hydrate formation at the surface and bulk solution was examined using a multi cell photo-sensor instrument (MCPSI) and Differential Scanning Calorimetry (DSC). Both measurements show that QAB exhibits the greatest crystal growth inhibition compared to PVP and QAB. On the other hand VC-713 has greatest influence on delaying hydrate nucleation. Lee et al. (2005) reported unusual kinetic inhibitor effect on gas hydrate formation for methane-ethane mixture at 273.7 K and 5100 kPa using water droplet and water contained in cylindrical glass column. The experiment was conducted in the presence of kinetic inhibitor GHI 101 and Luvicap EG. The unusual behaviour observed when water droplet in the presence of inhibitor collapsed and spread on the Teflon surface prior to hydrate nucleation. This is believed to be due to the droplet undergoes a hydrophobic to oleophilic transformation in the presence of kinetic inhibitor. Hydrate crystal formed in a narrow cylindrical glass column in the presence of GHI 101 grew upwards along the wall of the column. Ohmura et al. (2003) investigated the effect of kinetic inhibitors, PVP and PVCap, on formation and growth of structure-II hydrate crystals at the liquid/liquid interface

[1] Terpolymer of vinylcaprolactam (VCap), vinylpyrollidone (VP), and dimethylaminoethyl methacrylate (Sloan et al., 2008)

between HCFC-14b (CH_3CCl_2F) and inhibited water phase at atmospheric pressure. PVcap shows longer inhibition effect than PVP on the growth along the interface although it causes little change in the hydrate-crystal morphology. PVP promote crystal growth into the aqueous phase while retarded the growth along the interface. PVP also significantly changes the morphology of hydrate in both the interface and in the aqueous phase.

Crystal morphology studies provide valuable information on the mechanisms of hydrate crystal nucleation, growth and decomposition (Servio, 2003). The various geometries of hydrate crystal morphology are attributed to factors such as the hydrate forming gas, the subcooling and the pressure.

Hydrate kinetics can be broken into two main stages: nucleation and growth (Figure 5.4). In nucleation, microscopic hydrate clusters grow and break down attempting to exceed a critical size for stability. Once a sufficient concentration of nuclei has become stable, they begin to grow and agglomerate. Once sufficient hydrate particles are present, a growth stage is observed until the reaction begins to terminate due to mass or heat transfer limitations and compositional changes.

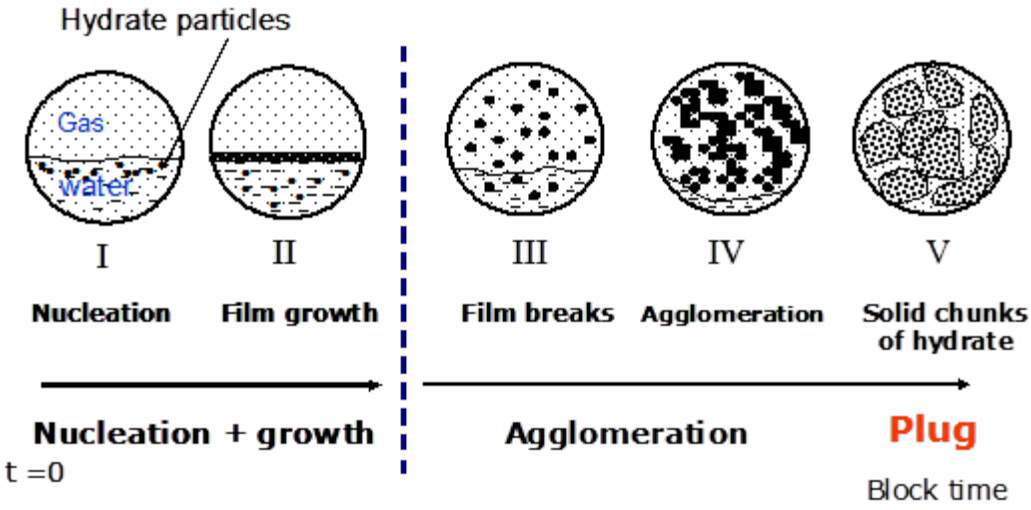

Figure 5.4. Schematic of hydrate plug formation in the pipeline (taken from Lingelem et al., 1994

5.2. TECHNIQUE FOR THIS STUDY

5.2.1 Review Experimental Techniques

There is a wide range of experimental set-up used to perform LDHI hydrate study. It ranges from low cost atmospheric pressure glassware equipment using THF as the hydrate former to a very expensive large scale flow loops using multi-barrel quantities of recombined live oils. A review of experimental techniques for studying gas hydrate formation and evaluating performance of LDHI (Table 5.1) shows that the High pressure reactor is the most common techniques to evaluate the performance of LDHI.

Talley et. al. (Talley et. al., 2002) had made comparison of laboratory results on hydrate induction rates in a THF rig, HP rocking cell, Miniloop and large flowloop. Based on these comparisons, flowloop was recommended for ranking kinetic inhibitors according to subcooling and induction times as a function of concentration. This is based on the preferred conditions of reproducible driving force and reliable hydrate detection. Large scale flowloop pilot plant for studying hydrate formation, plugging tendencies and the nature of plugging mechanism was reported by Matthews et.al. (Matthews et. al., 2000). Subcooling measured in the flowloop was found to be comparable to that measured in the field near hydrate formation plug. Palermo et. al. (Palermo et. al., 2000) reported the use of pilot loop tests to study the efficiency of threshold hydrate inhibitor (THI178) and kinetic inhibitor (THI370) under multiphase flow conditions. Sinquin (Sinquin, 2003) described experimental approach which includes semi batch reactor, laboratory loop and pilot loop used by France Petroleum Institute.

In this work, the kinetics of gas hydrate formation and inhibition for various fluid systems (gas-water, gas-oil-water, condensate-water system) are studied using visual techniques in the HP glass micromodel and glass capillary tube under static and dynamic conditions. The scope of work will incorporate the investigation of crystal growth and characteristic behaviour of hydrate plugging with and without LDHI (KHI, and AA) at various simulated pipeline conditions.

5.2.2 Visual Techniques

5.2.2.1 High Pressure Glass Micromodel

Micromodel studies (by means of 2D micromodels) have been around since 1961 when first reported (Mattax et al., 1961). It has mainly been used as a qualitative tool to study phenomena related to the flow of fluids in porous media. The application of glass micromodel is reported by several researchers. Corapcioglu et al. (Corapcioglu et al., 1999) carried out extensive literature review on the application of glass etched micromodels and glass bead micromodel for solute transport study.

Visualisation techniques are extensively applied for reservoir flow studies in a simulated pore structure under high pressure conditions to model microscopic phenomena. At Heriot Watt University several applications of glass micromodel has been reported. Sohrabi et al. (Sohrabi et al., 2000, 2001) reported the application of glass micromodel for visual observation of oil recovery by WAG injection in different wetting system. The wettability alteration in porous media was also investigated using glass micromodel by Buckley (Buckley, 1996). McDougall et al. (McDougall et al., 1998) examined the complex interaction between interfacial tension and buoyancy forces during gas evolution within porous medium containing oil, water and gas.

Other application of glass micromodel are investigating the pore scale behaviour of the Solution Gas Drive in Heavy Oil (Bora et al., 2000, 2003), the flow of oil through polymer gel (Al-Sharji et al., 1999; Grattoni et al., 2001), multiphase flow in porous media during water injection (Sun et al., 2004) and kinetics crystal growth of calcium carbonate (Dawe et. al., 1997).

Limited reported application of visual technique using glass micromodel for studying mechanism of gas hydrates inhibition and its morphology. Previous reported study was on visualisation of hydrate formation in porous media (Tohidi et al., 2001; 2002; Anderson et al., 2001**).** The study was focused on visual observation of hydrate formation from both a free gas phase (methane - water) and from dissolved gas only (Carbon dioxide - saturated water). It was reported in these studies that nucleation sites or water history (i.e. remnant ice structures) are required to form hydrates from dissolved gases for low solubility gases such as methane at low pressure (<8 MPa).

This is mainly due the pressure limit of the micromodel set-up which is 8 MPa (Anderson et al., 2001), hence low concentration of these gases.

Similar set–up was used to study the novel application of glass micromodel for Hydrate risk in WAG injection operation (Bashir et al., 2002). Preliminary application of glass micromodel for testing and evaluation of LDHI at static condition was reported (Yang et al., 2003).

In this study, High Pressure Glass Micromodel was developed and modified to study mechanism of gas hydrate formation and inhibition in the presence and absence of several LDHI at high pressure to mimic conditions in pipeline particularly for deepwater application. The effect of LDHI on hydrate crystals morphology was also investigated under static condition. The details are reported in Chapter 6 of this thesis.

5.2.2.2 Dynamic Multichannel Flow Conduits and Glass Capillary Tubes

Capillary Flow measurement or tube blocking method has been a laboratory test protocol adopted throughout the industry for evaluating performance of scale inhibitors (Zhang, et al, 2001; Graham, et al, 2002; Bazin, et al, 2005). Application was also reported for detecting asphaltene deposition by Broseta et al. (Broseta, et al., 2000). To our knowledge, the application of this technique is not being reported elsewhere for evaluating LDHIs with the exception of publication by Jonap, et al. (Jonap, et al., 2005). However, technique reported by Jonap, et al. is not a visual technique.

In our study, detail measurement of visual observation via dynamic multichannel flow conduit and glass capillary blockage technique to evaluate performance of LDHI is described (Chapter 7). The efficiency of inhibitor in the presence of synergist material and carrier/solvent fluid is examined. The performance of KHI in the presence of a corrosion inhibitor was also studied.

5.3. SUMMARY

The second part of this thesis is to investigate the mechanism of gas hydrate formation/growth, inhibition and morphology by Low Dosage Hydrate Inhibitors (LDHIs) by means of visualization technique for evaluation LDHI performance. These

techniques are based on visual observation in high pressure glass micromodel, multichanel flow conduit and glass capillary tube blockage. Therefore, this chapter provides an overview of mechanism of gas hydrates formation, inhibition and morphology based on published literature for system with and without LDHI. Techniques for studying the kinetic gas hydrate formation and inhibition was also review to support a novel technique adopted for this thesis.

Table 5.1: Experimental Techniques for Studying Gas Hydrate Formation and Evaluating Performance of LDHI

No	METHOD	SAMPLE	MESUREMENT INDICATOR/CRITERIA	INHIBITOR /ADDITIVES	REF.
1.	Rotated test tube with steel ball	Water-THF	• Induction time (> 1 hr) • Tube blockage (ball stop time > 6 hrs)	1500 commercial products	Lederhos et. al., 1996
	HP Autoclave reactor (300 mL)	NG-water (DI & 3.5 wt% salt)	• Induction time • Rate of gas consumption (initial, 10 hrs and final)	PVP, Pvcap, VC-713, Poly (VP/VC)	
2	HP Autoclave (750 mL) - pre-screen LDHI	Recombined black oil (Exxsol D60) with syn gas- water (oil-water system)	• Visual: (no hydrate > 50 hrs, Mobile slurry, no solid) • Thermal • Torque • Gas consumption	Surfactant, Polymer, Patented chemicals	Lund et. al. , 1996; Urdahl et. al., 1995.
	HP Wheel flow simulator (13.6 L)		• Degree of subcooling at hydrate initiation • Visual Hydrate macrostructure (slurry, slush powder like hydrate) • Flow resistant by Torque to correlate with visual (apparent fluid viscosity, deposits on the pipe wall and clogging of hydrate lump)		
3	HP Sapphire cell	Oil-water-gas system	• Induction time • Initial hydrate growth rate • Extent and time to agglomeration/plugging of the cell • Total hydrate conversion (gas consumption) and water conversion factor		Kelland et.al.,1994

4	HP Cell (300 cc)	Gas Condensate system: H_2O-HC* - NG * c6,c7,c8,c9,c10,c12	• Torque from motor current due to viscosity change, dispersion formation and plug formation; motor current > 50 mA - plug form	AA	Huo et.al., 2001
	Sapphire Screening Apparatus with steel ball	80% Octane - NG	• Ball stop time	AA+PVCap Small amount of AA (0.1-0.5 wt%) improve PVCap performance by 40.	
	Optical Cell (HP Visual Cell) with mixer	Octane-Di-water-NG	• Visual (> 5 days)	Commercial & custom design Colorado School of Mines Non-ionic surfactant	
5	HP Reactor with turbidimetric sensor	Water-methane	• Induction time • Gas rate consumption • Hydrate particle size distribution • Number of particles	KI	Cingotti et. al., 1999; Herri et al., 1999.
6	Acoustic resonance spectrometer	NG-water	• Detect onset formation: Sharp change in frequency at the onset due to sharp sonic speed change at the entrapment of NG by water molecules		Sivaraman, 2003.
	Differential Scanning Calorimeter	THF-water	• Onset and dissociation: Heat flow vs temp. • Time, temp. transformation (TTT) curves: Nucleation and growth kinetics	Methanol, PVP, PVCap, AA	
7	Viscometer	THF, CO2,NG	• Induction time	PVAP, Mirawet ASC, BASF F-127	Kalbus, 1995.

8	HP Sapphire Cell	Ethane/SNG/condensate-SNG mixture with synthetic salt water	• Induction time • Gas consumption rate	PVCAP	Startaas et. al., 2000
9	Multiple Additive Screening Equipment (similar to #1 and #4 with steel ball)	THF-water	• Appearance of crystal (turbidity) indicate induction time • End of formation indicate by stopping ball which correspond to blockage time	PVP, VC 713, THI178D, PVCap	Monfort et. al., 2000.
	Stirred reactor	Ethane and Propane-water system	• Gas consumption rate • Particle size distribution		
10	Flow loop plant (Quantify rheology of water in oil emulsion prior to crystallization & effect of dispersant additive on hydrate slurry behaviour after cryst.)	Methane-water-dedecane	• Flow rate • Rheology of hydrate slurry by Viscosity	PVP	Dufour et. al., 2000.

11	HP stress controlled rheometer • Time cure test (static approach, no gas bubbling and dynamic approach, gas bubbling) • Stress ramp test (stress vs strain profile: no flow behaviour or flow behaviour)	Gas-water and gas-water-oil systems	• Sudden increase in moduli – hydrate formation • Stress vs strain profile for degree of hydrate consistency - gas hydrate flow or do not flow	PVCap, PVAP, Anti-agglomerant	Chiappa et. al., 2003.

CHAPTER 6

INVESTIGATING INHIBITION MECHANISM OF KINETIC HYDRATE INHIBITORS (KHIs) BY VISUAL OBSERVATION OF GAS HYDRATE FORMATION, GROWTH PATTERN AND MORPHOLOGY

This chapter describe detail analysis of visual observation via High Pressure Glass Micromodel and Multichannel Flow Conduits. The performance and inhibition characteristics of typical commercial LDHIs were investigated by visual observation of hydrate morphology, growth patterns and hydrate particle size. This novel data will provide clues to explain reason for LDHI failure.

6.1. EXPERIMENTAL METHODOLOGY

6.1.1 Experimental Facilities and Materials

The heart of the micromodel facility is consisted of two glass plates, one with 2-dimension micro-models etched onto its surface and a plain cover plate, as shown in Figure 6.1. The models can be changed into geometrical networks, such as multi-channels pipeline configuration (Figure 6.2) which was used to study under dynamic/flowing condition. As shown in Figure 6.3, the micromodel is mounted in a steel vessel, subjected to a confining (overburden) pressure and fitted into its housing. The cover plate has an inlet and outlet, which allows fluids to be pumped through the enclosed model network. For studying gas hydrate formation, inhibition and morphology at static condition, fluids are injected and drained through the inlet and outlet valves using pistons operated by an HPLC pump or High precision Quizix pumps. System temperature is measured by a probe mounted under the model. The pressure transducers are connected to the model inlet and outlet lines for measuring system pressure. A digital magnifying camera was used to make video footages and take photographs of the glass micromodel during hydrate formation and dissociation. Modification were made to the high pressure micromodel (Figure 6.4) to further

improve the data capturing, visual observation and fluid injection paths (i.e., multi way valves system). This system was further modified to cater for the study under dynamic/flowing conditions which is described in the Chapter 7.

The natural gas composition for studying the mechanism of hydrate formation and morphology supplied by Air products is given in Table 6.1. All LDHI chemicals (Luvicap EG®, HI03-187, HI03-24, HI03-22) used in this study were supplied by Clariant Oil Services except PVCap base polymer and HT04-049 (BASF advanced polymer) which were supplied by BASF. The detail of the KHIs is provided in Table 6.2 of this thesis.

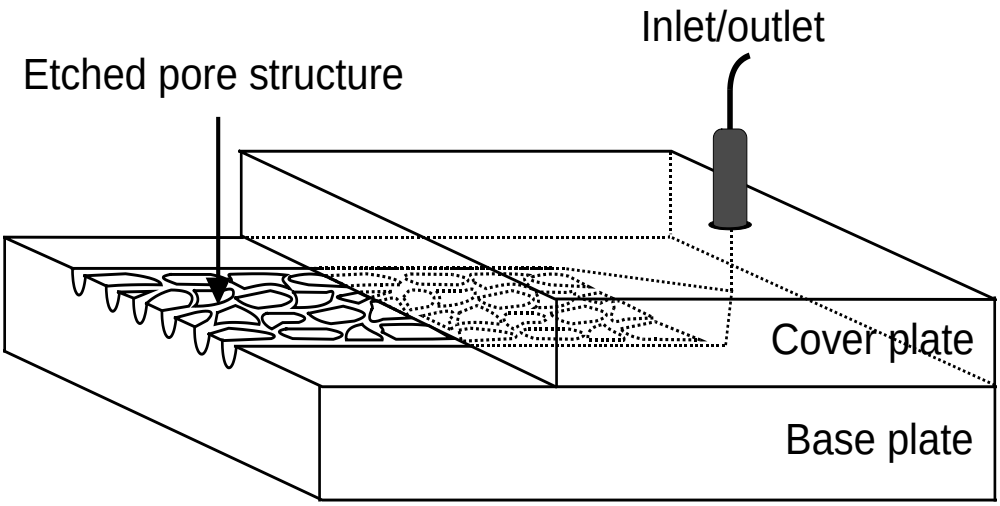

Figure 6.1 Basic glass micromodel pore structure network

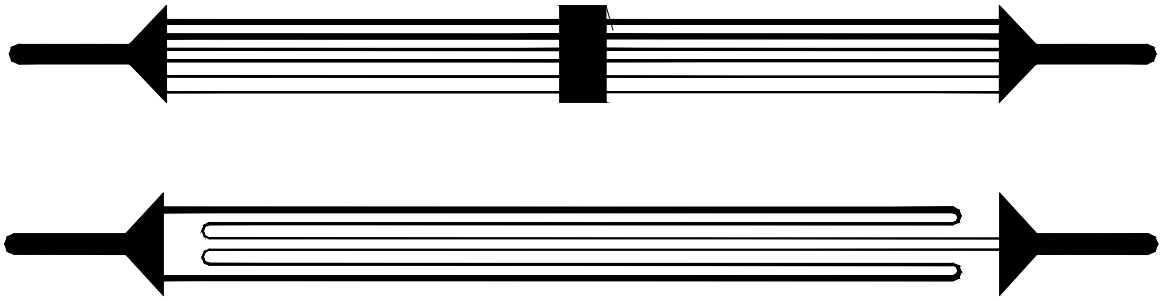

Figure 6.2 Multichannel glass conduit

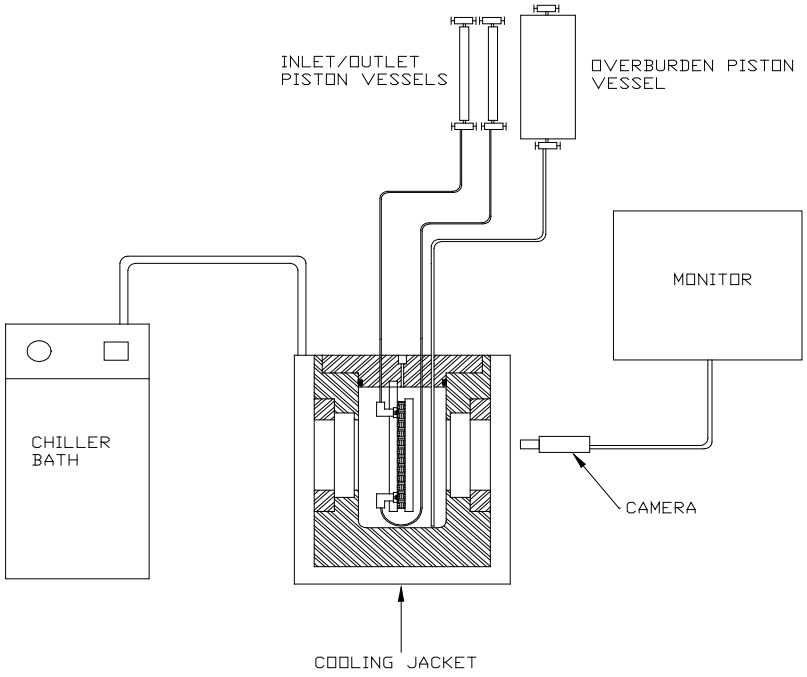

Figure 6.3 Experimental set-up

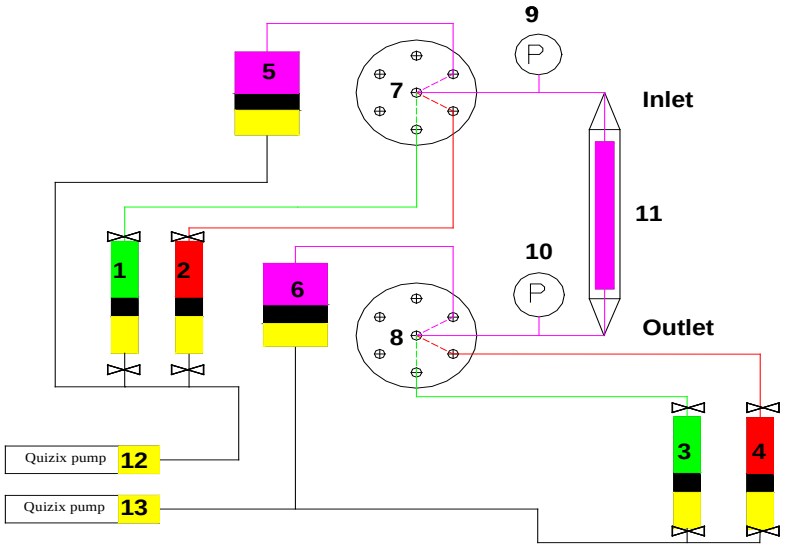

Description:

1 - 4: sample cylinders
5 - 6: cleaning cylinders
7 – 8: switching valves
9 – 10: inlet and outlet pressure transducers
11: Micromodel
12 – 13: High precision quizix pump

Figure 6.4 Schematic diagram of the HP Micromodel set-up

Table 6.1 Natural Gas Composition

Component	Mole%
N_2	3.86
CO_2	1.5
C_1	86.49
C_2	5.71
C_3	1.63
i-C_4	0.2
n-C_4	0.35
i-C_5	0.08
n-C_5	0.08
n-C_{6+}	0.1
Total	100

Table 6.2: Information on KHIs used for this study

Name of Inhibitor	Supplier	Concentration	Compound in inhibitors
Luvicap EG®	Clariant	2.5 mass% in deionised water (equivalent to 1 mass% PVCap)	40 mass% PVCap + 60 mass% EG
HI03-24	Clariant	5 vol% in deionised water (equivalent to 1 mass% PVCap)	PVCap + synergist chemical A + EG
HI03-22	Clariant	5 vol% in deionised water (equivalent to 1 mass% PVCap) 2 vol% in deionised water (equivalent to 1 mass% PVCap)	PVCap + synergist chemical A* + EG Note: * different ratio from HI03-24
HI03-187	Clariant	5 vol% in deionised water (equivalent to 1 mass% PVCap)	PVCap + synergist chemical B + EG
HT04-049	BASF	5 vol% in deionised water (equivalent to 1 mass% PVCap)	BASF advanced polymer + solvent
PVCap base polymer	BASF	1 mass% in deionised water	PVCap

6.1.2 Experimental Procedure

In general, aqueous solutions with or without LDHI using deionised water (dyed with methyl blue) were prepared and charged into the sample cylinder. These aqueous solutions are interchangeably called water in this thesis. A piston vessel/cylinder was used in sample preparation. The cylinder was connected to vacuum pump to remove air. Subsequently desired gas source was connected to the cylinder to saturate water with gas. The cylinder content was shaken several times to promote gas dissolution in the water and then it was left overnight. The saturated water and gas in the cylinder were pumped into the pore structure glass micromodel using high precision Quizix pump. The gas sample was injected into the system to create gas bubbles and to pressurise the system to the required test pressure. The system was then cooled down to 4 ^{o}C which was selected to simulate seabed temperature. The formation of hydrate was visually observed and recorded accordingly.

It is important to note that since the kinetic gas hydrate formation is very stochastic in nature and micromodel experiment is a static condition without any mixing, hence it is a

challenge to control the hydrate formation during experiment. Therefore the induction time which was measured from the time when the system pressure and temperature were stabilised was not very meaningful parameter in this study. It serves only as a qualitative indicator. During experiment, there is also the case where the hydrate had formed before the system reached to the stable conditions. In some cases, the temperature was reduced if hydrate did not form in the system for more than 24 hours. Conversely, if the hydrate formed earlier before reaching 4 ^{o}C, the system bath was maintained at the temperature which hydrates started to form. In this experiment, parameters such as degree of subcooling and qualitative observation of crystals growth with time was used for evaluating the mechanism of hydrate formation and inhibition with and without KHIs.

6.2. FLUID SYSTEMS

Fluid systems studied are methane-water and natural gas-water systems. Experiments were performed for blank samples which were methane with distilled water and natural gas with distilled water. Then similar systems were tested with various types of KHIs. The detail information on each KHI is summarised in Table 6.2. Experiments were performed for natural gas-water system with and without kinetic inhibitors as listed below:

- Natural gas – distilled water
- Natural gas with an aqueous solution of LUVICAP EG®
- Natural gas with an aqueous solution of PVCap
- Natural gas with an aqueous solution of HI03-22
- Natural gas with an aqueous solution of HI03-24
- Natural gas with an aqueous solution of HI03-187
- Natural gas with an aqueous solution of HT04-049 (BASF advanced polymer)

In the case of methane – water system, the following experiments were performed: Natural gas with distilled water:

- Methane with distilled water
- Methane with an aqueous solution of LUVICAP EG®
- Methane with an aqueous solution of HI03-22
- Methane with an aqueous solution of HI03-24

- Methane with an aqueous solution of HI03-187

6.3. EXPERIMENTAL RESULTS AND DISCUSSIONS

6.3.1 In the absence of KHIs

The mechanism of gas hydrate formation/growth and inhibition was investigated for two fluid systems. These are methane-water and natural gas-water systems. Methane represents structure I hydrate whereas natural gas form structure II hydrates. The result suggests that different mechanisms seem to be involved for different systems and hydrate can form at gas-water interface, from dissolved gas in the water phase, or from water in the vapour phase. The summary of results is provided in Table 6.3. In this thesis, experiment on natural gas – water systems is the major fluid system been studied. This is because they closely represent hydrate formation from real reservoir fluids, which are dominated by structure II systems. The detail of results for each fluid system is described next.

Table 6.3: Summary of gas hydrate formation for various fluid systems

Fluid system	Subcooling (^oC)	Pressure (psia/bar)	Temp. (^oC)	Comments (hydrate formation/growth, morphology)
Natural Gas	14.5	1500/103	4.0	Illustrated in Figure 6.5 • Hydrate form following gas bubble profiles forming dark, dense masses, spreading from bubble to bubble via crystalline extension in a continuous water phase • after 24 hours hydrates become translucent (white crystalline). • Hydrate grows in the dissolved gas of water phase
Natural Gas	12.0	1000/69	4.0	• hydrate form following gas bubble profiles and spread rapidly in a continuous gas phase • after 24 hours hydrates become translucent (white crystalline). • Hydrate grows in the dissolved gas of water phase.
Methane	17.0	2800/193	4.5	Illustrated in Figure 6.5 • large plugs of gas hydrate following the gas profile • at later stage, form translucent hydrate crystals possibly from dissolved gas within the water phase
Methane	13.0	2300/158	4.0	• dense masses hydrate from free gas bubbles and little growth in water phase • dense masses hydrate turned into translucent crystal at the interface of gas and water phases.

6.3.1.1 Natural gas –water systems

The tests for natural gas- water systems were conducted at two conditions; 14.5^{o}C and 12^{o}C subcooling at 103 bar and 69 bar, respectively. Figure 6.5 shows the sequential images of natural gas hydrate growth at 14.5^{o}C subcooling. The image in Figure 6.5(a) shows the condition before hydrate formation where the gas phase or bubbles is translucent and the water phase is dyed in blue. The image captured after 30 minutes of initial hydrate formation in Figure 6.5(b) showed that hydrate formed in the gas phase or bubbles (from free gas) as a non-translucent (dark coloured) crystals. Traces of translucent hydrate crystals formed from dissolved gas in the water phase were also observed. From the video footage, the hydrate crystal was transported through the water phase to the adjacent free gas bubbles to form hydrate. The process was continuous until all gas bubbles were converted to hydrate. After 24 hours, most of non-translucent hydrate crystals were converted to translucent crystals as the crystals structure were arranged in order to transmit more light. The induction time was approximately 10 minutes.

At 12.5^{o}C subcooling, hydrates formed following gas bubble profiles and spread rapidly in a continuous gas phase in the model as seen in the video footage. There was no still picture taken for this experiment. The induction time was approximately 20 minutes. Diffusion plays an important role during hydrate growth which was observed in this test. This phenomenon was earlier reported by Tohidi et al. (Tohidi et al., 2002). In their studies, it was observed that gas diffusion play important roles in gas hydrate growth especially at low degree of subcooling where some gas bubbles are dissolved in the water phase and transported to the hydrate forming regions.

From the results, it can be concluded that the degree of subcooling has effect on the mechanism of hydrate formation/growth for natural gas-water system. However, the hydrate morphologies were found to be similar in both cases. For example, as seen in Figure 6.5 (c) for growth at high degree of subcooling (14.5 ^{o}C), the hydrate crystal turned to translucent (white) crystalline solid and more consolidated after about 24 hours due to crystal rearrangement to become more stable crystal. Only some traces of hydrate crystal formed in the water phase due to low solubility of natural gas in the water phase to form hydrate.

6.3.1.2 Methane – water systems

For methane- water system, the formation of hydrate appeared to be quite rapid at 193 bar and 4.5 ^{o}C (17 ^{o}C subcooling) throughout the micromodel. They formed large plugs and generally kept the profiles of the gas bubbles. From the captured video footage, hydrate formation appeared to move inward from the edges toward the centre of the gas bubbles. Hydrate growth also occurred, in a later stage, from the edges of the gas bubble profiles, possibly from dissolved gas producing bright coloured crystals within the water phase (Figure 6.6). It was observed that, in one experiment with free methane bubbles, hydrate formation was at 158 bar and 4 ^{o}C (13 ^{o}C subcooling) with an induction time of 2.5 hours, and all the free gas in the micromodel had been converted into gas hydrates in approximately 6 minutes. For the test described earlier (193 bar), the induction time was around 4 hours to form hydrate. This illustrates the stochastic nature of hydrate formation, in particular in the glass micromodel at static conditions. In addition, the induction time measured in micromodel is only an estimated induction time. This is due to the fact that there is no mixing of fluid in the system since it was in fine pore structure of micromodel.

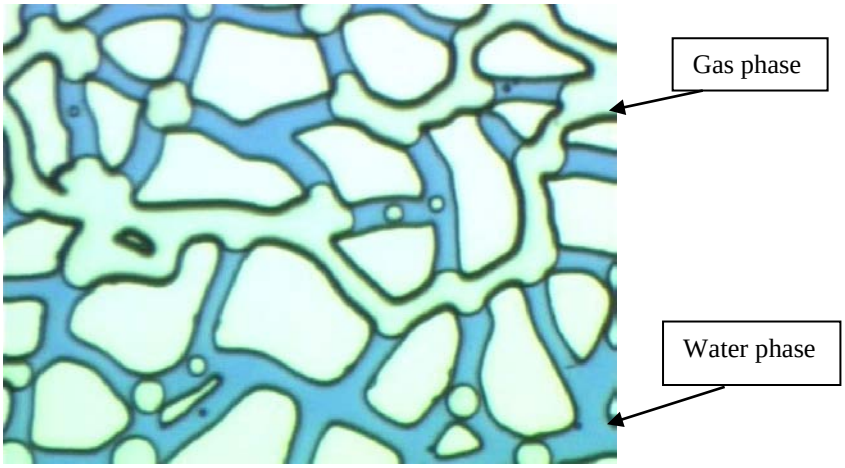

(a) Before hydrate formation

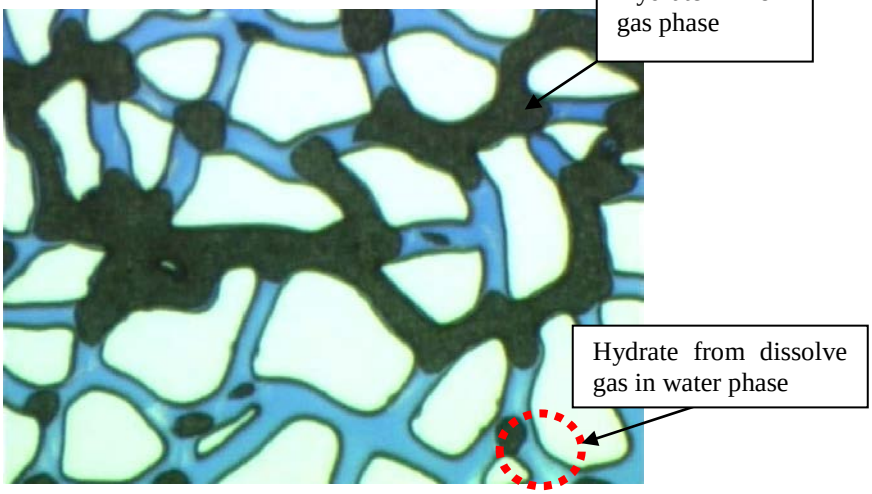

(b) 30 minutes after initial hydrate formation

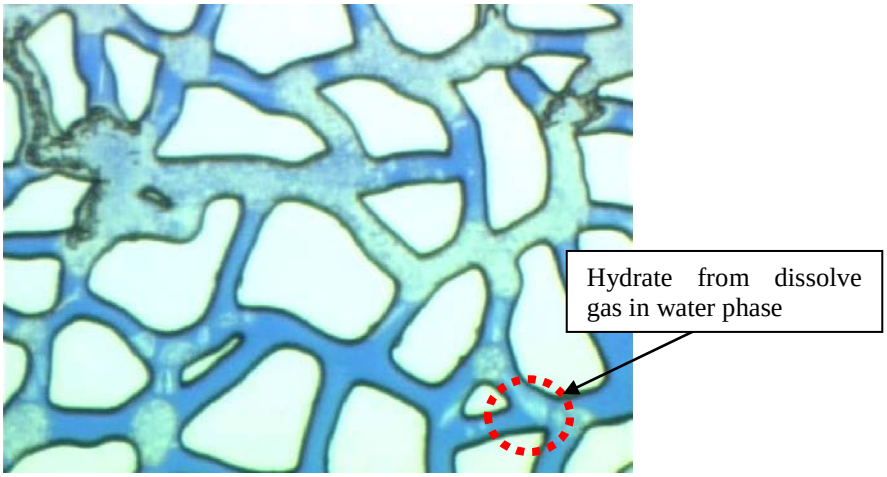

(c) 20 hours after initial hydrate formation

Figure 6.5 Images of natural gas hydrate growth at 103 bar / 1500 psia, 4.0^{o}C (14.5^{o}C subcooling). Hydrate growth in both free gas phase and dissolved gas within water phase

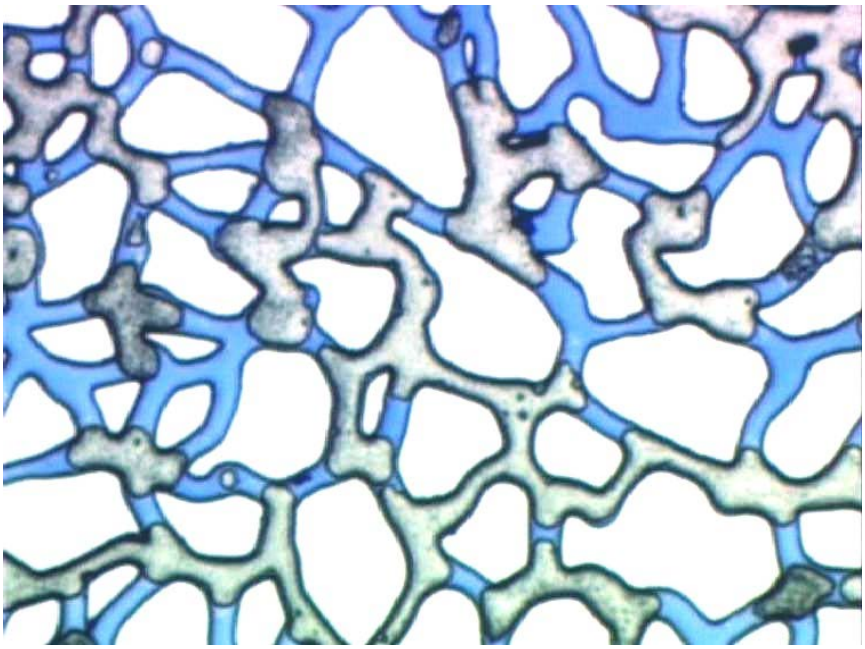

(a) immediately after formation

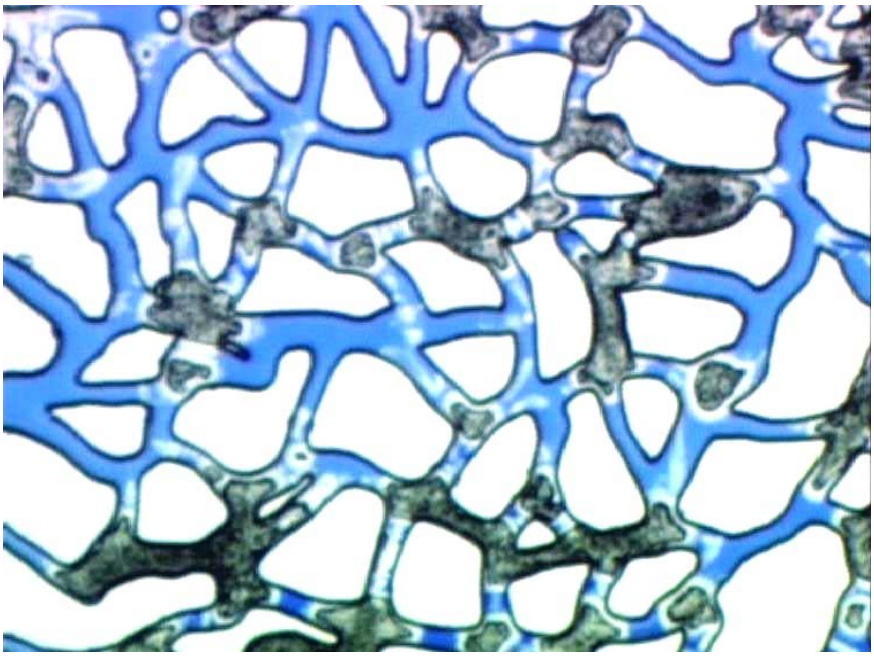

(b) 24 hours after formation

Figure 6.6 Images of methane hydrate growth at 193 bar / 2800 psia, 4.5^{o}C (17^{o}C subcooling). Hydrate growth in both free gas phase and dissolved gas within water phase

6.3.2 In the Presence of KHI

6.3.2.1 In the Presence of LUVICAP EG®

A series of tests were conducted to examine the effect of PVCap which is a base polymer in KHI formulations. In these experiments aqueous solutions containing 2.5 mass% of LUVICAP EG® in deionised water with 1 mass% PVCap active polymer were used. This KHI is composed of 40 mass% PVCap and 60 mass% ethylene glycol (as a carrier fluid). The tests were performed for methane-water and natural gas-water systems at several conditions. The results are summarised in Table 6.4.

Table 6.4: Summary of gas hydrate formation in the presence of 1 mass% PVCAP (2.5 mass% LUVICAP EG®)

Fluid system	Subcooling (^oC)	Pressure (psia/bar)	Temperature (^oC)	Comments (hydrate formation/growth, morphology)
Methane	13.0	2300/158	4.0	Illustrated in Figure 6.11 • smaller and discrete gas bubbles before hydrate formation • more dispersed hydrate from free gas bubbles • hydrate grow in water phase
Methane	10.5	1700/117	4.0	Illustrated in Figure 6.12 • large plugs formed following profiles of gas bubbles with dark masses of hydrate
Natural Gas	14.0	1300/90	4.0	Illustrated in Figure 6.7 • hydrate form as dark solid masses in free gas then become transparent hydrate crystals. • a very slow growth in dissolved gas within water phase

Natural gas-water system with LUVICAP EG®

Tests for natural gas-water system were conducted at 90 bar and 4^oC (14^oC subcooling) to study the effect of LUVICAP EG® on gas hydrates formation and their morphology. The induction time of the system in the presence of LUVICAP EG® was 8 hours, which was, as expected, longer than the blank test carried out earlier at similar conditions. Similar to the system without LUVICAP EG®, hydrate initially formed non-translucent solid masses crystals then turned to translucent crystalline with time as they became more dense and solid crystals (Figure 6.7).

Figure 6.8 shows the still pictures comparing the hydrate growth rate with and without LUVICAP EG®. It indicates that without LUVICAP EG®, more oriented and perfect hydrate crystals were observed and the edges were changed to translucent (white) crystals after 20 hours (Figure 6.8(a)). On the other hand in the presence of LUVICAP EG® hydrate growth was still continuing but at a slower rate after 72 hours which can be seen from the non-transparent solid masses of hydrate (Figure 6.8(b)). This evidence suggests that the LUVICAP EG® significantly reduces rate of hydrate growth in free gas of natural gas-water systems. The spread of hydrates through the model seems to also occur through traces of hydrates forming from dissolved gas, which suggests that LUVICAP EG® promotes a very slow growth of hydrate formation from dissolved gas in the water phase at the test condition

An interesting observation from the video footage during hydrate growth was that some of the gas bubbles were expelled from the hydrate structure. This could be due to fractionation of components in the natural gas. The gas bubbles are possibly consisting of light component such as methane and nitrogen. With time these gas bubbles turned to hydrate crystals. The explanation to this phenomenon is that larger size gas molecules will have more tendencies to fill-up or fit into water cavity to make the structure of hydrate more stable as compared to the smaller size gas molecules such as methane and nitrogen.

Methane-water system with LUVICAP EG®

The images of gas phase and water phase distribution in the micromodel are shown in Figure 6.9. An interesting difference was that upon the introduction of the gas into the system many small and discrete bubbles formed in the presence of LUVICAP EG® as shown in Figure 6.9 (b) compared to the larger gas bubbles that occurred when no inhibitor was present (Figure 6.9 (a)). This was also observed for natural gas-water system (Figure 6.7 (a)). However, it is not as significant as in methane-water system showed in Figure 6.9.

This observation indicates that LDHIs could have significant effect on the interfacial tension between water and gas phases. This could be due to a reduction of the interfacial tensions between the gas and water phases when the inhibitor is present. Analysis of

interfacial tension for methane-water, aqueous solution of ethylene glycol–methane and aqueous solution of LUVICAP EG® - methane was performed and included in internal report (Tohidi et al., 2005) using visual wax-hydrate rig. The plot of IFT is shown in Figure 6.10. The results reveal that the addition of 1.5 mass% of ethylene glycol to the water reduces the IFT compared to the distilled water data. The addition of LUVICAP EG® at 2.5 mass% also reduces the IFT compared to the distilled water data; however, the IFT measurements for ethylene glycol –methane and LUVICAP EG® - gas systems are similar. This suggests that the ethylene glycol present in the LUVICAP EG® has the effect of reducing the IFT but there is no effect of the PVCap polymer present in the LUVICAP EG® on the water/vapour IFT.

In the presence of LUVICAP EG®, hydrates formed at 158 bar and 4 ^{o}C (13^{o}C of subcooling). It appeared that hydrate formation was initiated within 10 minutes and occurred quite rapidly. The inhibitor not only failed to delay hydrate formation at this condition, but shorten the induction time compared to the test results obtained without the inhibitor (3 hours of induction time). This could be due to the stochastic nature of hydrate formation which prevails at high degree of subcooling. Figure 6.11 shows the images of hydrates formed after 24 hours with and without inhibitor. Massive hydrate crystal formed and the pores were blocked quickly for the case without the inhibitor (Figure 6.11 (a)). It should be noted that more dispersed hydrates (or smaller hydrate particles) were formed in the system with the inhibitor (Figure 6.11 (b)) compared to those without the inhibitor. This could be attributed to similar reason as observed previously in which IFT reduction in the present of the inhibitor which generate small gas bubbles and then small hydrate particles. Hydrates were also formed from dissolved gas in both cases, but less in the system with the inhibitor. This indicated that Luvicap is very effective in preventing hydrate formation in water phase.

Another test was conducted at 117 bar and 4^{o}C (10.5^{o}C of subcooling). Figure 6.12(a) shows the image taken for this test before hydrate formation. Video footage showed that hydrates started to form after approximately 13 hours of induction time. Once hydrate started to form, it formed quickly (in less than 15 minutes the whole gas bubble was converted into hydrates) with no hydrate formed from dissolved gas. As shown in Figure 6.12(b), after 50 hours, only hydrate crystals at the interface converted into

translucent crystals while the remaining was still non-translucent. This observation may suggest that Luvicap also slows down the process of crystal re-arrangement.

The tests carried out in the presence of LUVICAP EG® showed that it significantly reduces the rate of hydrate growth in the water phase for natural gas –water system. However, for methane-water system, LUVICAP EG® appeared to be less effective in reducing the hydrate growth and inhibiting hydrate formation in water phase as compared to natural gas-water system. As this is a static test, it is possible that changes in gas composition (due to hydrate formation) reducing the driving force for Natural Gas System.

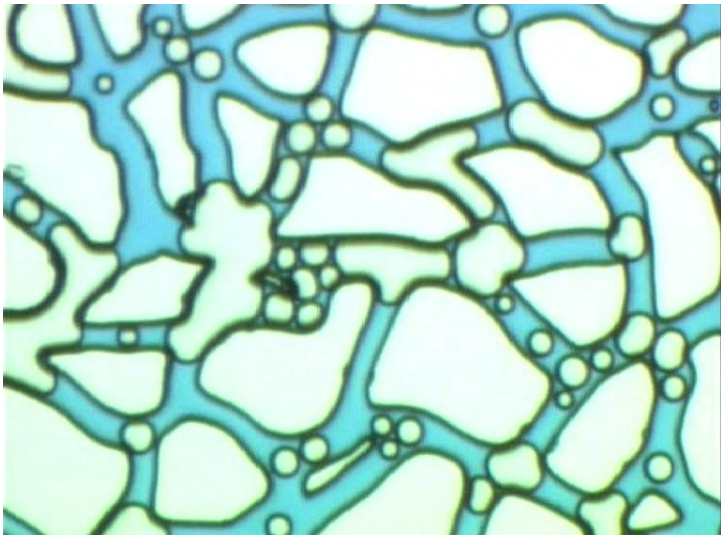

(a) Before hydrate formation

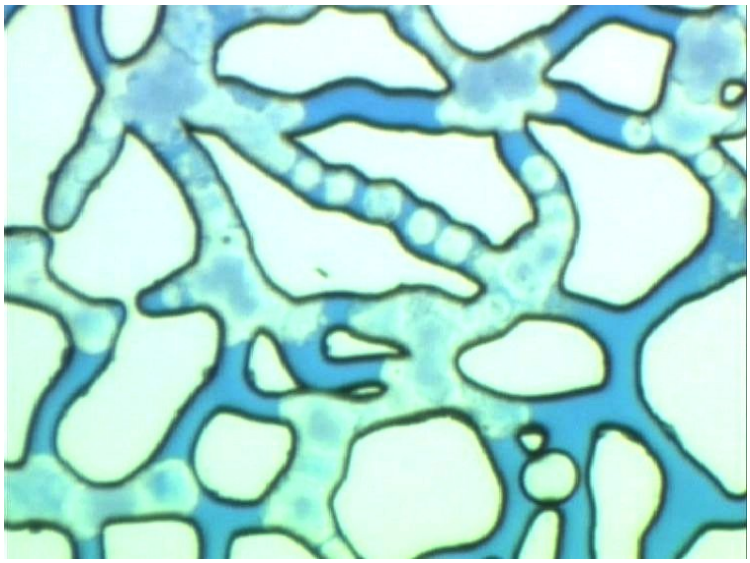

(b) 72 hours after hydrate formation

(a) Before hydrate formation (b) 72 hours after hydrate formation

Figure 6.7. Hydrate formation in natural gas-water system in the presence of LUVICAP EG® at 90 bar / 1300 psia, 4 ^{o}C (14 ^{o}C subcooling).

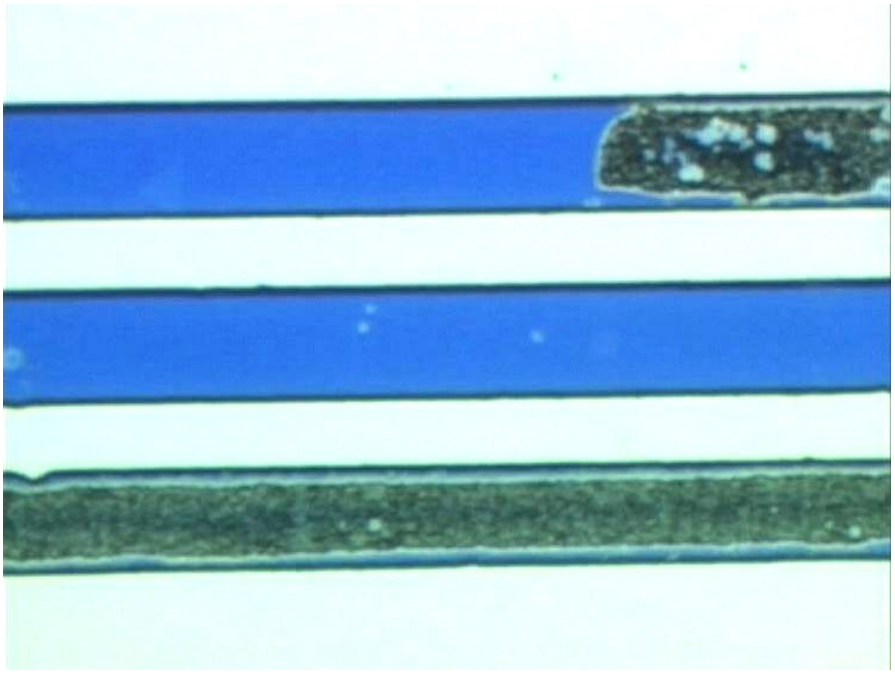

(a) 20 hours after initial formation without LUVICAP EG®

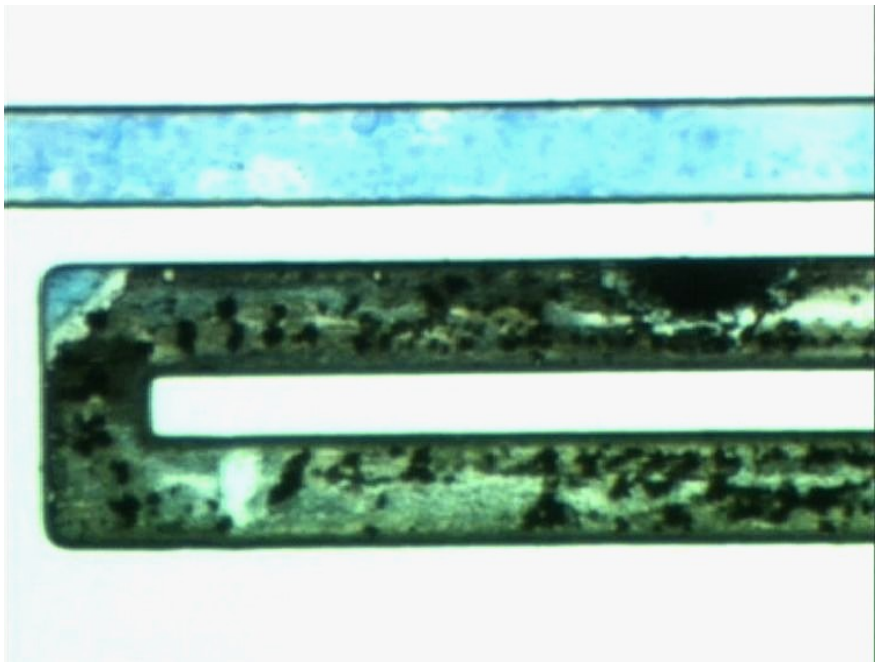

(b) 72 hours after initial formation with LUVICAP EG®

Figure 6.8. Natural gas hydrate formation (a) without LUVICAP EG® (103 bar / 1500 psia, 4 ^{o}C, 14.5 ^{o}C subcooling) and (b) with LUVICAP EG® (90 bar / 1300 psia, 4 ^{o}C, 14 ^{o}C subcooling). Slow growth of hydrate in free gas with LUVICAP EG® and traces in dissolved gas within water phase

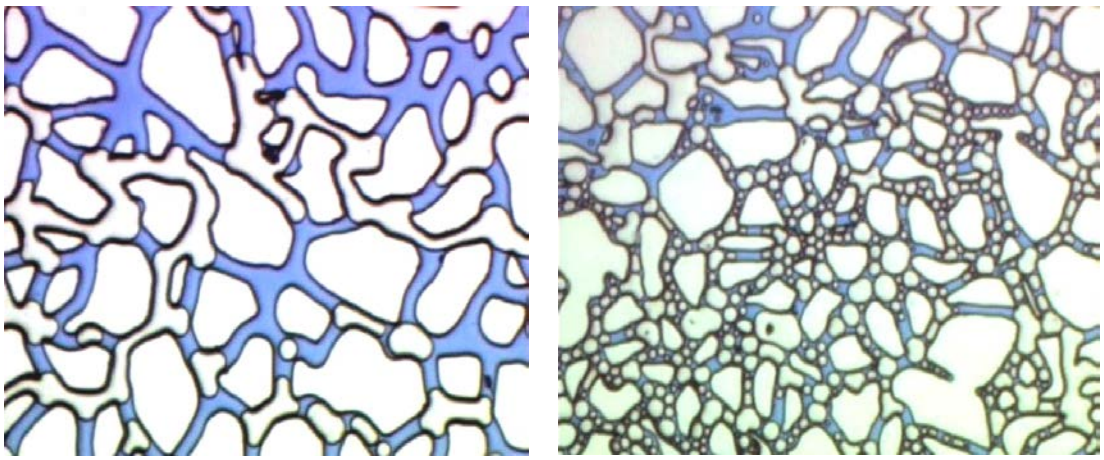

(a) without PVCap (large gas bubbles) (b) with PVCap (small and discrete gas bubbles)

Figure 6.9 Size of gas bubbles for methane-water system before hydrate formation with and without PVCap

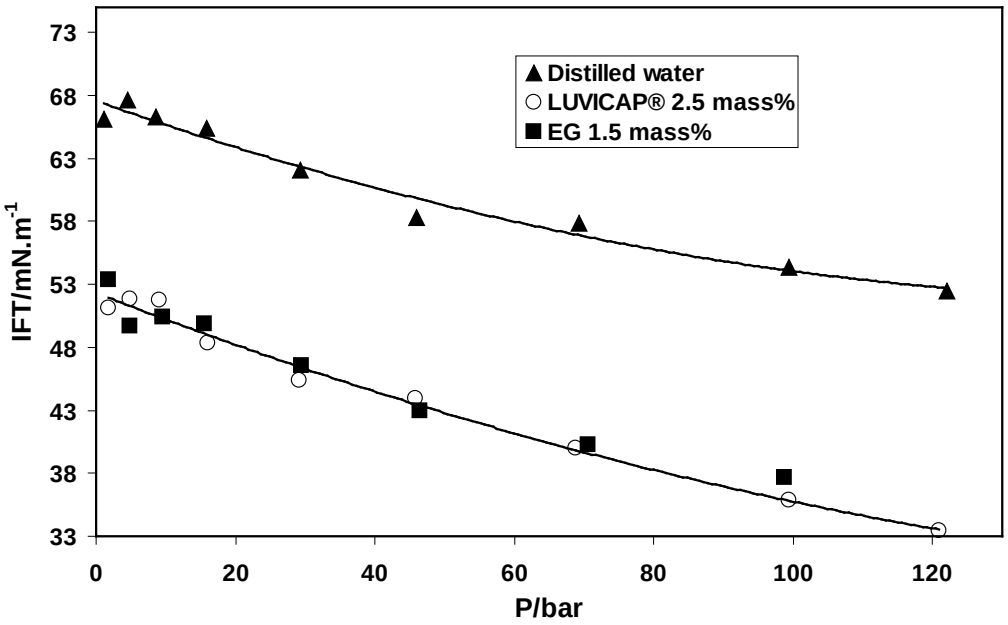

Figure 6.10 Experimental IFT measurements between aqueous and vapour phases for methane/water and methane/aqueous solutions of ethylene glycol 1.5 mass% and LUVICAP EG® 2.5 mass% at 10ºC (Tohidi et al, 2005).

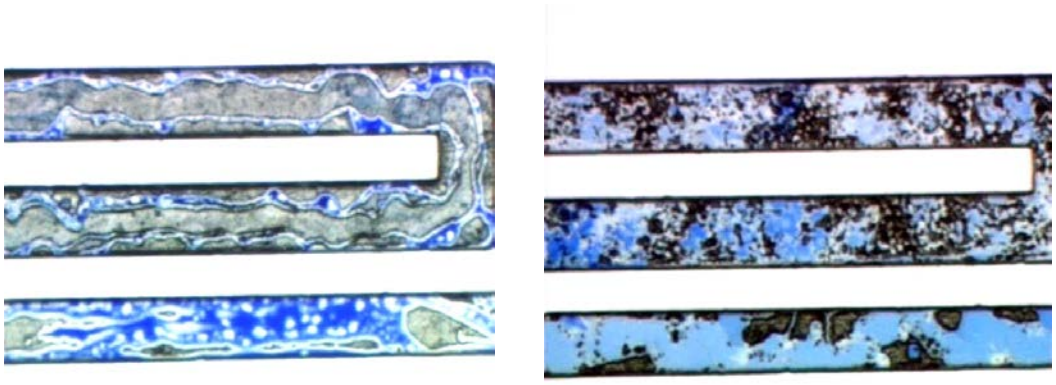

(a) without PVCap (solid masses hydrate) (b) with PVCap (more dispersed hydrate)

Figure 6.11 Methane hydrate growth after 24 hours of hydrate formation at 158 bar / 2300 psia, 4.0^{o}C (13^{o}C subcooling)

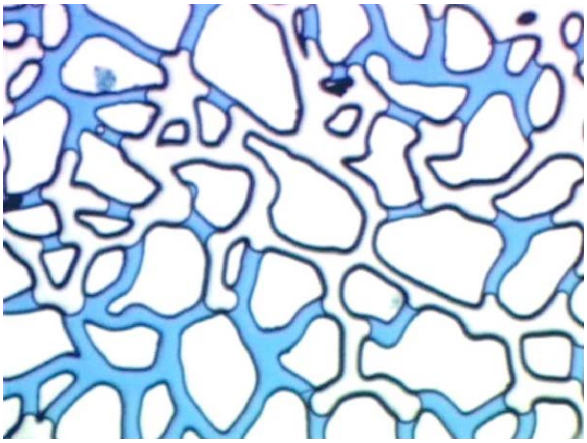

(a) before hydrate formation

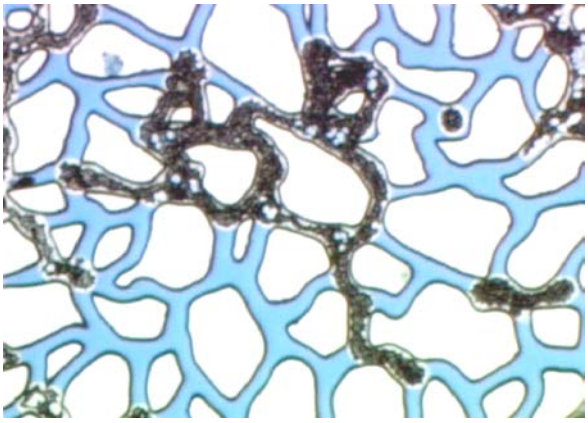

(b) after 50 hours of hydrate formation

Figure 6.12 Methane hydrate formation in the presence of LUVICAP EG® at 117 bar / 1700 psia and 4^{o}C (10.5^{o}C subcooling).

6.3.2.2 In the presence of HI03-24

Natural gas-water system with HI03-24

Several tests were conducted for natural-gas water systems in the presence of 5 vol% of HI03-24 (equivalent to 1 mass% PVCap which comprise of PVCap, synergist chemical A, ethylene glycol and water) to investigate the mechanism of hydrate formation and to study the hydrate morphology at different degrees of subcooling and comparing it with other inhibitors. Experiments were conducted at three conditions; 11.4 ^{o}C subcooling at 103 bar / 1500 psia, 12.4^{o}C subcooling at 103 bar / 1500 psia and 14.4 ^{o}C subcooling at 93 bar / 1350 psia.

In the presence of HI03-24 inhibitor, it was observed that different degrees of subcooling lead to different mechanisms of hydrate formation and morphologies. In the first experiment, hydrates formed immediately as the system reached 7.1^{o}C (11.4^{o}C subcooling). The sequential pictures of hydrate formation are shown in Figure 6.13.

The video footage showed that hydrate formation was initiated in water phase as the gas phase shrinks, leaving behind hydrate crystal forming in the water phase. At the interface, non-translucent masses of hydrate layer appeared as soon as the hydrate layer touched the gas bubbles. This hydrate layer turned into translucent crystals within few minutes. The sequential pictures showed the progress of before hydrate formation at one location of the glass micromodel (Figure 6.13(a)). After 3 hour, the hydrate in the water phase turned to a smooth whiskery type hydrate and a thread like hydrate crystals formed in the gas phase as shown in Figure 6.13(b). After leaving the hydrate crystals for 34 hours, they grew further and each individual type of hydrate morphology became more prominent (Figure 6.13(c)). Since this morphology was not commonly observed during our studies, the pictures during dissociation was further analysed to confirm the presence of each crystal morphology in both phases.

The sequential images of gas hydrate dissociation from 7.6 ^{o}C to 12.6 ^{o}C are shown in Figure 6.14. From the dissociation pictures shown in Figure 6.14, it is observed that after increasing the temperature from 7.6 ^{o}C to 9.6 ^{o}C, the whiskery hydrate crystals in bulk of water dissociate earlier than thread like hydrate crystals in gas phase (Fig 6.14 (a) and (b)). Finally at 12.6 ^{o}C, all hydrate crystals are fully dissociated leaving the gas and water phases in the system.

This microscopic level of observation on whiskery hydrate formation has been reported by Makogon (Makogon, 1997) for the bulk growth of natural gas in the windowed cell. It is described that during the formation of whiskery crystal, hydrate forming molecules go to the surface of growing whiskery crystal by tunnel diffusion at the gas-water interface. The crystals are pushed from the base when the molecules of water and gas arrive at the same geometric location to the base of crystals.

At the test conditions, hydrate formed in water phase in the presence of HI03-24 which indicated that it is not as effective as LUVICAP EG® in preventing hydrate formation from dissolved gas in the aqueous phase.

In another experiment on the above system, at 12.4^{o}C subcooling hydrates were first formed as a non-translucent particle at the interface of water and gas in the inlet of the micromodel where the video footage was taken. Still pictures were taken at several stages of hydrate formation shown in Figure 6.15 starting from before hydrate formation (Figure 6.15 (a)). While hydrate particles were continuously growing in the water phase, a thin layer of small dendrite and round shape hydrate crystals were slowly growing in the gas phase (Figure 6.15(b)) based on images taken after 24 hours. Similar hydrate growth is expected in the pores. However it cannot be observed visually due to many hydrate particles overlapping and both water and gas phases being covered with non-transparent particles. Some patches of gas bubbles and traces of water phase, which were initially trapped within the hydrate crystals, remained without converting to hydrate in the pore structure (Figure 6.15(c)).

The next test was carried out at 14.4 ^{o}C subcooling. The sequential still pictures are shown in Figure 6.16. At these conditions hydrates formed at the interface of water and gas growing into the gas bubbles as non-transparent hydrate masses. After 3 hours of initial hydrate formation, the hydrate particles within the gas profile turned to a thin circular shape hydrate crystals and some parts of them dissolved in water phase leaving a contour of thin circle lines of transparent hydrate crystal in the gas bulk volume at the inlet of the micromodel. The transparent hydrate crystal is formed as the crystal minimise the surface area to orientate into more perfect crystal arrangement. Some gas bubbles were expelled from the existing hydrate particles (Figure 6.16(a)). They dissolved in the water phase and contributed to the formation of other hydrate crystals in

the water phase (Figure 6.16(c)). It is worth to note that at lower degrees of subcooling 11.4 ^{o}C and 12.4 ^{o}C (Figures 6.13 and 6.14) hydrate crystals also formed in the water phase. It appears that at above conditions HI03-24 is not as effective as PVCap in preventing hydrate formation from dissolved gas in water phase.

Methane-water system with HI03-24

An experiment was carried out in methane – water system in the presence of 5 vol% of HI03-24. After charging the system, the temperature was reduced to 5 ^{o}C, and kept for one day. The hydrate did not form; therefore the temperature was decreased step by step to 3^{o}C (within 2 days) where it formed. The sequence of still pictures of hydrate formation is shown in Figure 6.17. As can be seen the growth of the hydrate initiated and progressed in the gas bubbles profile only in the form of grey hydrate layer with a thick interface (Figures 6.17 (b)) after 1 hour. It then turned to black masses of hydrate particles, which preserved the shape of gas bubbles. Finally these particles changed to many thick and rough hydrate crystals, which were separated within the original gas profiles (Figures 6.17 (c)).

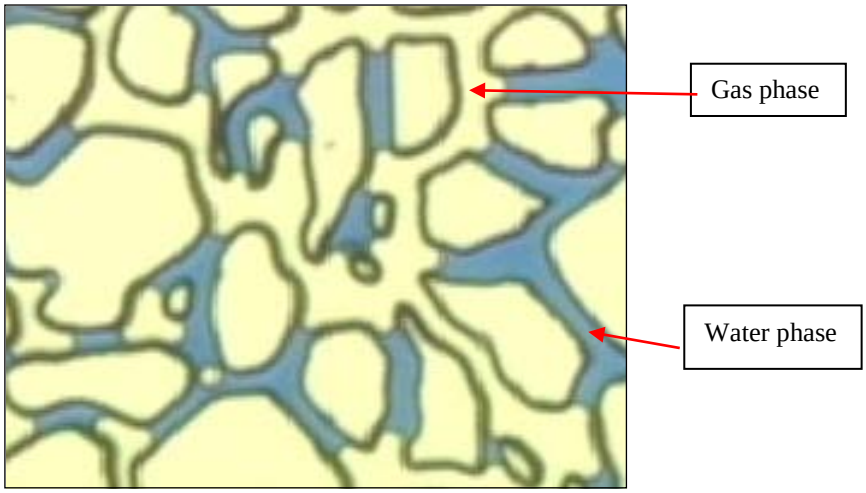

(a) Before hydrate formation

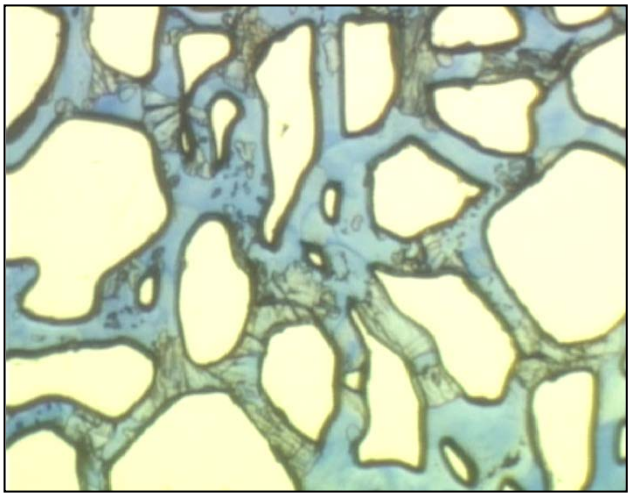

(b) 3 hrs after hydrate formation

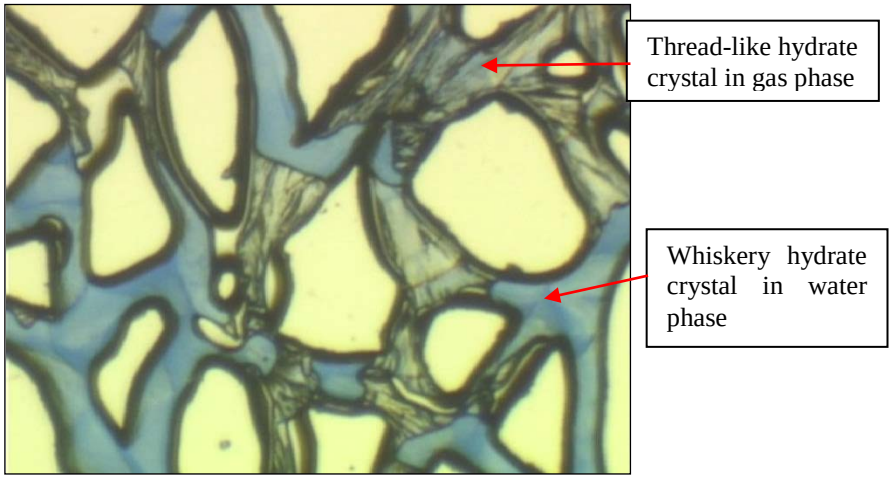

(c) 34 hours after hydrate formation

Figure 6.13. Hydrate formation in natural gas-water system in the presence of 5 vol% HI03-24 at 103 bar / 1500 psia/, 7.1^{o}C (11.4^{o}C subcooling)

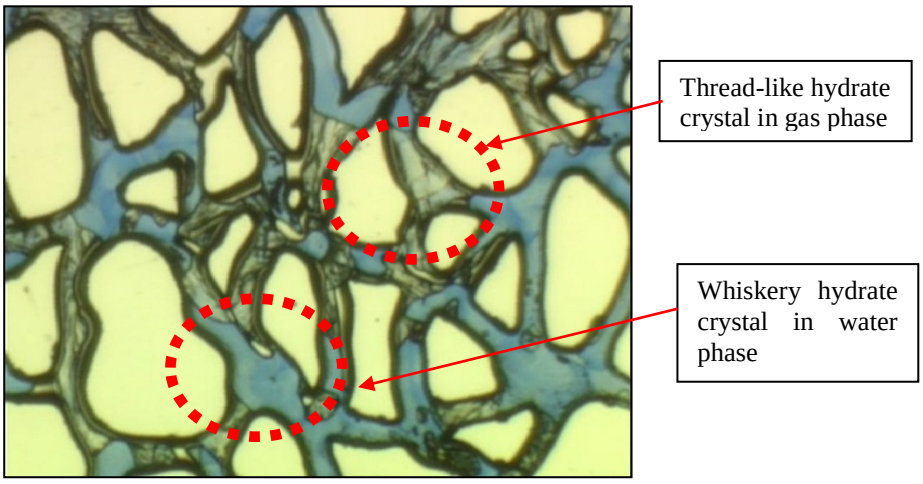

(a) T = 7.6°C

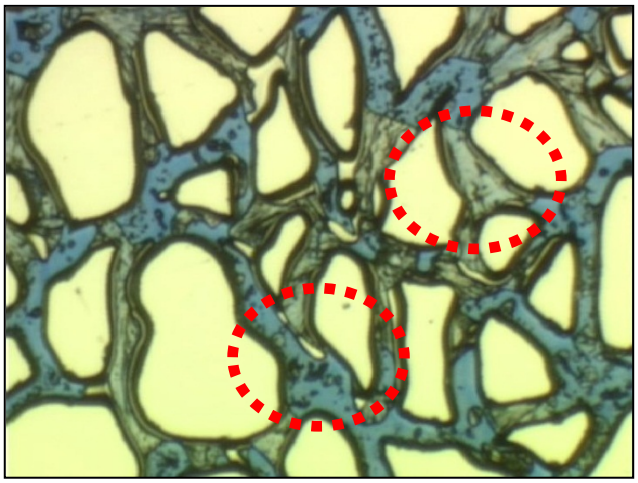

(b) T = 9.6°C

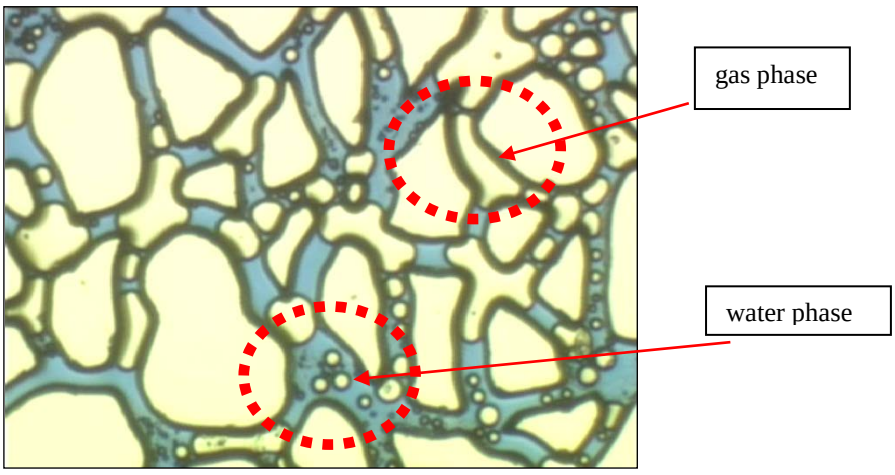

(c) T = 12.6°C

Figure 6.14. Hydrate dissociation in Natural Gas-Water System in the presence of 5 vol% HI0324 at 1500 psia/103 bar.

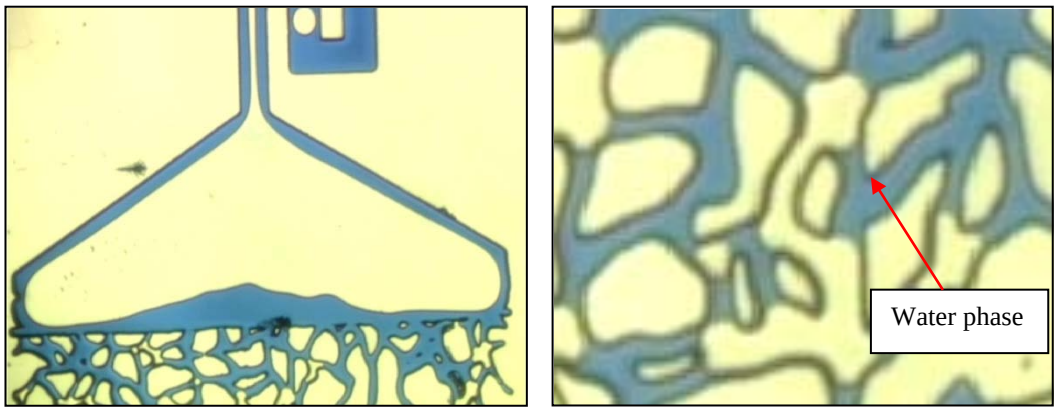

(a) before hydrate formation

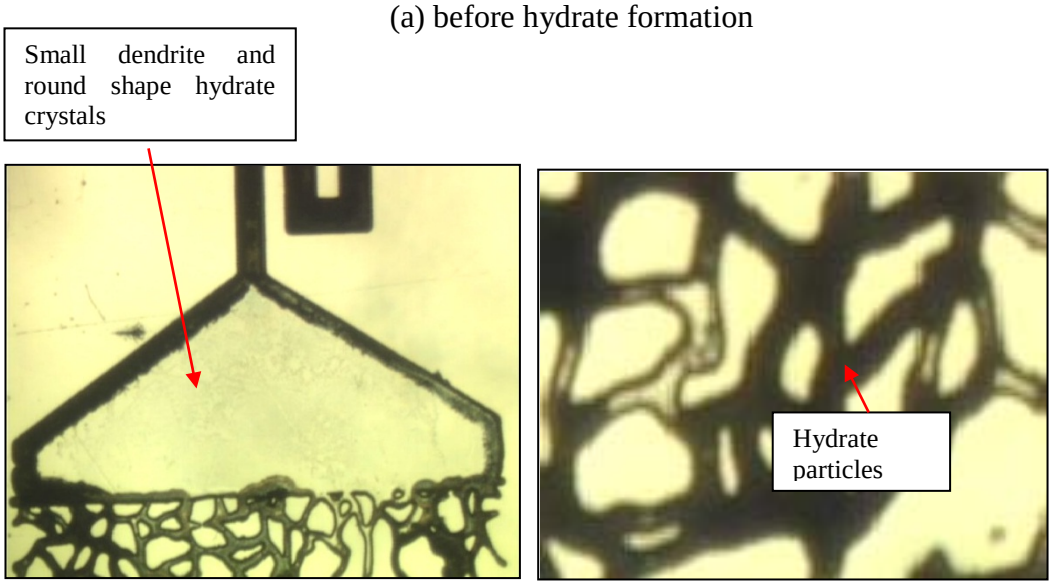

(b) 24 hrs after initial formation

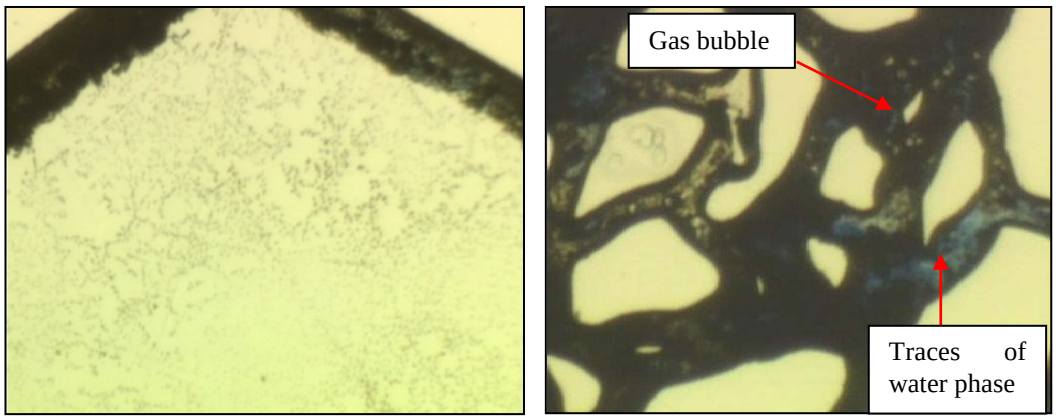

(c) 40 hrs after initial formation

Figure 6.15. Hydrate formation in natural gas-water system in the presence of 5 vol% HI0-324 at 103 bar / 1500 psia, 6.1 ^{o}C (12.4 ^{o}C subcooling)

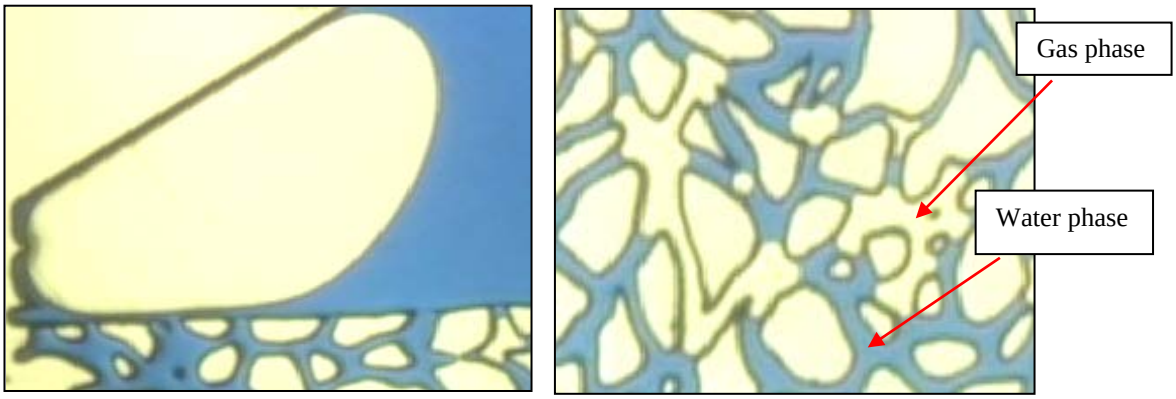

(a) before hydrate formation

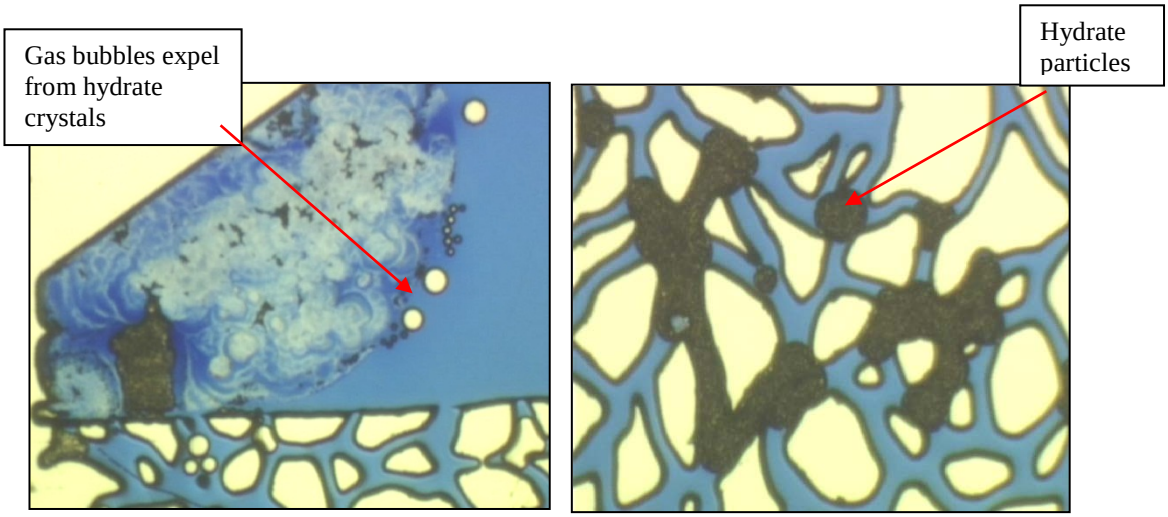

(b) 3 hrs after initial formation

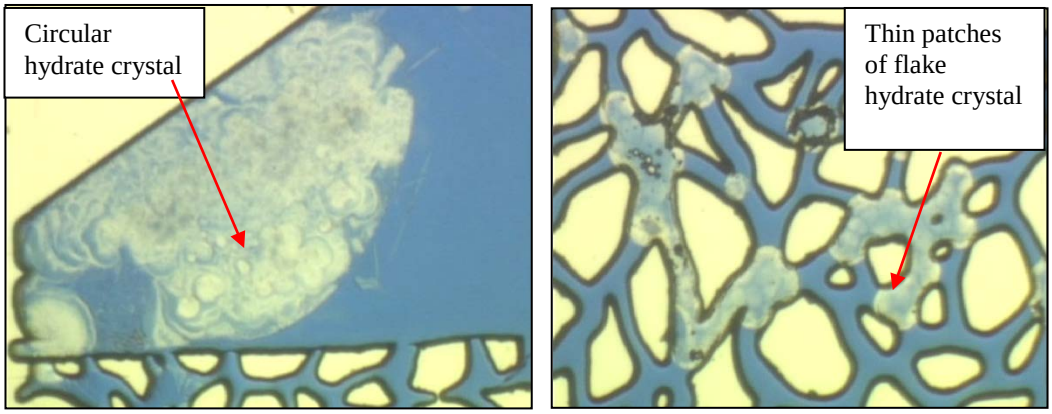

(c) 20 hrs after initial formation

Figure 6.16. Hydrate formation in natural gas-water system in the presence of 5 vol% HI03-24 at 93bar / 1350 psia, 4.1 ^{o}C (14.4 ^{o}C subcooling).

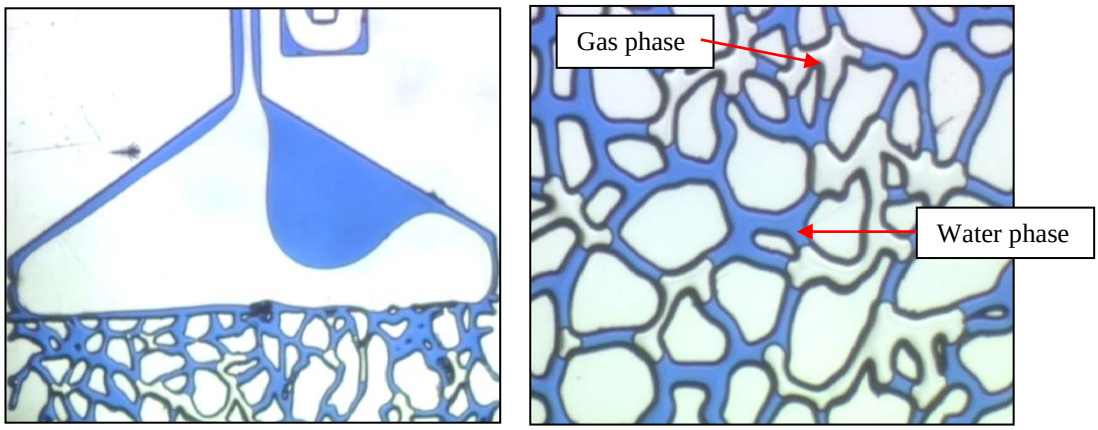

(a) Before hydrate formation

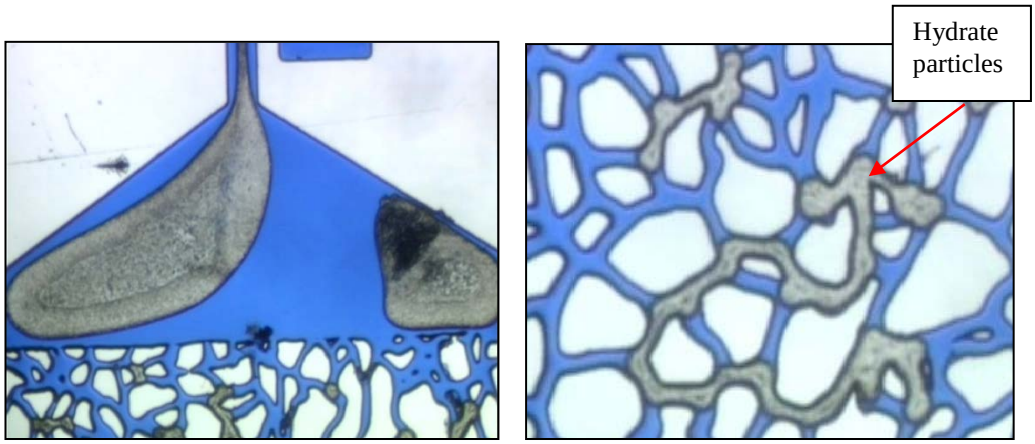

(b) 1 hr after hydrate formation

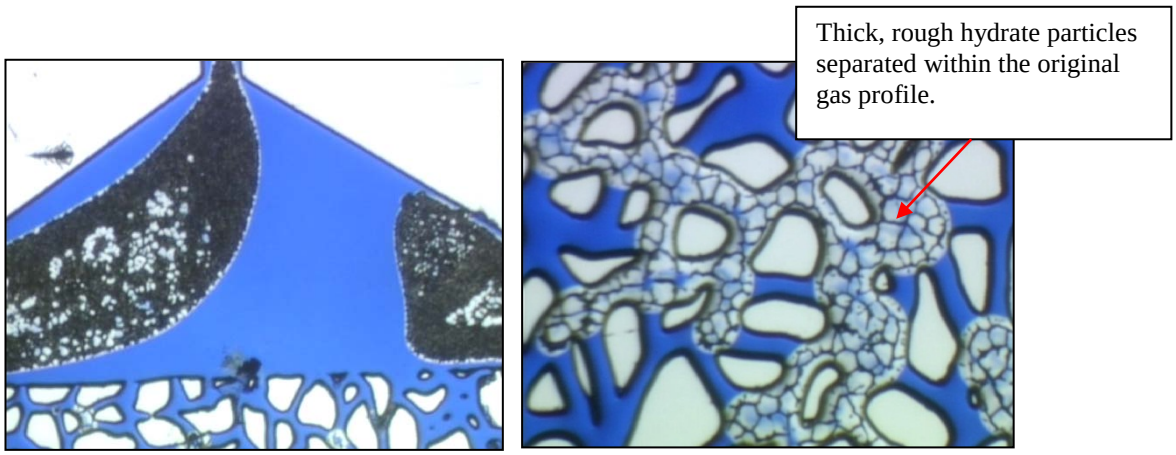

(c) 39 hrs after hydrate formation

Figure 6.17. Hydrate formation in methane-water system in the presence of 5 vol% HI03-24 at 117 bar / 1700 psia, 3 ^{o}C (11.5 ^{o}C subcooling).

6.3.2.3 In the Presence of HI03-22

Natural gas-water system with HI03-22

Several tests were conducted at different conditions (90 bar / 1300 psia and 69 bar / 1000 psia) to study the effect of KHI inhibitor HI03-22 (composed of PVCap, a synergist chemical A similar to the one added to HI03-24 but different ratio, water and ethylene glycol) on the hydrates formation and their morphologies. Two concentrations of the inhibitor were tested; 2 vol% and 5 vol%.

The results show that this inhibitor formed hydrate at 90 bar / 1300 psia (11.6^{o}C subcooling) without induction time. This was due to the testing condition, which was beyond the strength of the new inhibitor to delay hydrate formation and growth. In comparison, the induction time of natural gas-water system in the presence of LUVICAP EG® at 90 bar / 1300 psia and higher degree of subcooling of 14^{o}C was 8 hours longer than that of above system.

Two interesting phenomena were observed during the experiments. The first observation was the dynamic growth of hydrate in the gas phase as shown in Figure 6.18. This observed phenomenon was described by Makagon (Makagon, 1997) based on his experiments on the kinetics and morphology of gas hydrates. His study on the locations of formation and growth of hydrate nuclei has shown that with large volumes of water in the presence of a free gas-water interface, nucleation proceeds at the surface of a gas-water interface. Once the hydrate film formation covers the whole gas-water interface, the surface contact process becomes a diffusive surface. Massive crystal grows in the gas phase because of different molecular sizes of gas and water and different diffusion coefficients through a previously formed hydrate film at the gas-water interface. This phenomenon supports the role of diffusion in hydrate formation.

The second observation was the dissociation of hydrate molecules within the hydrate crystals following the profile of gas phase as a function of time illustrated in Figure 6.19. However, it is unclear what caused the dissociation of hydrates. The possible scenario is that hydrate shell rapidly formed on the glass surface and re-distributed within the system. Some gas was observed in the shell and fine hydrate particles formed in the aqueous phase.

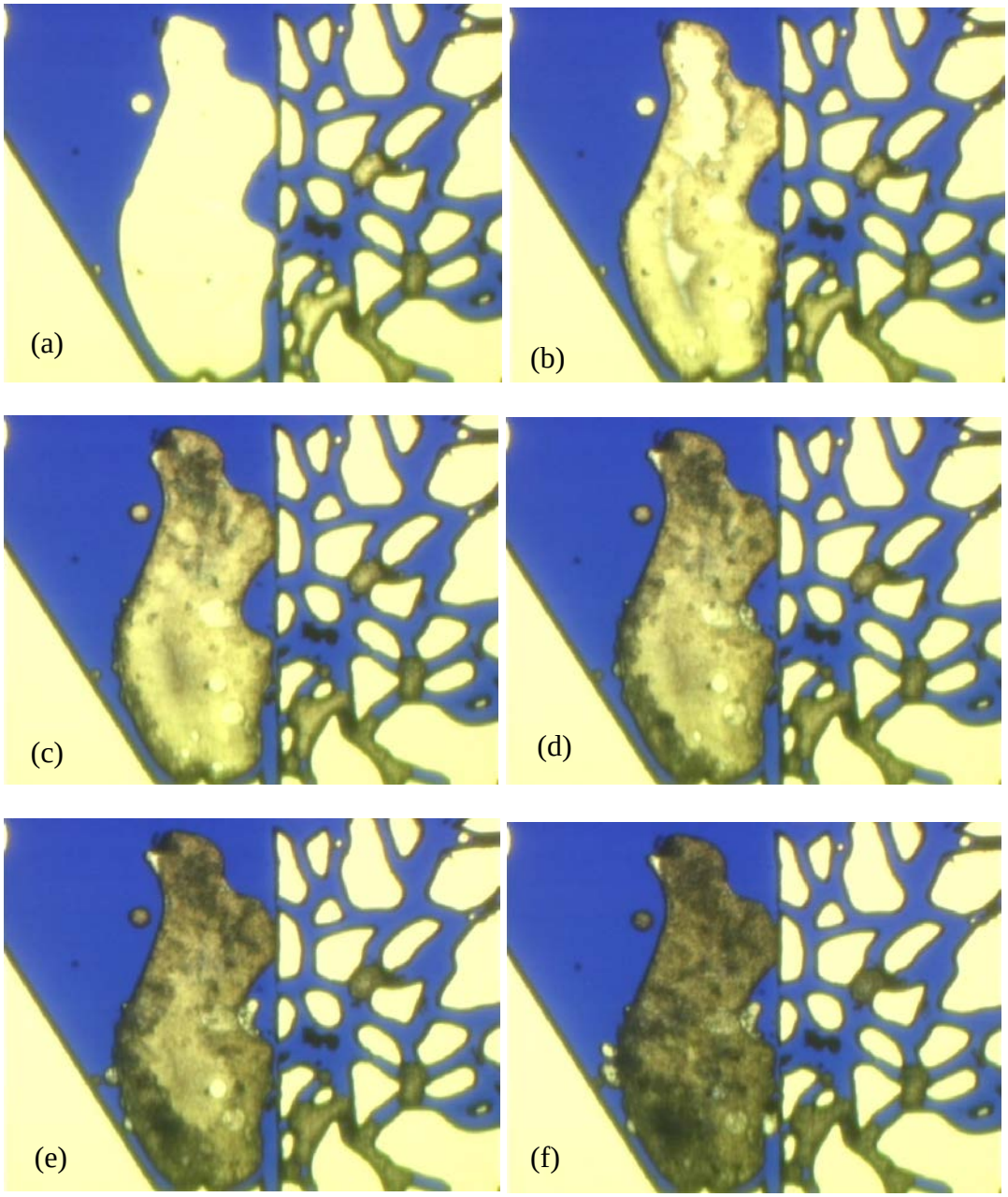

Figure 6.18. Dynamics of natural gas hydrate formation/growth in the presence of HI03-22 within 6 minutes of initial growth (90 bar/1300 psia and 6.4 ^{o}C, 11.6 ^{o}C subcooling). Hydrate begins to form at the gas-water interface and grow toward the middle of gas bubble with another layer of hydrate grow due to the diffusion and sorption influx of gas and water molecules from the forming crystal surface.

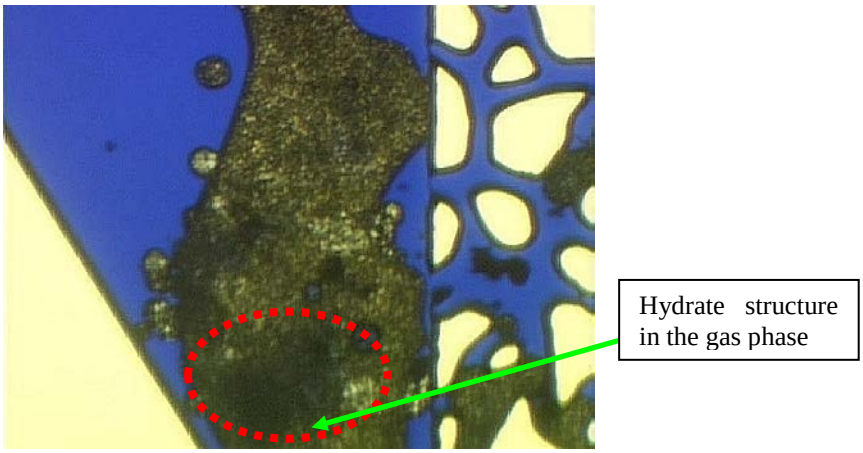

2 hrs after initial hydrate formation (continuous growth)

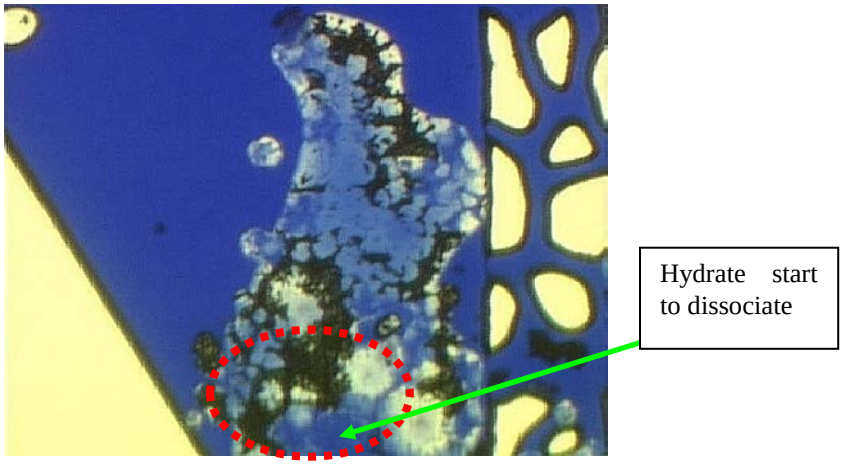

15 hrs after initial hydrate formation (slow growth)

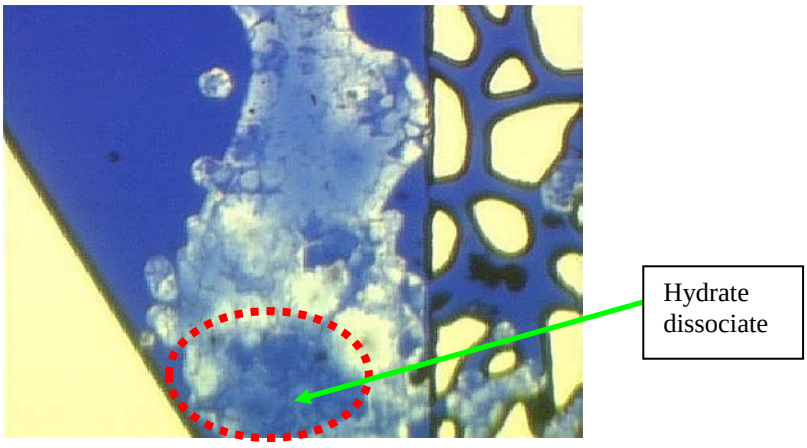

120 hrs after initial hydrate formation (Termination of growth)

Figure 6.19. Changes in natural gas hydrate morphology in the presence of HI03-22 inhibitor with time at 90 bar / 1300 psia and 6.4 ^{o}C, 11.6 ^{o}C subcooling. Observed hydrate dissociate within hydrate structure.

Visual observations also suggest that the rate of hydrate growth is faster in the presence of 2 vol.% HI03-22 in comparison with LUVICAP EG® based on the still pictures shown in Figure 6.20. As seen, in the presence of LUVICAP EG® (Fig 6.20 (a)) and at 14°C subcooling, after passing 72 hours from the first hydrate particles formation, the hydrate crystals have not turned to transparent, however in the presence of HI03-22, and at lower degree of subcooling than former (11.6 °C), after 30 hours (Figure 6.20 (b)) all hydrate crystals turned into transparent (their final stage in structural formation). This suggests that 2 vol% HI03-22 is weaker than LUVICAP EG® in delaying hydrate formation and growth probably due to low concentration of active polymer (PVCap) which reduces its performance and effectiveness.

The above experiment was repeated at the same conditions after heating up the system to 35°C for about 24 hours to remove water history. After cooling down the system, a small amount of hydrates formed earlier than the first test, at 6.3°C (~ 10°C subcooling). The formation occurred at the gas phase in some parts of the micromodel and most of the gas phase and water phase remained in the system without conversion into hydrates. This observation could be because of water condensation due to cooling that resulted in a water droplet without KHI. This agrees with the other observation that hydrates did not form in the main body of the micromodel as KHI delay hydrate formation. However, the rate of growth appeared to be slower than the earlier tests possibly due to the lower degree of subcooling. Reducing the temperature by another 2°C (or 12°C subcooling) caused hydrates to form throughout the model while the earlier hydrate crystals formed at 10°C subcooling remained unchanged. All gas phase was converted into hydrate at 12°C subcooling.

HI03-22 inhibitor was further tested for natural gas-water system with 5 vol% (equivalent to 1 mass% PVCap, as active polymer). The test was carried out to study the mechanism of hydrate formation and crystal morphology at this concentration in comparison with LUVICAP EG® (1 mass% PVCap). In order to make the comparison at similar conditions, the inhibitor solution (5 vol%) and natural gas were charged into the micromodel at 94 bar. The system was cooled down to 4 °C (14 °C subcooling) and hydrate did not form after 24 hours. The system temperature was further decreased step by step until it formed at 0.5 °C (17 °C subcooling). As shown in Figure 6.21, initial

hydrate formation began at the interface of gas and water as water diffused into the gas bubble to form non-transparent masses of hydrate layer (Figure 6.21 (b)). This is similar to what had been observed in the presence of 2 vol% of the inhibitor and also 1 mass% of PVCAP. At the final stage hydrate particles turned into thin patches of flaky hydrate crystals (Figure 6.21 (c)). It was also noted that hydrate growth from dissolved gas in the water phase was not observed at this conditions even after leaving the system for 47 hours.

The previous study showed that hydrate formed at 14 ^{o}C subcooling in the presence of 1 mass% of PVCAP, whereas the current results showed that it formed at 17 ^{o}C subcooling in the presence of 5 vol% of HI03-22. This indicates that HI03-22 (PVCAP with synergist) appears to be more effective in delaying hydrate formation as compared to PVCAP (without synergist) at static conditions. This results also supported by the kinetic rig and ultrasonic test results, which showed that HI03-22 inhibitor appeared to be better (i.e. longer induction time) than PVCAP at static (shut-in) conditions.

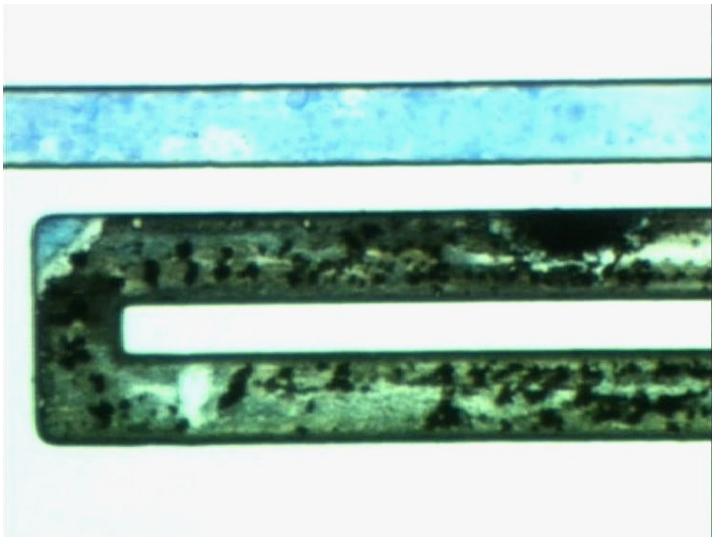

(a) 72 hours after hydrate formation with PVCAP

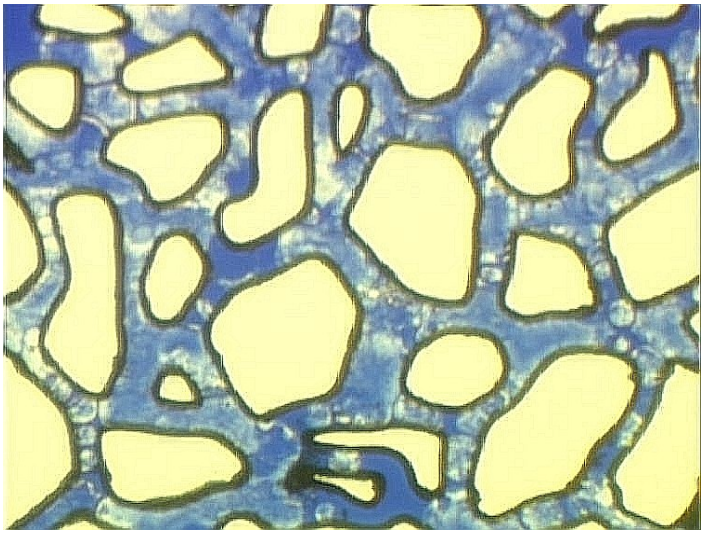

(b) 30 hours after hydrate formation with HI03-22

Figure 6.20. Comparison of natural gas hydrate growth at 90 bar / 1300 psia, (a) with 1 mass% PVCAP at 14 ^{o}C subcooling (b) with 2 vol% HI03-22 and at 11.6 ^{o}C subcooling.

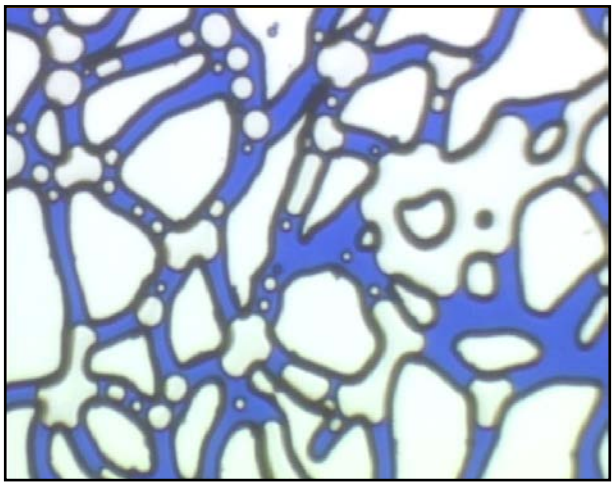

(a) Before hydrate formation

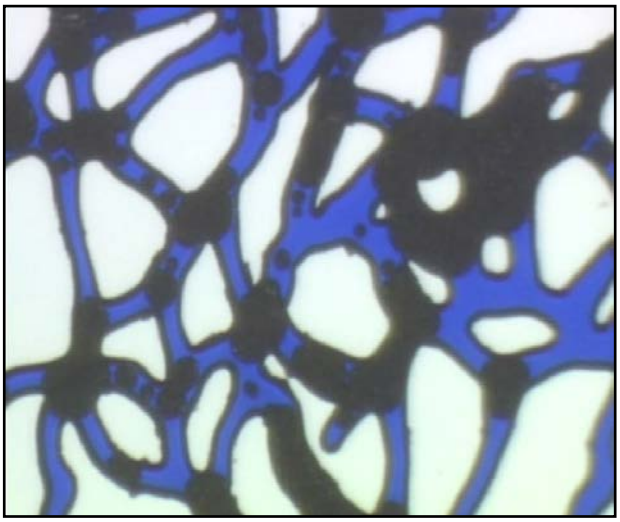

(b) 1 hr after hydrate formation

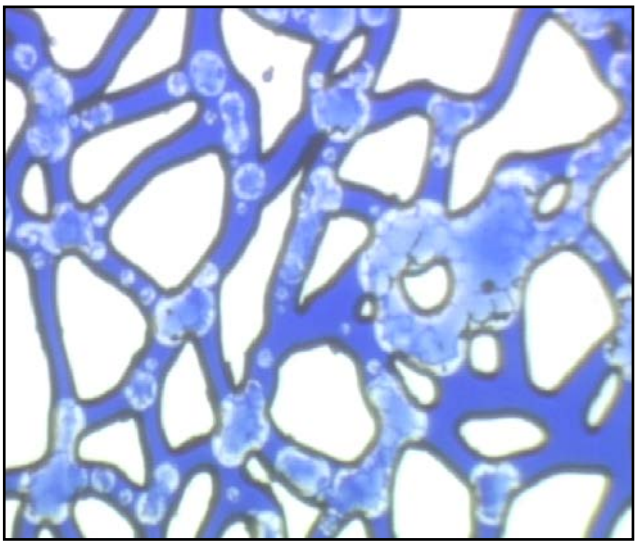

(c) 47 hrs after hydrate formation

Figure 6.21. Hydrate formation in natural gas-water system in the presence of 5 vol% HI03-22 at 94 bar / 1360 psia, 0.5 ^{o}C (17 ^{o}C subcooling).

Methane-water system with HI03-22

Test was conducted for methane – water system in the presence of 2 vol % of HI03-22. After charging the micromodel with test fluids and cooling down the system, hydrate formed immediately at 4.3^{o}C and 1700 psia/117 bar (i.e., 10.5^{o}C subcooling) with no induction time as compared to the system in the present of PVCap where the induction time was about 13 hours.

Figure 6.22 described the progress of hydrate growth in this system with time. As shown in the pictures, hydrate started to form as dark (non transparent) masses of hydrate particle, which appeared to consist of many small particles following the profile of, gas bubbles (Figure 6.22(a)). After 24 hours, some of the hydrate particles turned into white (transparent) crystal, mainly at the edges of hydrate crystal structure. The growth of non-transparent crystal were obvious after 74 hours of hydrate formation where the hydrates formed shells inside the gas bubbles and water molecules appeared to be remained in the middle (Figure 6.22(b)). With time, the hydrate crystal developed a continuous thin hydrate crystal and appeared to be agglomerated to each other and not separated into small crystal flakes (Figure 6.22(c)). From the still picture shown in Figure 6.23, it was observed that some traces of gas hydrate formed in the water phase after 24 hours of hydrate formation. This suggests that this inhibitor, in the presence of methane, may not prevent hydrate formation in water phase.

Comparison of hydrate crystal growth rate for Natural gas system

Natural gas hydrate crystals growth in the presence of different kinetic inhibitors was compared. It is observed that hydrate crystal growth in the presence of synergist (for HI03-22 and HI03-24) is faster than PVCAP (without synergist) as shown in Figure 6.24.

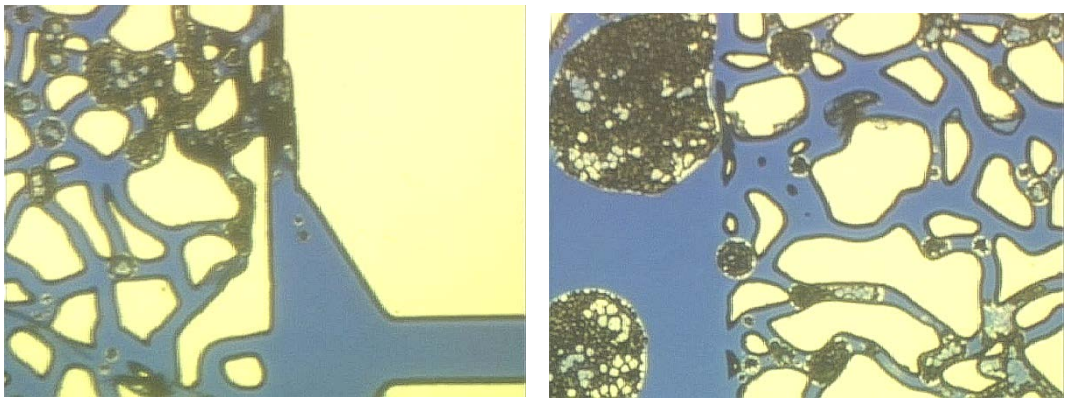

(a) 24 hrs after hydrate formation (inlet and outlet micromodel)

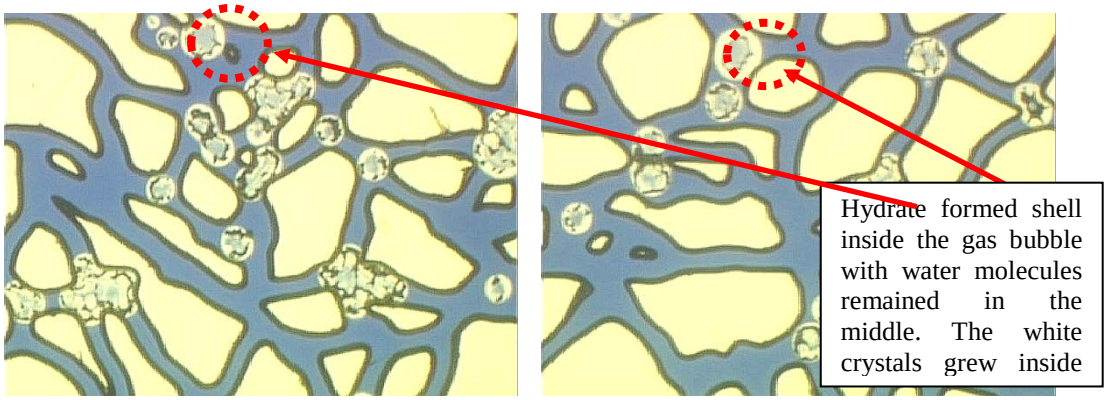

(b) 72 hrs after hydrate formation

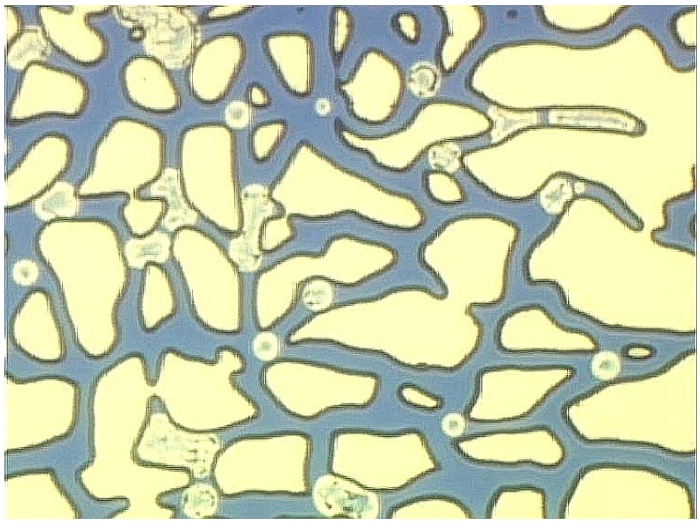

(c) 96 hours hrs after hydrate formation

Figure 6.22. Changes in methane hydrate morphology in the presence of HI03-022 inhibitor with time at 1700 psia/117 bar and 4.3°C, 10.5°C subcooling.

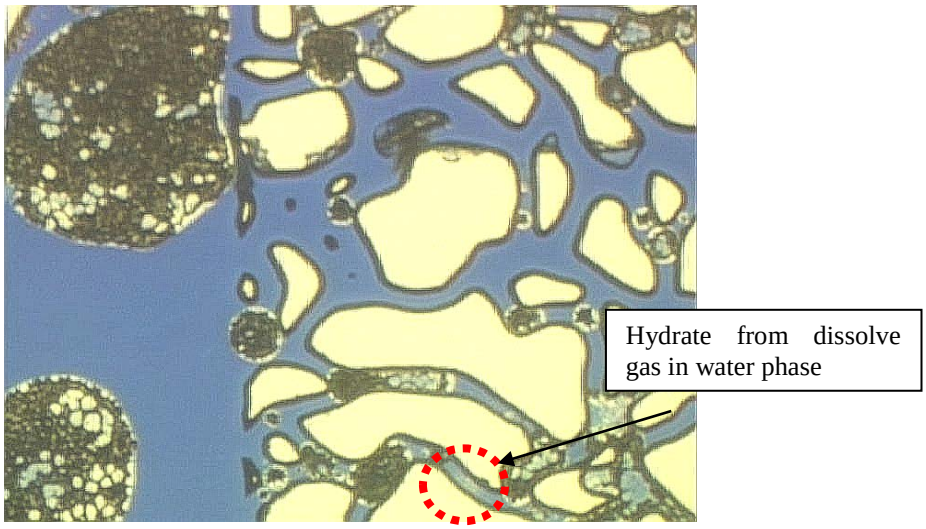

Figure 6.23. Methane hydrate morphology in the presence of HI03-022 inhibitor after 24 hours at 1700 psia/117 bar and 4.3^{o}C, 10.5^{o}C subcooling. Observed traces of hydrate crystal formed in water phase

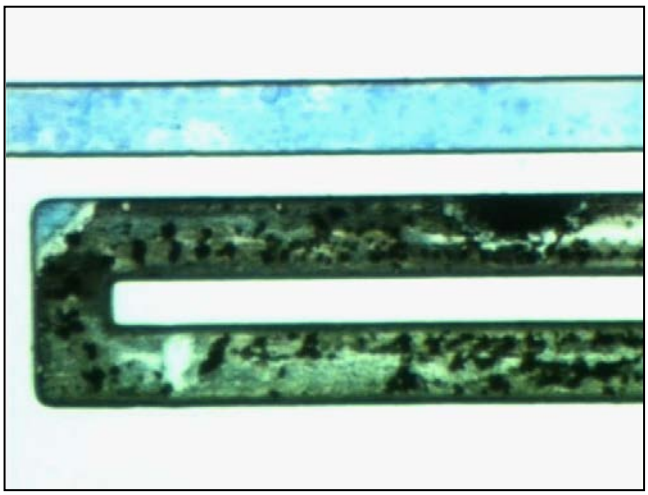

(a) 72 hours after formation (PVCAP)

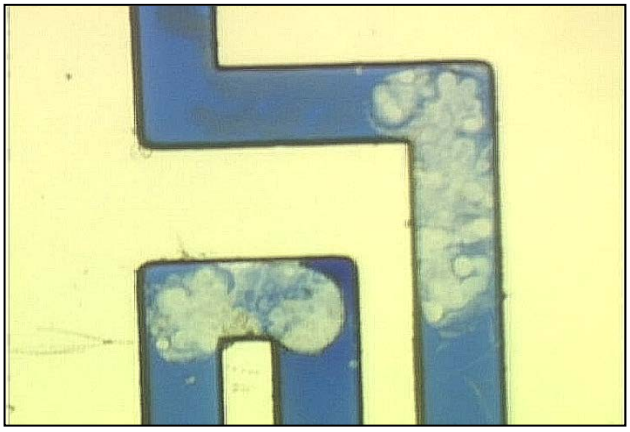

(b) 20 hours after formation (HI03-24)

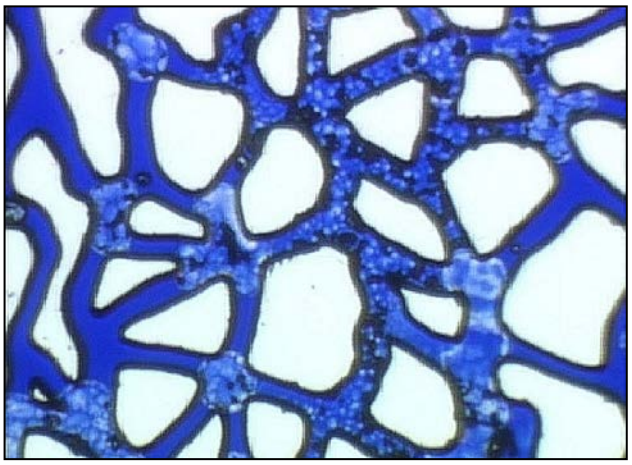

(c) 20 hours after formation (HI03-22)

Figure 6.24. Comparison of hydrate growth for Natural Gas – Water system for (a) 1 mass% PVCAP at 14 ^{o}C subcooling (c) 5% vol HI03-24 at 14.4 ^{o}C subcooling (d) 5 vol% HI03-22 at 13.6 ^{o}C subcooling

6.3.2.4 In the presence of HI03-187

Natural gas-water system with HI03-187

A test was carried out in the presence of 5 vol% HI03-187, another PVCap base polymer with a synergist, at 90 bar (13.9 ^{o}C subcooling) with natural gas-water system. In this test, the temperature of the system was reduced to 4.1^{o}C and hydrates formed after about 80 hours of induction time. As shown by still pictures in Figure 6.25, it was observed that hydrates formed followed gas bubbles profile (Figure 6.25(b)). The non-transparent hydrate particles in the gas bubbles profile turned into white (translucent), thin patches of hydrate crystals with snowy and flake type morphology (Figure 6.25 (c)) after 24 hours in the system. The morphology indicated a more porous hydrate, less packed and with disorder in the structure leading to higher porosity. In comparison with LUVICAP EG®, this inhibitor with synergist seems to be far more effective in preventing hydrate formation based on longer induction time for hydrate formation (compared to LUVICAP EG® with 8 hrs induction time at 14^{o}C subcooling). This inhibitor appeared to be very effective in preventing hydrate formation in water phase for natural gas-water systems.

Methane-water system with HI03-187

A test was carried out one a methane-water system at 117 bar (13.6^{o}C subcooling). The system temperature was reduced step by step from 4.3^{o}C to 3^{o}C within 92 hours. Then the temperature was set at 1.6^{o}C for 48 hrs and hydrates did not form. When the system temperature was further reduced to 0.7^{o}C, hydrate immediately formed within the gas bubbles with non-transparent hydrate particles as shown in Figures 6.26 (a) and 6.26 (b). After 24 hours of hydrate formation, the edges of hydrate particles turned into translucent hydrate crystal forming more order crystal morphology (Figure 6.26 (c)). Finally the hydrate crystal formed shells inside the gas bubble profile and water molecules remained in the middle. Similar to natural gas–water system, this inhibitor prevents hydrate formation in water phase at this condition. Based on these results, it is clear that HI03-187 kinetic inhibitor has also changed hydrate morphology for different hydrate structure at similar degree of subcooling.

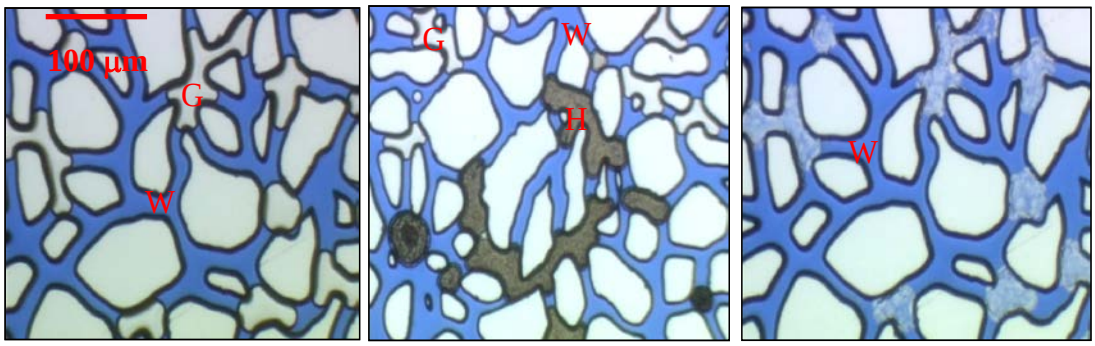

(a) Before hydrate formation (b) 30 min after formation (c) 24 hrs after formation

Figure 6.25. Hydrate formation in natural gas-water system in the presence of 5 vol% HI03-187 at 90 bar / 1300 psia, 4.1 ^{o}C (13.9 ^{o}C subcooling).

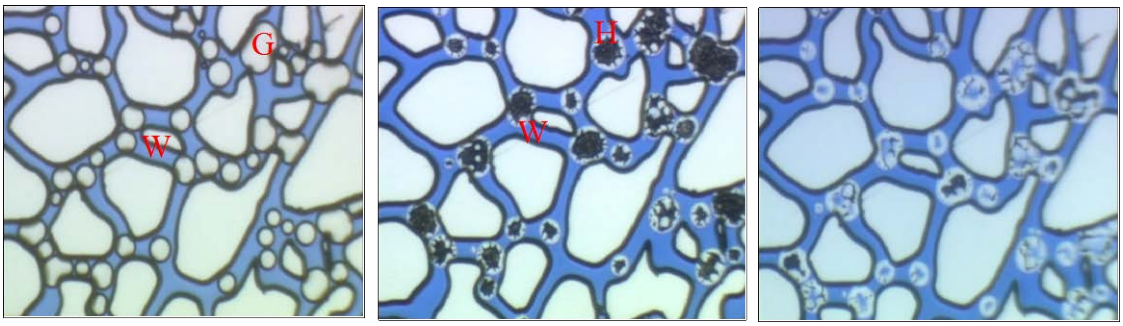

(a) before hydrate formation (b) 24 hrs after formation (c) 65 hrs after formation

Figure 6.26. Hydrate formation in methane -water system in the presence of 5 vol% HI03-187 at 117 bar / 1700 psia, 0.7 ^{o}C (13.6 ^{o}C subcooling).

6.3.2.5 In the presence of HT04-049

Natural gas-water system with HT04-049

The experiments for natural gas-water system with 5 volume% HT04-049 inhibitor (containing the BASF advanced polymer, water and a solvent) were carried out to study the mechanism of hydrate formation and crystal morphology in comparison with those of LUVICAP EG® (1 mass% PVCAP). Tests were carried out at two different pressures: 105 bar and 95 bar. At 105 bar, the system was cooled down step by step until hydrate formed at 2.5 ^{o}C (16 ^{o}C subcooling). As shown in Figure 6.27, the initial hydrate formation started at the interface between gas and water and formed a thick non-translucent layer that outlined the profile of gas bubbles (Figure 6.27(b)). Then a slow growth of small hydrate particles appeared within the gas bubbles. After about 24 hours (Figure 6.27(c)), most of the gas bubbles profiles were covered with these hydrate particles. The growth of hydrate crystals completed after 72 hours as shown in Figure 6.27(d). The hydrate particles turned into transparent and thin patches of crystal. The sequential still pictures taken during hydrate dissociation (Figure 6.28) showed clearly how the hydrate dissociated (from 10.4 ^{o}C to 22.9 ^{o}C) into tiny hydrate particles within gas bubbles as observed during initial hydrate formation. At static condition there is a still remnant of hydrate particles left within gas bubbles, which may require longer time to dissociate at temperature above dissociation temperature.

In another experiment carried out at 95 bar and 4.2 ^{o}C (13.7 ^{o}C subcooling), hydrate formed in the outlet of the micromodel that turned into transparent thin patches of hydrate crystal (Figure 6.29). However, it was observed that hydrates did not grow further inside the micromodel. After leaving the system for 24 hours, temperature was further reduced and more hydrate started to form in the pore structure of the micromodel at 2.6 ^{o}C (15.4 ^{o}C subcooling) as shown in Figure 6.30. It is observed that the mechanism of initial hydrate formation and morphology was similar to that at 13.7 ^{o}C subcooling. There was still remaining gas bubbles and water, which did not convert into hydrate. Larger driving force (higher degree of subcooling) may be required to covert the remaining water and gas molecules to hydrate.

The natural gas hydrate crystals growth in the presence of LUVICAP EG® and HT04-049 are compared. Based on still pictures shown in Figure 6.31(a), in the presence of

LUVICAP EG®, the hydrate crystals have not turned into translucent after passing 72 hours from the first hydrate particle formation. On the contrary, all hydrate crystals turned into translucent (their final stage in structural formation) in the presence of HT04-049 (Figure 6.31(b)) at similar degree of subcooling after passing 24 hours of hydrate formation. This suggests that 5 vol% HT04-049 is less effective than LUVICAP EG® (1 mass% PVCap) in delaying hydrate growth.

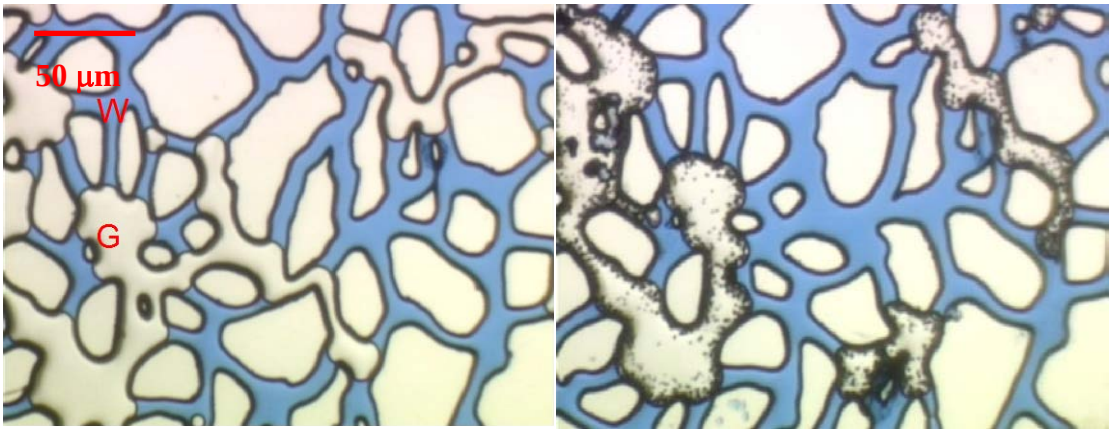

(a) before hydrate formation (b) 0.5 hrs after formation

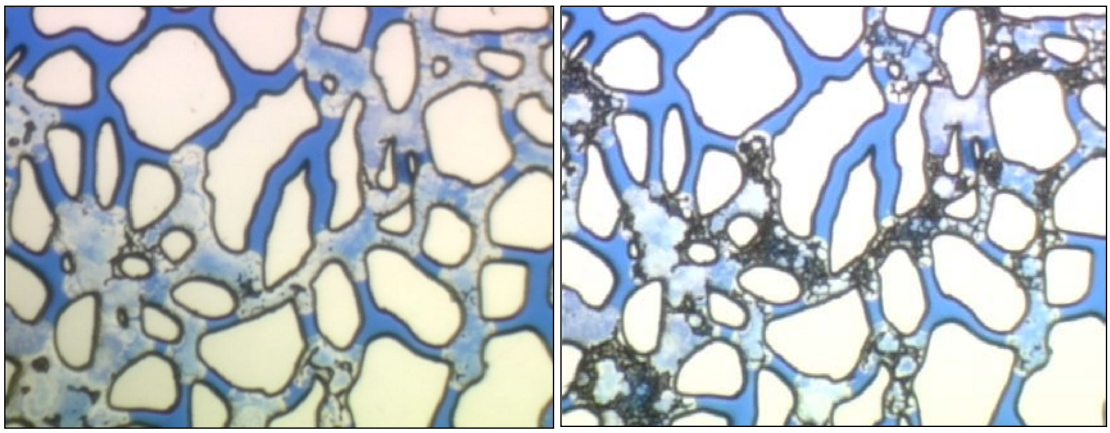

(c) 24 hrs after formation (d) 72 hrs after formation

Figure 6.27. Hydrate formation in natural gas-water system in the presence of 5 vol% of HT04-049 at 105 bar / 1522 psia, 2.5 ^{o}C (16 ^{o}C subcooling).

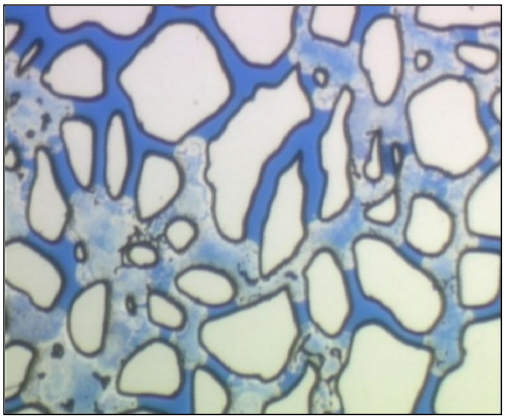

(a) T = 10.4^{o}C

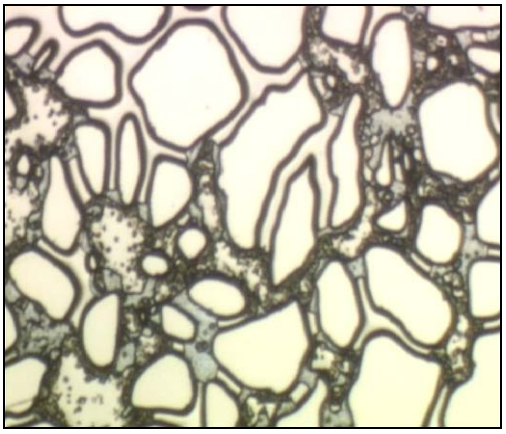

(b) T = 18.4^{o}C

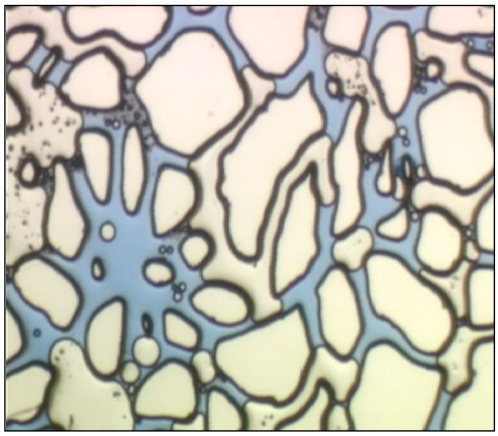

(c) T = 22.9^{o}C

Figure 6.28. Hydrate dissociation in the presence of 5 vol% of HT04-049 at 107 bar

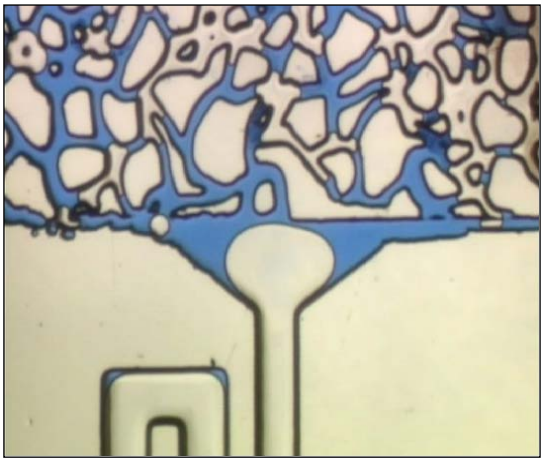

(a) before hydrate formation

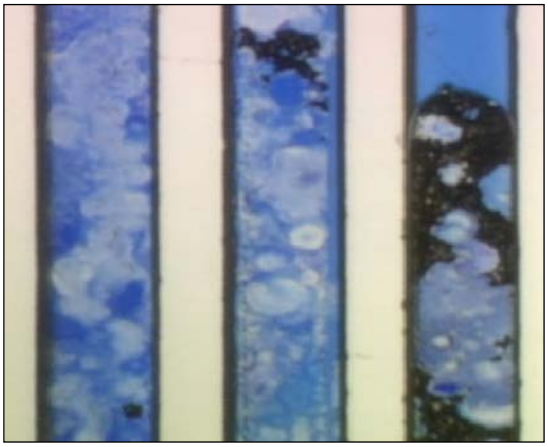

b) 2 hrs after formation

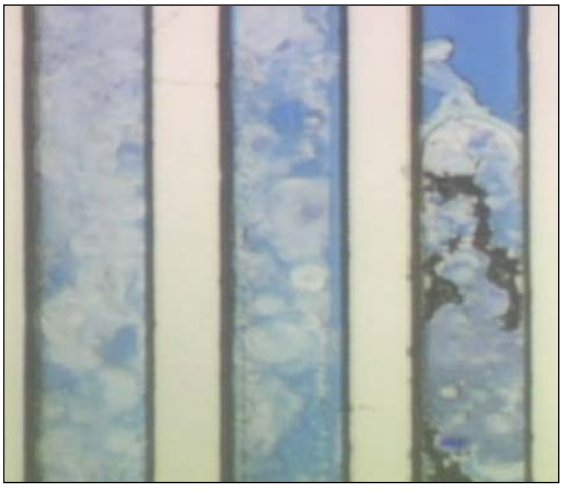

(c) 24 hrs after formation

Figure 6.29. Hydrate formation in natural gas-water system in the presence of 5 vol% of HT04-049 at 95 bar / 1378 psia, 4.2 ^{o}C (13.7 ^{o}C subcooling).

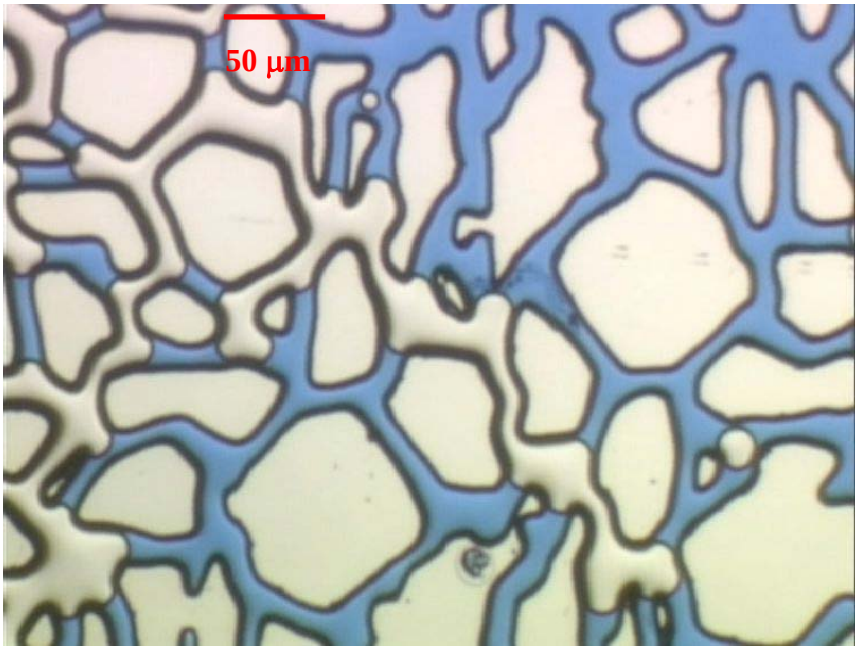

(a) before hydrate formation

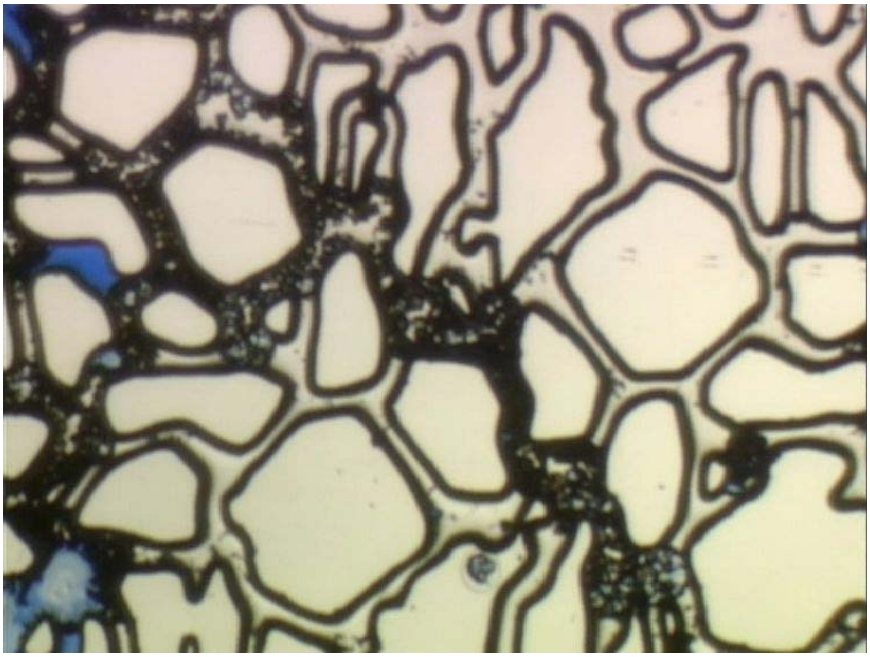

(b) 2 hrs after hydrate formation

Figure 6.30. Hydrate formation in natural gas-water system in the presence of 5 vol% of HT04-049 at 95 bar / 1378 psia, 2.6 ^{o}C (15.4 ^{o}C subcooling).

6.3.2.6 In the presence of PVCap base polymer

Natural gas-water system with PVCap base polymer

The experiments were conducted for the natural gas-water system with 1 mass% PVCap polymer (without solvent/carrier fluid) at 109 bar. The experiment was performed using a multichannel glass conduit shown in Figure 6.2. The sytem temperature was reduced to 4.7 ^{o}C with no hydrate formation after leaving the system for 62 hours. Then the temperature was further reduced and hydrate formed at 3 ^{o}C (15.5 ^{o}C subcooling) in the presence of 1.0 mass% PVCap. As seen from images in Figure 6.32, hydrate began to form at the water-gas interface and grew inside the gas phase or bubbles with a non-transparent crystals (Figure 6.32(b)). After about 24 hours, these hydrate crystals turned into small transparent crystals within the gas profile (Figure 6.32(c)). Hydrate deposits appeared to be more porous with the formation of patches of hydrate crystals (Figure 6.32(d)) which is similar morphology as seen under flowing conditions which is reported in Chapter 7.

6.3.3 Effect of KHs on Hydrate Crystals Morphology

6.3.3.1 Natural gas-water system

Based on the study reported in this thesis, it was observed that different hydrate morphologies in natural gas-water system formed in the presence of different kinetic inhibitors (all PVCap-based with different synergists). The summary of the morphology at various test conditions is provided in Table 6.5. The most common hydrate morphology observed during this study is dense masses solid, patches of hydrate crystals and thin patches crystal flakes. However, other different hydrate crystals were seen in the presence of HI03-187 and HI03-24. These are snowy crystal flakes, whiskery, threadlike, small dendrites and circular shape.

Effect of Synergistic Chemical: The different hydrate morphologies in natural gas-water system formed in the presence of different kinetic inhibitors (all PVCap-based with different synergists) at similar degrees of subcooling were compared. At the same degree of subcooling, the hydrate morphologies for the systems without inhibitor and the systems with PVCap are different as shown in Figures 6.33 (a) and (b). In the presence of PVCap, a dense solid hydrate crystal was observed in gas phase with little traces growth in dissolved gas. The morphology observed in the presence of HI03-24

and HI03-22 is significantly different from that in the presence of PVCap. The morphology in the presence of these inhibitors is mainly patches of very thin crystal flakes (Figure 6.33(c)) and small hydrate particles (Figure 6.33(d)). This suggests that the synergist chemicals have changed hydrate morphology and particle sizes for the same basic polymer. With formation of thin and small hydrate crystal, it suggest that even KHIs fail to inhibit hydrate formation at this test condition, the hydrate is still transportable and will not cause immediate blockage to the pipeline upon failure. For future work, it is recommended to investigate synergist chemical which could transport hydrate in the presence of KHI when it is failed. The effect of synergist chemical was further studied using multichannel flow conduit. The detail result is included in Chapter 7 of this thesis.

Effect of Different Base Polymer: The hydrate crystals morphology between the BASF advanced base polymer (HT04-049) and PVCap based polymers (LUVICAP EG® and HI03-24) were compared. As shown in Figure 6.34, while the morphology in the presence of LUVICAP EG® and blank sample without inhibitor exhibits mainly continuous solid hydrate crystals, in the presence of HT04-049 it exhibits thin patches of hydrate crystals. The transparent thin patches of hydrate crystals observed were similar to the one in the presence of HI03-24 (containing PVCap and a synergist chemical) at 14 ^{o}C subcooling (Figure 6.34(d)). This observation suggest that different base polymer will have an effect on hydrate morphology.

Effect of Carrier Fluid: The natural gas hydrate crystals morphology in the presence of 1 mass% PVCap with and without carrier fluid are compared in Figure 6.35. In the presence of PVCap with 1.5 mass% ethylene glycol as carrier fluid, a continuous solid hydrate formed in the micromodel (Figure 6.35(a)). On the other hand, without carrier fluid, thin patches of hydrate crystals were observed as shown in (Figure 6.35(b)). The results suggest that the carrier fluid have some effect on the morphology of hydrate crystal at the tested conditions.

This visual observation suggests various gas hydrate crystal morphology will form upon failure of KHIs. Hence, this methodology must be adopted as part of evaluating KHIs to provide understanding on the gas hydrate formation in the presence of KHIs.

Table 6.5 Summary of morphology, crystal growth and inhibition mechanism for natural gas hydrate

Inhibitor	Subcooling (^oC)	Pressure (psia/bar)	Temp. (^oC)	Observed Morphology, Crystal Growth and Inhibition Mechanism
Blank	14.5	1500/103	4	Dense masses solid in free gas phase and in dissolved gas (water phase) - Figure 6.5
	12	1000/69	4	Dense masses solid in free gas phase and in dissolved gas (water phase)
Luvicap EG ® (1 mass % PVCap)	14	1300/90	4	Dense masses solid in free gas phase and traces in dissolved gas (water phase) – Figure 6.7
	14	1300/90	4	Dense masses solid in free gas phase and traces in dissolved gas (water phase) – Figure 6.8 **Luvicap EG® is effective in inhibiting hydrate in dissolved gas (water phase)**
PVCap base polymer (1 mass %)	15.5	1580/109	3	Patches of hydrate crystal – Figure 6.32 **PVCap is effective in inhibiting hydrate formation in dissolved gas (water phase)**
BASF advanced base polymer HT04-049 (5 vol%)	16	1522/105	2.5	Thin patches crystal flakes in gas phase – Figure 6.27 & Figure 6.28
	13.7	1378/95	4.3	Thin patches crystal flakes in gas phase – Figure 6.29
	15.4	1378/95	2.6	Thin patches crystal flakes in gas phase – Figure 6.30 **H104-049 is effective in inhibiting hydrate formation in dissolved gas (water phase)**
H103-187 (5 vol%)	13.9	1300/90	4.1	Thin patches and snowy crystal flakes in gas phase – Figure 6.25 **H103-187 is effective in inhibiting hydrate formation in dissolved gas (water phase)**
H103-24 (5 vol%)	11.4	1500/103	7.1	Threadlike in free gas phase and whiskery in dissolved gas (water phase) – Figure 6.13
	12.4	1500/103	6.1	Small dendrite round shape in gas phase and non-transparent masses in dissolved gas (water phase) – Figure 6.15
	14.4	1350/93	4.1	Circular and thin patches crystal flakes in gas phase – Figure 6.16 **H103-24 is less effective in inhibiting hydrate formation in dissolved gas (water phase)**
H103-22 (5 vol%)	14	1360/94	4.3	Small hydrate particles and thin patches crystal flakes
	17	1360/94	0.5	Thin patches crystal flakes in gas phase - Figure 6.21 **H103-22 is effective in inhibiting hydrate formation in dissolved gas (water phase)**
H103-22 (2 vol%)	11.6	1300/90	6.4	Thin patches crystal flakes in gas phase – Figure 6.18 & Figure 6.19
	10	1000/69	6.3	Thin patches crystal flakes in gas phase
	12.5	1000/69	4	Thin patches crystal flakes in gas phase

Note: Refer to Table 6.2 for compound in inhibitors

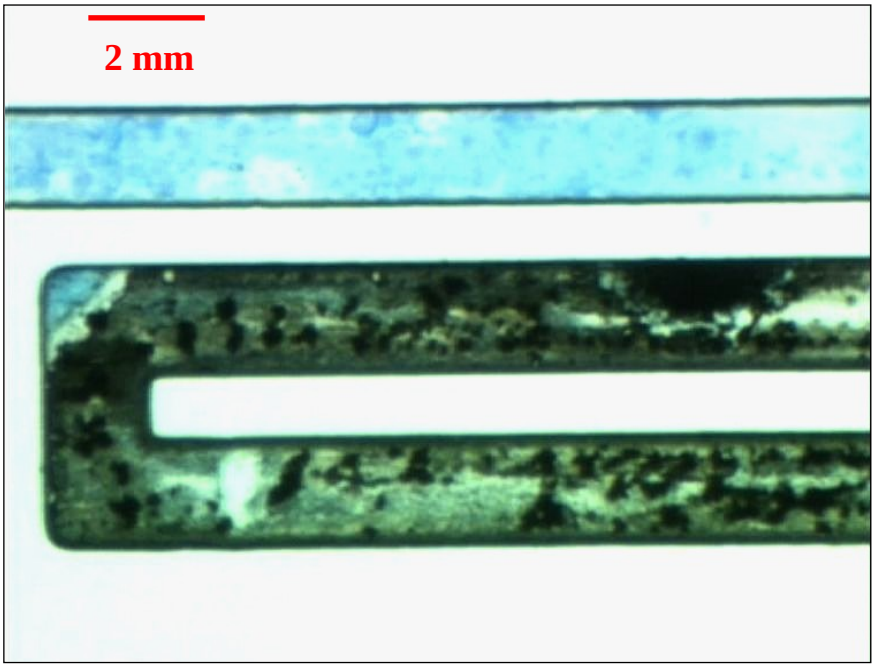

(a) 72 hours after formation (Luvicap EG ®)

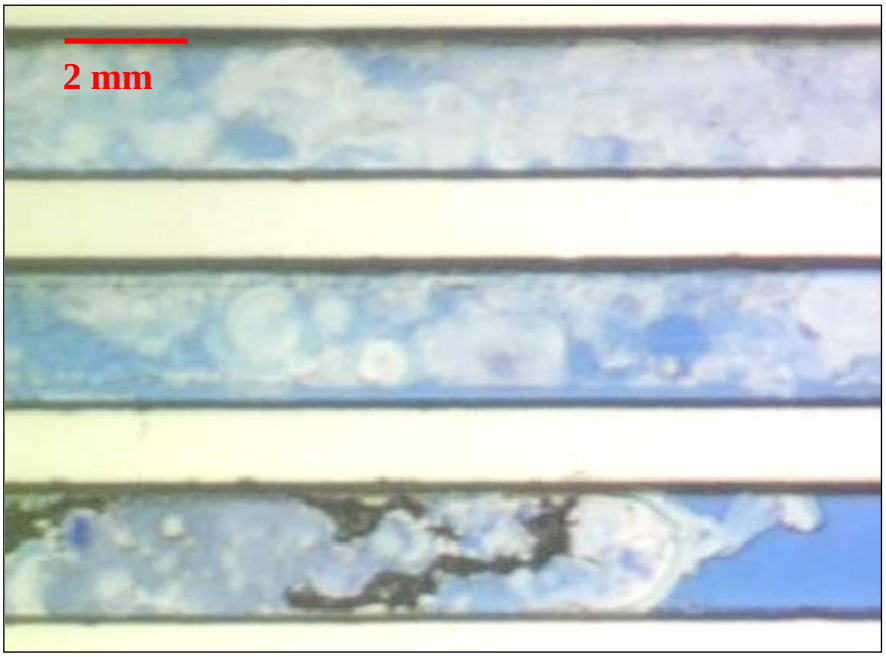

(b) 24 hours after formation (HT04-049)

Figure 6.31. Comparison of hydrate growth for natural gas – water system for (a) Luvicap EG ® (1 mass % PVCap) at 14 ^{o}C subcooling (b) 5 vol% HT04-049 at 13.7 ^{o}C subcooling

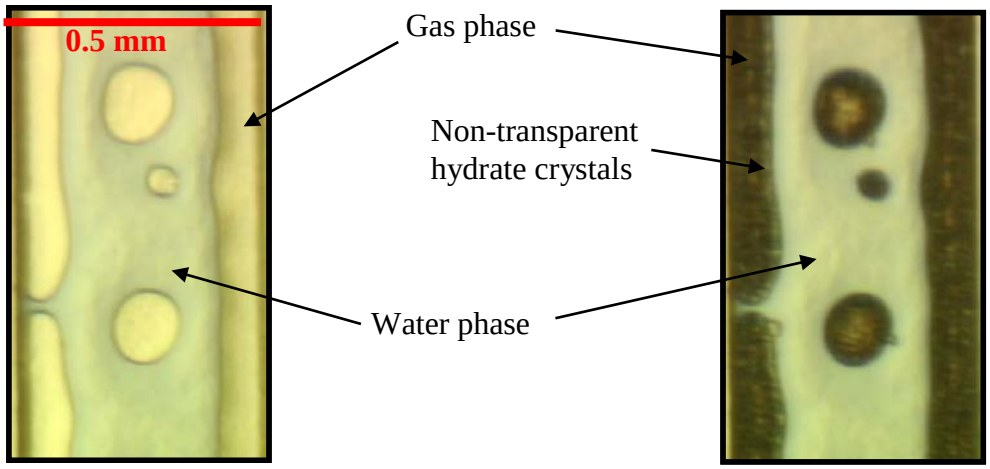

(a) Before hydrate formation (b) 3 hrs after formation

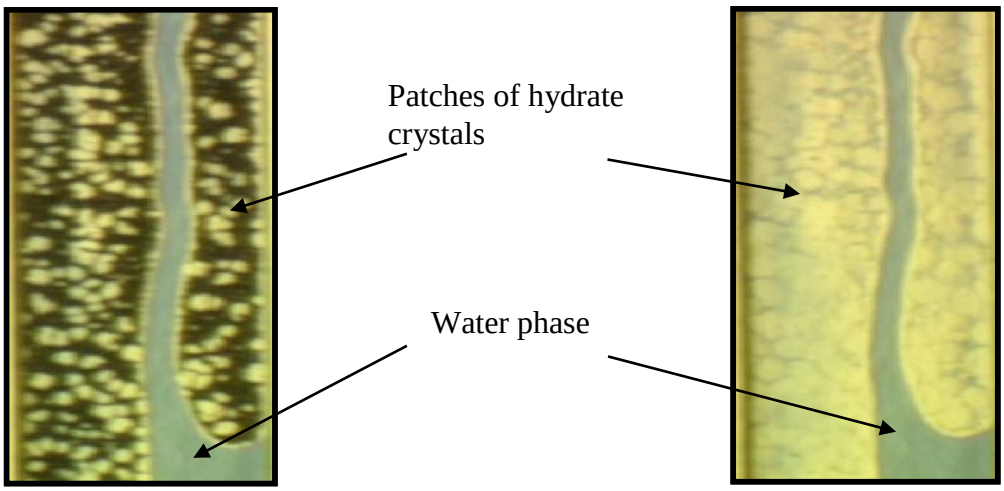

(c) 24 hrs after formation (d) 72 hrs after formation

Figure 6.32 Images of hydrate formation for natural gas-water system in the presence of 1 mass% PVCap base polymer at 109 bar / 1580 psia, 3.0 ^{o}C (15.5 ^{o}C subcooling).

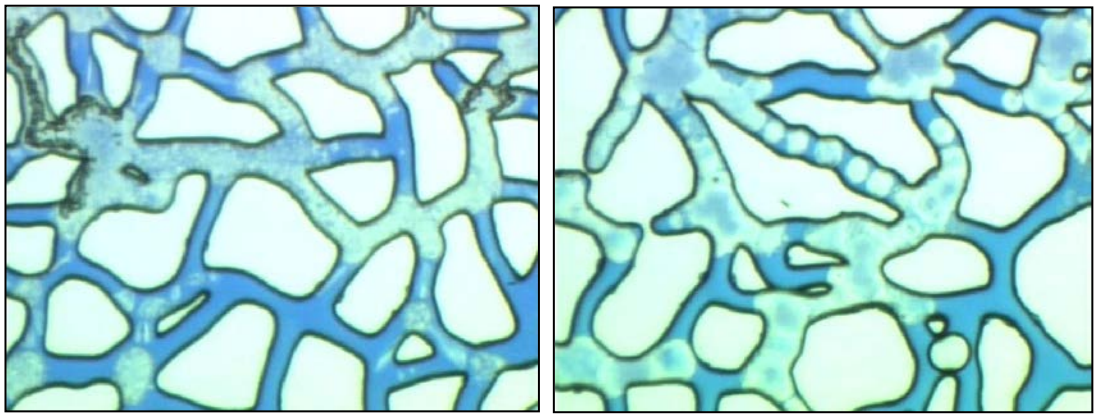

(a) Without inhibitor (b) With LUVICAP EG®

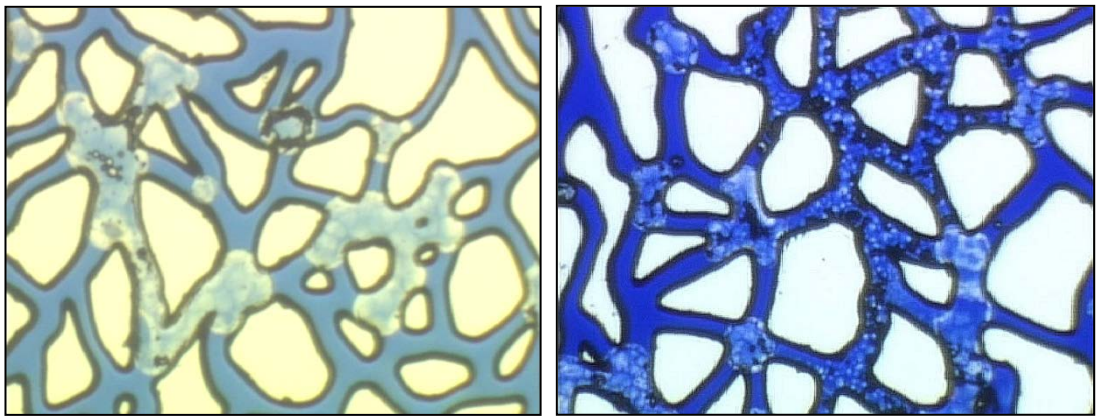

(c) With HI03-24 (d) With HI03-22

Figure 6.33. Comparison of hydrate morphology for natural gas – water system at 14 ^{o}C subcooling (a) without inhibitor - dense masses solid (b) with LUVICAP EG® - dense masses solid (c) with HI03-24 - thin patches (d) with HI03-22 - thin patches & small hydrate particles. Effect of Synergist.

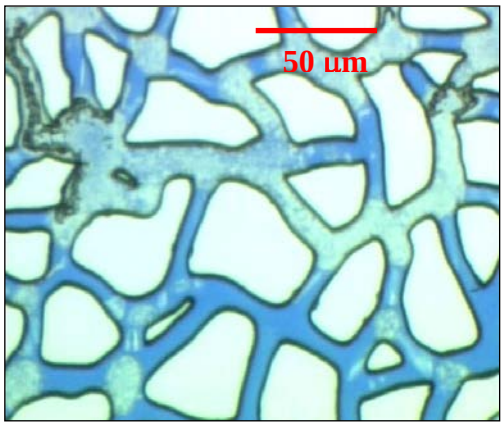

(a) Without inhibitor

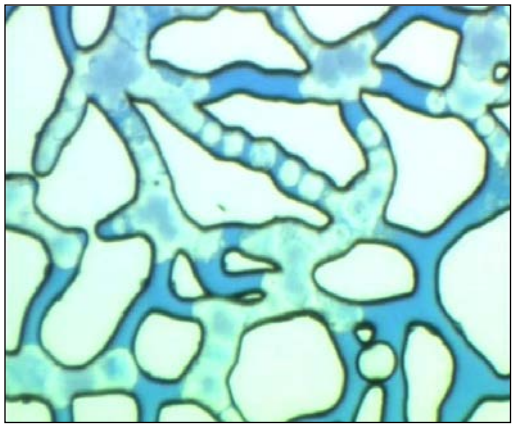

(b) LUVICAP EG® (PVCap + EG)

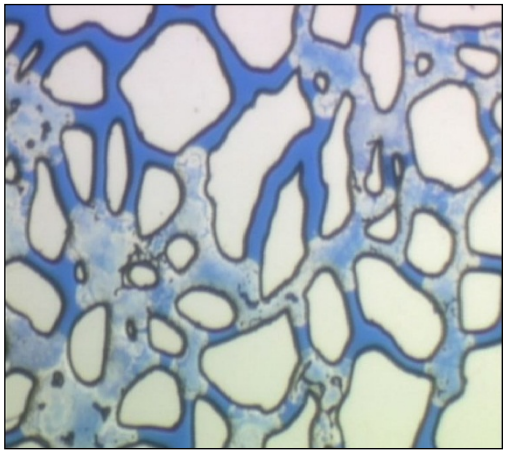

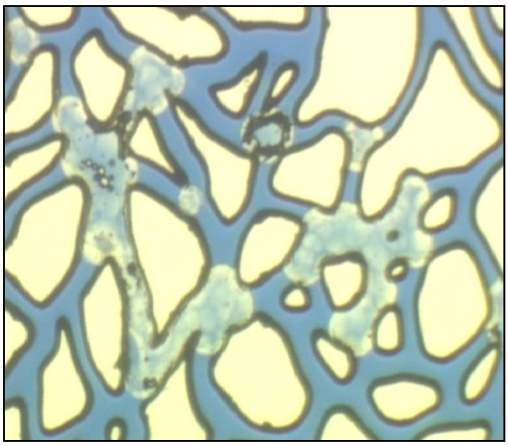

(c) HT04-049 (BASF base polymer + solvent) (d) HI03-24 (PVCap+EG+Synergist)

Figure 6.34. Comparison of hydrate morphology for natural gas – water system at 14 ^{o}C subcooling (a) without inhibitor - dense masses solid (b) with LUVICAP EG® - dense masses solid (c) with HT04-049 at 16 ^{o}C subcooling – thin patches (d) with HI03-24 – thin patches. Effect of different base polymer.

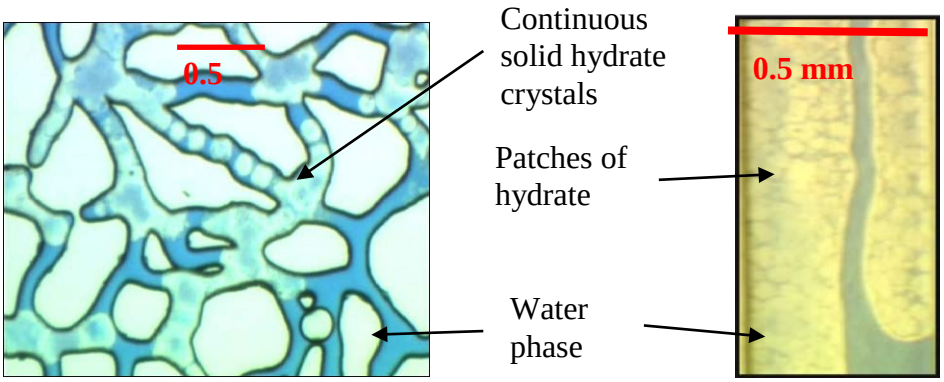

(a) LUVICAP EG® (40% PVCap+60% EG) (b) PVCap base polymer

Figure 6.35. Comparison of hydrate morphology for natural gas – water system in the presence of 1 mass% PVCap (a) with carrier fluid at 14 ^{o}C subcooling) (b) without carrier fluid at 15.5 ^{o}C subcooling.

6.3.3.2 Methane-water system

Several types of crystal morphology were observed for methane-water system with and without inhibitor as summarised in Table 6.6. Comparison was made between methane hydrate with PVCap, HI03-22 and HI03-24 inhibitor tested at about the same degree of subcooling. As shown in Figure 6.36(a), the hydrate crystals in the presence of PVCap, after 50 hours have not changed to transparent crystals (more ordered structure) while in the presence of HI03-22 (Figure 6.36(b)) and HI03-24 (Figure 6.36(c)) the hydrate crystals turned into ordered structures (transparent crystals). It seems that after hydrate formation the conversion of hydrate crystal to an ordered structure in the presence of synergist is faster than PVCap (without synergist). The hydrate crystal morphology is dense solid in the presence of PVCap and a continuous thin crystal in the presence of HI03-22 inhibitor. In the presence of HI03-24 thick and rough hydrate crystals were formed.

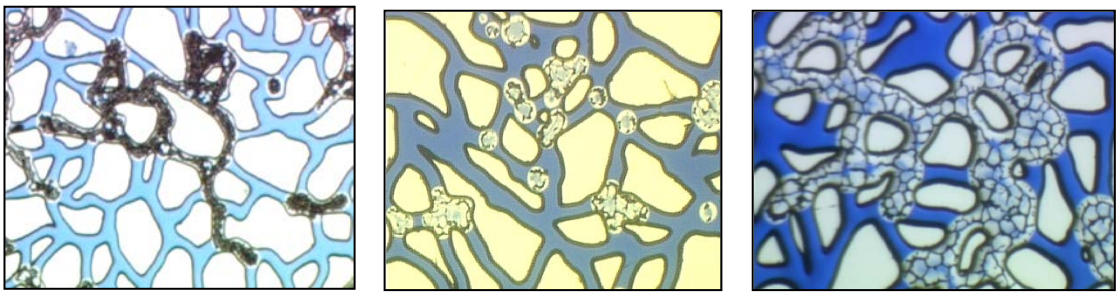

(a) PVCap (after 50 hours) (b) HI-0322 (after 54 hours) (c) HI0-324 (after 39 hours)

Figure 6.36. Comparison of hydrate morphology for methane – water system at 10.5 – 11.5^{o}C subcooling for (a) 1 mass% PVCAP (b) HI03-22 (c) HI03-24

Table 6.6 Summary of morphology for Methane gas hydrate

Inhibitor	Subcooling (^{o}C)	Pressure (psia/bar)	Temp. (^{o}C)	Observed Morphology, Crystal Growth and Inhibition Mechanism
Blank	17	2800/193	4.5	Large hydrate crystal plugs in gas phase and also hydrate crystal in dissolve gas (water phase) – Figure 6.6
	13	2300/158	4	Dense masses hydrate crystal – Figure 6.11(a)
Luvicap EG ® (1 mass % PVCap)	13	2300/158	4	More dispersed hydrate crystal from gas phase and grow into dissolved gas (water phase) – Figure 6.11(b)
	10.5	1700/117	4	Large plug and massive solid hydrate following profile of gas phase with dark masses of hydrate – Figure 6.12
H103-187 (5 vol%)	13.6	1700/117	0.7	Hydrate shell in gas phase with water remain in the middle – Figure 6.26
H103-24 (5 vol%)	11.5	1700/117	3	Thick and rough crystal separated within original gas profile – Figure 6.17
H103-22 (2 vol%)	10.5	1700/117	4.3	Hydrate shell inside the gas phase, water remain in the middle, continuous agglomerated thin crystal – Figure 6.22; Traces of hydrate crystals in water phase – Figure 6.23

6.3.4 Effect of KHIs on Morphology of different Hydrate Structure

A comparison between natural gas – water (s-II) and methane-water (s-I) systems were made to observe different morphologies of hydrates in the presence of HI03-22 and HI03-24. In the presence of HI03-22, it was observed that thin flakes of hydrate crystals formed from natural gas (s-II) and continuous thin solid hydrate crystals formed from methane (s-I) as shown in Figure 6.37. In the presence of HI03-24, a mixture of whiskery and thread like hydrate crystals are formed in natural gas systems (s-II), while at similar degrees of subcooling, thick and rough hydrate crystals are formed in methane

systems (s-I) as shown in Figure 6.38. This comparison suggests that KHIs have different effect on hydrate morphology for different hydrate structure.

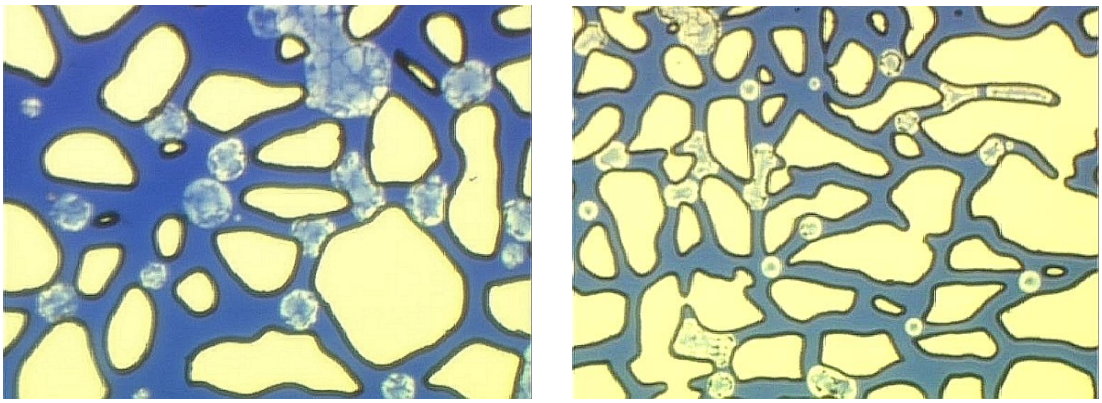

(a) Natural gas - water system (s-II) - thin patches

(b) Methane-water system (s-I) - hydrate shell inside gas phase

Figure 6.37. Comparison of hydrate morphologies for natural gas and methane in the presence of HI03-22 at 10 ^{o}C subcooling

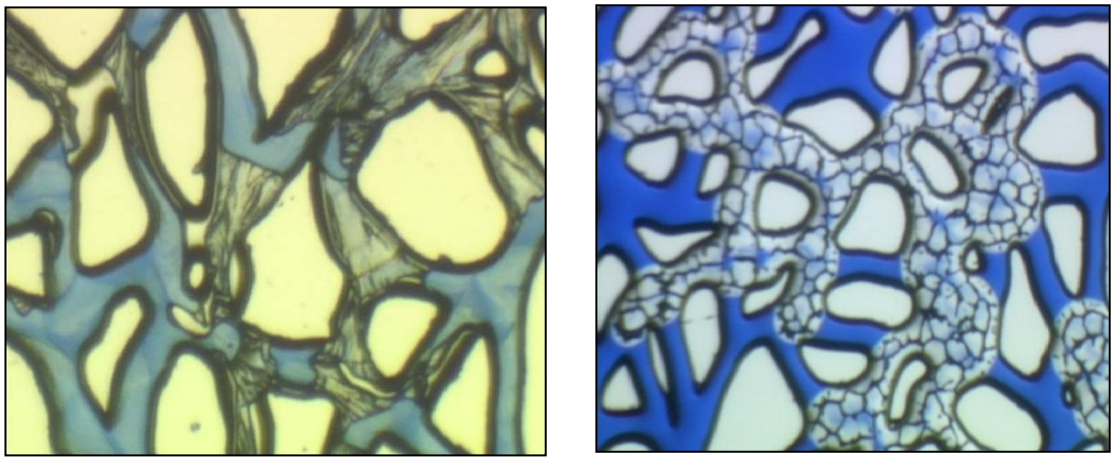

(a) Natural gas - water system (s-II) - threadlike (gas phase), whiskery (water phase)

(b) Methane-water system (s-I) thick and rough crystals

Figure 6.38. Comparison of hydrate morphologies for natural gas and methane in the presence of HI03-24 at 11.4 ^{o}C subcooling. Effect of KHIs on Morphology of different hydrate structure

6.4. SUMMARY AND CONCLUSIONS

In this thesis, extensive novel data and knowledge was generated to study gas hydrate in the absence and presence of KHIs for various fluid systems. The objective is to investigate the inhibition mechanism of typical commercial KHIs by visual observation of hydrate morphology, growth patterns and hydrate formation. The investigation was conducted using High Pressure Glass Micromodel with pore structure network and multichannel glass conduit.

The study was investigated for methane-water and natural gas – water systems. Methane represents structure I hydrate, whereas natural gas for structure II hydrates. In this thesis, experiment on natural gas – water systems is the major fluid system been studied. This is because they closely represent hydrate formation from real reservoir fluids, which are dominated by structure II systems. The result suggests that different mechanisms seem to be involved for the different systems. This study shows that hydrate can form at gas-water interface or from dissolved gas in the water phase or from water in the gas phase as summarised in Table 6.3 of Chapter 6. For example, based on the video footage captured for natural gas - water system at 14.5^{O}C subcooling, hydrate formed in the gas phase or bubbles (from free gas) as a non-translucent (dark coloured) crystals. The hydrate crystal was transported through the water phase to the adjacent free gas bubbles to form hydrate. The process was continuous until all gas bubbles were converted to hydrate. There was also evidence of traces of translucent hydrate crystals formed from dissolved gas in the water phase.

Several commercial KHIs which are polymer base were used in this study to investigate the inhibition mechanism of the natural gas-water and methane-water system. These KHIs are LUVICAP EG®, HI03-24, HI03-22, HI03-187, HT04-049 and pure PVCap. These inhibitors are mainly PVCap based polymer in combination with Ethylene Glycol as a carrier fluid. A synergist chemical is additional compound present in inhibitor HI03-24, HI03-22 and HI03-187 whereas inhibitor HT04-049 is another base polymer used for this investigation. In this thesis, hydrate crystal morphology and growth pattern in the presence of different KHIs was reported. The effect of synergistic chemical, carrier fluid and different base polymer on hydrate morphology was also documented.

The finding of this study shows that various hydrate morphologies formed in the presence of different KHIs. The common hydrate morphology observed for inhibition characteristic of natural gas-water system by majority of tested KHIs was dense masses solid, patches of hydrate crystals and thin patchy crystal flakes. However, different hydrate crystals morphology was observed in the presence of HI03-187 and HI03-24. These are snowy crystal flakes, whiskery, threadlike, small dendrites and circular shape. Results of morphology are summarised in Table 6.5 of Chapter 6. For methane-water system the inhibition characteristic resulted in thick rough crystals, hydrate shell thin crystals and large massive solid crystals as summarised in Table 6.6 of Chapter 6.

The morphologies in the presence of KHIs with and without synergistic chemical (all PVCap-based with different synergists) for natural gas-water system at similar degrees of subcooling were investigated and compared. At the same degree of subcooling, the hydrate morphologies for the systems without inhibitor and the systems with LUVICAP EG® are different. In the presence of LUVICAP EG®, a dense solid hydrate crystal was observed in gas phase with little traces growth in dissolved gas. The morphology observed in the presence of HI03-24 and HI03-22 is significantly different from that in the presence of LUVICAP EG®. The morphology in the presence of these KHIs is mainly patches of very thin crystal flakes and small hydrate particles. This suggests that the synergist chemicals have changed hydrate morphology and particle sizes for the same basic polymer. With formation of thin and small hydrate crystal, it suggests that even KHIs fail to inhibit hydrate formation at this test condition, the hydrate is still transportable and potentially will not cause immediate blockage to the pipeline upon failure. For further work, it is recommended to investigate synergist chemical which could transport hydrate in the presence of KHIs when it is failed. The effect of synergist chemical was studied using multichannel flow conduit and the detail result is included in Chapter 7 of this thesis.

The natural gas hydrate crystals morphology in the presence of PVCap with and without carrier fluid was investigated. In the presence of PVCap with ethylene glycol as the carrier fluid, a continuous solid hydrate formed in the micromodel. On the other hand, without carrier fluid, thin patches of hydrate crystals were observed. The results suggest that the carrier fluid have some effect on the morphology of hydrate crystal at these test conditions.

For methane-water system, the hydrate morphology and growth pattern was investigated in the presence of PVCap, HI03-22 and HI03-24 tested at about the same degree of subcooling. The hydrate crystal morphology is a dense solid in the presence of PVCap, a

continuous thin crystal in the presence of HI03-22 inhibitor and thick rough hydrate crystals in the presence of HI03-24.

The effect of KHIs on hydrate crystal morphology for different hydrate structure was analysed by comparing morphologies of natural gas (s-II) and methane (s-I) hydrates in the presence of HI03-22 and HI03-24. In the presence of HI03-22, it was observed that thin flakes of hydrate crystals formed from natural gas (s-II) and continuous thin solid hydrate crystals formed from methane (s-I). In the presence of HI03-24, natural gas S-II) exhibits a mixture of whiskery-like and thread-like hydrate crystals, while at similar degrees of subcooling, methane gas (s-I) forms a thick and rough hydrate crystal. This suggests that different hydrate crystal morphology is generated from different hydrate structure in the presence of KHIs.

The following conclusion can be drawn from investigating inhibition mechanism of Kinetic Hydrate Inhibitors (KHIs) by visual observation of gas hydrate morphology, growth pattern and formation:

i. Various hydrate morphologies formed in the presence of different KHIs for Natural gas hydrate. This morphology are dense masses solid, patches of hydrate crystals, thin patchy crystal flakes, snowy crystal flakes, whiskery, threadlike, small dendrites and circular shape. For methane hydrate the morphology are thick rough crystals, hydrate shell thin crystals and large massive solid crystals
ii. Synergistic chemical as a compound in the KHIs have significant effect on hydrate morphology. The morphology in the presence of synergistic chemical was found to exhibit patches of very thin crystal flakes and small hydrate particles. This suggests that the synergist chemicals have changed hydrate morphology and particle sizes for the same basic polymer. With formation of thin and small hydrate crystal, it suggests that even KHIs fail to inhibit hydrate formation at this test condition, the hydrate is still transportable and potentially will not cause immediate blockage to the pipeline upon failure.
iii. The present of carrier fluid in the KHIs have effect on hydrate crystal morphology. The result shows that in the presence of PVCap with ethylene glycol as the carrier fluid, continuous solid hydrate morphology was formed. On

the other hand, thin patches of hydrate crystals were observed without carrier fluid.

iv. Different hydrate crystal morphology is generated from different hydrate structure in the presence of KHIs.

CHAPTER 7
INVESTIGATING INHIBITION MECHANISM OF LOW DOSAGE HYDRATE INHIBITOR (LDHI) BY DYNAMIC VISUAL OBSERVATION

This chapter describes the detail measurement of visual observation via dynamic multichannel flow conduit and glass capillary blockage technique to investigate the mechanism of gas hydrate morphology, growth pattern and inhibition. The main objective is to understand the mechanism of gas hydrate growth and inhibition in the presence of LDHI under dynamic condition and its effect on plugging. In this chapter, evaluation of Kinetic Hydrate Inhibitor (KHI) and Anti-agglomerant (AA) were studied. The second objective is to investigate the effect of synergist material and corrosion inhibitor on the performance of KHI based on characteristic behaviour of hydrate plugging.

7.1 EXPERIMENTAL METHODOLOGY

7.1.1 Experimental facilities and materials

The high pressure micromodel was modified as shown in Figure 7.1 to cater for the study under dynamic/flowing conditions. Two experimental model set-up which are multichannel flow conduit and capillary glass tube were used for evaluation of KHI and AA respectively.

All LDHI chemical (LUVICAP-EG®), Corrosion inhibitor (Corrtreat 799) and Anti-agglomerant (HT04-106) used in this study was supplied by Clariant Oil Services except for PVCap base polymer which was supplied by BASF. Propylene glycol propyl ether (PGPE) with 99% purity was supplied by Aldrich. Details are provided in Table 7.1.

The natural gas (composition listed in Table 7.2) supplied by Air products and the North Sea condensate sample with composition listed in Table 7.3 were used for evaluation of Anti-agglomerate under dynamic/flowing condition.

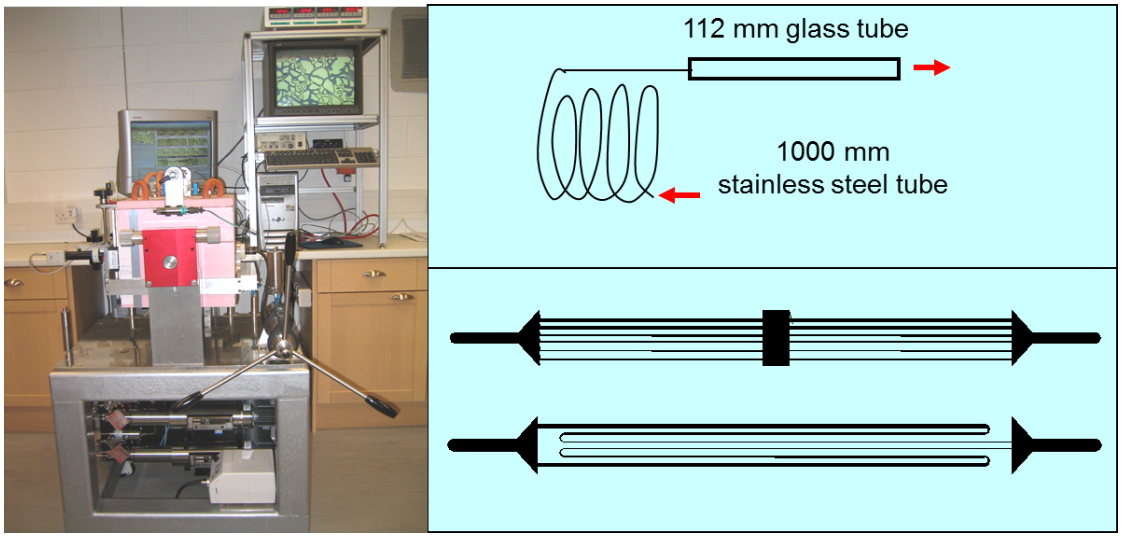

Figure 7.1 Schematic diagram of the Multi-channel Flow Conduit and Glass Capillary Tube set-up

Table 7.1: Information on Chemicals used for this study

Name of Inhibitor	Supplier	Concentration
Luvicap EG®	Clariant	2.5 mass%
PVCap base polymer	BASF	0.5 mass%
PGPE	Aldrich	0.75 mass%
HT04-106	Clariant	2.5 mass%
Corrotreat 799	Clariant	500 ppm
PVCap base polymer	BASF	1 mass%
NaCl	Aldrich	3 mass%

Table 7.2 Natural Gas Composition

Component	Mole%	Component	Mole%
N_2	2.673	i-C_4	0.182
CO_2	1.756	n-C_4	0.284
C_1	88.553	i-C_5	0.072
C_2	5.051	n-C_5 +	0.042
C_3	1.387		

Table 7.3 North Sea Condensate Composition

Component	Mole %	Component	Mole %
C_1	0.032	C_{10s}	13.921
C_2	0.147	C_{11s}	7.470
C_3	0.640	C_{12s}	3.622
iC_4	0.445	C_{13s}	1.766
nC_4	1.045	C_{14s}	0.638
iC_5	1.295	C_{15s}	0.272
nC_5	1.512	C_{16s}	0.059
C_{6s}	5.810	C_{17s}	0.015
C_{7s}	14.384	C_{18s}	0.011
C_{8s}	26.458	C_{19s}	0.003
C_{9s}	20.453	C_{20s}	0.003

7.1.2 Experimental procedure

7.1.2.1 Application of Multichannel flow conduit

The pore structure glass micromodel was replaced with a multichannel flow conduit for testing under flowing/dynamic conditions. The deionised water (dyed with methyl blue) with or without kinetic inhibitor was saturated with natural gas at 103 bar in high-pressure cylinders. The cylinder content was shaken several times to promote gas dissolution in the water and it was left for 12 hours to reach equilibrium. About 20 ml of this presaturated solution was charged into the sample cylinder of micromodel set-up at constant pressure using HPLC pump. Another sample cylinder was filled with the natural gas at the desired test pressure. Deionised water or natural gas inside the system was then displaced with pre-saturated solution at constant pressure and allowed to equilibrate at the desired temperature and pressure conditions.

Flow test began by simultaneous injection of the pre-saturated solution and natural gas at constant rate (0.1 cc/hr) into the system through outlet (bottom) of micromodel using a high-pressure quizix pump. The system temperature was reduced step by step if the hydrate had not been formed after more than 24 hours. Pressure inside the micromodel was maintained at 104 bar by backpressure regulator at the inlet (top) side. The formation of hydrate was visually observed and recorded accordingly. The measured and observed parameters are characteristic of hydrate build-up, hydrate deposits on the glass walls (e.g. no deposit, traces, thin hydrate layer, large deposits) and also estimated induction time. In some cases, changes in the differential pressure across

micromodel due to hydrate blockage were measured. In this case, the blockage is defined as when the injection pressure has reached to the maximum set pressure limit (e.g. 156 bar) of the micromodel. The induction time was estimated from the time when the injection started at stabilised conditions of pressure and temperature until hydrate formation.

7.1.2.2 Application of Glass capillary tube

The evaluation of Anti-agglomerant was conducted using a glass capillary tube. In this study, the micromodel system was modified to a single glass capillary tube (length of 112 mm and internal diameter of 0.5 mm), which was connected to the 1-meter stainless steel tube inside the bath. In general, similar procedure was followed for preparing the system for injection as described above in the tests using multi-channels flow conduit. The changes in the differential pressure, which indicate, hydrate formation and visual observation within the capillary tube was recorded for analysis. During the experiments, shut-in conditions were also investigated by stopping the injection and closing all the valves. After 24 hours the injection was restarted until the maximum set point pressure limit was reached.

In the case of studying hydrate crystal size in the presence of Anti-agglomerant, the water in oil emulsion was prepared by mixing water (containing 0.5 mass% of AA labelled as HT04-106) and the condensate. The mixing ratio of water-condensate is 30:70. Stable emulsion, milky colour, was formed using high pressure mixer with 24000 rpm. The water in oil emulsion was saturated with natural gas at 69 bar (1000 psi). Subsequently, this mixture was injected into the system to displace deionised water. The natural gas was injected to pressurize the system at the desired test pressure which is 102 bar (1500 psi). The system was left for 12 hours to equilibrate prior to reducing the system temperature to 4 ^{o}C to initiate hydrate formation.

7.2 Fluid system

Fluid system for Evaluation of KHIs: A study was performed to investigate the system under flowing conditions using multichannel flow conduit. The main objective is to understand the mechanism of gas hydrate morphology, growth pattern and inhibition in the presence and absence of LDHI under dynamic condition. The procedure is developed to compliment other existing laboratory protocol (HP cell rig,

Ultrasonic, Visual rig, static Visual HP Micromodel). During flow test, characteristic behaviour of hydrate plugging with and without LDHI and/or synergist at simulated pipeline condition was investigated. Experiments were performed for natural gas-water system with and without kinetic inhibitors as listed below:

- Natural gas with distilled water
- Natural gas with an aqueous solution of PVCap base polymer
- Natural gas with an aqueous solution of PVCap base polymer and PGPE

A study on compatibility of the corrosion inhibitor (CI) with PVCap was reported by Tohidi et. al. (Tohidi et al, 2005). The finding based on kinetic rig shows that CI have adversely affected the performance of PVCap. Therefore, the study using micromodel was designed to investigate this effect. These studies were performed on the following systems:

- Natural gas with an aqueous solution of LUVICAP-EG®
- Natural gas with an aqueous solution of LUVICAP-EG® and Corrtreat 799

Fluid system for evaluation of AA: A series of tests was designed to evaluate the anti-agglomerant using capillary tube blocking technique under flowing/dynamic and static conditions. The characteristic behaviour of hydrate plugging and time for blockage was observed. In addition, the hydrate particles size and distribution was also investigated for natural gas–condensate-water in the presence of anti-agglomerant at static conditions. Analysis related to evaluation of anti-agglomerant were performed for the following systems:

- Natural gas with distilled water
- Natural gas - condensate with an aqueous solution of 3 mass% NaCl
- Natural gas - condensate with an aqueous solution of HT04-106
- Natural gas - condensate with an aqueous solution of 3 mass% NaCl and HT04-106
- Gas condensate with an aqueous solution of 3 mass% NaCl and HT04-106

7.3 EXPERIMENTAL RESULTS AND ANALYSIS

7.3.1 Evaluation of kinetic hydrate inhibitor

7.3.1.1 Effect of Synergist

The experiments were conducted for natural gas-water system in the presence of 0.5 mass% polyvinyl caprolactam (PVCap) based polymer and a mixture of 0.5 mass% PVCap base polymer with 0.75 mass% Propylene glycol propyl ether (PGPE). PGPE was selected as synergist chemical to study the effect of known synergist on kinetic inhibitor performance and also its influence on hydrate morphology and plugging. This combination of inhibitor and concentration was selected in line with the series of tests performed in the kinetic rig and ultrasonic rig under bulk and static conditions (Tohidi et al, 2005). Schematics of these rigs are illustrated in the Appendix D of this thesis. PGPE, a non-toxic chemical, was reported to be the second best glycol ether solvents acts as synergist to PVCap and VC-713 [terpolymer of vinylcaprolactam, vinylpyrrolidone, and (dimethylamino) ethyl methacrylate] (Cohen et al, 1997).

During experiment, induction time was estimated from the start of the injection at stabilised condition, and differential pressure across micromodel was recorded. It is important to take note that induction time for this aspect of experiment is only based on estimation since there is no reproducible data similar to that generated from kinetic rig for a proper induction time measurement. The estimated induction time for the analysis conducted in this chapter is monitored based on the time for hydrate formation at specific subcooling. A more measureable data is based on the reported time for blockage to occur. These data were used to indicate initial hydrate formation and duration for total blockage in the micromodel under flow conditions. Visual observation on hydrate growth, build-up and deposits were captured through video recording and still pictures.

Natural gas with distilled water

The blank test was first established by simultaneously injecting presaturated water and natural gas at 11 ^{o}C subcooling and 109 bar. Based on the differential pressure profile shown in Figure 7.2, hydrate started to form after 0.25 hour of induction time. The

system pressure was continuously build-up due to injection of fluid and more hydrate formation until the blockage occurred after passing 7.2 hours of initial hydrate formation. The sequential still pictures are shown in Figure 7.3. As can be seen, a continuous solid and non-porous hydrate blocked the capillary tubes.

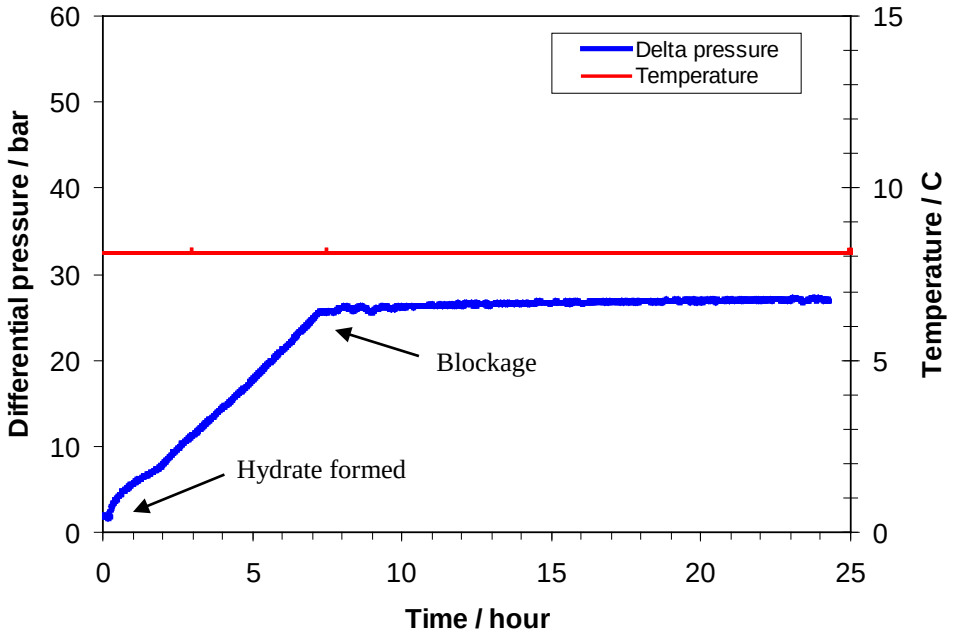

Figure 7.2. Differential pressure profile for natural gas – water system at 109 bar. Hydrate formed at 8 ^{o}C (11 ^{o}C subcooling)

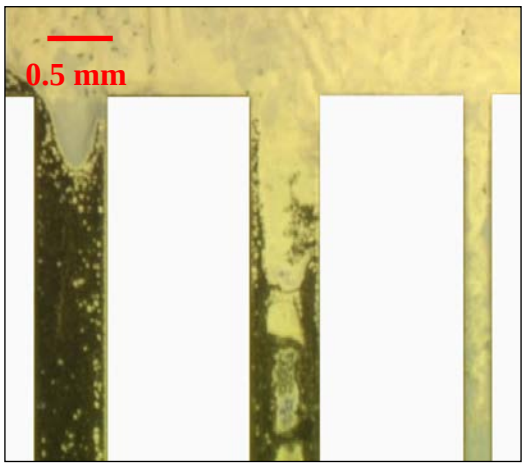

(a) 3 hrs after formation, ΔP = 12 bar

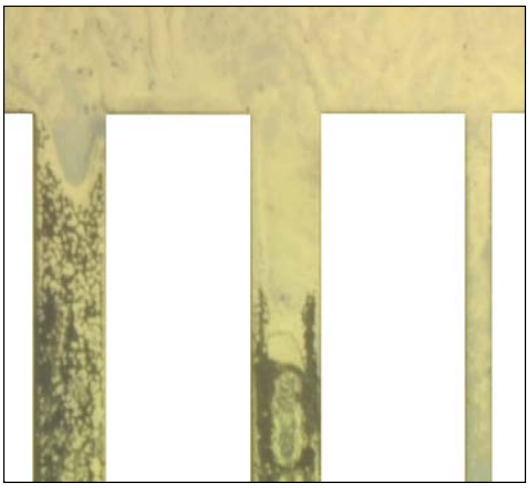

(b) 8 hrs after formation, ΔP = 26 bar

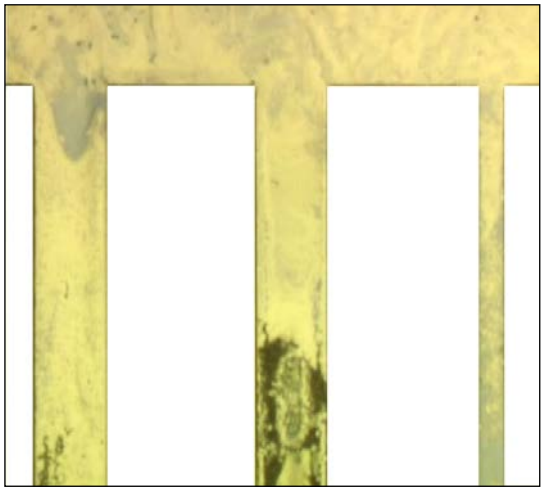

(c) 24 hrs after formation, ΔP = 27 bar

Figure 7.3. Images of hydrate deposits for natural gas – water system at 109 bar, 8 ^{o}C (11 ^{o}C subcooling)

Natural gas with an aqueous solution of PVCap

In the presence of 0.5 mass% PVCap, hydrate did not formed at 8 ^{o}C (11 ^{o}C subcooling) after leaving the system at this condition for 64 hours. Then, the system temperature was further reduced to 6 ^{o}C (13 ^{o}C subcooling). Hydrate formed at this condition with induction time of 1.23 hours as shown by the differential pressure profile in Figure 7.4. In this case, total blockage in the capillary tubes occurred after 13.6 hours of the initial hydrate formation. As expected, the presence of PVCap would slow down hydrate growth, delay blockage and also prevent hydrate formation in the water phase as compared to blank test without inhibitor. As seen in Figure 7.5, hydrate deposits initially appeared to be more porous. As time progressed, more hydrates are formed which finally could turn to a non porous solid and lead to blockage within capillary tubes.

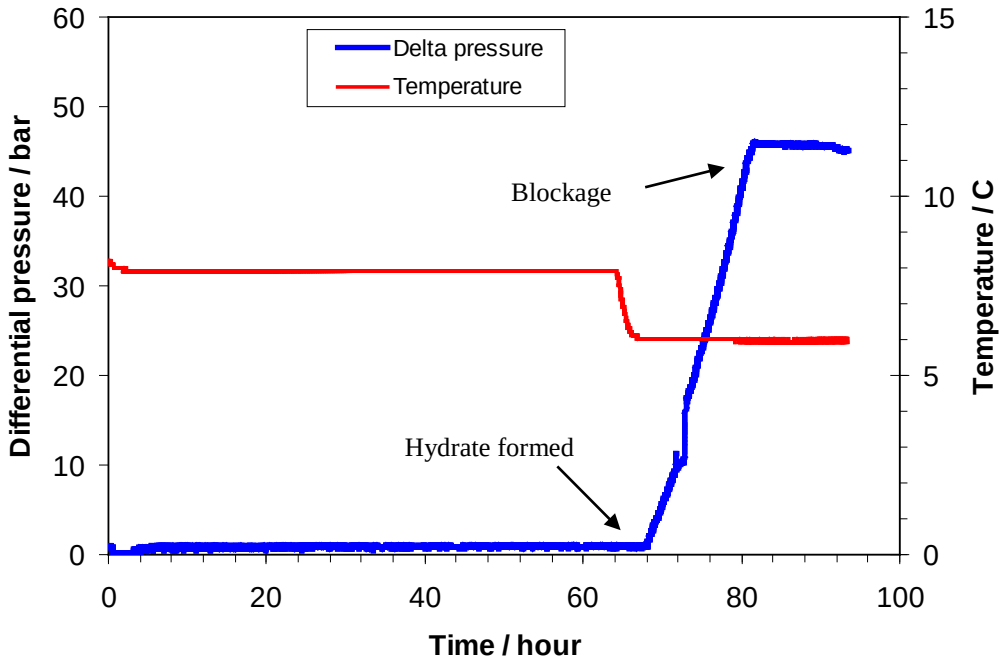

Figure 7.4. Differential pressure profile for natural gas – water system with 0.5 mass% PVCap at 109 bar. Hydrate formed at 6 ^{o}C (13 ^{o}C subcooling).

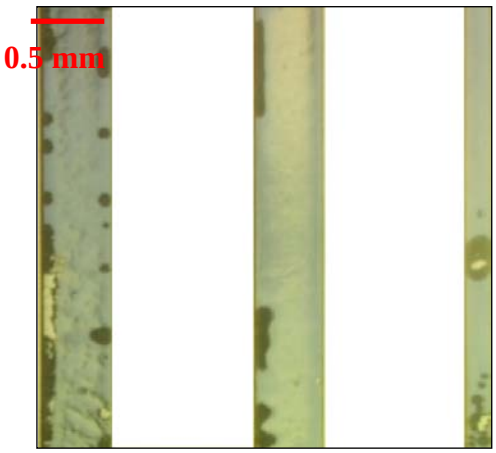

(a) 0.8 hrs after formation, ΔP = 3 bar

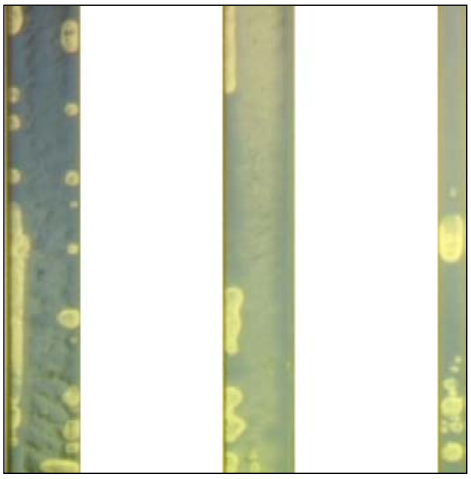

(b) 4 hrs after formation, ΔP = 10 bar

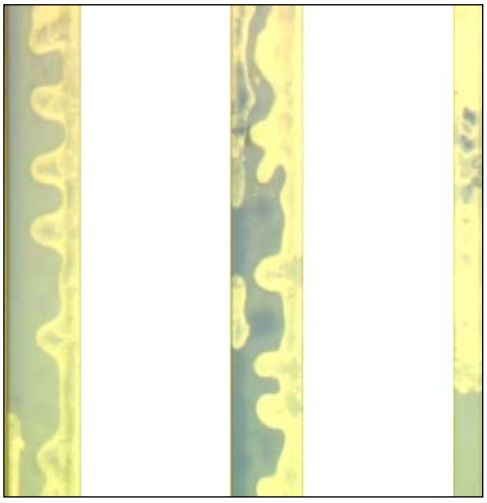

(c) 10 hrs after formation, ΔP = 32 bar

Figure 7.5. Images of hydrate deposits for natural gas – water system with 0.5 mass% PVCap base polymer at 109 bar, 6 ^{o}C (13 ^{o}C subcooling).

Natural gas with an aqueous solution of PVCap base polymer and PGPE

Another test was carried out in the presence of mixture 0.5 mass% PVCap base polymer and 0.75 mass% PGPE. Hydrate did not form at 8 ^{o}C (11 ^{o}C subcooling) after 45 hours. The temperature was further reduced to 6 ^{o}C (13 ^{o}C subcooling) and left for more than 60 hours. The temperature was further decreased to 4 ^{o}C (15 ^{o}C subcooling) and hydrate formed after 1.63 hours induction time. The blockage occurred 23.8 hours after the initial hydrate formation (Figure 7.6). Hydrate formed as a thin deposit and also solid hydrates in several parts of capillary tubes (Figure 7.7).

The summary of results for flow test is given in Table 7.4. It is interesting to note that in the presence of PGPE as a synergist for PVCap, hydrates form at higher degree of subcooling with slightly longer induction time and more delay in hydrate blockage as compared to PVCap without synergist. This suggests that PGPE enhances the performance of PVCap base polymer to inhibit hydrate formation and delays hydrate growth.

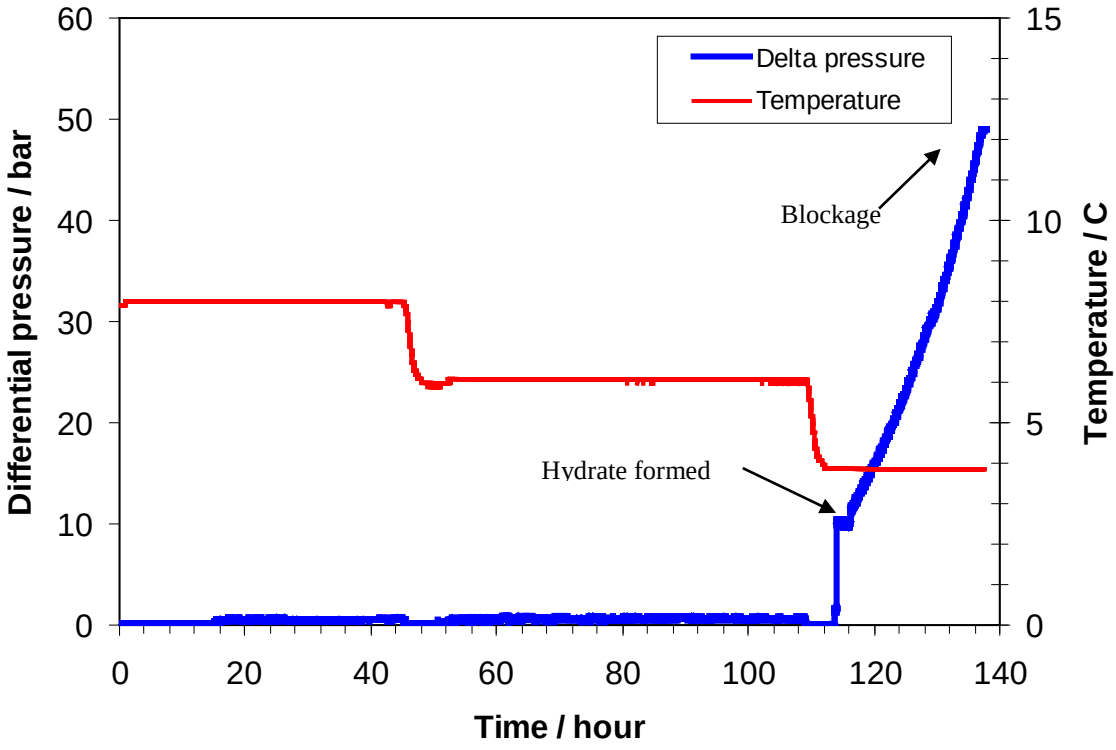

Figure 7.6. Differential pressure for natural gas – water system with 0.5 mass% PVCap base polymer + 0.75mass % PGPE at 109 bar. Hydrate formed at 4 ^{o}C (15 ^{o}C subcooling)

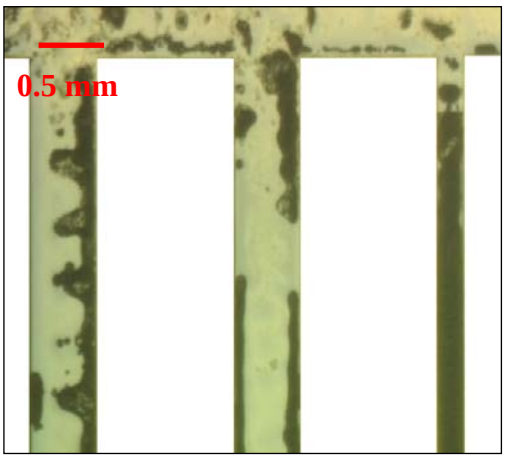

(a) 0.3 hrs after formation, ΔP = 2 bar

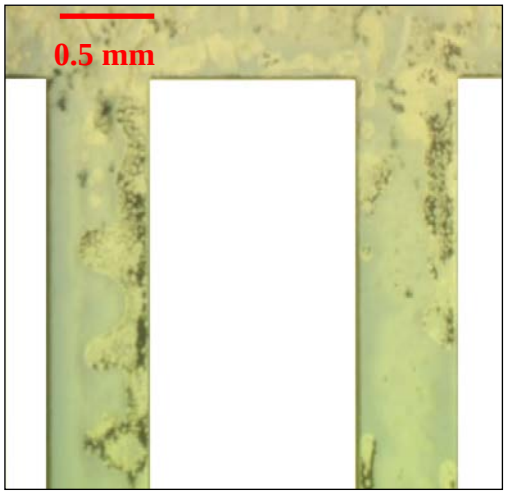

(b) 2 hrs after formation, ΔP = 10 bar

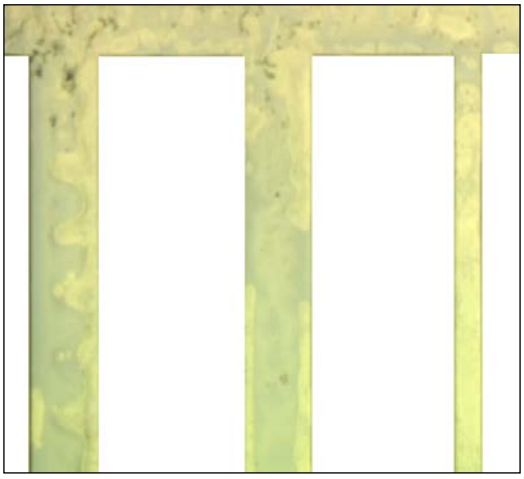

(c) 24 hrs after formation, ΔP = 49 bar

Figure 7.7. Images of hydrate deposits for natural gas – water system with 0.5 mass% PVCap base polymer + 0.75 mass% PGPE at 109 bar, 4 ^{o}C (15 ^{o}C subcooling)

Table 7.4: Summary of results: The effect of synergist

Sample	Hydrate formation temperature (^oC)	Subcooling (^oC)	Induction time at subcooling (hr)	Time for blockage (hr)	Observation (growth & crystal morphology, inhibition etc.
Blank	8	11	0.25	7.2	Continous solid hydrate in both phases – Figure 7.2 & 7.3
0.5 mass% PVCap	6	13	1.23	13.6	Non porous hydrate crystal in gas phase. Inhibit in dissolved gas and delay hydrate growth in gas phase – Figure 7.4 & 7.5
0.5 mass% PVCap + 0.75 mass% PGPE	4	15	1.63	23.8	Thin patches of hydrate crystal in gas phase. Inhibit in dissolved gas (water phase) and synergistic effect of delaying hydrate growth – Figure 7.6 & 7.7

7.3.1.2 Effect of corrosion inhibitor

The objective was to investigate the effect of corrosion inhibitor (CI) on the performance of kinetic hydrate inhibitor (KHI) using multichannel flow conduit under both static and flowing conditions. The experiment was performed using the mixture of 0.5 mass% PVCap (in 1.25 mass% LUVICAP-EG®) and 500 ppm CI (Corrtreat 799). The results were compared with the earlier data reported for 0.5 mass% PVCap without corrosion inhibitor.

Natural gas with an aqueous solution of LUVICAP-EG®

The differential pressure profile for Natural Gas – Water system in the presence of 0.5 mass% PVCap (in 1.25 mass% LUVICAP-EG®) without corrosion inhibitor at 109 bar is presented in Figure 7.8. As shown in this figure, the initial growth of hydrate was observed at 8^{o}C (11^{o}C subcooling) after about 4 hours of fluid injection at the rate of 0.1 cc/hr. However, there was no further growth of hydrate after leaving the system at this condition for 64 hours. Then, the system temperature was further reduced to 6 ^{o}C (13 ^{o}C subcooling) which induce catastrophic hydrate formation after 1.23 hours of induction time at this condition. Hydrate deposits initially appeared to be more porous (Figure 7.9(b)). As the time progressed, more hydrate formed which finally turned to a non porous solid and led to blockage of capillary tubes (Figure 7.9(c)). In this case,

total blockage in the capillary tubes occurred after 13.6 hours of catastrophic hydrate formation.

Natural gas with an aqueous solution of LUVICAP-EG® and CI

Similar procedure was repeated to investigate the effect of corrosion inhibitor. The differential pressure profile for Natural Gas – Water system in the presence of 0.5 mass% PVCap with corrosion inhibitor at 109 bar is presented in Figure 7.10. As shown in the figure, the catastrophic growth began after approximately 1.8 hours at 8 ^{o}C (11 ^{o}C subcooling). During the test, it was observed that many small gas bubbles present in the glass conduit. It was also observed that from time to time there was a gas breakthrough in the system which redistributed hydrate particles or pushed it out of the conduit. This may explain the differential pressure fluctuations as observed in Figure 7.10. It should be noted that there was a sudden pressure drop at about 19 hours after injection. This was due to power failure which temporarily stopped the injection pump. The fluid injection was resumed/continued and the pressure was built up which led to continuous hydrate formation within the conduit. After 26 hours, the system temperature was further reduced to 6 ^{o}C (13 ^{o}C subcooling). The increase in differential pressure suggested that more hydrate build-up formed in the conduit which continued until the temperature was further cooled down to 4 ^{o}C for several hours before terminating the test.

The above test was repeated by reducing system temperature directly to 6 ^{o}C (13 ^{o}C subcooling). The reason of repeating this test was to observe if the pressure fluctuation during previous flow test is typical characterisric in the presence of corrosion inhibitor, as well as comparing the time for blockage for the system with and without corrosion inhibitor. As shown in Figure 7.11, the catastrophic growth of hydrate was observed after about 3 hours reaching the stabilised condition and similar fluctuation in pressure profile was observed. The induction time at this condition was slightly longer than that the test without corrosion inhibitor (1.23 hrs), which may be due to the direct cooling of the system to 6 ^{o}C. The time of blockage (47 hours) was also longer which may suggest slower rate of growth of hydrate. The sequential images of hydrate formation is presented in Figure 7.12. From these images, it was observed that hydrate formed both in water and gas phases. This suggest that PVCap has failed to prevent hydrate formation in the water phase in the presence of the corrosion inhibitor.

Natural gas with an aqueous solution of LUVICAP-EG® and CI under static condition

Another test was carried out for this mixture of inhibitors under static conditions at 109 bar. Hydrate formed as soon as the temperature reached 4 ^{o}C (14.5 ^{o}C subcooling). Images of hydrate dissociation are shown in Figure 7.13. As shown in the figure (Figure 7.13 (a)), the morphology of hydrate formation was a thin layer of hydrate deposits. It was observed that at this condition, hydrate are formed mainly from dissolved gas in the water phase.

A summary of the results is presented in Table 7.5. Based on these preliminary experiments, the results suggest that the presence of corrosion inhibitor affect the performance of PVCap. This was observed from the fact that catastrophic hydrate formation began at 11 ^{o}C subcooling in the presence of corrosion inhibitor, while in the absence of CI, the catastrophic hydrate growth began at 13 ^{o}C subcooling. In addition, PVCap failed to prevent hydrate formation in the water phase in the presence of corrosion inhibitor.

Table 7.5: Summary of Results: Effect of corrosion inhibitor at 109 bar

Sample	Hydrate formation temperature (^{o}C)	Subcooling (^{o}C)	Induction time at subcooling (hr)	Time for blockage (hr)	Comments (growth & crystals morphology, etc.)
LUVICAP®	8	11	4 *	-	* Initial slow growth – Figure 7.8
	6	13	1.23	13.6	Catastrophic growth of hydrate; non porous solid hydrate in gas phase – Figure 7.8 & 7.9
LUVICAP® + CI	8	11	1.8	-	Catastrophic growth of hydrate; small gas bubbles present; ΔP fluctuate – Figure 7.10
	6	13	0	-	Catastrophic growth of hydrate; increase in ΔP due to hydrate build-up; terminate test at 4 ^{O}C – Figure 7.10
LUVICAP® + CI	6	13	3	~ 47	Catastrophic growth of hydrate; hydrate formed in both phases – Figure 7.11 & 7.12
LUVICAP® + CI at static condition	4	14.5	0		Thin deposit of hydrate crystals in both phases - Figure 7.13

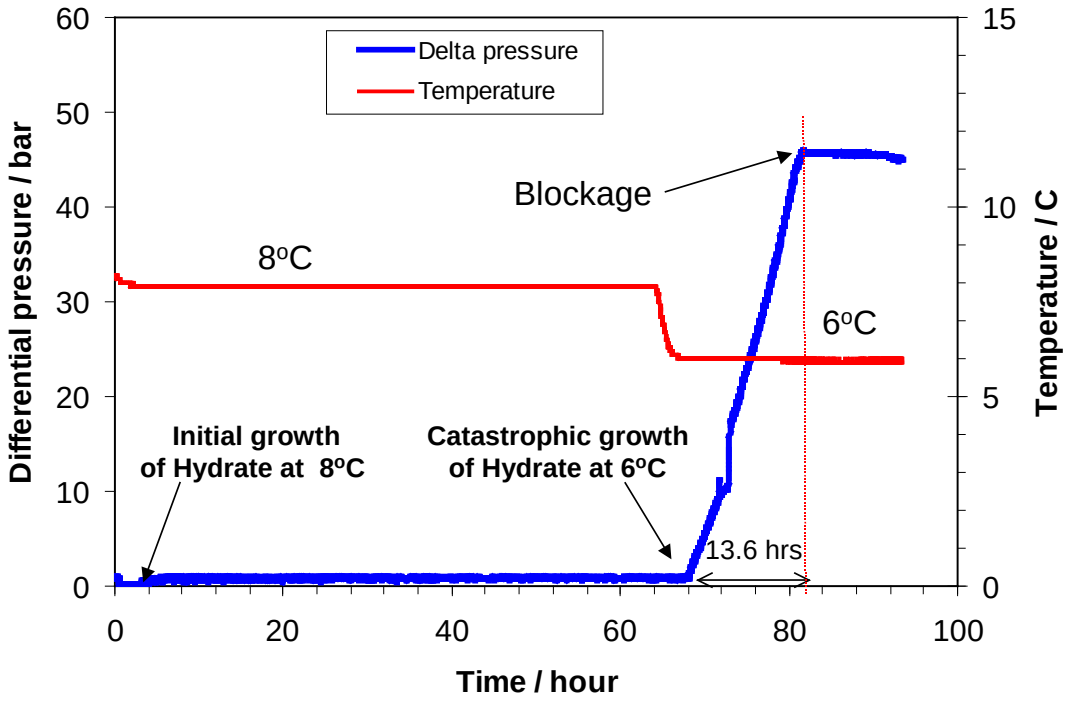

Figure 7.8. Differential pressure profile for natural gas – water system in the presence of 0.5 mass% PVCap at 109 bar. Hydrate formed at 6°C (13°C subcooling).

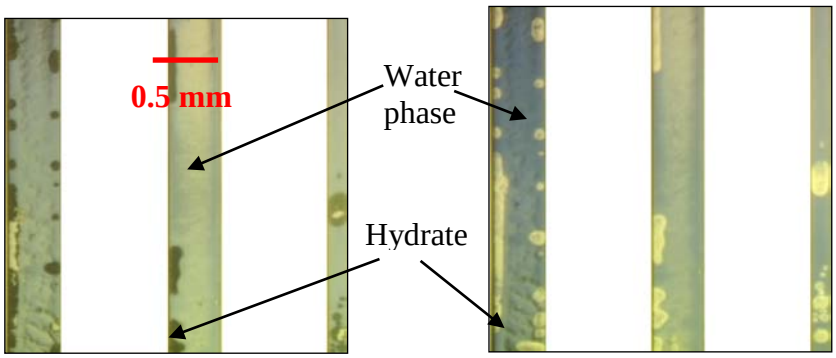

(a) 0.8 hrs after formation, ΔP = 3 bar (b) 4 hrs after formation, ΔP = 10 bar

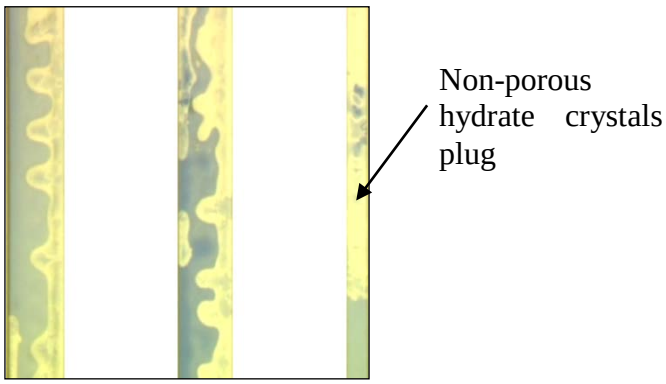

(c) 10 hrs after formation, ΔP = 32 bar

Figure 7.9. Images of hydrate deposits for natural gas – water system with 0.5 mass% PVCap at 109 bar, 6°C (13°C subcooling).

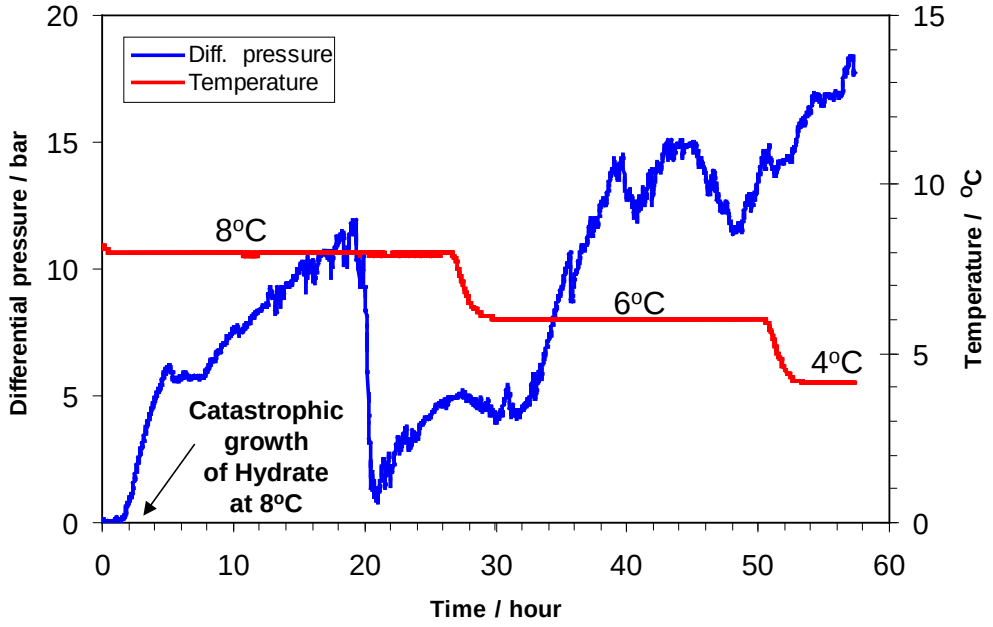

Figure 7.10. Differential pressure profile for natural gas – water system in the presence of 0.5 mass% PVCap + 500 ppm Corrosion Inhibitor at 109 bar. Hydrate formed at 8°C (11°C subcooling). Differential pressure drop at 21 hours is due to power failure.

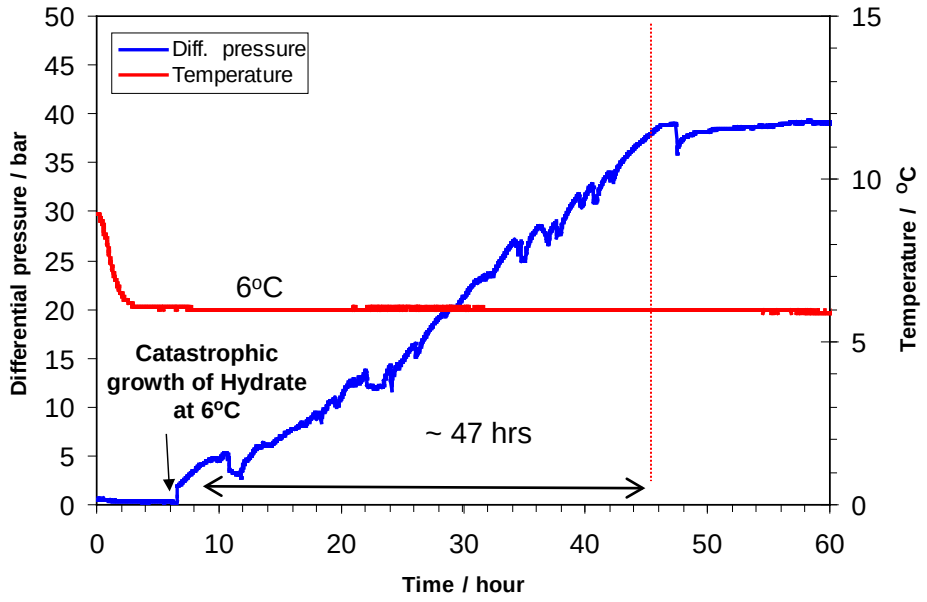

Figure 7.11. Differential pressure profile for natural gas – water system in the presence of 0.5 mass% PVCap + 500 ppm Corrosion Inhibitor at 109 bar. Hydrate formed at 6°C (13°C subcooling).

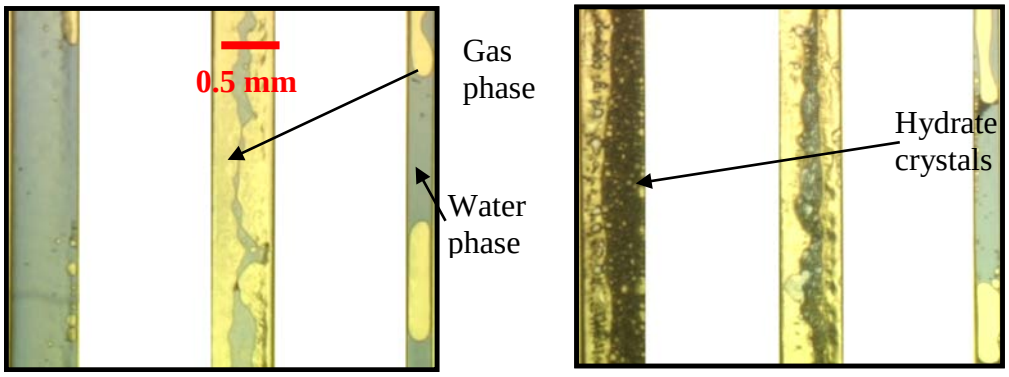

(a) Before hydrate formation, ΔP = 0 bar (b) 15 hrs after formation, ΔP = 50 bar

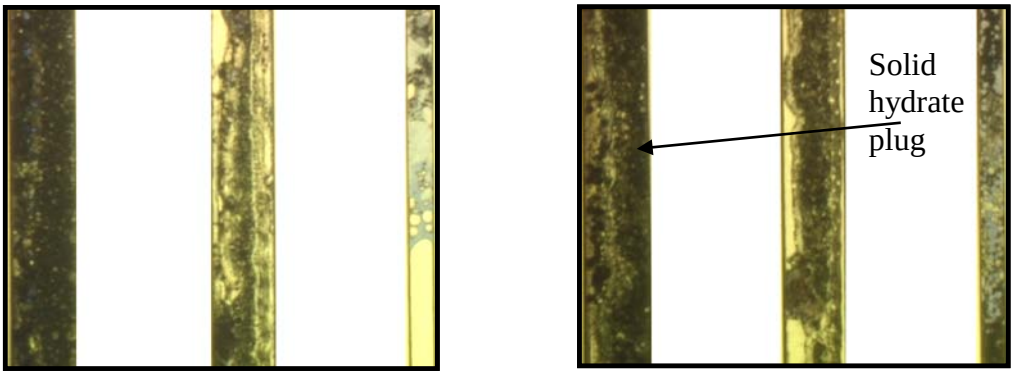

(c) 40 hrs after formation, ΔP = 630 bar (c) 72 hrs after formation, ΔP = 650 bar

Figure 7.12. Images of hydrate formation for natural gas-water system in the presence of 0.5 mass% PVCap + 500 ppm Corrosion Inhibitor at 109 bar. Hydrate formed at 6^{o}C (13^{o}C subcooling) under flowing conditions.

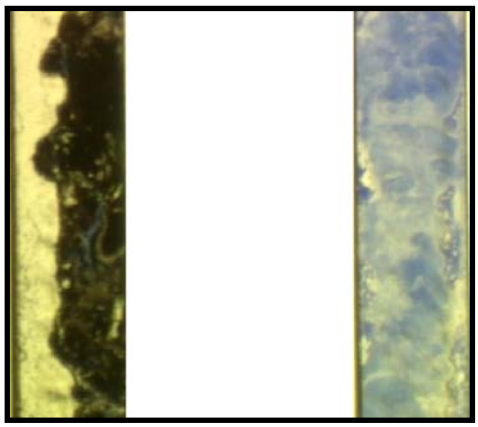

(a) T = 4 ^{O}C, ΔP = 5.5 bar

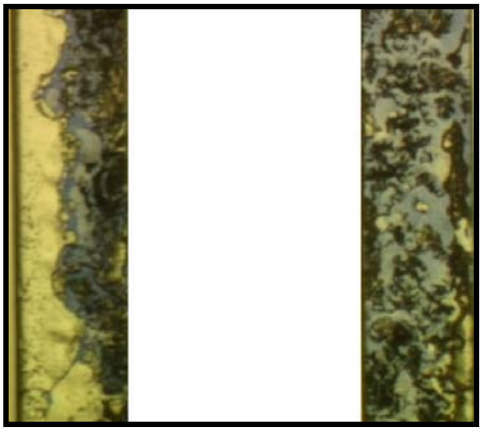

(b) T = 16 ^{O}C, ΔP = 5 bar

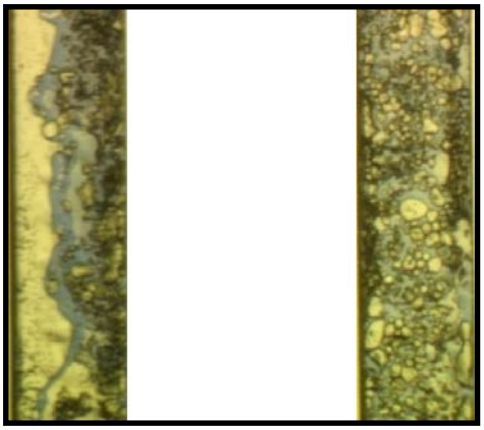

(c) T = 19.4 ^{O}C, ΔP = 1 bar

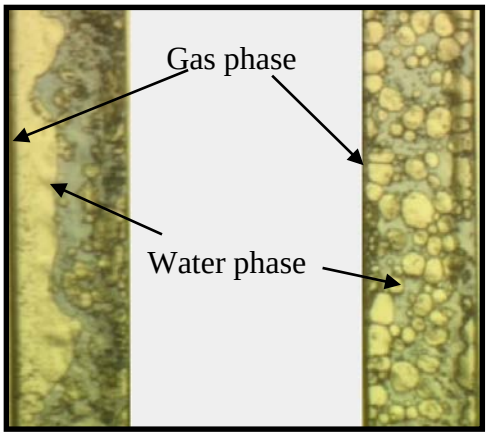

(c) T = 20 ^{O}C, ΔP = 0.2 bar

Figure 7.13. Images of hydrate dissociation for natural gas-water system in the presence of 0.5 mass% PVCap + 500 ppm Corrosion Inhibitor at 109 bar. Hydrate formed at 4 ^{o}C (14.5 ^{o}C subcooling) under static conditions.

7.3.2 Evaluation of Anti-agglomerant

The experimental work is designed to evaluate the anti-agglomerant with 3 mass% of NaCl for natural gas-water condensate system using capillary tube blocking technique. The study was conducted under flowing/dynamic and static conditions based on characteristic behaviour of hydrate plugging and time for blockage. Tests were performed for natural gas-water system, natural gas-condensate-water system with and without 0.5 mass% anti-agglomerant and finally gas condensate-water system with 0.5 mass% anti-agglomerant. The remaining study was focused on evaluating the hydrate crystal size and distribution for NG-water-condensate system at static conditions in the presence of anti-agglomerant. The water in oil emulsion sample and glass micromodel with a symmetric pore structure was used for this study.

7.3.2.1 Natural gas – water system

Test on natural gas – water system was first established using the capillary tube. The objective was to visually observe hydrate formation within capillary tube. In this study, hydrate formed after 1.7 hours at 10 ^{o}C (8 ^{o}C subcooling) as shown by differential pressure profile in Figure 7.14. Hydrate began to form at the interface of gas and water within capillary tube. It moved forward in the tube under flowing conditions and finally blocked the system after 60 hours of initial hydrate formation (Figure 7.15). The sequential image of hydrate plug dissociated by depressurisation into gas and water phases at two locations are shown in Figure 7.16. The images of fluid phases and hydrate formation could be clearly observed through out the capillary tube with the exception of gas phase. The visualisation of gas phase is limited to the center of capillary tube, which is darkened at the side due to light diffraction. This experiment suggest that single glass capillay tube could be applied as the technique for visual observation of hydrate formation with some limitation.

7.3.2.2 Natural gas-condensate-water (with 3 mass% NaCl)

Three phase fluid flow was simulated by simultaneously injecting water (with 3 mass% of NaCl), natural gas and condensate. The system temperature was reduced to 4 ^{o}C while the fluid was flowing through the capillary tube. Hydrate was formed after 1.8 hrs at the above conditions as indicated in Figure 7.17. After about 64 hours, the differential pressure reached to 33-34 bar and the injection was stopped for 24 hours. The objective was to simulate shut-in conditions. The injection was resumed for another 5 hours until the pump stopped as it reached to the set pressure (i.e. 156 bar) for blockage. The images of progressive changes in the hydrate formation within the capillary tube are shown in Figure 7.18. It was observed that hydrate crystals accumulated with time after initial hydrate formation and continued to block the capillary tube with a massive hydrate plug.

7.3.2.3 Natural gas-condensate-water (with 3 mass% NaCl) + 0.5 mass% AA

Similar procedure was followed for the test in the presence of 0.5 mass% of anti-agglomerate (labelled as HT04-106). For this case, it was observed that hydrates formed after 9.3 hours at 4 ^{o}C as shown in Figure 7.19. For this experiment, the challenge was to control three phase flow in the system. At certain times the gas phase will dominate

the flow in the system, leaving water phase behind. The gas injection was stopped to allow water and condensate to be injected into the system. As seen in the Figure 7.19, a sudden drop in pressure was mainly due to pressure drop caused by opening of gas and condensate sample valves after closing it for 1 hour to build-up pressure for water phase. In this case, after about 70 hours of flowing, the system was shut-in after the differential pressure reached 34 – 35 bars. The injection was continued and the system was finally blocked after 12 hours of flowing. The images of hydrate formation at three different locations are shown in Figure 7.20. Massive hydrate plug is formed after 4 hours within the capillary tube as shown in Figure 7.20(a). This observation was made at the outlet side of capillary tube. Hydrate formation at the gas-water interface is shown in Figure 7.20(b). A thin layer of hydrate deposits was also observed on the wall of the capillary tube (Figure 7.20(c)). In general, it was observed from this experiment, the distribution of phases within the system under flowing condition will have significant influence on the hydrate crystal morphology under dynamic/flowing conditions.

7.3.2.4 Recombined Gas condensate-water (with 3 mass% NaCl) + 0.5 mass% AA

Several tests were performed for gas condensate-water system in the presence of 0.5 mass% anti-agglomerate. As described in the procedure section, the condensate sample was saturated with natural gas to form a single phase fluid. Gas condensate and water phases were then simultaneously injected into the capillary tube at the test condition to observe hydrate formation. As shown in Figure 7.21, hydrate formed after 0.5 hours at 4 ^{o}C when the system temperature was reduced from 14 ^{o}C to 4 ^{o}C. As can be seen from the differential pressure profile, the reduction in differential pressure was observed at about 11 hour which could be due to redistribution of hydrate particles and movement of plug within the capillary tube. The differential pressure began to build-up again at 17 hour and reached to the maximum pressure limit after 8 hours of flowing. Images of hydrate formation were shown in Figure 7.22 with patches of hydrate crystals sticking on the wall of glass capillary tube. The test was repeated using a fresh sample by reducing temperature from 20 ^{o}C to 4 ^{o}C. As shown by differential pressure profile in Figure 7.23, hydrate formed after 17 hours at 4 ^{o}C and the blockage was observed after 6 hours under flowing condition. The images captured for this test (Figure 7.24) indicated that hydrate particles grow in the condensate phase and also in the gas-water interface.

7.3.2.5 Summary of Hydrate Morphology in the Presence of AA

The results for the tests described above are summarised in Table 7.6. The hydrate morphology observed for the natural gas- condensate water system in the presence of anti-agglomerate is a mix of thin layer and patchy hydrate crystals formed in the system at tested condition. Whereas in the absence of anti-agglomerate, massive hydrate plug formed at some part of capillary tube. In the case of hydrate formation from gas condensate-water system, hydrate particles was mostly observed to form and dispersed in the condensate phase and it also formed at the water-gas interface. Based on the above results, both estimated induction time and blockage time under shut in and flowing conditions are longer for the system with anti-agglomerant. The result is expected where the anti-agglomerant, fundamentally polymeric surfactants, prevent hydrates from agglomerating and depositing in the pipelines. These anti-agglomerant keep the particles small and well dispersed in the hydrocarbon liquid. Although in principle, anti-agglomerant allows hydrate to form and have no intended effect on hydrate nucleation/growth kinetics (i.e. induction time), it shows some significant differences for the series of tests that was performed using this system under flowing conditions.

It is also noted that for the case of gas condensate-water system, the starting cooling temperature seems to have some influence on the induction time for hydrate formation. For instant, starting cooling outside the hydrate phase boundary will give longer induction time (i.e. 17 hours) for hydrate formation in the system.

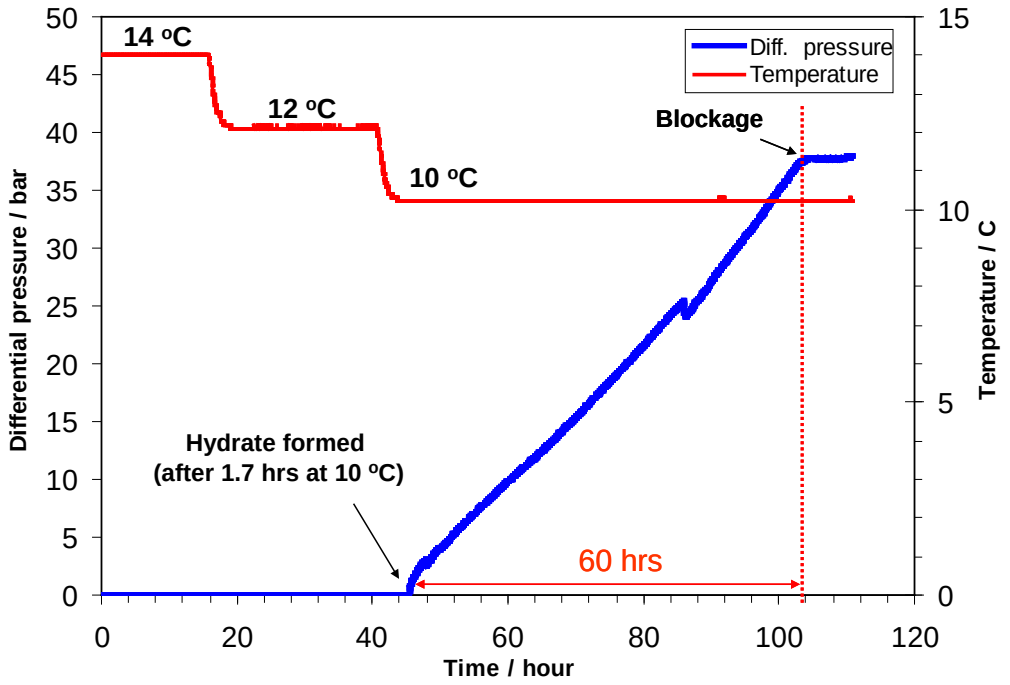

Figure 7.14. Differential pressure profile for natural gas – water system at 113 bar. Hydrate formed at 10 °C (8 °C subcooling). WGR= 0.5, total injection rate: 0.1 cc/hr

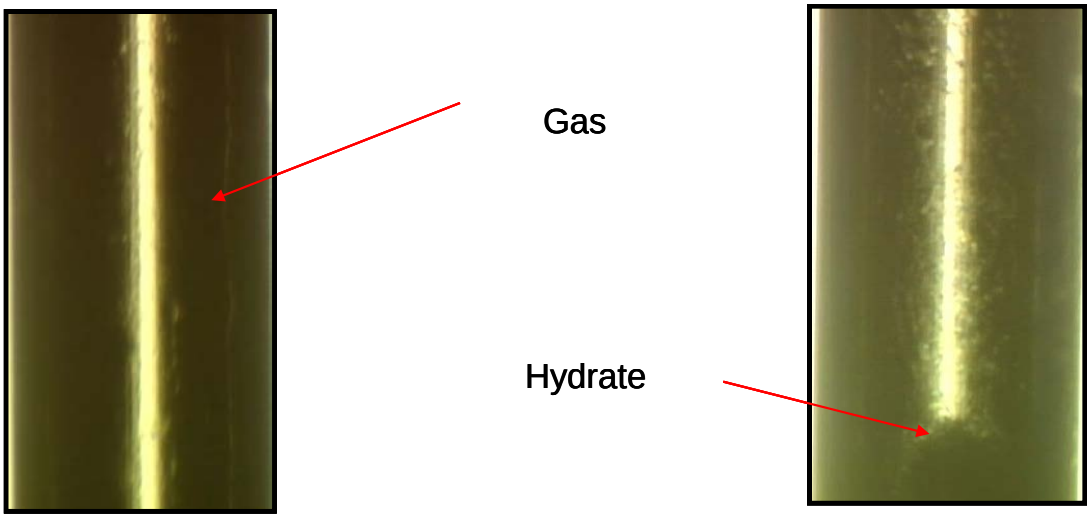

(a) Before formation, ΔP = 0 bar (b) After 18 hrs, ΔP = 12 bar

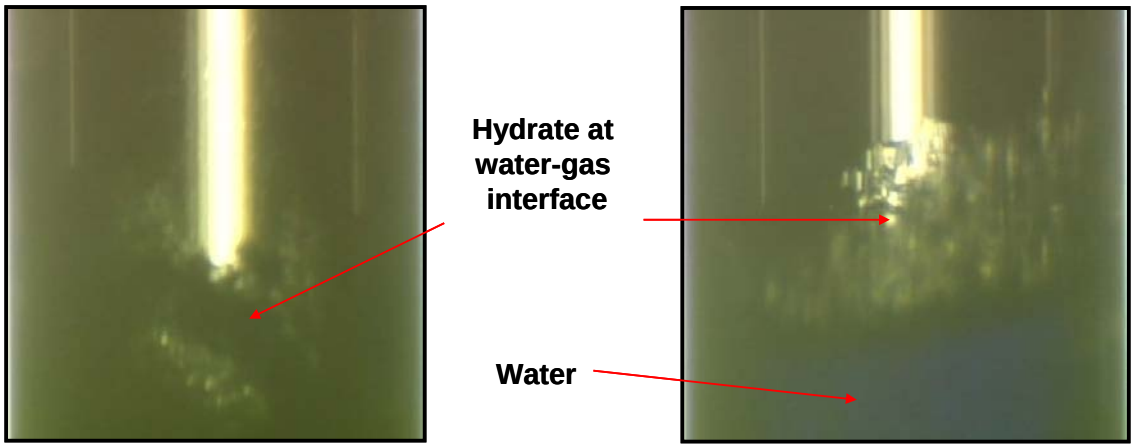

(c) After 47 hrs, ΔP = 29 bar (c) After 65 hrs, ΔP = 38 bar

Figure 7.15. Images of hydrate formation for natural gas-water System at 113 bar, 10 ^{o}C (8 ^{o}C subcooling) under flowing conditions.

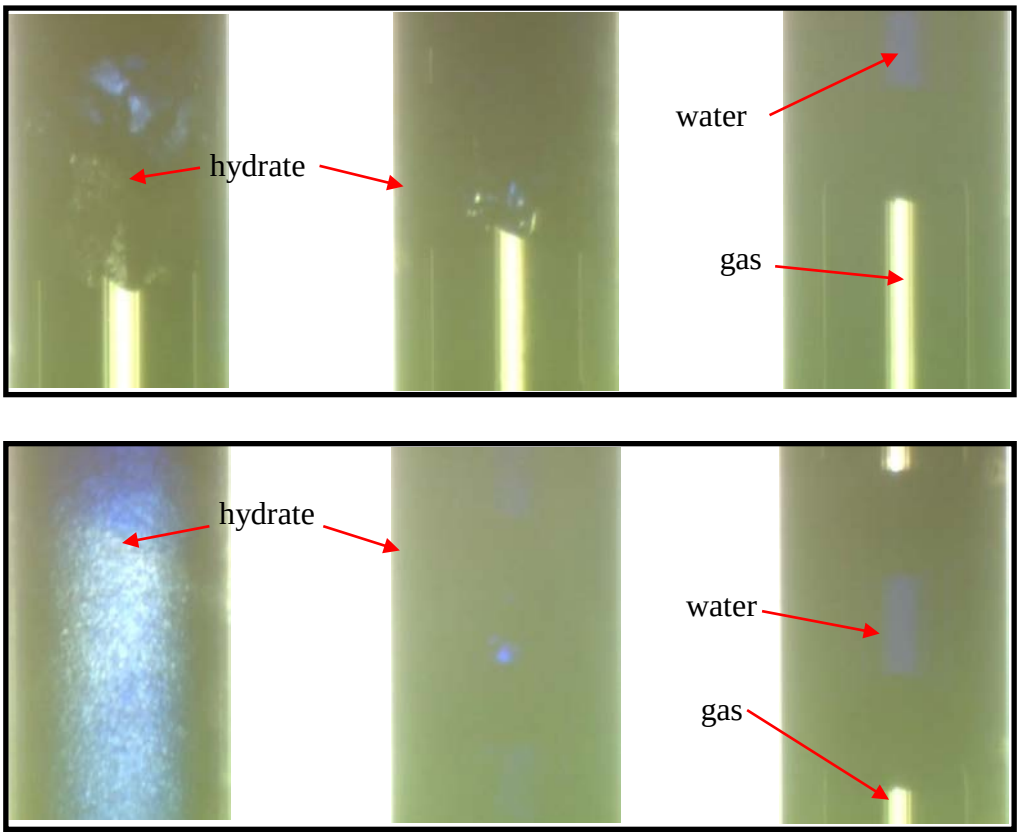

ΔP = 37 bar ΔP = 10 bar ΔP = 2 bar

Figure 7.16. Images of hydrate dissociation during depressurisation for natural gas-water system at 4 ^{o}C.

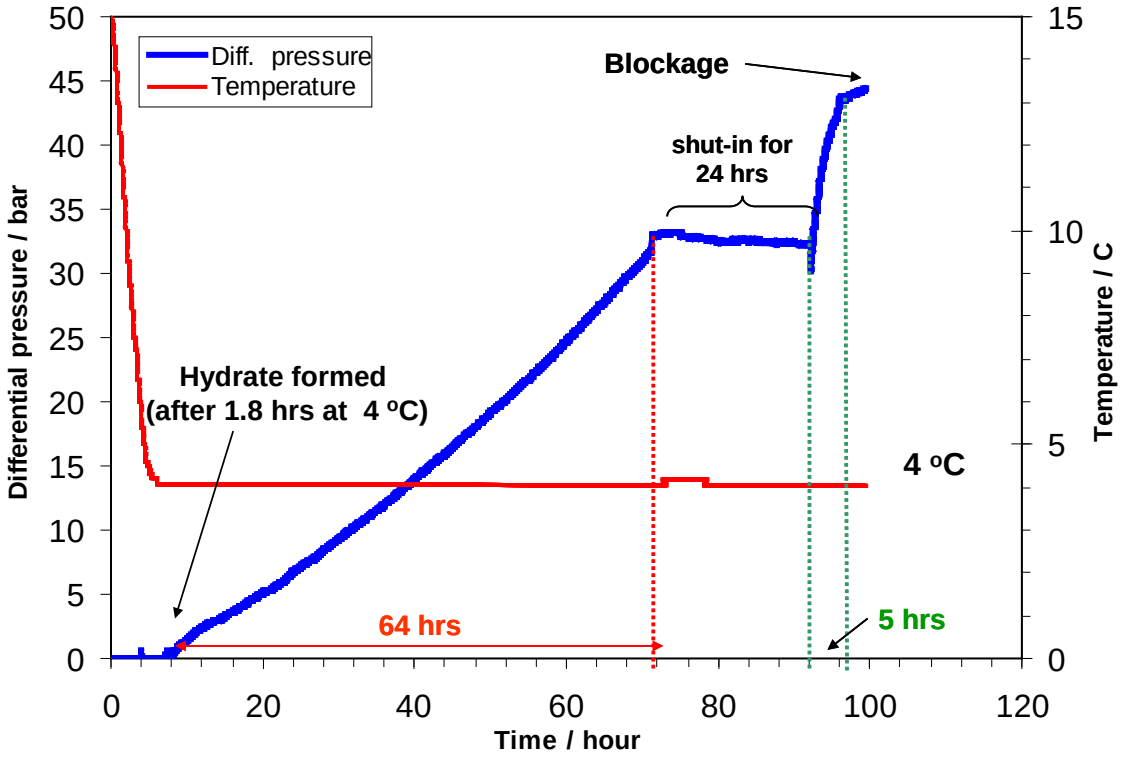

Figure 7.17. Differential pressure profile for natural gas–condensate-water system in the presence of 3 mass% NaCl at 110 bar. Hydrate formed at 4 °C (14 °C subcooling). WGR= 0.7, total injection rate: 0.1 ml/hr

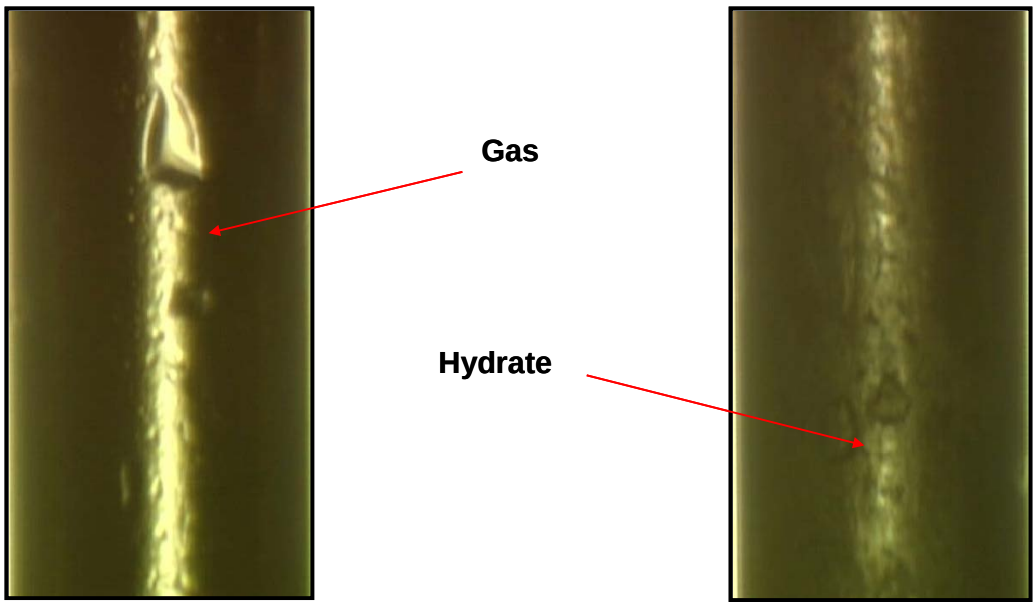

(a) Before formation, ΔP = 0 bar (b) Immediately after formation, ΔP = 0 bar

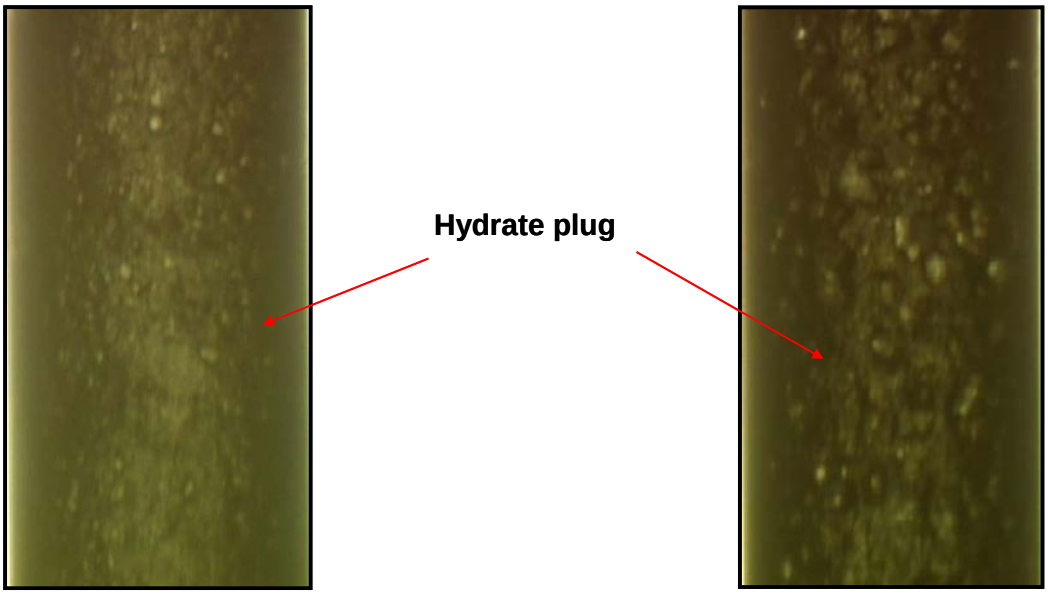

(c) After 19 hrs, ΔP = 8 bar (c) After 100 hrs, ΔP = 43 bar

Figure 7.18. Images of hydrate formation for natural gas–condensate-water system in the presence of 3 mass% NaCl at 110 bar, 4 ^{o}C (14 ^{o}C subcooling).

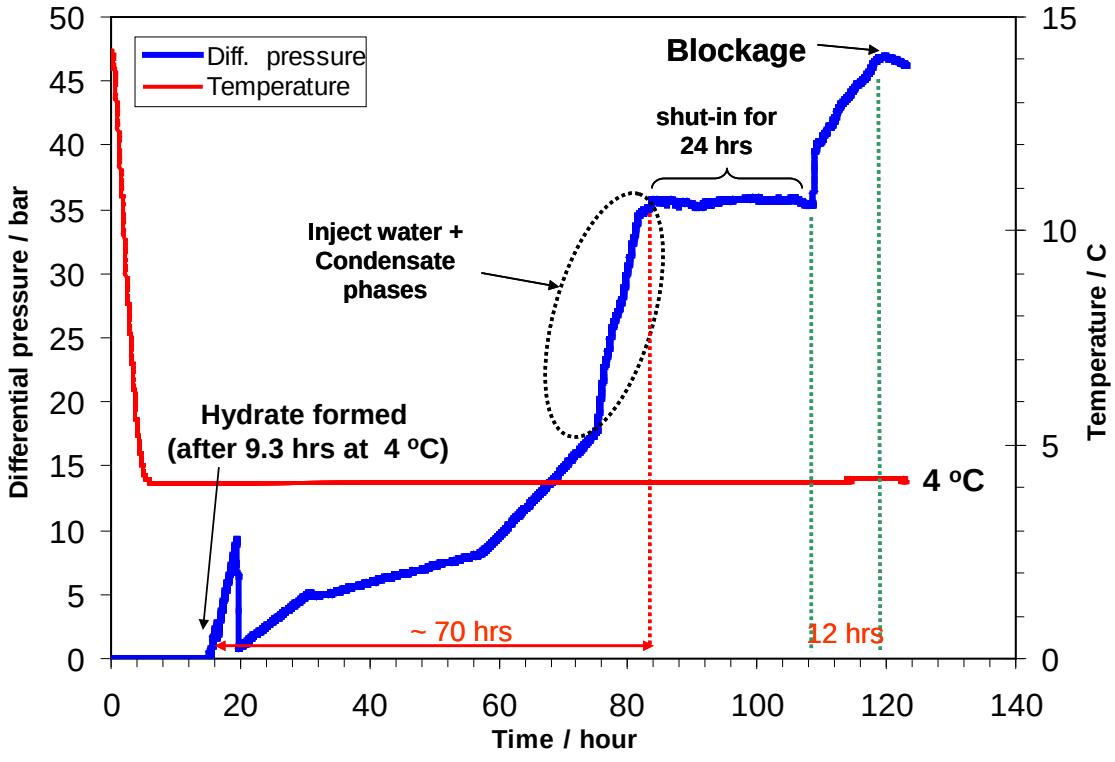

Figure 7.19. Differential Pressure profile for natural gas–condensate-water system in the presence of 3 mass% NaCl and 0.5 mass% AA at 110 bar. Hydrate formed at 4 ^{o}C (14^{o}C subcooling). WGR= 0.7, total injection rate: 0.1 ml/hr

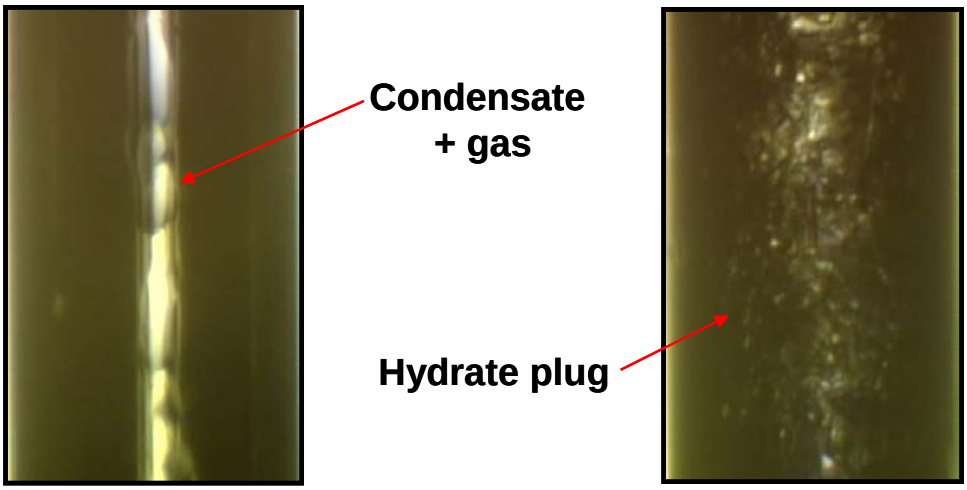

(a)Before formation (b) after 4 hrs, ΔP = 6 bar

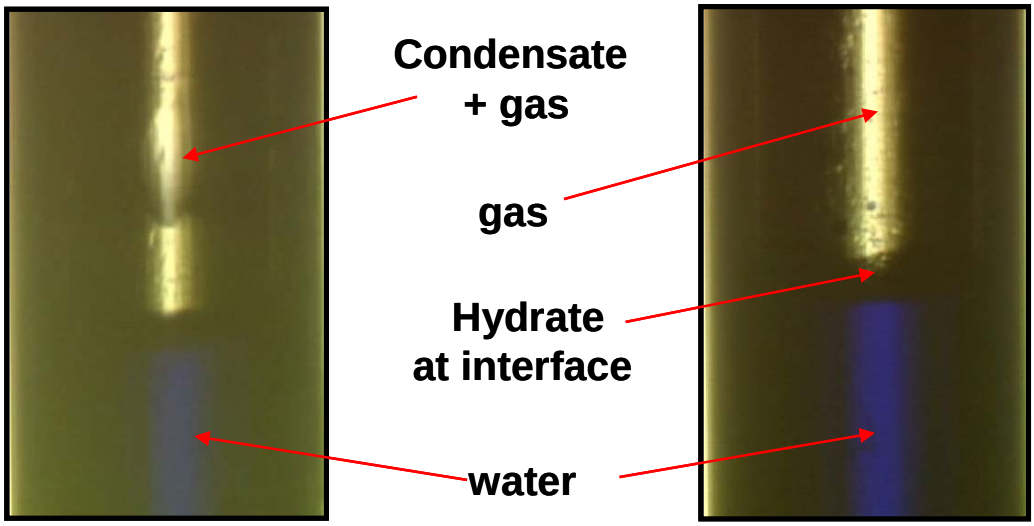

(b) Before formation after 32 hrs, ΔP = 7 bar

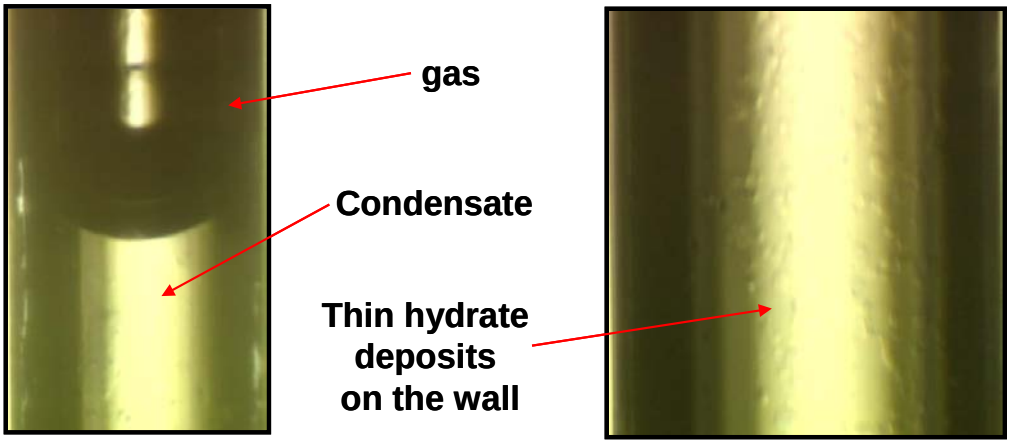

(c) After 30 hrs, ΔP = 6 bar after 108 hrs, ΔP = 32 bar

Figure 7.20. Images of hydrate formation for natural gas–condensate-water system in the presence of 3 mass% NaCl and 0.5 mass% AA at 110 bar, 4 ^{o}C (14 ^{o}C subcooling).

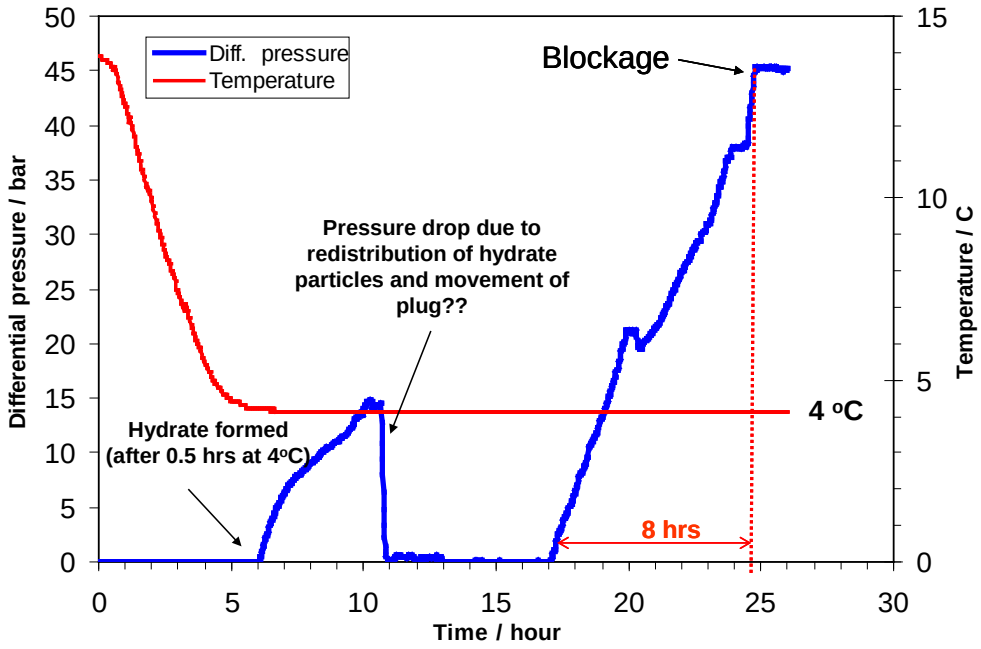

Figure 7.21. Differential Pressure profile for gas condensate-water system in the presence of 3 mass% NaCl and 0.5 mass% AA at 110 bar. Hydrate formed at 4 °C (14°C subcooling). WGR= 0.7, total injection rate: 0.1 ml/hr

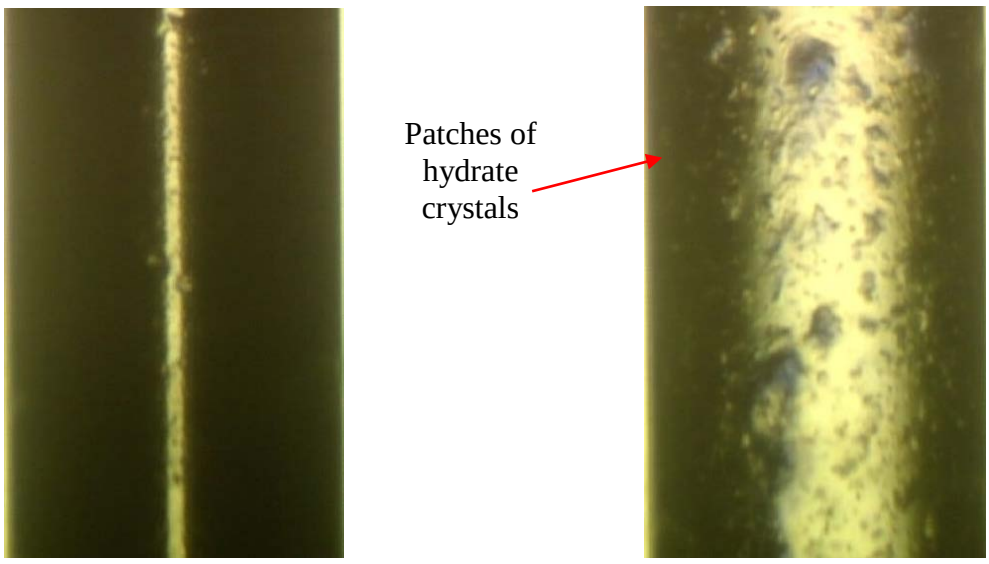

(a) before formation (b) after 26 hrs, ΔP = 45 bar

Figure 7.22. Images of hydrate formation for gas condensate-water system in the presence of 3 mass% NaCl and 0.5 mass% AA at 110 bar, 4 °C (14 °C subcooling).

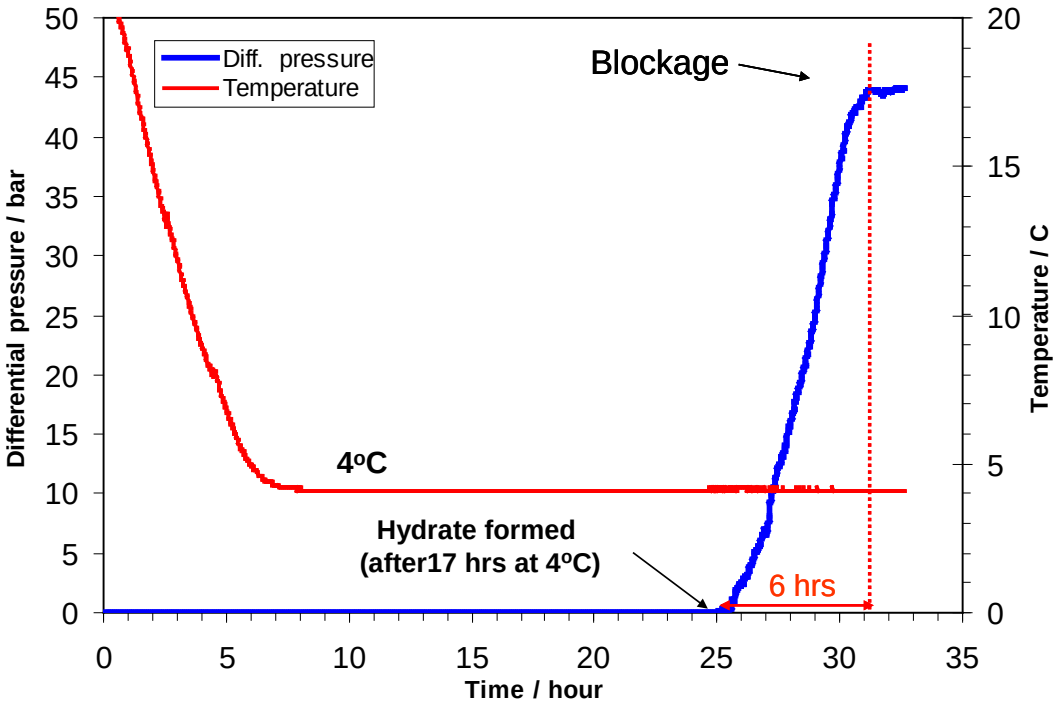

Figure 7.23. Differential Pressure profile for gas condensate-water system in the presence of 3 mass% NaCl and 0.5 mass% AA at 110 bar. Hydrate formed at 4 °C (14°C subcooling). WGR= 0.7, injection rate: 0.1 ml/hr

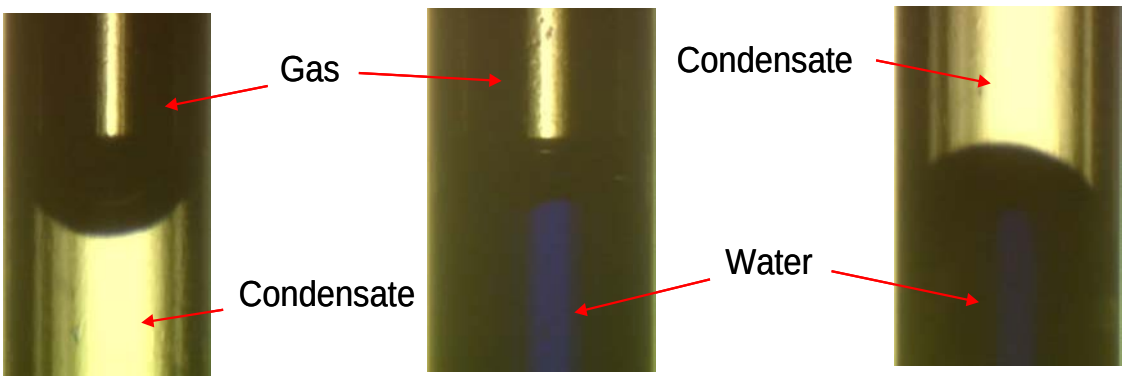

(a) before formation

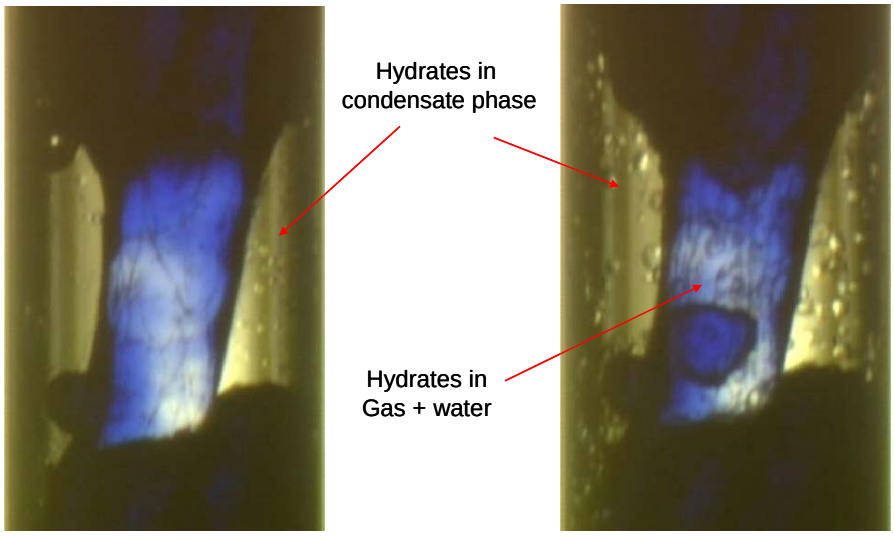

(b) after 10 hrs (c) after 30 hrs

Figure 7.24. Images of hydrate formation for gas condensate-water system in the presence of 3 mass% NaCl and 0.5 mass% AA at 110 bar, 4 ^{o}C (14 ^{o}C subcooling).

Table 7.6 Summary of results: Evaluation of AA by Capillary tube blockage
110 bar, 4 ^{o}C (14 ^{o}C subcooling)

Sample	Hydrate formation temperature (^{o}C)	Subcooling (^{o}C)	Induction time at subcooling (hr)	Time for blockage (hr)	Comments (growth & crystals morphology)
NG- water	10	8	1.7	60	Massive hydrate plug – Figure 7.15 & 7.16
NG-Condensate-water (3 mass% NaCl)	4	14	1.8	64 5 (after shut-in)	Massive hydrate plug, Hydrate at gas-water interphase, thin layer deposit on wall – Figure 7.17 & 7.18
NG-Condensate-water (3 mass% NaCl) + AA	4	14	9.3	~ 70 12 (after shut-in)	Thin deposit of hydrate Figure 7.19 & 7.20
Gas Condensate-water (3 mass% NaCl) + AA*	4	14	0.5	8	Patch of hydrate on the wall, hydrate in gas and water phase, hydrate in condensate phase (?) – Figure 7.21 & 7.22
Gas Condensate-water (3 mass% NaCl) + AA**	4	14	17	6	Patch of hydrate on the wall, hydrate in both gas and water phase, Hydrate in condensate phase (?) – Figure 7.23 & 7.24

Note:

* Reduce temperature from 14 ^{o}C to 4 ^{o}C

** Reduce temperature from 20 ^{o}C to 4 ^{o}C

7.3.2.6 Hydrate Particles size and Distribution for Natural Gas-Condensate-Water System

An experiment was conducted for natural gas-water-condensate system in the presence of anti-agglomerant at 102 bar (1500 psia). The water in oil emulsion (mixing ratio of 30% water:70% oil) was prepared by mixing water (containing 0.5 mass% of AA labelled as HT04-106) with the condensate. The stable emulsion, milky colour, was formed using high pressure mixer with 24000 rpm and the sample was saturated with natural gas at about 69 bar (1000 psia) prior to injecting into the system. The system was pressurised to 102 bar (1500 psia) by injecting natural gas. The system was allowed to equilibrate and the temperature was reduced to 4 ^{o}C to allow hydrate to form. The system temperature was further reduced to 0 ^{o}C when hydrate did not form after two days. After several days, the system temperature was increased to 4 ^{o}C to estimate the hydrate particle size in the presence of anti-agglomerant.

The water in oil emulsion sample was analysed using Scanning Electron Microscope (SEM) to estimate the size of water droplet in the condensate phase prior to hydrate prevention. The SEM images are shown in Figure 7.25. The results indicate that the water droplet size is in the range of 20 – 30 μm (Figure 7.25 (a)) with a mixture of smaller water droplets at 366x magnification. A higher magnification (1462x magnification) of these water droplets showed that it made up of agglomeration of smaller water droplets. This water droplet size is estimated to be in the range of 2 – 5 um (Figure 7.25 (b)) which will be the basis for estimating the size of hydrate particles forming in the system at the test conditions.

As shown by the sequential images in Figure 7.26, some condensate phase separated out from emulsion at the test conditions. Therefore, three phases, which consists of gas, condensate and emulsion, were present in the system prior to hydrate formation (Figure 7.26 (a)). It was observed that hydrate particles mainly formed and distributed within the water in oil emulsion phase (Figure 7.26 (b)). Increasing the system temperature from 0 ^{o}C to 4 ^{o}C caused redistribution of some of the hydrate particles within the phases as shown in Figure 7.26 (c). The hydrate particle size which dispersed in the condensate phase was estimated from images shown in Figure 7.27. Based on this image the hydrate particle size is estimated in the range of 5 – 10 μm which is slightly

larger than the size of water droplet in emulsion.

The sequential images of hydrate dissociation from natural gas-water-condensate system are shown in Figure 7.28. It is observed that the gas phase was slowly released from the hydrate crystal when the temperature increases. By increasing the system temperature up to 16 ^{o}C, the hydrate particles dissociated into gas, condensate and water phases.

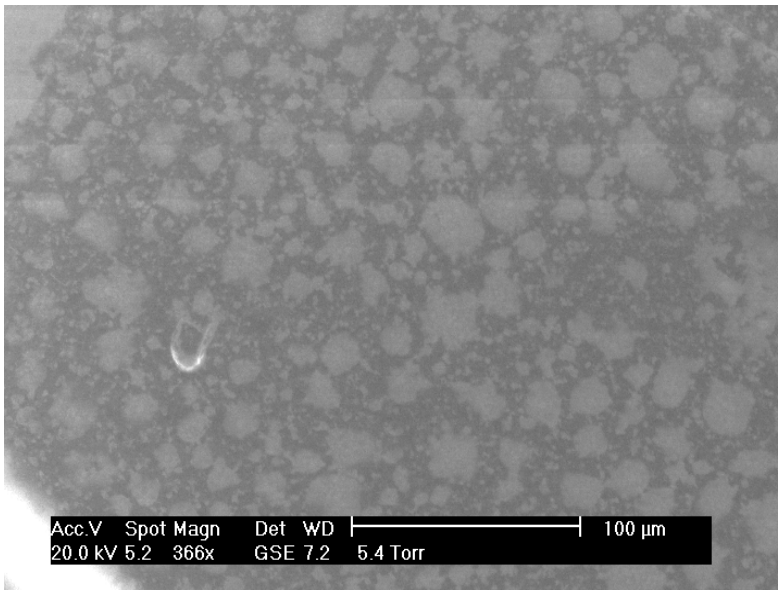

(a) 366x magnification

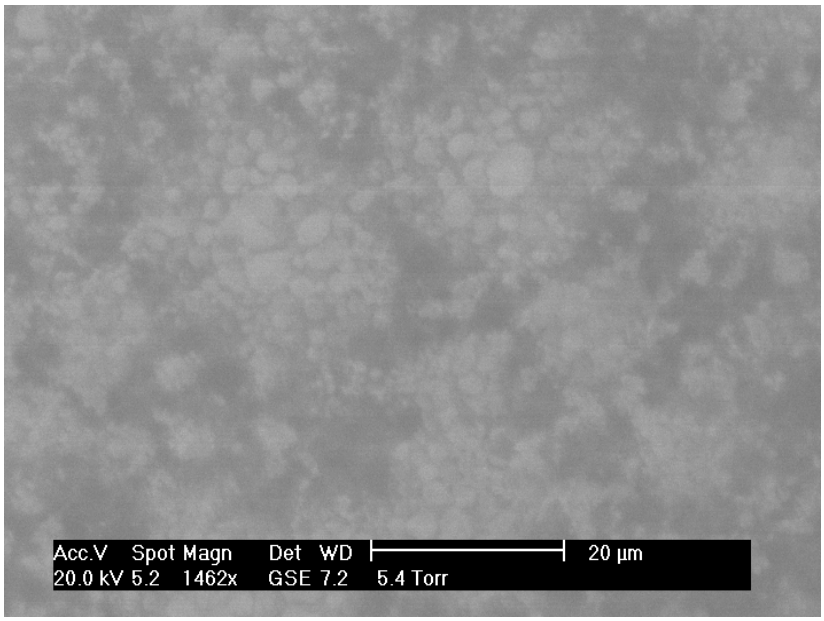

(b) 1462x magnification

Figure 7.25. SEM Images of water in condensate emulsion

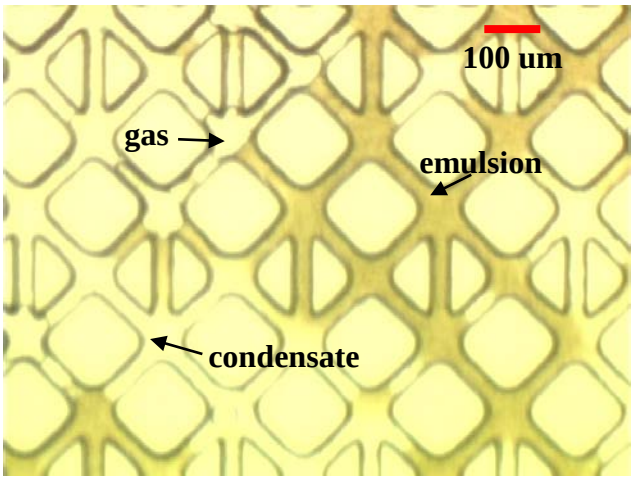

(a) Before hydrate formation (4 ^{o}C)

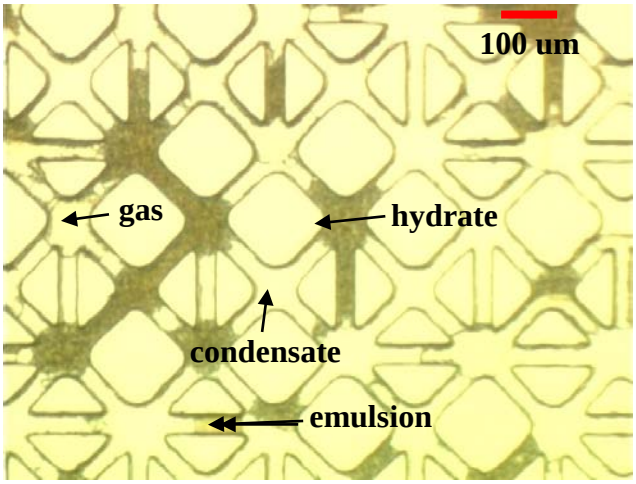

(b) 0.5 hrs after formation (0 ^{o}C)

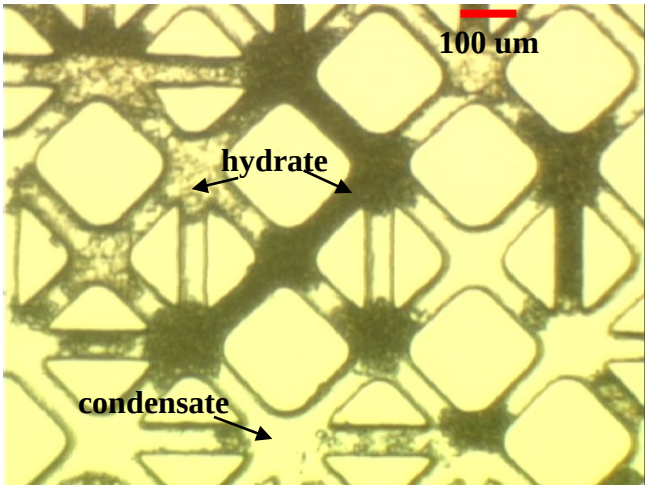

(c) 170 hrs after formation (4 ^{o}C)

Figure 7.26 Images of hydrate formation for natural gas-condensate-water system in the presence of 0.5 mass% HT04-106 at 102 bar, 4^{o}C (14 ^{o}C subcooling).

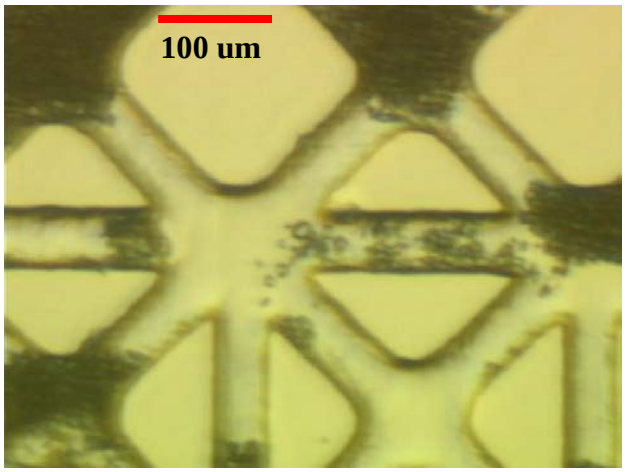

Figure 7.27 Images of hydrate formation for natural gas-condensate-water system in the presence of 0.5 mass% HT04-106 at 102 bar, 4 ^{o}C (14 ^{o}C subcooling). Particle size estimated range: 5 – 10 μm.

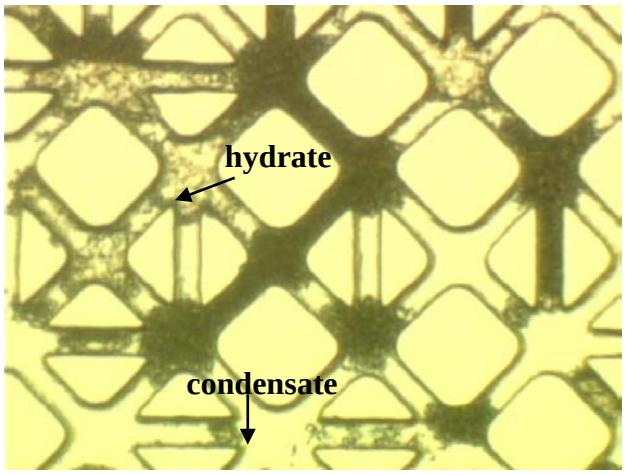

(a) Before dissociation, 4 ^{o}C (14 ^{o}C subcooling)

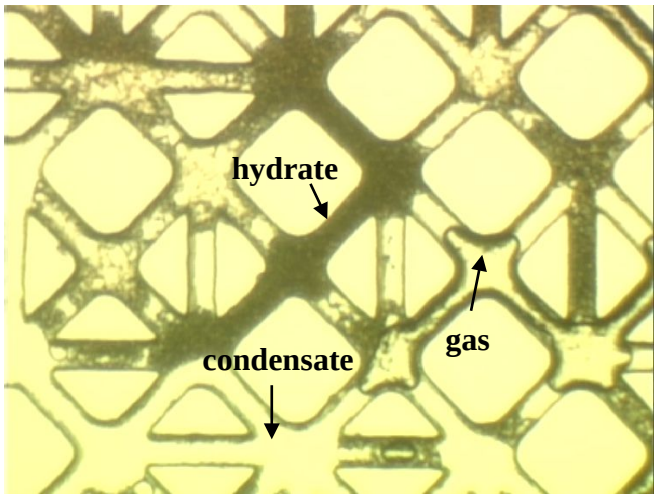

(b) 6 ^{o}C (12 ^{o}C subcooling)

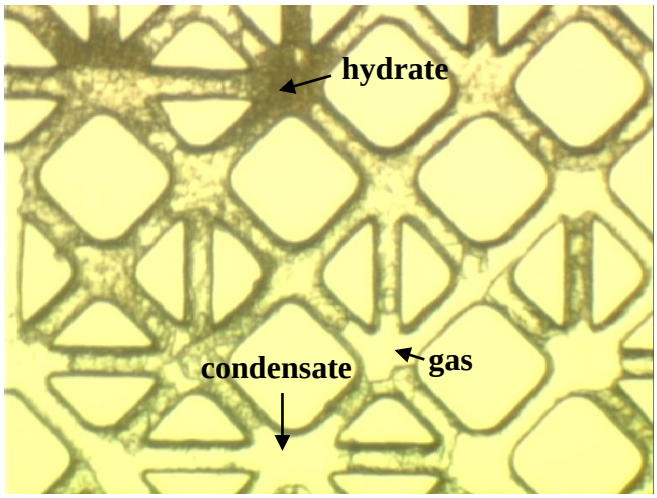

(c) 10 ^{o}C (8 ^{o}C subcooling)

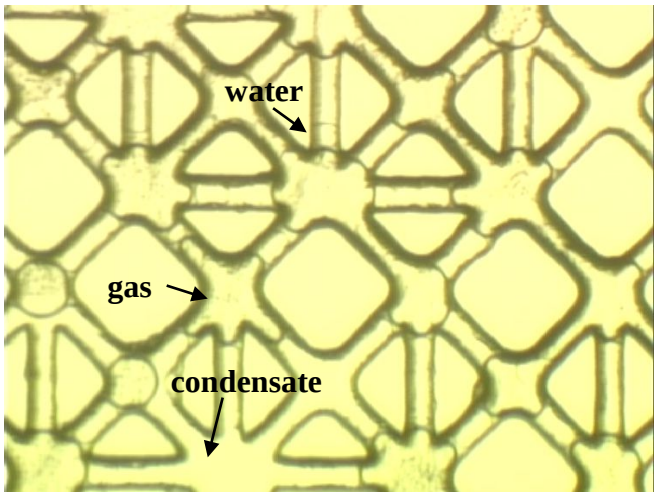

(d) 16 ^{o}C (2 ^{o}C subcooling)

Figure 7.28 Images of hydrate dissociation for natural gas-condensate-water system in the presence of 0.5 mass% HT04-106 at 102 bar.

7.4 SUMMARY AND CONCLUSIONS

This chapter describes the detail measurement of visual observation via dynamic multichannel flow conduit and glass capillary blockage technique to investigate the mechanism of gas hydrate morphology, growth pattern and inhibition. The main objective is to understand the mechanism of gas hydrate growth and inhibition in the presence of LDHI. In this chapter, evaluation of Kinetic Hydrate Inhibitor (KHI) and Anti-agglomerant (AA) were studied. The second objective is to investigate the effect of synergist material and corrosion inhibitor on the performance of KHI based on characteristic behaviour of hydrate plugging.

For evaluation of Kinetic Hydrate Inhibitor (KHI), the experiments were conducted using natural gas-water system in the presence of 0.5 mass% polyvinyl caprolactam (PVCap) based polymer and a mixture of 0.5 mass% PVCap base polymer with 0.75 mass% Propylene glycol propyl ether (PGPE). PGPE was selected as synergist chemical to study the effect of known synergist on kinetic inhibitor performance and also its influence on hydrate morphology and plugging. The results showed that PGPE enhances the performance of PVCcap base polymers to inhibit hydrate formation and delay hydrate growth. In the presence of PGPE as a synergist to PVCap, hydrate formed at higher degree of subcooling with slightly longer induction time and further delayed in hydrate blockage as compared to PVCap without synergist and also the blank test.

The morphology for the blank test (Natural Gas – Water System) was in the form of a continuous non-porous solid hydrate, while in the presence of PVCap, hydrate deposits initially appeared to be more porous and proggressively turned to a non-porous solid. In the presence of a mixture with synergist i.e. PGPE, hydrate initially formed as a layer of thin patches of hydrate crystal in gas phase and solid hydrate in several parts of capillary tubes. Continuous flow of water and gas into the capillary tubes led to buildup of solid hydrate and finally blocked the capillary tubes.

A study on compatibility of the corrosion inhibitor (CI) with PVCap was reported by Tohidi et. al. (Tohidi et al, 2005). The finding based on kinetic rig shows that CI has adversely affected the performance of PVCap. Therefore, the study using micromodel was designed to investigate this effect. The effect of the corrosion inhibitor (500 ppm Corrtreat 799) on the performance of the kinetic hydrate inhibitor (1.25 mass%

LUVICAP®) under both static and flowing conditions was investigated. The results shows that catastrophic hydrate formation began at 11°C subcooling in the presence of the corrosion inhibitor. On the other hand, in the test without the corrosion inhibitor hydrate formed at 13 °C subcooling. In addition, PVCap failed to prevent hydrate formation in the water phase in the presence of corrosion inhibitor.

For evaluation of Anti-agglomerant, a series of experimental studies were designed to evaluate the anti-agglomerant with 3 mass% of NaCl for natural gas-water condensate system using capillary tube blocking technique. The study was conducted under flowing/dynamic and static conditions based on characteristic behaviour of hydrate plugging and time for blockage. Tests were performed for natural gas-water system, natural gas-condensate-water system with and without 0.5 mass% anti-agglomerant and finally gas condensate-water system with 0.5 mass% anti-agglomerant. The remaining study was focused on evaluating the hydrate crystal size and distribution for NG-water-condensate system at static conditions in the presence of anti-agglomerant.

The hydrate morphology observed for the natural gas- condensate water system in the presence of anti-agglomerate is a mix of thin layer and patchy hydrate crystals formed in the system at tested condition. Whereas in the absence of anti-agglomerate, massive hydrate plug formed at some part of capillary tube. In the case of hydrate formation from gas condensate-water system, hydrate particles was mostly observed to form and dispersed in the condensate phase and it also formed at the water-gas interface. Based on the above results, both estimated induction time and blockage time under shut in and flowing conditions are longer for the system with anti-agglomerant. The result is expected where the anti-agglomerant, fundamentally polymeric surfactants, prevent hydrates from agglomerating and depositing in the pipelines. These anti-agglomerant keep the particles small and well dispersed in the hydrocarbon liquid. Although in principle, anti-agglomerant allows hydrate to form and have no intended effect on hydrate nucleation/growth kinetics (i.e. induction time), it shows some significant differences for the series of tests that was performed using this system under flowing conditions.

Hydrate particles size and distribution for natural gas-condensate-water system in the presence of anti-agglomerant was studied at static condition using symmetric pore

structure conduit in the micromodel. The results showed that hydrate particles mainly formed and distributed within the water in oil emulsion phase. The hydrate particle size is estimated in the range of 5 – 10 μm which is slightly larger than the size of water droplet in emulsion.

In summary, a dynamic visual observation using micromodel generates new data to support understanding of hydrate inhibition mechanism, growth pattern and morphology in the presence of various LDHIs.

CHAPTER 8

CONCLUSIONS AND RECOMMENDATIONS

8.1 INTRODUCTION

The theme of this thesis has been the new approaches in avoiding gas hydrate problems in offshore and deepwater operation. This thesis has focused on the following aims:

(i) Develop a novel approach for early warning system and monitoring against initial hydrate formation, and

(ii) Investigate the mechanism of gas hydrate formation/growth, inhibition and morphology in the presence of Low Dosage Hydrate Inhibitors (LDHIs) by means of visualization technique.

Results on development of novel early warning methods by investigating water memory using dielectric constant and on-set of ice formation is presented respectively in Chapters 3 and 4 of this thesis. The work also includes investigating the main factors influencing the water memory. Sustainability of memory at atmospheric pressure for potential surface application and at low pressure for potential on-line application was also investigated. Other important factors such as heating to remove memory, influence of sample preparation path and the effect of impurities were studied.

Potential novel method to understand the mechanism of gas hydrate formation/growth and inhibition for evaluation of LDHI's under static and dynamic conditions is presented. Details are provided in Chapters 6 and 7 of this thesis. These techniques are based on visual observation using high pressure glass micromodels, multichannel flow conduits and glass capillary tubes.

Specific technical conclusions with regards to detection of hydrate water memory as indicator for early warning system using various techniques and the methodology of using LDHI for hydrate prevention through understanding the mechanism and potential novel method of evaluation have evolved from the results of each chapter. In this final chapter, the important conclusions from each part of the study with a summary of main

contributions of this dissertation and recommendations for future directions are presented.

8.2. CONCLUSIONS AND CONTRIBUTIONS

Investigation of Water Memory by Dielectric Constant

A new approach for hydrate early warning system using dielectric properties was studied. The main idea was based on the phenomena of water memory which was extensively reviewed. The experiments were designed to answer several key questions. These key questions are the potential application of dielectric constant as an indicator to detect the presence of water memory, the main factors contributed to the water memory (changes in water structure or dissolved gas or combination of both), the sustainability of water memory, the effect of heating, the effect of sample preparation path on water memory, the effect of sample preparation path on water structure, the effect of impurities and the water memory under pressure for potential on-line application.

The dielectric constant can be applied to detect the presence of water memory in a water sample after hydrate formation and dissociation. This is based on significant different in dielectric constant (measure with DW) between HDW and SDW. The results also suggested the presence of water memory is a combined effect of both dissolved gas and presence of remnant water structure which remains for a longer time (2 to 3 hours) after hydrate dissociation as compared to the sample with soluble gas at atmospheric and 4 ^{o}C. In practice, this result implies the produced water must be analysed within 2 to 3 hours after sampling to detect the presence of water memory as hydrate early warning.

The debatable phenomena on the hypothesis of main factors contributing to the presence of water memory were investigated in this thesis. The experiments was designed to confirm that water memory is mainly attributed to dissolved gas, which keeps the structure of water until the excess gas is evolved from solution. Investigation on the presence of water structure suggests that hydrate water memory is influenced significantly by dissolved gas which causes the water memory to remain for some time. The presence of water structure was found to be very weak based on the procedure adopted for this study. This results support the notion that hydrate water memory is mainly a function of dissolved gas.

The effect of heating on the water memory was investigated. The result confirmed that water memory is totally removed after heating at 35 ^{o}C for more than 12 hours. It was recognized that 12 hours heating time is too long for practical purposes. The effect of time required further investigation which could not be covered in this thesis.

In pipelines, hydrates may be dissociated through gradual change in temperature or pressure. To simulate this process, the hydrate water samples were prepared following different paths, along a depressurization track inside or just outside the hydrate stability zone. The effect of different depressurisation path on water memory was investigated. The result shows that the hydrate memory remain up to 1 hour for depressurization path inside hydrate phase boundary and approximately 0.5 hour for that outside hydrate phase boundary. Reduction in temperature and pressure from step by step dissociation cause significant release of soluble gas especially outside hydrate phase boundary and hence reduce the stability of water memory.

The compositional analysis of each aqueous phase was conducted at atmospheric pressure and room temperature after dissociation/depressurisation based on different paths. The results of analysis show that in the presence of hydrate water memory (for HDW samples), the ratio of C_2 to C_1 concentration is higher than that without water memory (for SDW samples). The ratio is significantly higher in the case of HDW depressurised along the path inside hydrate phase boundary. This is likely due to the longer sustainability of water memory as detected by dielectric constant technique. The ratio of C_2 and C_1 concentration was higher in the case of HDWV as compared to SDWV. This indicated that even with the two stages vacuum procedure to remove excess dissolved gas, there was detectable dissolved gas present in the aqueous sample which may contribute to the water memory at the test conditions. This results support the finding from dielectric constant study that dissolved gas is the main factor contributing to the water memory of hydrates.

Investigation was done on Tetrahydrofuran (THF), a water soluble hydrate former, to further understand the influence of water structure on water memory in the absence of dissolved gas. The result shows that there is no significant difference between dielectric constant after dissociation and after heating. This could be attributed to a very weak water memory presence in water-soluble hydrate former and reduction of water activity

at atmospheric pressure, which is agreeable with the conclusion that dissolved gas plays an important role as a main factor contributed to water memory.

The effect of salt (3 wt% NaCl) as impurities on hydrate water memory was investigated. The finding shows that the presence of salt has a negative effect on the memory. It is understood that the presence of salt in water, similar to THF, reduces the activity of water and solubility of natural gas in the water. It is expected that, the amount of gas hydrate form is less for the system with salt as impurity and hence reduces the water memory.

Potential online measurement technique for monitoring and early warning system of hydrate formation in the closed system such as pipeline is of interest to oil companies and field operators. In this thesis, the potential application of dielectric properties measurement at medium pressure was investigated. The result shows that dielectric properties measurement can be applied to detect the initial hydrate formation and the presence of solid hydrate particles based on reduction of dielectric constant value demonstrated in this study. The water memory remains for a much longer time (12 hours) in the system under pressure than that of atmospheric conditions. This could be evidence that the water memory is a strong function of dissolved gas and remnant of hydrate nuclei which keep the memory for some period of time. The difference in dielectric constant between DW and HDW is significantly lower after heating as compared to after dissociation. This again suggests that most of water memory was removed after heating.

The results demonstrate that dielectric properties at microwave frequencies has potential to be used as a downstream analysis and/or online system for detecting the initial hydrate formation and/or changes in the water memory due to hydrate formation. This could be used as an indicator for early warning system. The results are very encouraging and could make significant impact on the industrial approach to gas hydrate control strategy.

Investigation of Water Memory by Onset of Ice Nucleation

Onset of ice formation by freezing method was considered as one of the potential techniques for early warning system. The main idea in this thesis is to generate data to

confirm the applicability of onset of ice formation method, which could provide a simple method to detect memory of hydrate formation in produced water from the field.

The effect of different sample preparation paths on water history was investigated. The nucleation probability distribution based on classical nucleation theory was applied to describe the stochastic nature of the nucleation data. The results suggest that the samples with water history tend to freeze earlier and to nucleate faster than those without water history regardless of the sample preparation paths are inside or outside the hydrate stability zone.

The role of dissolved gas in the sustainability of water structure was studied by removing excess dissolved gas. The results suggest that removing dissolved gas could significantly eliminate the effect of water structure on ice nucleation, but the presence of water history is still measurable based on the observed effect on ice nucleation rate.

As a conclusion, the results demonstrate that changes in water memory due to hydrate formation could be detected using freezing method. This could provide a simple method to identify the memory of hydrate formation in produced water, hence an early warning against pipeline blockage.

Investigating Inhibition Mechanism of KHIs by Visual Observation of Gas Hydrate Formation, Growth Pattern and Morphology

In this thesis, extensive novel data and knowledge was generated to study gas hydrate in the absence and presence of KHIs for various fluid systems. The objective is to investigate the inhibition mechanism of typical commercial KHIs by visual observation of hydrate morphology, growth patterns and hydrate formation. The investigation was conducted using High Pressure Glass Micromodel with pore structure network and multichannel glass conduit.

The study was investigated for methane-water and natural gas – water systems. Methane represents structure I hydrate, whereas natural gas for structure II hydrates. In this thesis, experiment on natural gas – water systems is the major fluid system been studied. This is because they closely represent hydrate formation from real reservoir fluids, which are dominated by structure II systems. The result suggests that different mechanisms seem to be involved for the different systems. This study shows that hydrate can form at gas-water interface or from dissolved gas in the water phase or from water in the gas phase (Table 6.3 of Chapter 6). For example, based on the video

footage captured for natural gas - water system at 14.5^{O}C subcooling, hydrate formed in the gas phase or bubbles (from free gas) as a non-translucent (dark coloured) crystals. The hydrate crystal was transported through the water phase to the adjacent free gas bubbles to form hydrate. The process was continuous until all gas bubbles were converted to hydrate. There was also evidence of traces of translucent hydrate crystals formed from dissolved gas in the water phase.

Several commercial KHIs which are polymer base were used in this study to investigate the inhibition mechanism of the natural gas-water and methane-water system. These KHIs are LUVICAP EG®, HI03-24, HI03-22, HI03-187, HT04-049 and pure PVCap. These inhibitors are mainly PVCap based polymer in combination with Ethylene Glycol as a carrier fluid. A synergist chemical is additional compound present in inhibitor HI03-24, HI03-22 and HI03-187 whereas inhibitor HT04-049 is another base polymer used for this investigation. In this thesis, hydrate crystal morphology and growth pattern in the presence of different KHIs was reported. The effect of synergistic chemical, carrier fluid and different base polymer on hydrate morphology was also documented.

The finding of this study shows that various hydrate morphologies formed in the presence of different KHIs. The common hydrate morphology observed for inhibition characteristic of natural gas-water system by majority of tested KHIs was dense masses solid, patches of hydrate crystals and thin patchy crystal flakes. However, different hydrate crystals morphology was observed in the presence of HI03-187 and HI03-24. These are snowy crystal flakes, whiskery, threadlike, small dendrites and circular shape (Table 6.5 of Chapter 6). For methane-water system the inhibition characteristic resulted in thick rough crystals, hydrate shell thin crystals and large massive solid crystals (Table 6.6 of Chapter 6).

The morphologies in the presence of KHIs with and without synergistic chemical (all PVCap-based with different synergists) for natural gas-water system at similar degrees of subcooling were investigated and compared. At the same degree of subcooling, the hydrate morphologies for the systems without inhibitor and the systems with LUVICAP EG® are different. In the presence of LUVICAP EG®, a dense solid hydrate crystal was observed in gas phase with little traces growth in dissolved gas. The morphology observed in the presence of HI03-24 and HI03-22 is significantly different from that in the presence of LUVICAP EG®. The morphology in the presence of these KHIs is mainly patches of very thin crystal flakes and small hydrate particles. This suggests that the synergist chemicals

have changed hydrate morphology and particle sizes for the same basic polymer. With formation of thin and small hydrate crystal, it suggests that even KHIs fail to inhibit hydrate formation at this test condition, the hydrate is still transportable and potentially will not cause immediate blockage to the pipeline upon failure. For further work, it is recommended to investigate synergist chemical which could transport hydrate in the presence of KHIs when it is failed. The effect of synergist chemical was studied using multichannel flow conduit and the detail result is included in Chapter 7 of this thesis.

The natural gas hydrate crystals morphology in the presence of PVCap with and without carrier fluid was investigated. In the presence of PVCap with ethylene glycol as the carrier fluid, a continuous solid hydrate formed in the micromodel. On the other hand, without carrier fluid, thin patches of hydrate crystals were observed. The results suggest that the carrier fluid have some effect on the morphology of hydrate crystal at these test conditions.

For methane-water system, the hydrate morphology and growth pattern was investigated in the presence of PVCap, HI03-22 and HI03-24 tested at about the same degree of subcooling. The hydrate crystal morphology is a dense solid in the presence of PVCap, a continuous thin crystal in the presence of HI03-22 inhibitor and thick rough hydrate crystals in the presence of HI03-24.

The effect of KHIs on hydrate crystal morphology for different hydrate structure was analysed by comparing morphologies of natural gas (s-II) and methane (s-I) hydrates in the presence of HI03-22 and HI03-24. In the presence of HI03-22, it was observed that thin flakes of hydrate crystals formed from natural gas (s-II) and continuous thin solid hydrate crystals formed from methane (s-I). In the presence of HI03-24, natural gas S-II) exhibits a mixture of whiskery-like and thread-like hydrate crystals, while at similar degrees of subcooling, methane gas (s-I) forms a thick and rough hydrate crystal. This suggests that different hydrate crystal morphology is generated from different hydrate structure in the presence of KHIs.

The following conclusion can be drawn from investigating inhibition mechanism of Kinetic Hydrate Inhibitors (KHIs) by visual observation of gas hydrate morphology, growth pattern and formation:

i. Various hydrate morphologies formed in the presence of different KHIs for Natural gas hydrate. This morphology are dense masses solid, patches of hydrate

crystals, thin patchy crystal flakes, snowy crystal flakes, whiskery, threadlike, small dendrites and circular shape. For methane hydrate the morphology are thick rough crystals, hydrate shell thin crystals and large massive solid crystals

ii. Synergistic chemical as a compound in the KHIs have significant effect on hydrate morphology. The morphology in the presence of synergistic chemical was found to exhibit patches of very thin crystal flakes and small hydrate particles. This suggests that the synergist chemicals have changed hydrate morphology and particle sizes for the same basic polymer. With formation of thin and small hydrate crystal, it suggests that even KHIs fail to inhibit hydrate formation at this test condition, the hydrate is still transportable and potentially will not cause immediate blockage to the pipeline upon failure.

iii. The present of carrier fluid in the KHIs have effect on hydrate crystal morphology. The result shows that in the presence of PVCap with ethylene glycol as the carrier fluid, continuous solid hydrate morphology was formed. On the other hand, thin patches of hydrate crystals were observed without carrier fluid.

iv. Different hydrate crystal morphology is generated from different hydrate structure in the presence of KHIs.

Investigating Inhibition Mechanism of Low Dosage Hydrate Inhibitor (LDHI) by Dynamic Visual Observation

This chapter describes the detail measurement of visual observation via dynamic multichannel flow conduit and glass capillary blockage technique to investigate the mechanism of gas hydrate morphology, growth pattern and inhibition. The main objective is to understand the mechanism of gas hydrate growth and inhibition in the presence of LDHI. In this chapter, evaluation of Kinetic Hydrate Inhibitor (KHI) and Anti-agglomerant (AA) were studied. The second objective is to investigate the effect of synergist material and corrosion inhibitor on the performance of KHI based on characteristic behaviour of hydrate plugging.

For evaluation of Kinetic Hydrate Inhibitor (KHI), the experiments were conducted using natural gas-water system in the presence of 0.5 mass% polyvinyl caprolactam (PVCap) based polymer and a mixture of 0.5 mass% PVCap base polymer with 0.75 mass% Propylene glycol propyl ether (PGPE). PGPE was selected as synergist chemical

to study the effect of known synergist on kinetic inhibitor performance and also its influence on hydrate morphology and plugging. The results showed that PGPE enhances the performance of PVCcap base polymers to inhibit hydrate formation and delay hydrate growth. In the presence of PGPE as a synergist to PVCap, hydrate formed at higher degree of subcooling with slightly longer induction time and further delayed in hydrate blockage as compared to PVCap without synergist and also the blank test.

The morphology for the blank test (Natural Gas – Water System) was in the form of a continuous non-porous solid hydrate, while in the presence of PVCap, hydrate deposits initially appeared to be more porous and proggressively turned to a non-porous solid. In the presence of a mixture with synergist i.e. PGPE, hydrate initially formed as a layer of thin patches of hydrate crystal in gas phase and solid hydrate in several parts of capillary tubes. Continuous flow of water and gas into the capillary tubes led to buildup of solid hydrate and finally blocked the capillary tubes.

A study on compatibility of the corrosion inhibitor (CI) with PVCap was reported by Tohidi et. al. (Tohidi et al, 2005). The finding based on kinetic rig shows that CI has adversely affected the performance of PVCap. Therefore, the study using micromodel was designed to investigate this effect. The effect of the corrosion inhibitor (500 ppm Corrtreat 799) on the performance of the kinetic hydrate inhibitor (1.25 mass% LUVICAP®) under both static and flowing conditions was investigated. The results shows that catastrophic hydrate formation began at 11^{o}C subcooling in the presence of the corrosion inhibitor. On the other hand, in the test without the corrosion inhibitor hydrate formed at 13 ^{o}C subcooling. In addition, PVCap failed to prevent hydrate formation in the water phase in the presence of corrosion inhibitor.

For evaluation of Anti-agglomerant, a series of experimental studies were designed to evaluate the anti-agglomerant with 3 mass% of NaCl for natural gas-water condensate system using capillary tube blocking technique. The study was conducted under flowing/dynamic and static conditions based on characteristic behaviour of hydrate plugging and time for blockage. Tests were performed for natural gas-water system, natural gas-condensate-water system with and without 0.5 mass% anti-agglomerant and finally gas condensate-water system with 0.5 mass% anti-agglomerant. The remaining study was focused on evaluating the hydrate crystal size and distribution for NG-water-

condensate system at static conditions in the presence of anti-agglomerant.

The hydrate morphology observed for the natural gas- condensate water system in the presence of anti-agglomerate is a mix of thin layer and patchy hydrate crystals formed in the system at tested condition. Whereas in the absence of anti-agglomerate, massive hydrate plug formed at some part of capillary tube. In the case of hydrate formation from gas condensate-water system, hydrate particles was mostly observed to form and dispersed in the condensate phase and it also formed at the water-gas interface. Based on the above results, both estimated induction time and blockage time under shut in and flowing conditions are longer for the system with anti-agglomerant. The result is expected where the anti-agglomerant, fundamentally polymeric surfactants, prevent hydrates from agglomerating and depositing in the pipelines. These anti-agglomerant keep the particles small and well dispersed in the hydrocarbon liquid. Although in principle, anti-agglomerant allows hydrate to form and have no intended effect on hydrate nucleation/growth kinetics (i.e. induction time), it shows some significant differences for the series of tests that was performed using this system under flowing conditions.

Hydrate particles size and distribution for natural gas-condensate-water system in the presence of anti-agglomerant was studied at static condition using symmetric pore structure conduit in the micromodel. The results showed that hydrate particles mainly formed and distributed within the water in oil emulsion phase. The hydrate particle size is estimated in the range of 5 – 10 μm which is slightly larger than the size of water droplet in emulsion.

In summary, a dynamic visual observation using micromodel generates new data to support understanding of hydrate inhibition mechanism, growth pattern and morphology in the presence of various LDHIs.

Summary of Main Contributions of this Thesis

The primary part of this thesis is to develop a new approach for early warning system and monitoring against initial hydrate formation. The techniques investigated in this thesis are dielectric properties and onset of ice formation. The aim is to give the operator adequate time to initiate remedial steps prior to massive hydrate

formation/build up which could result in pipeline blockage. The new approach demonstrate that dielectric properties at microwave frequencies has the potential to be used as a downstream and online analysis for detecting the initial hydrate formation and/or presence of hydrate particles and/or changes in water structure due to hydrate formation. Characteristic of onset of ice formation by freezing method for water samples with and without hydrate water memory shows that samples with water memory nucleate faster than that without water memory. These new approach have potential to be developed for early warning and online hydrate monitoring. The results are very encouraging and could potentially change the industrial approach to gas hydrate control strategy.

The second part of this thesis is to investigate the mechanism of gas hydrate formation/growth, inhibition and morphology by Low Dosage Hydrate Inhibitors (LDHIs) by means of visualization technique for evaluation LDHI performance. These techniques are based on visual observation in high pressure glass micromodel, multichanel flow conduit and glass capillary tube blockage. Extensive novel data and knowledge was generated from these techniques which demonstrate that different mechanisms seem to be involved for different systems and that hydrates can form at gas-water interface, from dissolved gas in the water phase or from water in the vapour phase. Different hydrate morphologies formed in the presence of different kinetic hydrate inhibitors. It was concluded that these techniques provides a new data to supplement the lacking of knowledge on the kinetics of gas hydrate inhibition and morphologies.

8.3. RECOMMENDATIONS FOR FUTURE WORK

This thesis reports experimental work on the following areas:

(i) development of new approach for early warning system and monitoring against initial hydrate formation which is focused on detection of hydrate memory using dielectric constant and onset of ice nucleation

(ii) investigating the mechanism of gas hydrate formation/growth, inhibition and morphology in the present of Low Dosage Hydrate Inhibitors (LDHIs) by application of visualization techniques using Glass micromodel and dynamic multiconduit and glass capillary tube blockage.

Although much has been discovered during this work, there is still many aspects of the techniques need to be improved and studied in detail in the future. Some of the areas for future study are listed below:

(i) **Factors which effect hydrate water memory**. This work should be further extended to include other factors which also have significant impact on the presence of water memory. This factor includes the minimum temperature required while heating to remove water memory. The limitation of temperature is the main parameter to be established for technique based on water memory. This information will further refine the suitability of this technique for certain specific cases as an early warning system. Another factor is to investigate the effect of impurities such as various percentages of salt, alcohol and KHI which is present in the system and its effect on hydrate water memory. Investigation on relationship between the amounts of hydrate formation with hydrate water memory is another factor recommended to be studied. This will provide a clue if this technique have limitation detecting water memory.

(ii) **Potential application of dielectric under various pressures for hydrate water memory**. In the current work, limited investigation was conducted for condition under pressure considering the pipeline application. The limitation on pressure is mainly due to the limitation of pressure limit on available dielectric probe. With the advance technology and availability of improved dielectric probe, this effect must be further investigated to discover its potential for application in various pipeline conditions.

(iii) **Monitoring compositional changes as indicator for early warning system.** Preliminary work was initiated to investigate the potential of this technique. The detail is provided in Appendix B. This preliminary results based on water samples taken from hydrate dissociation used in dielectric constant water memory detection study. The idea was to investigate on prominent components which remains in the vapour and liquid phase which was be used as an indicator for early warning system at pipeline condition.

(iv) **Improved techniques on onset of ice formation by freezing methods**. Hydrate nucleation is stochastic by nature. Obtaining repeatable /transferable data is often highly problematic and time consuming, making robust evaluation difficult. Hence, improved technique in term of larger batch facilities to establish data set for freezing methods application on early warning system